Cobalt(II)/(III) Based Redox Mediators for Dye-Sensitized Solar Cells

Thesis submitted for the fulfillment of Degree of

Doctor of Philosophy

Muhammad Kalim Kashif

M.Phil.

Department of Materials Engineering

MONASH University

Australia

September 2013

Abstract

This thesis focuses on the search for alternative redox mediators, a critical component of the electrolyte used in dye-sensitized solar cells (DSCs). The redox couple plays the important role of facilitating dye regeneration, which occurs following the light-induced electron injection from the dye into the semiconductor. The maximum photovoltage (V_{OC}) achievable with DSCs strongly depends on the redox potential of the mediator used in these devices. The redox potential of the classical iodide/triiodide redox couple typically sits 600-700 mV above that of the dye ($E(D/D^{+})$). As a consequence, a sizable amount of energy is dissipated during the dye-regeneration process, restricting the maximum achievable V_{OC}. Currently major efforts are being made to use alternative redox mediators in place of iodide/triiodide.

Very recently, cobalt(II)/(III)-based redox mediators have been used to fabricate DSCs with record efficiency. These DSCs were made using $[Co(bpy)_3]^{2+/3+}$ as a redox mediator. The 2,2'-bipyridine (bpy) used in this case is a bidentate ligand that coordinates to the metal centre via two nitrogen donor atoms. Modification in the architecture of these ligands offers an opportunity to tune the redox potential of their respective cobalt complexes. Many derivatives of bpy and the tridentate ligand, 2,2',6',2"-terpyridine (terpy), have been used to synthesize redox couples for DSCs. However, the use of redox couples based on the complexes of higher denticity ligands was virtually unexplored prior to this research.

In this thesis, pentadentate (L = $PY5Me_2$) and hexadentate (L' = bpyPY4) polypyridyl ligands have been used to prepare novel cobalt complexes for application as redox couples in DSCs. Based on the chelate effect, the new complexes were expected to be thermodynamically more stable than analogues prepared from lower denticity ligands, such as bpy and terpy. In case of the pentadentate ligand complexes with the general formula $[Co(L)(X)]^{2+/3+}$, where L = pentadentate ligand and X = weakly binding ligand, two complexes were isolated in which the cobalt center resides in a slightly distorted octahedral geometry. For these complexes, there is an opportunity to fine-tune the potential

of the redox couple by simply replacing the monodentate ligand X with another Lewis base with a stronger binding affinity for cobalt(II)/(III). The Lewis bases chosen for this study are common DSC electrolyte additives, which are generally believed to act as surface passivating agents. Using a number of analytical techniques, it was shown that *t*-butylpyridine (tBP) and *N*-methylbenzimidazole (NMBI) can easily replace the monodentate acetonitrile ligand (X) to form a redox couple with the general formula $[Co(L)(B)]^{2+/3+}$. By applying an organic sensitizer, efficiencies of 8.4% and 9.4% were attained under simulated light intensity of 100% sun (1,000 W m^{-2} AM 1.5) and 10% sun, respectively, with an open circuit voltage (V_{OC}) of 1V at 100% sun for the tBP based mediator.

To further develop a thermodynamically stable redox mediator capable of extending the long term stability of the DSCs, a hexadentate polypyridyl ligand (L') was used to prepare novel cobalt(II)/(III) complexes, which were characterized using techniques such as single crystal X-ray crystallography. These $[Co(L')]^{2+/3+}$ complexes were then applied as redox mediators in DSCs in combination with an organic sensitizer, MK2. The newly synthesized redox couple, $[Co(L')]^{2+/3+}$, results in higher DSC efficiencies than the $[Co(bpy)_3]^{2+/3+}$ couple. Most importantly, the lab scale DSCs made with this redox mediator exhibit superior stability under continuous full sun illumination compared to those based on $[Co(bpy)_3]^{2+/3+}$, highlighting the importance of the thermodynamic stability of the complex for future applications in commercial DSCs.

The oxidation of the cobalt(II) complex to the corresponding cobalt(III) complex is an important part of the synthesis of the redox couple. Efforts to oxidize $[Co(L)(X)]^{2+/3+}$ by $NOBF_4$ resulted in an unwanted reaction product, which was further investigated. Single crystal X-ray analysis revealed the formation of $[Co(L)(F)]^{2+}$, which resulted from the decomposition of BF_4 over time. The synthesis and structural elucidation of $[Co(L)(F)^{3+}$ is provided, as it could find potential application as redox couple or as a catalyst. A preferable method for the oxidation of cobalt(II) polypyridyl complexes is also suggested.

In conclusion, new non-corrosive redox mediators based on cobalt(II)/(III) complexes comprising multidentate polypyridyl ligands were developed in this

thesis. The ability to adjust the redox properties of these mediators provides the scope to fine-tune the mediator properties to those of specific sensitizers. This in turn should allow the minimization of dye-regeneration driving forces, which would consequently improve the energy conversion efficiencies.

Dedicated to my

Loving Parents

&

Sweet Family

General Declaration

The following declarations are made for the thesis based on conjointly published or unpublished work according to the Monash University regulation 17.

I hereby declare that this thesis includes no research work, which has been accepted for the award of any other degree at any institution. To the best of my knowledge, this thesis contains no work published or written by other person, except where due references are provided within the thesis.

This thesis consists of five chapters with two published papers included in the thesis as Chapter 3 and Chapter 4. One unpublished paper is incorporated into the thesis as Chapter 5. In the preparation of these three chapters (3, 4 and 5), I was the main responsible person. The extent of my contribution is described and signed by the main supervisor in form of a declaration before each chapter.

I am also a co-author of one published paper, which is not included in the thesis but attached as an appendix to the thesis.

The inclusion of co-authors in my work suggests that this research outcome was the result of an active collaboration between our group at the Monash University and Jeffrey R. Long at the University of California Berkeley (UCB).

In short, I was solely responsible for the design of experiments, synthesis of cobalt(III) complexes, their characterization, their incorporation into the solar cells followed by the solar cell characterization and drafting the papers. All the respective cobalt(II) complexes were received from UCB. Intensity modulated photovoltage and photocurrent spectroscopy including charge extraction measurements were carried on the instruments in the care of Dr. Noel Duffy at CSIRO, Clayton, who also helped me in the interpretation of results. Dr. Craig M. Forsyth helped me to do the structural characterization of the complexes and also taught me the technique of single crystal X-ray crystallography.

This thesis consists of the following papers, where the candidate was the main responsible person:

- Muhammad K. Kashif, Jordan C. Axelson, Noel W. Duffy, Craig M. Forsyth, Christopher J. Chang, Jeffrey R. Long, Leone Spiccia, Udo Bach, **A New Direction in Dye-Sensitized Solar Cells Redox Mediator Development: In Situ Fine-Tuning of the Cobalt(II)/(III) Redox Potential through Lewis Base Interactions**, *Journal of the American Chemical Society*, 2012, *134*, 16646-16653.

- Muhammad K. Kashif, Michael Nippe, Noel W. Duffy, Craig M. Forsyth, Christopher J. Chang, Jeffrey R. Long, Leone Spiccia, Udo Bach, **Stable Dye-Sensitized Solar Cell Electrolytes Based on Cobalt(II)/(III) Complexes of a Hexadentate Pyridyl Ligand**, *Angew. Chem. Int. Ed.*, **2013**,*52*, 5527-5531.

- Muhammad K. Kashif, Jordan C. Axelson, Craig M. Forsyth, Christopher J. Chang, Jeffrey R. Long, Udo Bach, Leone Spiccia, **Stabilization of a Very Short Co-F Bond with a Cobalt Pentapyridyl Ligand Cavity,** *To be submitted to the Australian Journal of Chemistry (as an invited article)*, Manuscript.

In the following article, the candidate was not the main responsible person, but contributed to the work (article attached as appendix):

- Wanchun Xiang, Akhil Gupta, Muhammad Kalim Kashif, Noel Duffy, Ante Bilic, Richard A. Evans, Leone Spiccia, Udo Bach, **Cyanomethylbenzoic Acid: An Acceptor for Donor–π–Acceptor Chromophores Used in Dye-Sensitized Solar Cells**, *ChemSusChem*, **2013**, *6*, 256-260.

General Declaration

Monash University

Declaration for thesis based or partially based on conjointly published or unpublished work

In accordance with Monash University Doctorate Regulation 17.2 Doctor of Philosophy and Research Master's regulations the following declarations are made:

I hereby declare that this thesis contains no material which has been accepted for the award of any other degree or diploma at any university or equivalent institution and that, to the best of my knowledge and belief, this thesis contains no material previously published or written by another person, except where due reference is made in the text of the thesis.

This thesis includes two original papers published in peer reviewed journals and one unpublished publication. The core theme of the thesis is cobalt(II)/(III) redox mediators for dye-sensitized solar cells. The ideas, development and writing up of all the papers in the thesis were the principal responsibility of myself, the candidate, working within the department of Materials Engineering under the supervision of Associate Prof. Udo Bach.

The inclusion of co-authors reflects the fact that the work came from active collaboration between researchers and acknowledges input into team-based research.

In the case of three chapters, my contribution to the work involved the following:

Thesis chapter	Publication title	Publication status*	Nature and extent of candidate's contribution
3	A New Direction in Dye-Sensitized Solar Cells Redox Mediator Development: In Situ Fine-Tuning of the Cobalt(II)/(III) Redox Potential Through Lewis Base Interactions	Published	Synthesis of the cobalt(III)complexes, experimental designs and measurements, interpretation of results and drafting of the manuscripts
4	Stable Dye-Sensitized Solar Cell Electrolytes based on Cobalt(II)/(III) Complexes of a Hexadentate Pyridyl Ligand	Published	Synthesis of the cobalt(III)complexes, experimental designs and measurements, interpretation of results and drafting of the manuscripts
5	Stabilization of a Very Short Co-F Bond with a Cobalt Pentapyridyl Ligand Cavity	To be submitted as invited paper	Synthesis of the cobalt(III)complexes, experimental designs and measurements, interpretation of results and drafting of the manuscripts

I have not renumbered sections of submitted or published papers in order to generate a consistent presentation within the thesis.

Signed: …… 

Date: ……**17/09/13**

Acknowledgement

All praises be to the Almighty Allah, the creator of all and the sustainer of all. Many thanks to Him, Who blessed me with the knowledge to differentiate between the right and wrong. All gratitude to Him as He blessed me with the guidance of the last Holy Prophet, Muhammad (PBUH).

I feel great pleasure in expressing my ineffable thanks to my encouraging and inspirational supervisors Assoc. Prof. Dr. Udo Bach and Prof. Dr. Leone Spiccia. Their personal interest, thought provoking guidance, valuable suggestions and discussions enabled me to complete this tedious work. My special thanks to Dr. Udo Bach, who supported my application during my transfer to Clayton Campus and to Dr. Leone Spiccia who agreed to co-supervise my PhD work. Both of my supervisors remained fully involved throughout my PhD work. The in-depth knowledge of Dr. Udo Bach particularly in the field of solar cells and in chemistry, in general, helped me to design my PhD project. He always listened to my crazy ideas and guided in the right direction. Vast knowledge of Dr. Leone Spiccia, especially in the field of coordination chemistry always remained a source of inspiration and motivation for me and encouraged me through difficult times of research.

My special thanks to my teachers, especially, Prof. Muhammad Taufique, Prof. Shahid Hameed and Prof. Khwaja Ansar Yaseen for my training as a researcher. Nevertheless, I also express my acknowledgments to Prof. Dr. Samuel Adeloju (Monash Gippsland), who initially supported my application, for PhD scholarship and happily allowed me to transfer to the Clayton Campus. I appreciate and acknowledge Monash University, for providing me scholarships (MIPRS and MGS) to complete my PhD degree.

I would like to thank my parents who always supported my studies and remained a source of inspiration throughout my life. I thank to my wife for being supportive and helpful in my research work and amusing me in difficult times. Thanks to my brother and sisters who always encouraged my higher studies.

I would like to express my sincere appreciation to Jordan C. Axelson, Dr. Michael Nippe and Prof. Jeffrey R. Long for their cooperation and collaboration; also for hosting me during my visit to UC Berkeley.

At the commencement of my PhD work, Dr. Torben Daeneke showed me how to construct the solar cells. His friendly behavior and nice suggestions always remained helpful and are much appreciated. Coordination chemistry discussions with Yan Mulyana are also acknowledged. Craig M. Forsyth taught me the crystallography and his continuous support is expressed with gratitude. I would like to thank Dr. Noel W. Duffy, who helped me to carry out IMVS-IMPS and charge extraction measurements during my work.

I would like to thank all my lab fellows including; the Bach group, the Spiccia group and the Cheng group for their help and friendly behavior. I also express my deepest appreciation to those whom I could not mention but are important part of my work and life.

I appreciate Jane Moodie and Amanda Everaert (research student academic support, Monash University) for helping me to improve my writing skills. I also thank and acknowledge, Dr. Alex McKnight, who helped in proofreading my literature review chapter (Chapter 2).

Abbreviations and Acronyms

Abbreviations and Acronyms	Name
ACN	Acetonitrile
BZN	Benzonitrile
bpy	2,2'-Bipyridine
bpyPY4	6,6'-bis(1,1-di(pyridine-2-yl)ethyl)-2,2'-bipyridine
CV	Cyclic voltammetry
Co^{2+}/Co^{3+} or Cobalt(II)/(III)	Cobaltous/Cobaltic
Co-bpy	$[Co(bpy)_3]^{2+/3+}$
DSC	Dye-sensitized solar cell
Fc/Fc^+	Ferrocene/ferrocenium redox couple
FTO	Fluorine doped tin oxide
FF	Fill factor
HOMO	Highest occupied molecular orbital
Hexadentate ligand (bpyPY4)	6,6'-bis(1,1-di(pyridine-2-yl)ethyl)-2,2'-bipyridine
IPCE	Incident photon to electron conversion efficiency
***IV*- and *JV*- Characterization**	Current-potential and current density-potential measurements
ITO	Indium doped tin oxide
IMVS	Intensity modulated photovoltage spectroscopy
IMPS	Intensity modulated photocurrent spectroscopy
J_{SC}	Short-circuit current density
LiTFSI	Lithium bis(trifluoromethane)sulphonamide
LUMO	Lowest unoccupied molecular orbital
LED	Light emitting diode
MPN	4-Methoxypropionitrile
NHE	Normal hydrogen electrode
NMBI	*N*-methylbenzimidazole
NMR	Nuclear magnetic resonance
OTf	Trifluoromethanesulphonate anion
PV	Photovoltaic
PEDOT	Poly[3,4- ethylenedioxythiophene]
Pentadentate ligand ($PY5Me_2$)	2,6-(bis(bis-2-pyridyl)methylmethane)pyridine
Phen	Phenanthroline
tBP	*tert*-butylpyridine

TCO	Transparent conducting oxide
TEMPO	[2,2,6,6-Tetramethylpiperidin-1-yl]oxyle
terpy	2,2',6',2"-terpyridine
TFMP	4-Trifluoromethyl-pyridine
TFSI	Bis(trifluoromethane)sulphonimide anion
UV-Vis	Ultraviolet and visible light
V_{OC}	Open circuit voltage
η	Energy conversion efficiency
τ_n	Electron lifetime
τ_d	Mean charge transport time
λ	Reorganization energy
$\Delta G°$	Gibbs free energy

Table of Contents

Chapter 1

Introduction

Chapter 1

Introduction

1.1. Energy and Environment

Since the beginning of the industrial revolution, the world has seen ever-increasing prosperity and economic growth. However, consumption of conventional energy resources as a result of industrialization has resulted in increased concentration of carbon compounds in the environment as well as in the atmosphere. In order to reduce the stress induced by pollution on our ecological and socio-economic systems and to augment the industrial and commercial growth, access to clean and inexpensive energy is of prime importance. In 2011, the atmospheric CO_2 concentration reached 390 ppm, which is 40% higher than its preindustrial level of 278 ppm and by May 2013, CO_2 concentration had climbed to 399.7 ppm.[1] Figure 1.1 shows the human contribution to the present atmospheric carbon dioxide content. This alarming increase in greenhouse gases and the cumulative carbon footprint necessitates enormous effort and decisive actions to tackle this issue.

The United Nations Framework Convention on Climate Change held 20 years ago urged participants to make policies to mitigate or prevent the anthropogenic effects of climate change.[2]

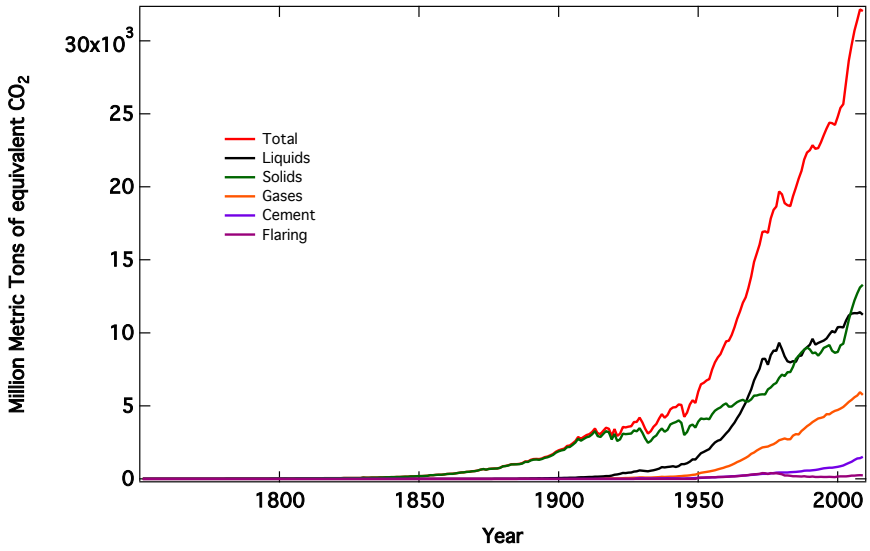

Figure 1.1: Emission estimates expressed in million metric tons of carbon from major contributors to the carbon footprint: fossil-fuel burning in its three different forms, cement manufacture and gas flaring[1]

Unfortunately, the effects of significant climate change have been adverse particularly for developing countries. Over 95% of deaths resulting from natural disasters have occurred in developing countries during the period of 1970 to 2008.[1,2] Thus, the quest for cheap, green and abundant energy is urgent and the modern world desperately needs innovative, environmentally friendly, alternative energy sources. Alternative energy sources can be defined as energy sources that are not based on fossil fuel burning or the atomic fission, since the recent Fukushima Daiichi (2011) and the Chernobyl (1986) nuclear disasters have turned many against nuclear power. Five major sources of clean energy include biomass, wind, hydro, geothermal and solar energy.

Solar energy in the form of light radiation is the most abundant energy source. Massive amounts of radiant energy are generated by the continuous nuclear fusion processes taking place in the sun. The energy striking the earth in an hour is more than the energy consumed globally in a year.[3] In order to use this energy to effectively fill the energy gap, a number of technologies have been devised, including solar heating, solar thermal electricity, solar fuels and photovoltaics (PV) technologies. Amongst these the most promising methodologies for generating power from the sun are PV technologies that transform radiation energy from the sun to generate an electric current, which is then fed directly into the electricity

transmission grid. Such photovoltaic technologies are thus regarded as utility-scale solar energy facilities.

Increasing investment interest shown by global companies has facilitated the application of solar energy into mainstream energy technologies. The current price of PV modules is less than half of their price in mid 2008. This steep reduction in cost is also supported by significant policy support in a number of key markets. A further expected decrease in PV module prices will help the public sector to adopt this technology and thus assist in the decarbonization of the electric grid.

There are a number of factors that affect the potential of a country to benefit from PV technologies. The most obvious factor is the geographic location of the country, as this not only changes the intensity of the solar irradiation but also the whole spectral distribution. Many other factors including the size of gross domestic product, financial stability, business environment and policies on renewable energy are considered to be important. A recent study by the European Photovoltaic Industry Association mapped all these factors for sunbelt countries (i.e., countries within 35° of the Equator). The resulting chart is given in Figure 1.2. As can be seen, Australia has great potential to benefit from PV technologies.

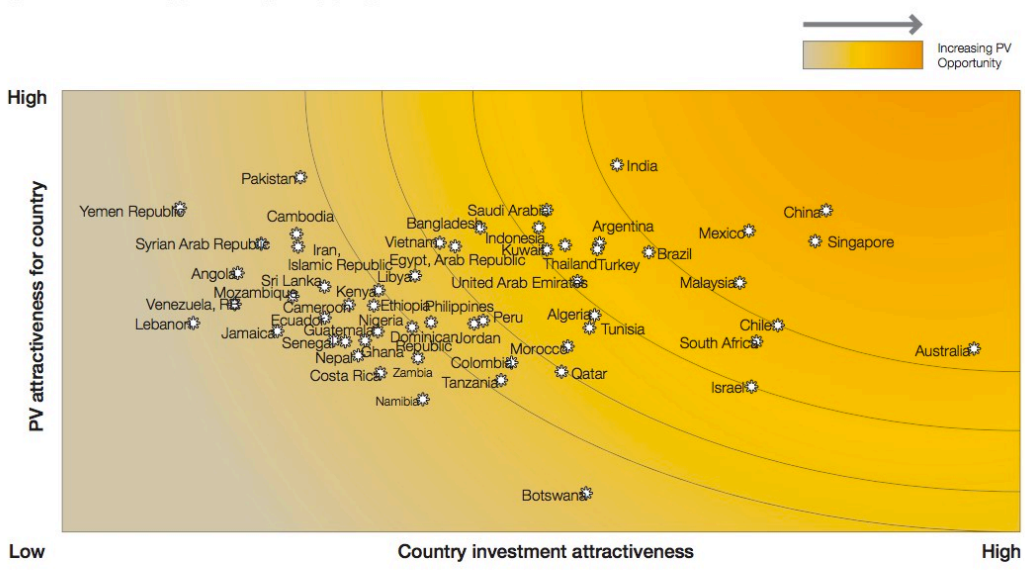

* Following countries are not shown on the mapping due to poor availability of data: Chad, Côte d'Ivoire, Congo Democratic Republic, Cuba, Iraq, Madagascar, Mali, Myanmar, Somalia, Sudan, Uganda.

Figure 1.2: Photovoltaic opportunity mapping of Sunbelt countries.[4]

1.2: Brief History of the Photovoltaic Technology

The solar PV cell is the fundamental semiconductor device responsible for converting light into electricity. The dominant PV technology is based on single-crystal silicon or polycrystalline silicon. In this section, a brief history of the concept development of PV is provided.

The photovoltaic (PV) effect was discovered in 1893 by Edmond Becquerel when he observed that electrical currents arise from certain light stimulated chemical reactions. In the late 1940s, the first solid-state device with 6% efficiency was available to industry. In PV solar cells, the incoming photons are absorbed by the semiconductor material and are converted into electron-hole pairs. The decisive parameter in this conversion efficiency is the bandgap energy, E_{gap}, of the semiconductor. Photons with an energy $hv < E_{gap}$ will not contribute to the photogeneration, whereas all photons with $hv > E_{gap}$ will take part in the overall photogeneration process. The maximum achievable photogenerated electric current density, J_{SC}, is thus given by the photons with an energy $hv > E_{gap}$. Estimates of the maximum achievable efficiency have been made since the discovery of the photovoltaic effect. In general, the solar-power conversion efficiency is strongly related to the initiation of electron-hole pairs caused by the incident photons followed by the propagation to the external circuit before the unwanted recombination reaction happens at a given voltage.

In 1960, Shockley-Queisser identified that the recombination mechanisms are the detailed balance counterpart of the generation mechanisms that are impossible to circumvent. Deeply rooted in the second law of thermodynamics, the detailed balanced principle of Shockley-Quiesser sets theoretical limits on the efficiency of the single junction solar cell. The first generation crystalline solar cells are already reaching the single junction solar cell's Shockley-Queisser limit of 31% under one sun illumination (air mass 1.5 G).[5] Currently, second generation and third generation solar cells are under intense investigation as the theoretical efficiency of these solar cells can be improved by using different materials and device architectures.

A comparison of the theoretical maximum efficiencies, best research cell efficiencies and typical module efficiencies has been provided by NREL for a number of

promising PV technologies (see Figure 1.3). Large gaps exist between the theoretical maximum efficiencies and the achieved module efficiencies. In particular, the large gap between the theoretical and module efficiency for triple junction (3J) concentrated photovoltaics (CPV) needs to be overcome to produce cost-effective CPV solar cells.

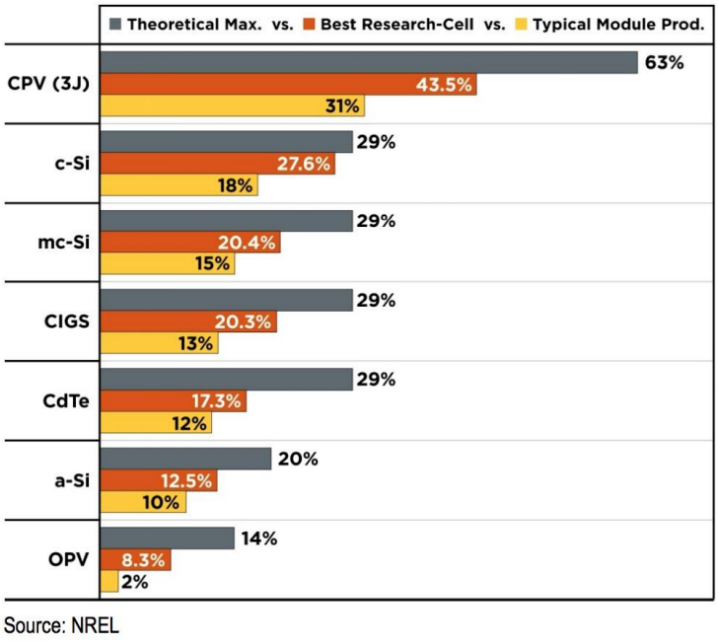

Figure 1.3: A comparison of theoretical maximum, best research cell and typical module efficiencies of a number of attractive PV technologies

1.3: Current Challenge for PV Technologies

The current challenge for the solar industry is to provide electricity at a cost of less than \$ 0.5/W_P at large scale. This requires simple mass production with cheap and effective infrastructure. Second and third generation solar cells are potential candidates for achieving this cost. These cells include amorphous silicon (a-Si), copper indium gallium diselinide (CIGS), CdTe and dye-sensitized solar cells (DSCs).[6] Figure 1.4 shows the highest efficiency records achieved by laboratory based research cells for most of the photovoltaic technologies currently under investigation. This useful compilation by Martin Green also shows the historic evolution of these technologies and the contribution towards this exciting research by different research groups in the world. This figure also provides the readers with an overview of the main classes of PV technologies and achievable efficiencies.

The classes of PV technologies described in the figure can be broadly divided into two major classes: single crystal solar cells and thin film technologies. Current attempts to reduce the cost and enhance the efficiency of single crystal based solar cells are limited. However, polycrystalline photovoltaic cells have emerged as a viable alternative technology to costly and laborious manufacturing of single crystal photovoltaics. Four main classes of thin film technologies are approaching or have exceeded the 10% landmark for solar-power conversion efficiencies. These technologies include: organic photovoltaics, solution-processed bulk inorganic photovoltaics colloidal quantum-dot solar cells and dye-sensitized solar cells (DSCs).[7] The DSC is a promising, inexpensive technology that can potentially be produced at low cost via well-established commercial printing technologies. DSCs are also very advantageous in their characteristic property of being able to operate in low sunlight as well.

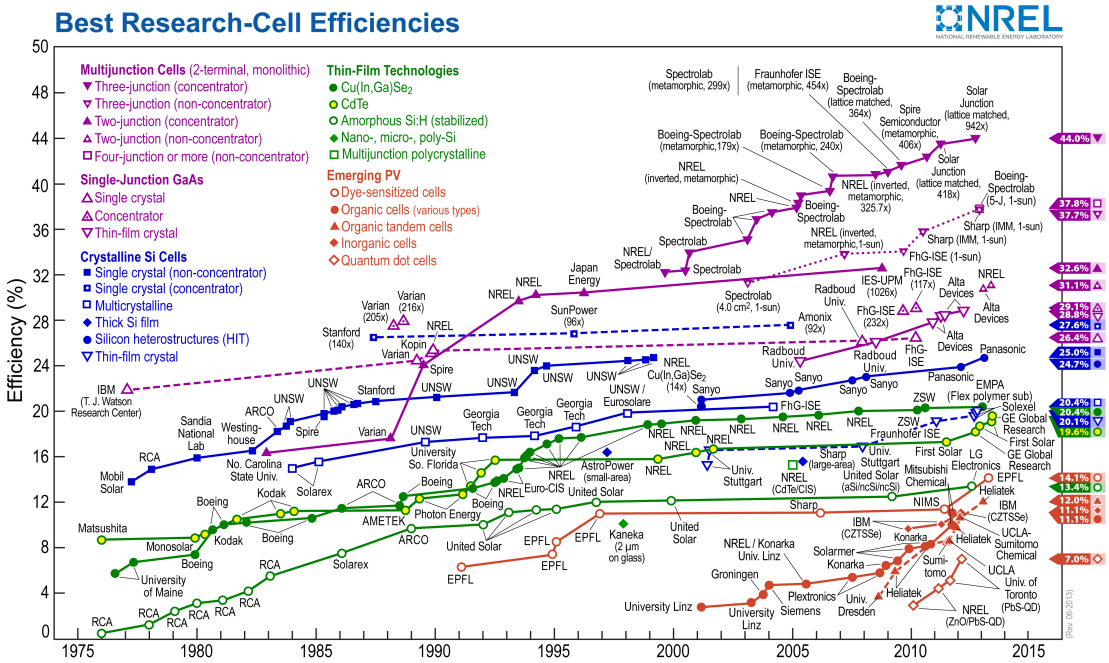

Figure 1.4: A comparison of best research cell efficiencies for different photovoltaic technologies. Reproduced from reference[8]

1.4: Dye-Sensitized Solar Cells

The functioning of DSCs is based on the large internal interface offered by the combination of a sensitizing dye and nanostructured titania in contrast to a built-in electric field in highly pure semiconductor materials. Low production cost, design opportunities, high temperature stability, flexibility, bifacial output and better diffused and low light performance are some of the characteristics which make these devices ideal candidates for future research and exploration as third generation PVs.

In a DSC, nanocrystalline semiconductor oxides, mostly TiO_2 sensitized with a dye, are used as the electrode and immersed into an electrolyte solution and redox mediators (see Figure 1.5). Upon optical excitation of the dye and subsequent electron injection into the titania, the redox mediator regenerates the dye. Dye regeneration in DSCs is an important part of the cascade of reactions that proceed on a pico to nano seconds time scale. The electrolyte present in the DSC device not only regenerates the dye but also transfers the charge to the adjacent counter electrode, typically through an ion diffusion mechanism.

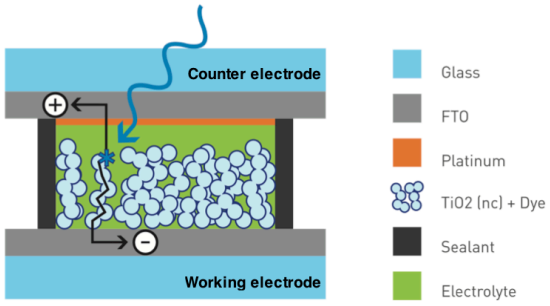

Figure 1.5: Schematic illustration of the operation principle of a molecular photovoltaic cell. The DSC components are divided into two major components: counter electrode (CE) and working electrode (WE). Both electrodes are fused together and filled with an electrolyte. Titania is printed on a conducting transparent layer applied on a transparent substrate (WE). A monolayer of dye is adsorbed onto the TiO_2 nanostructured film. A catalyst, usually Pt nanoparticles, is applied on the CE to catalyze the triiodide reduction.

The DSC is a complex system made up of strongly interacting individual components. Since the function of a DSC as a whole is larger than the sum of its components, the efficiency improvement of DSCs depends upon utilizing the full

potential of these individual components. The challenge is to develop these individual components in such a way that simultaneous interaction between them would allow better functioning of the DSC with maximum efficiency and enhanced stability enabling future industrial production of DSCs. These efforts include interdisciplinary research, involving electrochemistry, semiconductor physics, surface physics and chemistry, materials science aspects in organic and inorganic chemistry.[6,9] Figure 1.5 illustrates a schematic cross-section of a DSC. Figure 1.6 shows photoinduced processes occurring during photovoltaic energy conversion in a DSC. An ideal dye is capable of quantitative charge injection and of harvesting a wide spectral range of the solar spectrum (see processes 1 and 3 in Figure 1.6). Thus, a huge effort is being undertaken for the development of dyes.[9] The development of highly porous TiO_2 nanostructured films with a wide band gap is also very important as it allows superior charge percolation across the titania film.[10] In addition the electrolyte is a very important component that is responsible for dye-regeneration and is also under intense investigation.

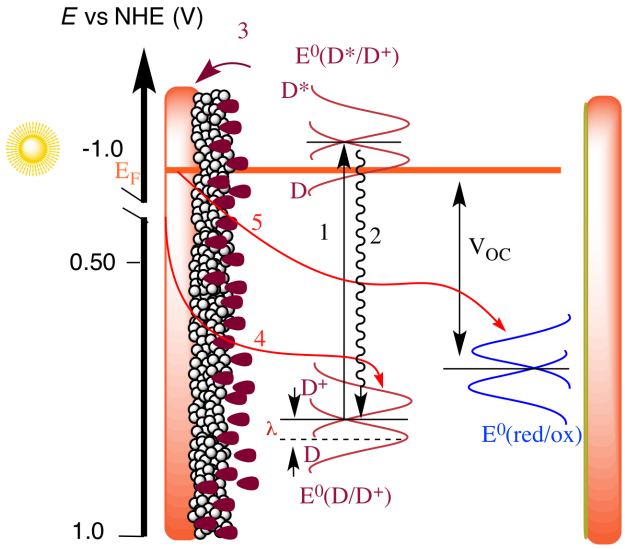

Figure 1.6: Photoinduced processes taking place during the photovoltaic energy conversion at the surface of the mesostructured titania films: (1) sensitizer excitation by light; (2) radiative or nonradiative deacay of the sensitizer; (3) electron injection into the conduction band; (4) recapture of the conduction band electron by the oxidized sensitizer (D^+); (5) recapture of the conduction band electrons by the oxidized form of the redox couple; $E^0(D/D^+)$ and $E^0(D^*/D^+)$ are the distribution functions for the redox energy levels of ground state and excited state of the dye, respectively. E^0(red/ox) is the redox distribution function for redox couple responsible for regenerating the sensitizer and transporting the positive charge to the counter electrode. Gray spheres: titania nanoparticles. Brown dots: sensitizer. Green and blue dots: oxidized and reduced forms of the redox couple. Gerischer distribution curves are used explicitly for all species undergoing a redox process, as the energy levels are not discrete.

1.4.1 Photoelectrochemical reactions in the DSC.

In the dark, an equilibrium is established between the Fermi levels of the titania and the electrolyte. However, when light falls on the sensitizer, electrons are excited from the HOMO level of the dye to the original LUMO level. The transfer of the electrons from the LUMO level of the dye to the titania increases the electron concentration in the conduction band of the titania and consequently, the quasi Fermi level is shifted upward. Subsequently, the sensitizer is regenerated by the reduced species of the redox shuttle in the electrolyte. In turn, the redox couple is regenerated at the counter electrode. A distribution of the energy levels occurs due to the fluctuations in the solvation shell surrounding the molecule.

The distribution functions of the unoccupied and occupied orbitals for the ground and excited states are equal areas showing that the corresponding concentrations of the redox species are the same (see Figure 1.7). Any variation in concentrations gives rise to different Fermi levels; $E_{F,\,redox}$ (D/D^+) and $E^*_{F,\,redox}$ (D^*/D^+). This variation will also lead to different driving forces for electron injection and for regeneration of the oxidized dye by the electrolyte. A high quality and well-sintered TiO_2 nanostructured film allows for efficient charge collection and percolation across the film (see process 3 in Figure 1.6).

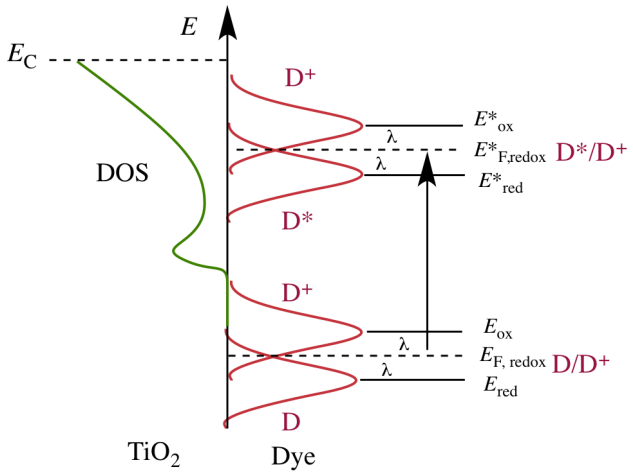

Figure 1.7: Energy distribution states of the dye in the ground state and the excited state. Optical excitation energy for excitation of the ground state of the dye, *D*, to the excited state *D is shown by an arrow. This optical excitation is then followed by the electron injection into unoccupied states within the conduction band of the mesoporous TiO_2 film.**[11]

The electrolyte has an important role in DSCs, as it is responsible for the dye regeneration as well as the charge conduction across the cell. The corresponding reorganization energies of the redox species (dye and redox couple) are very important for an efficient DSC device. For example, the reorganization energy for the D5 dye has been estimated to be 0.97 eV by a quantum chemical approach. Similarly the reorganization energy for the N3 dye has been estimated to be 0.35 eV (the structures of the dye N3 and D5 are shown in Figure 1.9).[11] The importance of the reorganization energy of the different redox species (dye and redox couple) in a DSC device is not very well understood. However, very recent developments in the field of alternative redox couples based on one-electron redox processes have provided very useful further insights into the importance of dye regeneration kinetics (discussed in detail in next chapter). The dye regeneration kinetics has also been very well studied for iodide/triiodide (two-electron process) based electrolytes. The process of dye regeneration following the electron injection into the titania by the excited dye is crucial. Ideally, dye regeneration must occur rapidly enough to avoid recombination reactions. Two types of unwanted recombination reactions occur in DSCs: 1) the recombination of photoinduced electrons in the titania and electron deficient species (oxidized form) in the electrolyte (see process 5 in Figure 1.6 and process 6 in Figure 1.8); and 2) the recombination of electrons from titania to the oxidized dye molecules (see process 4 in Figure 1.6 and process 5 in Figure 1.8).

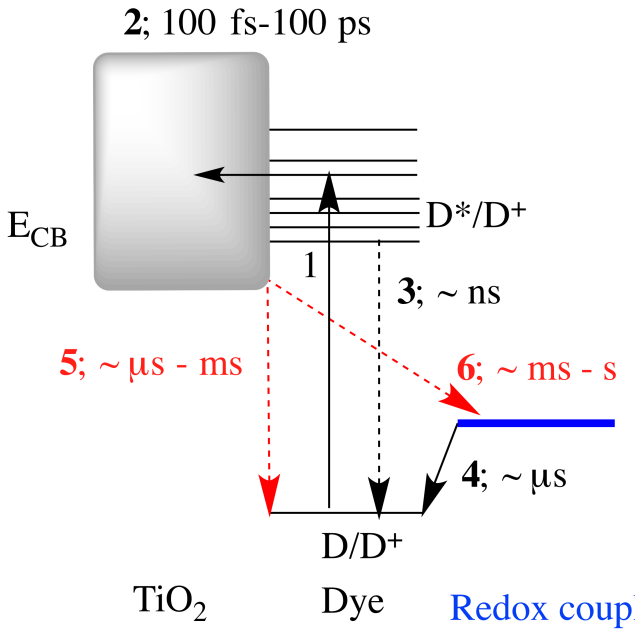

Figure 1.8: Diagram summarizing the interfacial electron transfer kinetics in a high performing DSC sensitized using a ruthenium dye and conventional iodide/triiodide electrolyte. Typical time ranges of the forward reactions (solid lines) and recombination reactions (dotted lines) are indicated.[12]

The successful operation of the DSC device is achieved as the forward electron transfer kinetics occur on a µs to fs scale. The electron injection from the excited state of the dye to TiO_2 (process 2 in Figure 1.8) occurs within 100 fs to 100 ps, which is much quicker than the relaxation of the dye, which occurs on the ns scale. However, dye regeneration (process 4 in Figure 1.7) occurs on µs scale, thus competing with the recombination reactions taking place on the s to µs scale (process 5 and 6 in Figure 1.8).[12]

1.4.2 The iodide/triiodide redox couple based electrolyte system

Despite record performance of I^-/I_3^- redox couple based electrolyte in DSCs, this redox couple has its own disadvantages. The corrosive nature of I^-/I_3^- particularly towards conductive metals is one of the serious concerns for the large scale production of DSCs as the production process involves the use of metallic grids. These grids are deposited on fluorine doped tin oxide (FTO) glass to minimize ohmic losses due to the high sheet resistance of the transparent conductive substrate [11]. The mismatch in the redox potential between I^-/I_3^- and the highest occupied molecular orbital (HOMO) of most dyes is also a serious issue. For N-719 (di-tetrabutylammonium-cis-bis(isothiocyanato)bis(2,2′-bipyridyl-4,4′-dicarboxylato)ruthenium(II)), a sensitizer used in high efficiency DSCs the HOMO

level is at 1.07 V (vs NHE).[13]Dye regeneration by the I^-/I_3^- redox couple involves the formation of the intermediate radical species $I_2^{\cdot-}$ with a more negative redox potential than the standard redox potential of I^-/I_3^-, representing an additional energy barrier. At high concentrations the I^-/I_3^- in the electrolyte absorb a significant part of the visible light, limiting the light harvesting efficiency of the sensitizer and hence limiting the achievable photocurrent.[14] In addition, the slow rate of regeneration for dyes with low redox potential, i.e., far-red-absorbing dyes, further limits the achievable photocurrent [15-17]. For sensitizers such as porphyrins with highly polarizable organic chromophores, the strong association of I_3^- results in enhanced dark currents and unwanted side reactions.[18,19]

The I^-/I_3^- redox couple was regarded as a robust redox couple in record performing DSCs for many years. In 2006, the important advance was reported by the Hagfeldt group by using cobalt(II)/(III) based redox mediators with donor-acceptor dyes. Later, in the seminal study by Grätzel *et al.*, I^-/I_3^- was replaced with the $[Co(bpy)_3]^{2+/3+}$ redox couple for record performing devices.[20] However, the industrial production of DSCs not only requires high performance but also stability. Thus, research into alternative redox mediators for DSCs is an ongoing research topic.

1.4.3 Finding a suitable redox mediator for DSCs

A number of different approaches have been considered to identify the optimum electrolyte of choice to bring the production of DSCs to an industrial scale. One approach is based on the use of the I^-/I_3^- redox couple supported by the ionic liquid, gel and polymer interface. However, the inherent issues associated with the I^-/I_3^- redox couple cannot be avoided using this strategy. Another parallel effort included the investigation of non-volatile components based organic and inorganic solid hole-conductors. These solid hole-conductors transfer the charge across the working electrode and counter electrode through a hole-transfer mechanism.[21-24] The main drawbacks associated with these solid hole-conductors include inefficient charge transfer and poor pore filling.[25]

Other approaches include the application of organic and inorganic redox couples dissolved in liquid solvents or supported by quasi-solids. These organic and inorganic redox couples have been selected from many redox processes taking place

in the nature as well other field of chemistry. A brief literature review of these redox couples is provided in the next chapter.

There are many examples of the use of metal-based redox mediators offering stable and efficient redox processes in nature, e.g. chlorophyll or metalloproteins. The ability of transition metal complexes to shuttle between two stable oxidation states makes them ideal candidates for alternative redox mediators. Our strategies to adhere to the challenge of finding suitable redox mediator for DSCs mainly include the exploration of redox mediators based on cobalt(II)/(III) (cobaltous/cobaltic) complexes. Cobalt(II)/(III) based redox mediator based on a bidentate and tridentate redox mediators have been recently explored. According to the literature, metal complexes based on higher denticity of the ligand result in higher stability of the complex as compared to the metal complexes based on lower denticity of the ligand.[26] Thus, the main emphasis of this thesis is to explore the usage of cobalt(II)/(III) based redox mediator as redox couples, with the general formula $[Co(L)_n]^{2+/3+}$, where L = polypyridyl ligand and n = 1-2.

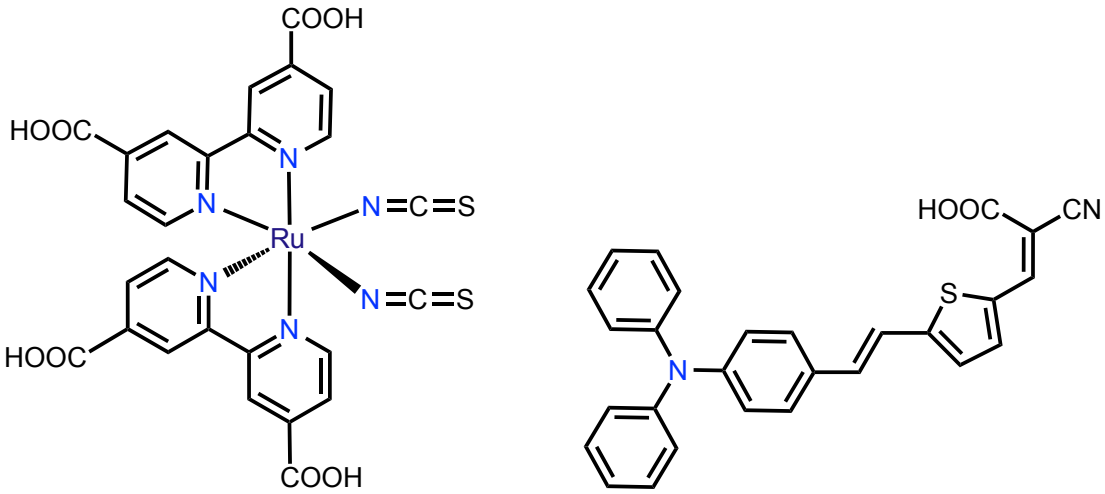

N3 **D5**

Figure 1.9: Structures of the dyes N3 and D5

1.5 References (Chapter 1)

1. a) Byrne, J.; Kurdgelashvili, L.; Taminiau, J., *WIREs Energy Environ,* **2012,** *1*, 17-40. b) Tans, P. NOAA/ESRL *(www.esrl.noaa.gov/gmd/ccgg/trends/)* and Dr. Ralph Keeling, Scripps Institution of Oceanography *(scrippsco2.ucsd.edu/).*

2. Pachauri, R. K., *WIREs Energy Environ.* **2012,** *1***,** 2-8.

3. Basic Research Needs for Solar Energy Utilization. *Report from Basic Energy Sciences Workshop on Solar Energy Utilization*, **2005,** April 18-21, Bethesda, Maryland. Washington, D.C.: Office of Science, U.S. Department of Energy, 2005.

4. Hauff, J.; Verdonck, M.; Derveaux, H.; Dumarest, L.; Alberich, J.; Malherbe, J-C., Unlocking the Sunbelt Potential of Photovoltaics, 2nd addition, *Report by EPIA*, October, **2010**.

5. Shockley, W.; Queisser, H. J., Detailed Balance Limit of Efficiency of p-n Junction Solar Cells, *J. Appl. Phys.* **1961**, *I32*, 510-519. b) Green, M. A., Third Generation Photovoltaics: Ultra-High Conversion Efficiency at low Cost, *Prog. Photovoltaics Res. Appl.* **2012**, *20*, 12-20.

6. a) Hagfeldt, A.; Henrik G. B.; Lindström, A.; Figgemeier, G.; Holmberg, A., A System Approach to Molecular Solar Cells. *Coord. Chem. Rev.* **2004,** *248*, 1501-1509. b) Grätzel, M.; Solar Energy Conversion by Dye-Sensitized Photovoltaic Cells. *Inorg. Chem.* **2005,** *44*, 6841-6851. c) Hagfeldt, A.; Boschloo, G.; Sun, L.; Kloo, L.; Pettersson, H., Dye-Sensitized Solar Cells. *Chem. Rev.* **2010,** *110*, 6595-6663.

7. Grätzel, M.; Janssen, R. A.; Mitzi, D. B.; Sargent, E. H., Materials Interface Eengineering for Solution-Processed Photovoltaics, *Nature,* **2012**, *488,* 304-312.

8. http://www.nrel.gov/ncpv/images/efficiency_chart.jpg

9. a) Mishra, A.; Fischer, M.; Bäuerle, P., Metal-Free Organic Dyes for Dye-Sensitized Solar Cells: From Structure: Property Relationships to Design Rules. *Angew. Chem. Int. Ed.* **2009,** *48*, 2474-2499. b) Caramori, S.; Cristiano, V.; Boaretto, R., Argazzi, Bignozzi, C. A.; Carlo, A. D., New Components for Dye-Sensitized Solar Cells. *Int. J. Photoenergy*. **2010**, Article ID 458614, 1-16.

10. Srikanth, K.; Rahman, M. M.; Tanaka, H.; Krishna, K. M.; Soga, T.; Mishra, M. K.; Jimbo, T.; Umeno, M., Investigation of the Effect of Sol Processing Parameters on the Photoelectrical Properties of Dye-Sensitized TiO_2 Solar Cells. *Sol. Energy Mat. Sol. Cells* **2001,** *65*, 171-177.

11. Kalyanasundaram, K., Dye-sensitized solar cells, EPFL Press, Page 351.

12. Feldt, S., Alternative Redox Couples for Dye-Sensitized Solar Cells, PhD Thesis, Uppsala University, **2013**.

13. Nazeeruddin, M. K.; Kay, A.; Rodicio, I.; Humphry-Baker, R.; Mueller, E.; Liska, P.; Vlachopoulos, N.; Grätzel, M., Conversion of Light to Electricity by cis-X_2bis(2,2'-bipyridyl-4,4'-dicarboxylate)ruthenium(II) Charge-transfer Sensitizers (X = Cl^-, Br^-, I^-, CN^-, and SCN^-) on Nanocrystalline Titanium Dioxide Electrodes. *J. Am. Chem. Soc.* **1993,** *115*, 6382-6390.

14. a) Nusbaumer, H.; Zakeeruddin, S. M.; Moser, J. E.; Grätzel, M., An Alternative Efficient Redox Couple for the Dye-Sensitized Solar Cell System. *Chem. Eur. J.* **2003,** *9*, 3756-3763; b) Hamann, T. W.; Farha, O. K.; Hupp, J. T., Outer-Sphere Redox Couples as Shuttles in Dye-Sensitized Solar Cells. Performance Enhancement Based on Photoelectrode Modification via Atomic Layer Deposition. *J. Phys. Chem. C* **2008,** *112*, 19756-19764.

15. Clifford, J. N.; Palomares, E.; Nazeeruddin, M. K.; Grätzel, M.; Durrant, J. R., Dye Dependent Regeneration Dynamics in Dye Sensitized Nanocrystalline Solar Cells: Evidence for the Formation of a Ruthenium Bipyridyl Cation/Iodide Intermediate. *J. Phys. Chem. C* **2007,** *111*, 6561-6567.

16. Kuciauskas, D.; Freund, M. S.; Gray, H. B.; Winkler, J. R.; Lewis, N. S., Electron Transfer Dynamics in Nanocrystalline Titanium Dioxide Solar Cells Sensitized with Ruthenium or Osmium Polypyridyl Complexes. *J. Phys. Chem. B* **2000,** *105*, 392-403.

17. Splan, K. E.; Massari, A. M.; Hupp, J. T., A Porous Multilayer Dye-Based Photoelectrochemical Cell That Unexpectedly Runs in Reverse. *J. Phys. Chem. B* **2004,** *108*, 4111-4115.

18. O' Regan, B. C.; Lopez-Duarte, I.; Martinez-Diaz, M. V.; Forneli, A.; Albero, J.; Morandeira, A.; Palomares, E.; Torres, T. S.; Durrant, J. R., Catalysis of Recombination and Its Limitation on Open Circuit Voltage for Dye Sensitized Photovoltaic Cells Using Phthalocyanine Dyes. *J. Am. Chem. Soc.* **2008,** *130*, 2906-2907.

19. Hagfeldt, A.; Boschloo, G.; Sun, L.; Kloo, L.; Pettersson, H., Dye-Sensitized Solar Cells. *Chem. Rev.* **2010,** *110*, 6595-6663.

20. Yella, A.; Lee, H. W.; Tsao, H. N.; Yi, C. Y.; Chandiran, A. K.; Nazeeruddin, M. K.; Diau, E. W. G.; Yeh, C. Y.; Zakeeruddin, S. M.; Grätzel, M., Porphyrin-Sensitized Solar Cells with Cobalt (II/III)-Based Redox Electrolyte Exceed 12% Efficiency. *Science* **2011**, *334*, 629- 634.

21. Saito, Y.; Azechi, T.; Kitamura, T.; Hasegawa, Y.; Wada, Y.; Yanagida, S., Photo-sensitizing Ruthenium Complexes for Solid State Dye Solar Cells in Combination with Conducting Polymers as Hole Conductors. *Coord. Chem. Rev.* **2004,** *248*, 1469-1478.

22. Bach, U.; Tachibana, Y.; Moser, J.-E.; Haque, S. A.; Durrant, J. R.; Grätzel, M.; Klug, D. R., Charge Separation in Solid-State Dye-Sensitized Heterojunction Solar Cells. *J. Am. Chem. Soc.* **1999,** *121*, 7445-7446.

23. Bach, U.; Lupo, D.; Comte, P.; Moser, J. -E.; Weissortel, F.; Salbeck, J.; Spreitzer, H.; Grätzel, M., Solid-state Dye-sensitized Mesoporous TiO_2 Solar Cells with High Photon-to-Electron Conversion Efficiencies. *Nature* **1998,** *395*, 583-585.

24. Tennakone, K.; Kumara, G.; Kumarasinghe, A. R.; Wijayantha, K. G. U.; Sirimanne, P. M., A Dye-Sensitized Nano-Porous Solid-State Photovoltaic Cell. *Semicond. Sci. Technol.* **1995,** *10*, 1689-1693.

25. Fukuri, N.; Masaki, N.; Kitamura, T.; Wada, Y.; Yanagida, S., Electron Transport Analysis for Improvement of Solid-State Dye-Sensitized Solar Cells Using Poly(3,4-ethylenedioxythiophene) as Hole Conductors. *J. Phys. Chem. B* **2006,** *110*, 25251-25258.

26. a) Izatt, R. M.; Pawlak, K.; Bradshaw, J. S.; Bruening, R. L., Thermodynamic and kinetic data for macrocycle interactions with cations and anions *Chem. Rev.* **1991**, *91*, 1721-2085. b) Hancock, R.D.; Martell, A.E., Ligand design for selective complexation of metal ions in aqueous solution, *Chem. Rev.* **1989**, *89*, 1875 -1914.

Chapter 2

Literature Review

Chapter: 2

Literature Review

In this chapter the importance of research into alternative redox mediators to the classical iodide/triiodide-based electrolyte is explained. In the second part of the chapter a broad classification of the alternative redox mediators is provided on the basis of organic and inorganic redox couples with a particular focus on cobalt(II)/(III)-based redox mediators.

2.1 Importance of Research into the Alternative Redox Couples

In DSC devices, upon optical excitation of the dye and subsequent electron injection into the nanocrystalline TiO_2, the redox mediator present in the electrolyte regenerates the dye. Thus, the redox couple, a very important component present in the electrolyte, is of prime importance. An efficient redox couple, when combined with an appropriate sensitizing dye, not only ensures efficient dye regeneration but also effectively transports positive charge to the catalyst-coated counter electrode. The redox potential of the electrolyte should be adjusted as close as possible to the HOMO level of the dye but should also provide sufficient driving force for quantitative dye regeneration. A comparison of HOMO levels of N719 dye and the redox levels of two highly successful redox couples; iodide/triiodide and $[Co(bpy)_3]^{2+/3+}$ are presented in the energy level diagram shown in Figure 2.1.

As explained in the previous section, dye regeneration is one of the very important mechanisms involved in DSC performance. The dye-regeneration mechanism using

the conventional iodide/triiodide electrolyte is not simple as it involves a two-electron process (as shown in Equation 1 and 2). In contrast, the redox process for cobalt (II)/(III)-based complexes is a very simple one-electron process (Equation 3) and it does not involve the disproportionation reaction shown in Equation 2 below.

$$D^+ + 2I^- \longrightarrow D + I_2^{-\bullet} \quad (1)$$

$$2I_2^{-\bullet} \longrightarrow I_3^- + I^- \quad (2)$$

$$D^+ + Co^{+2} \longrightarrow D + Co^{+3} \quad (3)$$

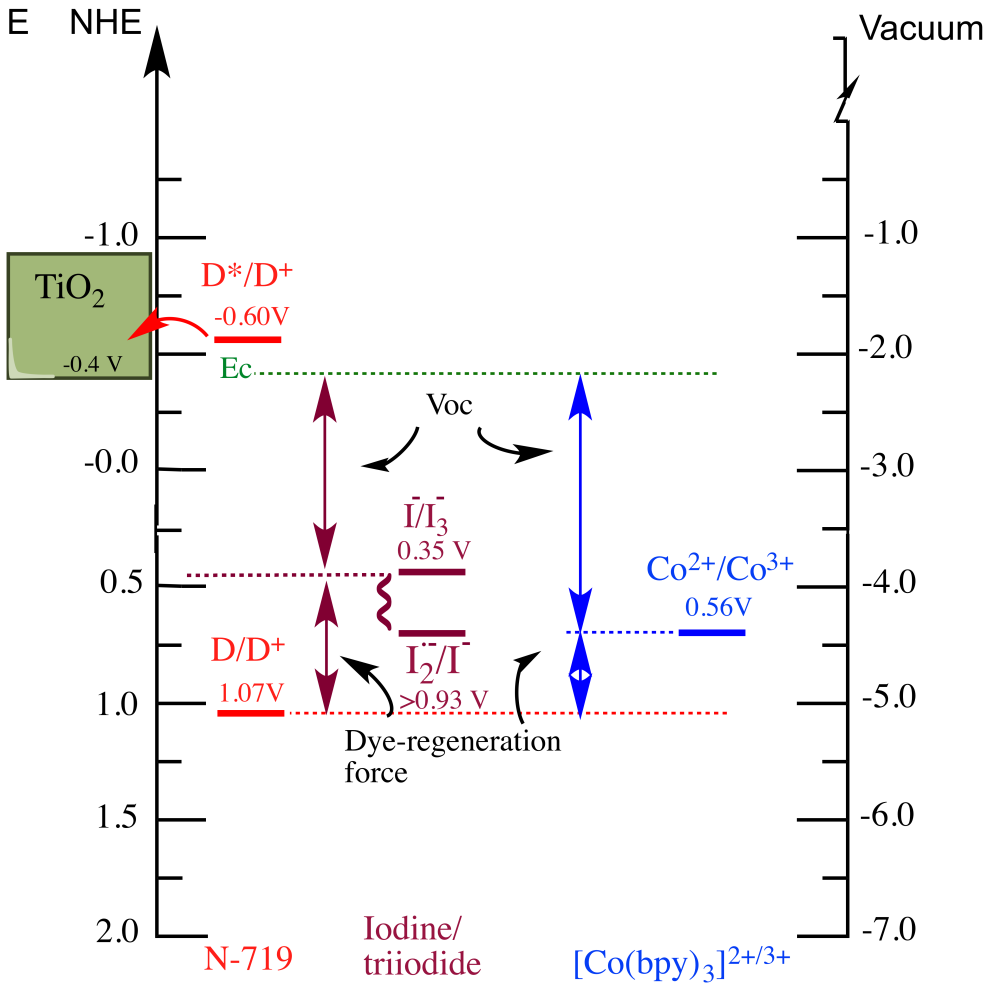

Figure 2. 1: Energy-level diagram of DSC components, approximate redox potentials of the electrolytes based on $[Co(bpy)_3]^{2+/3+}$ and classical iodide/triiodide redox couple. Data for N719 and both electrolytes are relative to the normal hydrogen electrode.

The disproportionation reaction leads to an appreciable energy loss (~ 0.4 eV in acetonitrile).[1] Thus, the careful design of an efficient redox couple is crucial to achieve the goal of high efficiency, commercially viable DSC technology.

The current-voltage (IV) characteristics of the DSCs define energy conversion efficiency, η, as given by:

$$\eta = \frac{I_{SC} \times V_{OC} \times FF}{P_{in} \times A_{cell}} \quad (4)$$

The characteristic parameters can be defined as: I_{SC} is the short circuit current, V_{OC} is the open circuit voltage, FF is the fill factor, P_{in} is the power density of the incident solar light and A_{cell} is the cell area under illumination. The above equation 4 shows that the energy conversion efficiency is directly proportional to three important parameters of a DSC (I_{SC}, V_{OC} and FF), which are dependent on the redox couple.

In 1999, Gregg and Pichot found that the open circuit potential realized in the DSC was highly correlated to the electrochemical potential of the redox couple.[2] By applying the reduced species of the three different redox systems based on iodide/triiodide, ferrocene/ferrocenium and quinone/hydroquinone redox couples they deduced important result. They found that the photoinduced chemical potential difference between the Nernst potential of the redox couple and the titania quasi-Fermi level is the photovoltage determining parameter. Their findings helped to predict the obtainable V_{OC} (open-circuit voltage) of a DSC based on a new redox couple. The advantage of alternative redox mediators was recently demonstrated by the use of the $[Co(bpy)_3]^{2+/3+}$ couple in DSCs, which achieved a record efficiency of 12.3% and V_{OC} of 965 mV.[3] Figure 2.1 shows a large potential difference between the Nernst potential of the $[Co(bpy)_3]^{2+/3+}$ redox couple and the E_C (quasi-Fermi level of titania) compared to the conventional iodide/triiodide electrolyte. This large potential difference translates to a higher V_{OC} when the $[Co(bpy)_3]^{2+/3+}$ redox couple is used.

The second very important IV-characteristic parameter, I_{SC}, also depends on the choice of the redox couple. One-electron redox process involved in dye-regeneration using alternative redox mediators, $[Co(bpy)_3]^{2+/3+}$, also offers fast dye-regeneration kinetics. As indicated in Figure 2.1, the $[Co(bpy)_3]^{2+/3+}$ redox mediator accomplishes

efficient dye-regeneration using lower electrochemical driving force as compared to the conventional iodide/triiodide electrolyte. It has been concluded that inefficient dye-regeneration leads to lower photocurrent (I_{SC}).[4] Therefore, finding a suitable redox mediator is important to not only increase V_{OC} but also to increase the I_{SC}.

In the following sections, a brief overview of different types of redox mediators used previously in DSC research is presented, broadly divided into two major classes: organic and inorganic redox mediators. The focus of the literature presented here is on the alternative redox couples used to ameliorate the performance and stability of liquid electrolyte-based DSCs in order to avoid corrosion issues associated with the classical iodide/triiodide redox couple.

2.2 Organic redox mediators

Organic redox mediators using one-electron and two-electron transfer reactions are discussed in the following sections. With the benefit of advances in synthetic organic chemistry, organic redox couples can be easily modified in order to tune the redox potential of the electrolyte for optimum performance in the DSCs.

2.2.1 Nitroxide radical based complexes

Nitronyl nitroxides are recognized as the most stable and robust organic radicals and have been widely explored.[5] 2,2,6,6-tetramethyl-1-piperidinylolxy (TEMPO) is an organic redox couple based on the nitroxide functional group. In 2008, the use of TEMPO/TEMPO$^+$ as a redox mediator resulted in an overall efficiency of 5% under simulated sunlight, AM1.5G, 1,000 W/m^2.[6a] This exciting result was obtained with the dye D149 (shown in Figure 2.3). However, TEMPO/TEMPO$^+$ redox mediator-based DSCs suffer from higher rates of recombination, which has been shown to be a general problem associated with all one-electron redox systems.[7] Poor stability of the devices arising from the high reactivity of the nitroxide radical towards dye functional groups like thiophene is also regarded as a major issue. Nishide *et al.* (2010) studied the effect of the different functional groups attached to the *4*-position of the TEMPO ring.[6b] They demonstrated that the redox potential could be fine-tuned by the substitution of *4*-H of the TEMPO ring with negatively

Table 2.1: Chemical structures of the nitroxide redox couples

Oxidized and reduced species	Common name with relevant oxidation state	Redox potential	Ref.
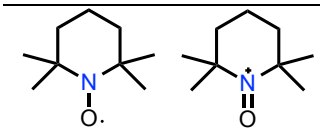	Tempo/Tempo$^+$	0.80 V vs. NHE	6a
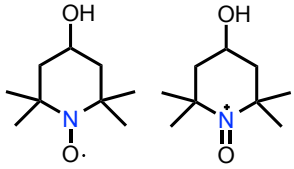	4-OH-Tempo/ 4-OH-Tempo$^+$	0.70 V vs. Ag/AgCl	6b
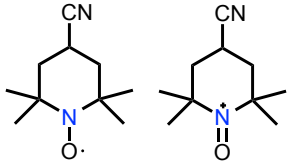	4-CN-Tempo/ 4-CN-Tempo$^+$	0.86 V vs. Ag/AgCl	6b
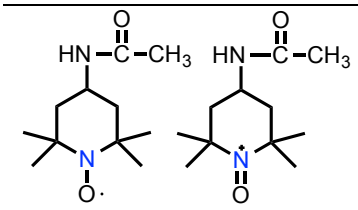	4-ACE-Tempo/ 4-ACE-Tempo$^+$	0.76 V vs. Ag/AgCl	6b
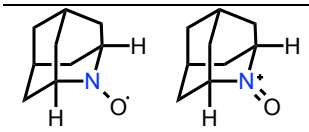	AZA/AZA$^+$	0.63 V vs. Ag/AgCl	6c

charged substituents. However, the device efficiencies were poor and recombination reactions were not effectively reduced using the new derivatives. In a recent publication (2012), Coote *et al.* have established a structure-activity relationship for five membered and six membered nitroxide bearing rings. They have predicted a number of structures suitable for their application as redox mediators in DSCs.[6d] Very soon after this publication one of the predicted structures was used as alternative redox mediators for DSCs. The nitroxide used in this research is 2-Azaadamantan-*N*-oxyl (AZA), a compound with 60 mV lower redox potential than TEMPO (690 mV vs. Ag/AgCl).[6c] The AZA/AZA$^+$ based redox mediator exhibits

10 times higher self-exchange reaction rates due to the rigid and symmetric adamantane framework than TEMPO and showed an impressive efficiency of 8.6% under full sun illumination conditions using a dye cocktail D205/D131.[6c]

2.2.2 Disulfide/thiourea and disulfide/thiolate based-redox shuttles

In 2010, Meng *et al.* investigated tetramethylthiourea (TMTU) and its dimer tetramethylformaminium disulfide dication ($TMFDS^{+2}$) as a redox couple in DSCs.[8] This colorless, low cost and non-corrosive redox system worked better in combination with carbon-based counter electrodes. An efficiency of 3.1 % was realized using the N3 sensitizer.

Wang *et al.* have reported a T_2/T^- (disulfide/thiolate) redox couple that led to a DSC efficiency of 6.4% under standard illumination test conditions.[9] Being non-corrosive towards other components in the cell is an obvious advantage of this redox couple, but it involves cleavage/formation of a disulfide bond, leading to slow reaction kinetics. The two-electron concerted electrochemical reaction showed a very reasonable overall efficiency of 6.4 %.

Sun and his co-workers developed a new redox system based on another type of disulfide/thiolate-based organic redox couple.[10] This new redox system contained $McMT^-$ (structures can be found in Table 2.2) as the thiolate form and its dimer BMT as the disulfide component. An efficiency of 4.0 % was achieved using an organic dye, TH305, and platinized counter electrode, under full sun illumination conditions. In their next publication, Sun *et al.* published a series of different disulfide/thiolate-based organic redox couples using PEDOT as counter electrodes catalyst.[11] This series consisted of $McMT^-$/BMT, $McMO^-$/BMO, $McPO^-$/BPO, $McBT^-$/BBT AND $McBO^-$/BBO (structures can be found in Table 2.2). The counter electrode catalyst, PEDOT, showed better performance with $McMT^-$/BMT. An efficiency of 6 % was achieved using a PEDOT counter electrode, mainly due to higher FF compared to the previously published 4 % efficiency with a platinized FTO counter electrode. These new redox couples, however, did not outperform the $McMT^-$/BMT redox couple.

Recently, Cheng *et al.* have reported the use of DMPIC/DMPIDC (L-cysteine/L-cystine) as an organic redox couple with a high efficiency of 7.7 % (structures shown in the table 2.2).[12] The inter-conversion of the redox couples follows the S-S bond making and breaking process.

Table 2.2: Molecular structures of the redox couples involving S-S bond making and bond breaking process

Oxidized and reduced species	Common name with relevant oxidation state	Redox potential	Ref.
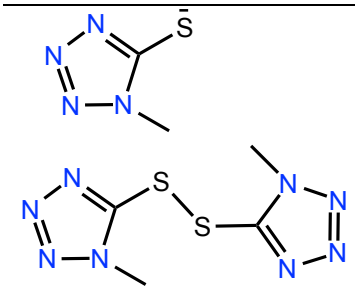	T^-/ T2	485mV vs. NHE	9
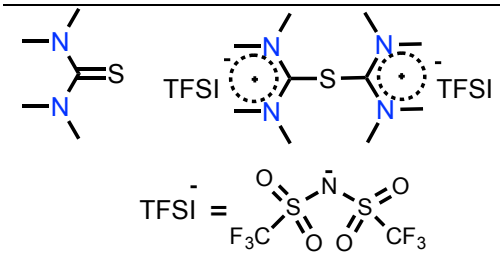	TMTU/ $TMFDS^{+2}$	303 mV vs. SCE	8
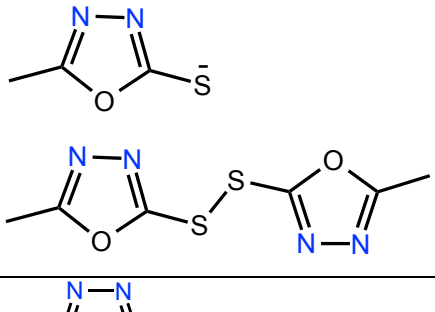	McMT/ BMT	150 mV vs. NHE	10
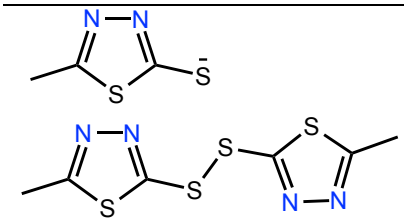	$McMO^-$/ BMO	250 mV vs. NHE	11

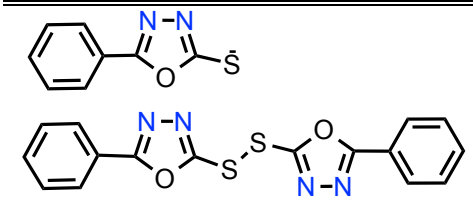	McPO^{-}/ BPO	370 mV vs. NHE	11
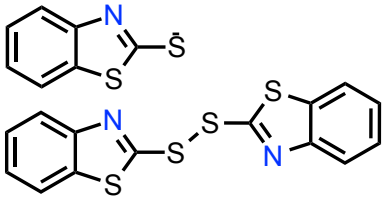	McBT^{-}/ BBT	10 mV vs. NHE	11
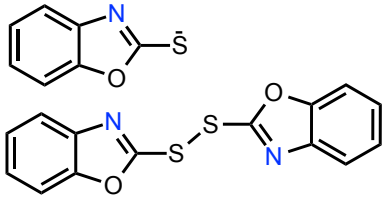	McBO^{-}/ BBO	290 mv vs. NHE	11
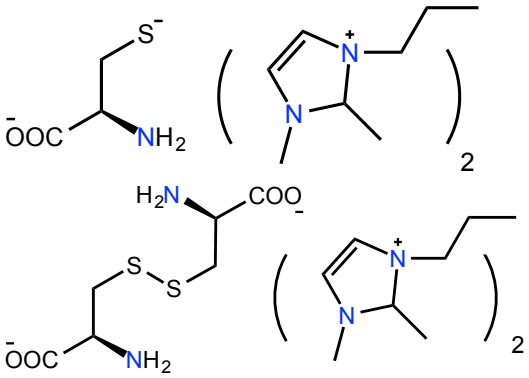	DMPIC/ DMPIDC	453 mV vs. NHE	12

2.2.3 Tetrathiafulvalene (TTF) based-redox shuttles

Tetrathiafulvalene has long been known for its characteristic charge transfer properties. Zhang studied its use as an alternative redox mediator with limited success in his PhD thesis.[13] Two more oxidation states for TTF and its derivatives can be accessed and used to make a redox couple, depending on the HOMO level of dye. The corresponding structures and possible oxidation states are explained in the following table.

Table 2.3: Redox couples based on tetrathiafulvalene moiety

Reduced/oxidized species	Common name with relevant oxidation state	Redox potential	Ref.
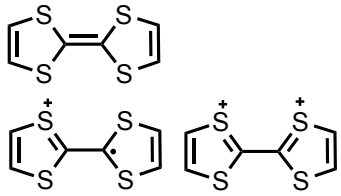	TTF/TTF^{+}	560 mV vs. NHE	14
	TTF^{+}/TTF^{2+}	910 mV vs. NHE	
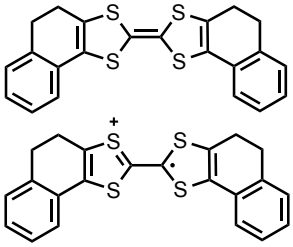	BDHNTTF/ BDHNTTF^{+}	-80 mV vs. Fc/Fc^{+}	13,14
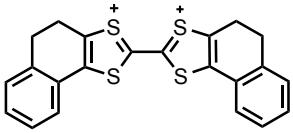	BDHNTTF^{+}/ BDHNTTF^{2+}	260 mV vs. Fc/Fc^{+}	

In 2012, Yu *et al.* further studied the application of TTF in DSCs as a redox mediator using dye D35 as sensitizer. An efficiency of only 1.24 % was realized under full sun illumination conditions, mainly due to competitive light absorption by the TTF electrolyte solution compared to the iodide/triiodide electrolyte. Factors like fast recombination reactions, mass transport limitations and inefficient electron transfer at the counter electrode were identified as efficiency-limiting issues in the detailed analysis.[14]

Replacing the liquid electrolyte with a solid state hole-conducting material results in the development of solid-state DSCs. Small organic molecules have also been used as hole-conducting materials to transport the charge across the working electrode and counter electrode in solid-state DSCs. Spiro-OMeTAD has proven to be the best for this purpose but other materials have also been investigated.[15] A new generation of DSCs has just been developed and have shown very promising results. This approach uses the same principle of a solid-state DSC, but differs in terms of

the sensitizer, which is an inorganic perovskite material. Spiro-OMeTAD is exclusively used as hole-conducting material in these kinds of solar cells.[16]

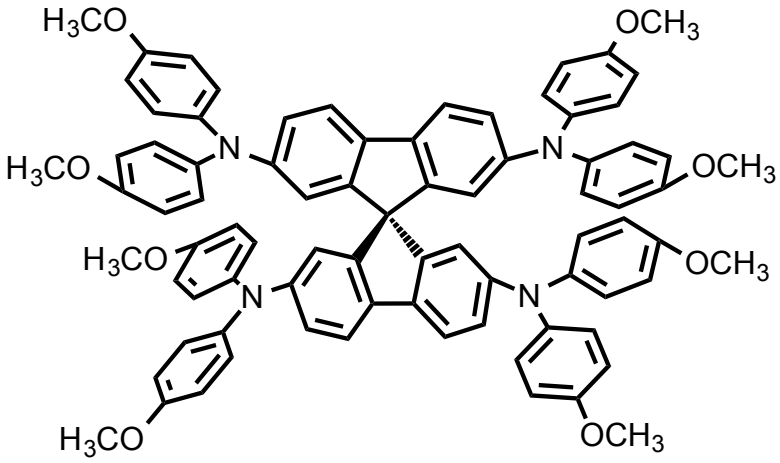

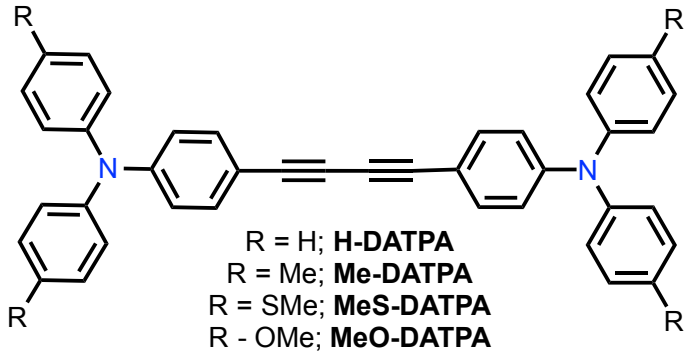

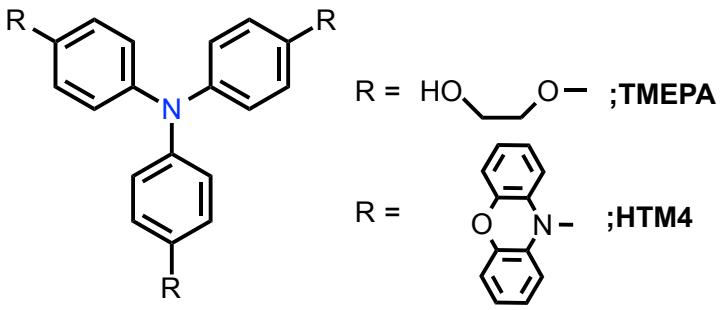

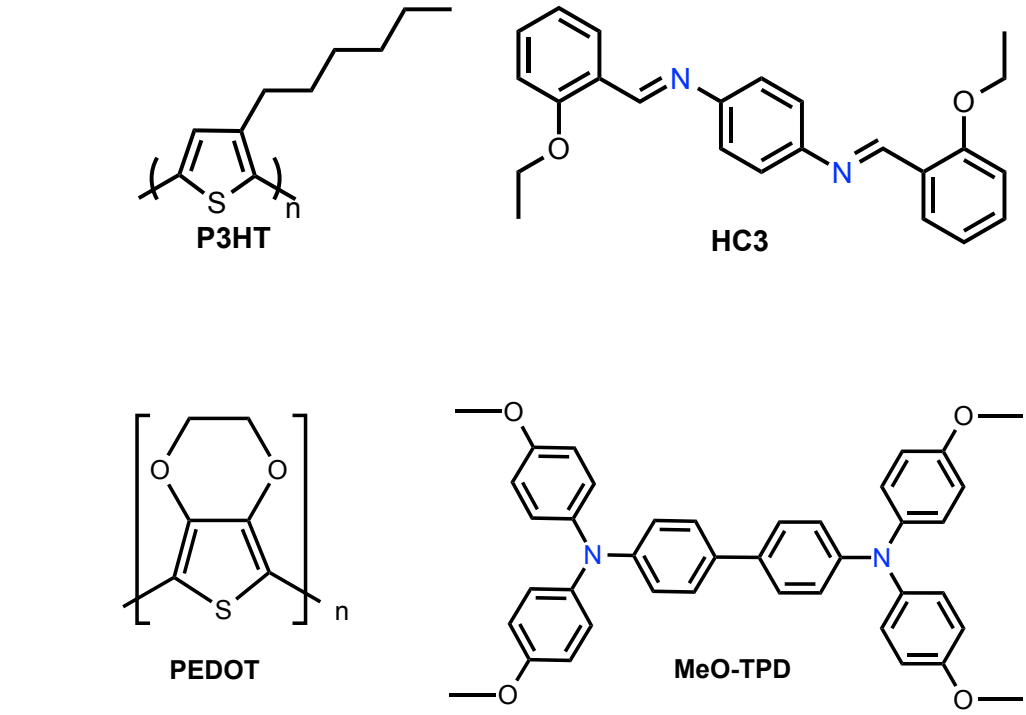

Figure 2.2: Molecular structures of the hole conducting materials used in solid state DSCs

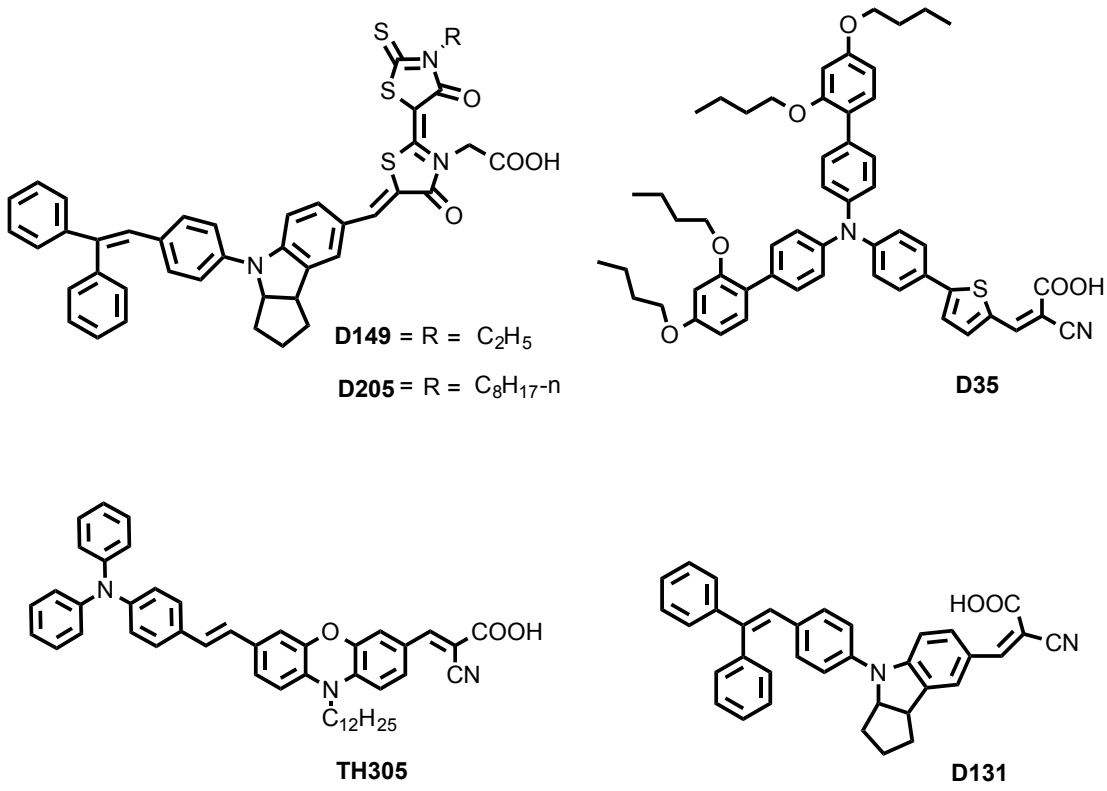

Figure 2.3: Organic dyes mostly used with organic redox couples

2.3 Inorganic redox mediators

The inorganic redox mediators include halogens such as iodine and bromine as well as organometallic and coordination metal complexes. Fine-tuning the redox potential of the redox couple cannot be achieved using the halogen and pseudohalogen redox shuttles, as very little structural modification is possible. However, the use of organometallic and coordination metal complexes offers the opportunity of fine-tuning the redox potential by the modification of the donor atoms (number and type) and the organic scaffold supporting the atoms coordinated to the metal center. This characteristic feature of the organometallic and coordination metal complexes opens up new avenues of research focusing not only on synthesis of new redox mediators but also the new sensitizer dyes which best match the potential of the redox mediators. The development of new dyes custom-designed for particular redox couples is also discussed.

2.3.1 Halogen and Pseudohalogen redox shuttles

The working principle, merits and demerits of I^-/I_3^- based electrolyte were described in the previous chapter. In the search for an alternative redox couple to I^-/I_3^-, other halogen-based redox couples like bromine have also been investigated. Higher V_{OC} have been achieved due to the large energy gap between the conduction band level of the TiO_2 and the Br^-/Br_3^- redox potential,[17]as compared to I^-/I_3^-, and promising DSC results were obtained. It was realized that Br^-/Br_3^- based electrolyte are suitable to achieve higher $V_{OC,}$ provided the sensitizer dye has a more positive potential than that of Br^-/Br_3^- (1.09 V vs. NHE) for efficient dye regeneration. A dye, Eosin Y, with more positive redox potential (1.15 V vs. NHE) than the redox potential of Br^-/Br_3^- has been shown to produce higher open-circuit voltage (0.81 V) and higher conversion efficiency, η (2.6 %) than the I^-/I_3^- based electrolyte system showing an open circuit voltage of only 0.45 V and conversion efficiency of 1.7 %.[18] However, comparatively lower IPCE values were observed for devices made using Br^-/Br_3^- as compared to I^-/I_3^-, mainly due to the lower electrochemical driving force (0.06 eV) for dye regeneration.

In 2009, Sun *et al.* designed two carbazole dyes, TC306 and TC301, having HOMO levels with further positive values, 1.38 and 1.59 V vs. NHE, respectively.[19] Very

promising efficiencies (5.2 % and 3.7 %) and higher open-circuit voltages (0.94 V and 1.16 V) were obtained by the DSCs made using TC306 and TC301, respectively, along with the Br^-/Br_3^- electrolyte system under full sun illumination conditions. Higher electrochemical driving forces of 0.29 and 0.50 eV for dye regeneration using TC306 and TC301, respectively, reflected superior overall efficiency compared to Eosin Y. In 2010, a series of organic dyes TC301-TC310 was investigated for their performance in DSCs using Br^-/Br_3^- redox couples with varying concentrations of lithium salt. Higher concentrations of lithium salt not only broadened the absorption spectra of the dyes but also suppressed electron recombination reactions.[20]

Mixed halogens or interhalogens redox systems have also been used as redox couples in the DSC electrolytes. A redox system based on IBr_2^- and the I_2Br^- has been studied in different solvent systems and ionic liquids using N3 dye, as sensitizer.[21] Conversion efficiencies of 6.4 % have been achieved under full sun illumination conditions. However, due to the complex equilibria established between different concentrations of halogens involved in the redox process, this electrolyte system is very difficult to fully characterize. However, a benefit of using interhalogen ionic liquids as compared to corresponding iodides is the higher viscosities associated with interhalogen systems, which is advantageous feature for ionic liquid based electrolytes.

The feasibility of using psuedohalogens as alternative redox couples has also been explored. The redox potential of $SeCN^-/(SeCN)_2^-$ and $SCN^-/(SCN)_2^-$ couples has been determined to be 0.43V and 0.19 V (vs. NHE) more positive than the redox potential of the I^-/I_3^-, respectively.[22-23] On the positive side, these redox couples are noncorrosive towards most metals that are typically used to form charge collector grids. Owing to the fact that some of these redox couples have a more positive redox potential than I^-/I_3^-, an increased V_{OC} should be expected, but an increase in V_{OC} was not necessarily found, primarily due to the fast recombination kinetics associated with the new redox couples.[23a] In 2004, Grätzel *et al.* used SeCN as redox mediator in ionic liquid electrolyte (1-ethyl-3methylimidazolium thiocyanate) and achieved

record efficiencies of 7.5-8.3%.[23b] However, good stability of the solar cells made using this electrolyte system could not be achieved.

2.3.2 Transition metal based-redox couples

Only four transition metals i.e. iron, cobalt, nickel and copper have been used to synthesize DSC redox mediators. In general, transition metals form complexes in more have more than one oxidation state, which is ideal for DSC redox mediator development. The following table shows common oxidation states and the corresponding number of d-electrons for the metals of interest in this study.

Table 2.4: Oxidation states of the transition metals commonly applied in the synthesis of redox couples for DSCs

Common oxidation states	**1+**	**2+**	**3+**
Iron (Fe)	×	d^6	d^5
Cobalt (Co)	×	d^7	d^6
Nickel (Ni)	×	d^8	×
Copper (Cu)	d^{10}	d^9	×

The metal cations forms of these metals behave as Lewis acids and form coordination complexes with ligands, which act as Lewis bases. Very common examples of ligands are ammonia (NH_3) and water (H_2O), both coordinating through a pair of nonbonding electrons. These ligands are called monodentate ligands because they occupy a single coordination site and six ligands surround the metal ion in a complex with octahedral geometry (the coordination number can vary from as little as 1 to 16, but is commonly found in the 2-6 range). With the advances in synthetic organic chemistry, ligands with varying denticity (typically1-6 donor atoms) and functional groups can be synthesized, so that the coordination sphere and geometry of the metal center can essentially controlled. Binding of the ligand to the metal center imparts characteristic properties to the metal complex, including the geometry of the complex, color, redox behavior, magnetic properties and solubility. In the next sections, Fe, Ni, Cu and Co complexes used as redox couples in DSCs

are discussed. Initially, metal complexes were selected keeping in mind properties like redox potential, solubility and color. Subsequently, more elaborate ligands have ben applied to better fine-tune the properties of the redox couples. The engineering of custom-synthesized organic and organometallic dyes particularly designed to operate with one-electron transfer redox mediators is also discussed.

2.3.2.1 Iron based redox couples

Ferrocene/ferrocenium (Fc/Fc^+) is recommended by IUPAC as a reference redox couple due to its well-defined and well-understood redox chemistry. Early attempts to incorporate this redox couple into DSCs have met with little success.[24] Our laboratory has reported energy conversion efficiencies of 7.5% (simulated sunlight, AM1.5, 1,000 W/m^2) for DSCs using a Fc/Fc^+ single electron redox couple with a metal-free organic donor-acceptor sensitizer (Carbz-PAHTDTT).[42] The judicious design of this dye makes it special due to its long spacer and bulky donor units, helping to restrict the charge recombination from titania to ferrocenium. These Fc/Fc^+ redox couple-based devices exceed the efficiency attained for devices prepared using I^-/I_3^- electrolytes under comparable conditions. This improved performance over the DSCs constructed with I^-/I_3^- electrolytes results from a more favourable matching of the redox potential of the Fc/Fc^+ couple with that of the new donor-acceptor sensitizer.

This study opened new opportunities for research into the use of ferrocene derivatives as redox mediators in DSCs. The commercial availability and ease of chemical modification provide the opportunity to fine-tune the redox potential of the redox couple to match the appropriate HOMO levels of the dyes and obtain optimum performance. In a recent publication by Daeneke *et al.*, a rigorous study was conducted in order to precisely identify the energy required for efficient dye-regeneration. A combination of six carbazole dyes and nine Fc-derivatives was used to afford 54 different driving-force conditions. A driving force of 20-25 kJ/mol (0.20-0.25 eV) was identified to be ideal for 99.9 % theoretical dye-regeneration.[25] It is important to note here that this identified ideal driving force for efficient dye-regeneration is for Fc and Fc-derivatives and not necessarily applicable for other redox couples. In the following section on cobalt(II)/(III)-based redox couples

results by the Hagfeldt group are reported which identify a higher energy requirement for efficient dye-regeneration using cobalt(II)/(III)-based redox couples. Dimethyl (dm) and dimethoxy (dMeO) derivatives of 2,2'-bipyridine ligand bound to iron(II)/(III) metal centre ($[Fe(dmbpy)_3]^{2+/3+}$, $[Fe(dMeObpy)_3]^{2+/3+}$) have also been studied in combination with the cobalt(II)/(III)-based electrolyte system.[26] It was realized that this mixed electrolyte system improved the charge collection efficiency by efficient dye-regeneration and also a maximum of 65 % IPCE at 510 nm was obtained.

In 2008, an aqueous $[Fe(CN)_6]^{3-/4-}$ redox couple was used by Tachibana et al. in quantum dot sensitized solar cells. This system produced an impressive efficiency of 1.0 % emphasizing the use of compact titania layers as blocking layers to retard recombination. Daeneke *et al.* in 2012 used aqueous $[Fe(CN)_6]^{3-/4-}$ redox couples in combination with a carbazole dye MK-2 in the fabrication of DSCs, and achieved an impressive efficiency of 4.1 %. However, the devices showed poor stability under simulated solar light, attributed to the decomposition of the redox shuttle. Solid-state solar cells were fabricated using a polynuclear inorganic material, $K_4Ni^{II}[Fe^{II}(CN)_6]$/ $K_3Ni^{II}[Fe^{III}(CN)_6]$. This mixed-valent cyanometallated system along with a ruthenium dye, N3 resulted in an impressive device efficiency of 4 %.[27b]

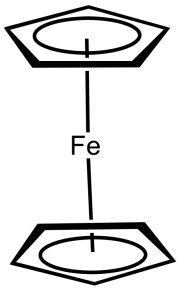

Fc-der	$E_{1/2}$ *vs.* NHE
Me_{10}-Fc	90
Et_2-Fc	510
i-Pr_2-Fc	499
Me_2-Fc	504
Et-Fc	570
Fc	630
$(Me_2Si)_2$-Fc	671
Br-Fc	800
Br_2-Fc	935

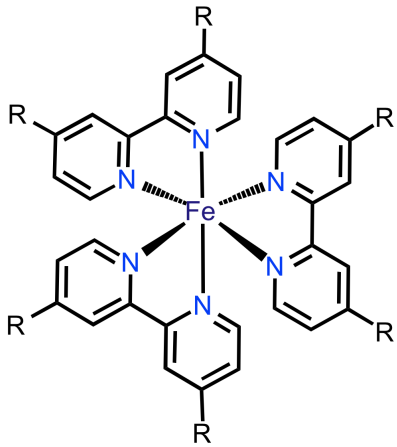

$E_{1/2}$ *vs.* SCE

R = CH_3= $[Fe(dmbpy)_2]^{2+/3+}$ = 850 mV

R = OCH_3 = $[Fe(dMeObpy)_2]^{2+/3+}$ = 750 mV

Ferricyanide redox shuttles	$E_{1/2}$
$K_4Ni^{II}[Fe^{II}(CN)_6]$/ $K_3Ni^{II}[Fe^{III}(CN)_6]$	850 *vs.* SCE
$[Fe(CN)_6]^{3-/4-}$	40 *vs.* I^-/I_3^-

Figure 2.4: Iron based redox couples with corresponding redox potentials[27]

2.3.2.2 Nickel-based redox mediators

In 2010, Hupp and co-authors introduced a novel nickel-based redox mediator, $[Ni(carbollide)_2]^{-/0}$.[28] The best efficiency with this redox shuttle was limited to 0.9 %. Later on Mirkin *et al.* demonstrated that through facile chemical functionalization of the Ni–bis(dicarbollide) moiety, the Ni^{III}/Ni^{IV} redox potential can be systematically tuned.[29] Power conversion efficiencies in the range of 0.7-2.0 % were achieved using derivatives of $[Ni(carbollide)_2]^{-/0}$.

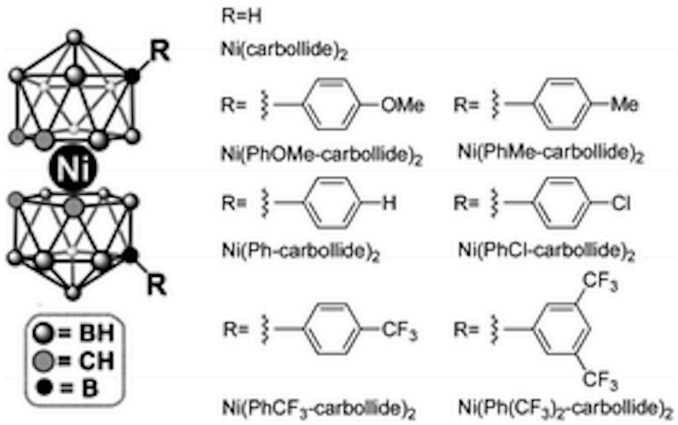

Figure 2.5: Nickel based redox couples (reproduced from 29)

2.3.2.3 Copper-based redox couples

There are only few studies on the use of copper complexes as redox shuttles in DSC electrolytes. In 2005, Hattori *et al.* studied a series of Cu complexes: $[Cu(phen)_2]^{+/2+}$ {bis(1,10-phenanthroline)copper}, $[Cu(dmp)_2]^{+/2+}$ {bis(2,9-dimethy-1,10-phenanthroline)copper}, and $[Cu(SP)(mmt)]^{-/0}$ {((-)sparteine-*N*-*N'*)(melonitriledithiolato-*S,S'*)copper}. They found that $[Cu(dmp)_2]^{+/2+}$ has a fast electron self-exchange rate in the light of Marcus theory of electron transfer, due to its small and distorted geometry. A maximum efficiency of 2.2 % was achieved for the $[Cu(dmp)_2]^{2+/+}$-based electrolytes under weak solar light irradiation of 20 mW/cm^2 intensity using N719 as sensitizer dye.[30] Recently, in 2011, Wang *et al.* applied the $[Cu(phen)_2]^{+/2+}$ redox shuttle with an organic dye, C218.[31] This dye contained alkoxy and alkyl chains in order to effectively restrict the approach of the $[Cu(phen)_2]^{2+}$ to the titania nanoparticles. This approach reduced the recombination

of photoinjected electron and resulted in an impressive conversion efficiency of 7.0 % under 100 mW/cm^2 simulated solar light intensity.

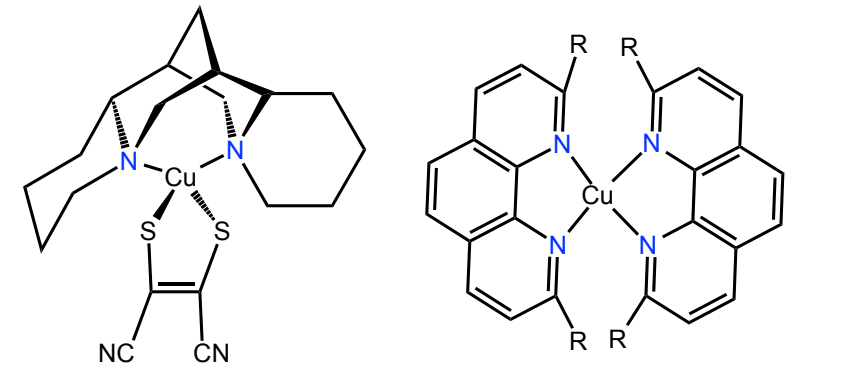

[Cu(SP)(mmt)]$^{-/0}$ = 290 mV vs SCE

R = H= [Cu(phen)$_2$]$^{+/2+}$ = -100 mV vs SCE
660 mV vs NHE
R = CH_3 = [Co(dmp)$_2$]$^{+/2+}$ = 660 mV vs SCE

Figure 2.5: Copper-based redox couples with corresponding redox potentials.

2.3.2.4 Cobalt-based complexes

Cobalt(II)/(III)-based redox mediators are to date the most extensively and successfully studied transition metal-based redox couples for DSCs. This is due to their reversible redox chemistry, favorable electrochemical redox potentials, negligible absorption and ease of synthesis. In the research literature, the most common accessible oxidation states for the cobalt-based complexes are Co^{2+} and Co^{3+}. In alternative redox couple research, these two oxidation states have been extensively used. The electrochemical redox potential associated with Co^{2+}/Co^{3+} can be tuned by varying the organic framework around the metal center.

In 2001, the first application of cobalt(II)/(III) based complexes as redox mediators in the DSC research was reported by Nusbaumer *et al.* In this investigation, the authors demonstrated that [Co(dbbip)$_2$]$^{2+/3+}$, where dbbip = 2,6-bis(1′-butylbenzimidazol-2′-yl)pyridine (structures are shown in the figure 2.6), can be successfully used as a redox shuttle in DSC research.[32] Using a ruthenium dye, Z316, they achieved an overall conversion efficiency of 2.2 % under full sun simulated conditions. This investigation opened a whole new era of research into alternative

redox mediators. One year later, Bignozzi *et al.* synthesized a range of cobalt(II)/(III) complexes based on substituted and unsubstituted bpy (2,2'-bipyridine), terpy (2,2',6',2"-terpyridine) and phen (phenanthroline) ligands (structures are shown in the figure 2.7). These redox couples were employed in DSCs sensitized using a ruthenium dye N3.[33] In this case presence of Li^+ in the electrolyte was found to improve the efficiency of DSCs up to 1.3 % using cobalt(II)/(III)-polypyridine complexes as redox couples, in contrast to the I^-/I_3^- system which also contain Li^+ as an important electrolyte additive.

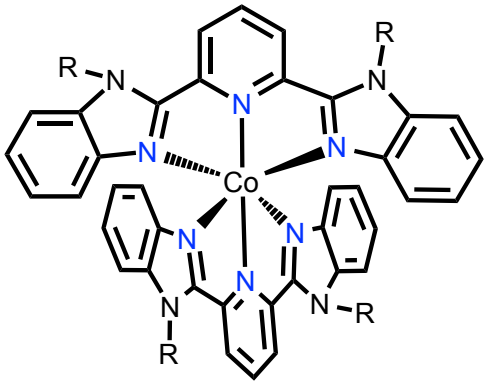

Name		***E*$_{1/2}$ (mV)**
R = CH_3	$[Co(dmbip)_2]^{2+/3+}$	440◆
R = C_4H_9	$[Co(dbbip)_2]^{2+/3+}$	600°, 385◆

Figure 2.6: First example of cobalt(II)/(III) polypyridyl-based redox couple in DSC electrolyte. Solid dot represents the redox potential vs. SCE and circle represents redox potential vs. NHE.

Nusbaumer *et al.* (2003), studied a variety of redox mediators based on bidentate and tridentate ligands including bpy, terpy, phen and dbbip. The effect of counterions on the solubility and performance of DSCs was also studied. Using a series of ruthenium dyes, they concluded that of the one-electron transfer redox mediators investigated, $[Co(dbbip)_2](ClO_4)_2$, outperformed all complexes. The favorable electrochemical properties of $[Co(dbbip)_2](ClO_4)_2$ and sterically hindered ruthenium dye, Z907, showed an efficiency of 4.2 % under full sun illumination conditions.[34] The in depth electron exchange kinetics at Pt and FTO (fluorine-doped tin oxide) electrodes were studied for $[Co(dbbip)_2]^{2+/3+}$. Slow diffusion through the electrolyte was a major performance limiting issue for this redox mediator.

Yanagida *et al.* (2005) studied the effect of different concentrations of Li^+ and *t*BP (*tert*-butylpyridine) in electrolyte systems based on $[Co(dtbbpy)_2]^{2+/3+}$, where dtbbpy = di-*tert*-butyl-2,2′-bipyridine and $[Co(abpn)]^{2+/3+}$, where abpn = propylene-1,2-bis(*o*-iminobenzylideneaminato).[35] By increasing Li^+ concentration up to 100 mM, an increase in electron lifetime and J_{SC} was observed. In the case of $[Co(abpn)]^{2+/3+}$, the addition of *t*-BP helped to reduce the reorganization energy of the cobalt(III) complex by coordinating to the cobalt and, hence, an increase in efficiency was observed. Klahr *et al.* (2009) used ALD (atomic layer deposition) technique to coat an ultrathin layer of Al_2O_3 on TiO_2 nanoparticles and used these as photoanodes for DSC construction. They reached a very important conclusion that device performance using $[Co(bpy)_3]^{2+/3+}$ redox couple was not limited by dye regeneration. Mass transport of the oxidized species of the redox couple through the mesostructured titania, however, was a performance limiting factor for the $[Co(bpy)_3]^{2+/3+}$ redox couple.[36] Thus, mass transport issues appear to be general problem associated with one-electron-transfer cobalt(II)/(III) redox mediators, leading to an increase in the charge recombination rates between the cobalt(III) complex and the TiO_2. To prevent fast recombination reactions, a co-mediator such as Fc/Fc^+, phenothiazine/phenothiazine$^+$, $[Fe(dmbpy)_3]^{2+/3+}$ or $[Fe(dMeObpy)_3]^{2+/3+}$ was used in conjunction with a relatively slow $[Co(dtbbpy)_2]^{2+/3+}$ redox couple. The charge recombination reactions were reduced by the interception of reduced species of the cobalt(II)(III) redox mediator by the fast oxidized forms of iron or phenothiazine redox couples.[26]

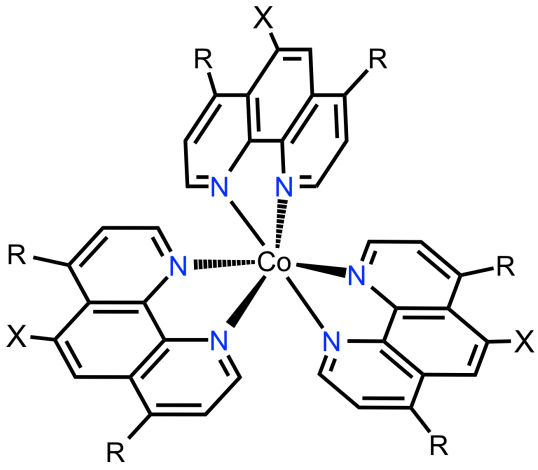

Structure			Name	$E_{1/2}$ (mV)
R = H	R' = H	X =H	$[Co(phen)_3]^{2+/3+}$	80*
R = phenyl	R = phenyl	X = H	$[Co(phen\text{-}phen)_3]^{2+/3+}$	-87*
R = H	R = H	X = Cl	$[Co(Cl\text{-}phen)_3]^{2+/3+}$	720°
R = H	R = H	X = NO_2	$[Co(NO_2\text{-}phen)_3]^{2+/3+}$	850°

Figure 2.7: Bidentated phenanthroline based cobalt(II)/(III) metal complex used as redox couples. Stars represent the redox potential vs. Ag/Ag^+ and circles represents redox potential vs. NHE.

Sun *et al.* (2009) engineered a series of metal-free, donor-pi-acceptor dyes. In the most efficient dye (D35), four insulating butyloxy chains efficiently retarded the recombination reaction. In 2010, Hagfeldt *et al.* using D35 as sensitizer, showed outstanding performance of 6.7 % with the $[Co(bpy)_3]^{2+/3+}$ based redox mediator. Use of the D35 dye helped to retard recombination reactions using hydrophobic butyloxy chains and at the same time facilitated the use of unsubstituted bpy ligand-based redox mediator, $[Co(bpy)_3]^{2+/3+}$.[37]

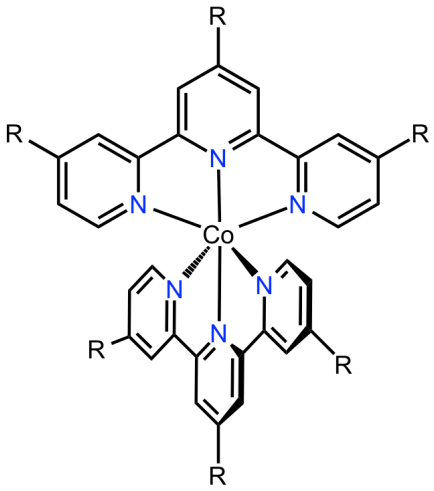

Name		$E_{1/2}$ (mV)
R = H	$[Co(terpy)_2]^{2+/3+}$	510°
R = phenyl	$[Co(te\text{-}terpy)_2]^{2+/3+}$	-103*
R = H	$[Co(ttb\text{-}terpy)_2]^{2+/3+}$	-229* 340°

Figure 2.8: Tridentate ligand, terpy based cobalt(II)/(III) metal complexes used in DSCs as redox shuttles. Stars represent the redox potential vs. Ag/Ag^* and circle represents redox potential vs. NHE.

With the successful application of D35 dye, primarily based on its structural features, new sensitizers were designed for the cobalt(II)/(III)-polypyridyl redox couples. Wang *et al.* (2012) designed a new metal-free, donor-pi-acceptor dye, C218, with the 4,4-dihexyl-4*H*-cyclopenta[1,2-b:5,4-b']dithiophene conjugated spacer.[38] Two hexyl chains were also introduced in the donor part of the dye. Energetics of dye and redox shuttle were judiciously matched to achieve an impressive efficiency of 8.3 % under full sun illumination conditions using the $[Co(phen)_3]^{2+/3+}$ based electrolyte system. The importance of the spacer features was examined using two dyes with different spacers, C228 and C229. The dye with 2,6-bis(thiophen-2-yl)- 4,4-dihexyl-4H-cyclopenta[2,1-b:3,4-b']dithiophene as the π-conjugated linker showed an impressive efficiency of 9.4 % with the $[Co(phen)_3]^{2+/3+}$ redox shuttle.[39] In a very recent publication, Grätzel *et al.* (2013) have used Co(II)/(III) redox couple based on a tridentate ligand, terpy and Cl-terpy: $[Co(terpy)_2]^{2+/3+}$, $[Co(Cl\text{-}terpy)_2]^{2+/3+}$, respectively. In combination with an organic dye Y123, the Cl-terpy-based redox couple showed an impressive efficiency of 8.7% at AM 1.5G simulated sunlight.[40]

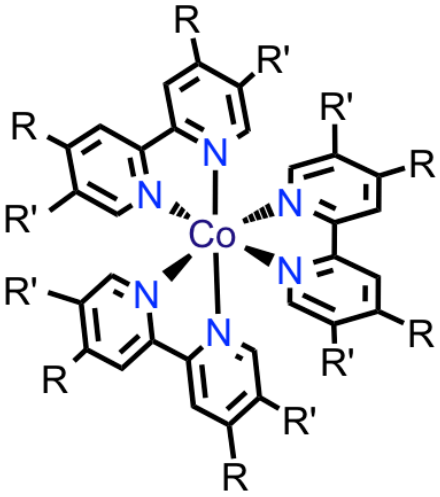

Structure		Name	$E_{1/2}$
R = H	R' = H	$[Co(bpy)_3]^{2+/3+}$	-7
R = CH_3	R = H	$[Co(4,4'\text{-dmb})_3]^{2+/3+}$	-139
R = H	R' = CH_3	$[Co(5,5'\text{-dmb})_3]^{2+/3+}$	-99
R = CH_3	R' = CH_3	$[Co(tm\text{-}bpy)_3]^{2+/3+}$	-225
R = CON(*n*-butyl)2	R' =H	$[Co(bdb\text{-}amd)_3]^{2+/3+}$	217
R = *t*-butyl	R' = H	$[Co(dtb\text{-}bpy)_3]^{2+/3+}$	-139
R = COO-*t*-butyl	R' = H	$[Co(dtb\text{-}est)_3]^{2+/3+}$	174
R = phenyl	R' = H	$[Co(dp\text{-}bpy)_3]^{2+/3+}$	-107
R = 3-pentyl	R' = H	$[Co(d3p\text{-}bpy)_3]^{2+/3+}$	-58
R = nonyl	R' = H	$[Co(dn\text{-}bpy)_3]^{2+/3+}$	-147

Figure 2.9: Electrochemical redox potentials of a series of cobalt-bipyridine complexes used to make redox couples for DSC electrolyte. The redox potentials are reported against Ag/Ag^+ reference electrode.

Grätzel and co-workers (2011) reported a novel cyclopentadithiophene-bridged donor-acceptor dye, Y123, containing four alkyloxy chains in the donor part. The spacer unit also contains two further hexyl chains, which make it ideal for retarding the recombination reactions. An impressive efficiency of 9.4 % was achieved using Y123 dye with $[Co(bpy)_3]^{2+/3+}$ redox couple. Higher V_{OC} values and distinct photovoltaic performance advantages mark Y123 as a model dye for use in one-electron transfer redox mediator research.[41] Mass transport has been regarded as an efficiency limiting issue for all Co-based polypyridyl redox shuttles. Kim *et al.*

identified that mass transport of the $[Co(bpy)_3]^{2+/3+}$ redox electrolyte is strongly dependent on porosity and pore size of mesoporous titania films. This problem was overcome by increasing the polymer content in the titania paste, which resulted in an and increased pore size and consequently an enhanced J_{SC} and overall efficiency.[42]

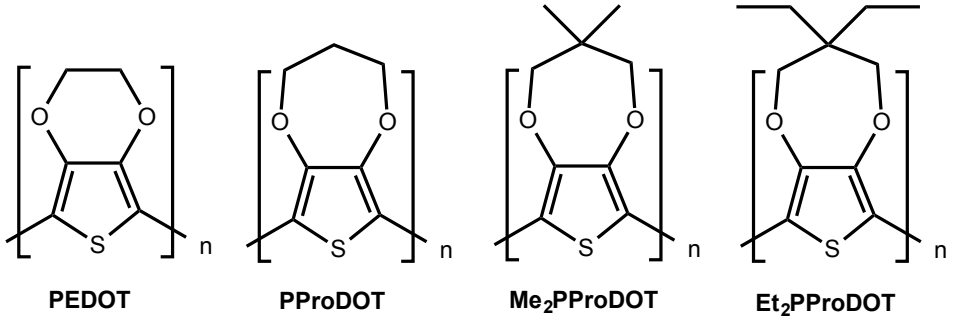

Figure 2.10: PEDOT and its derivatives used as counter electrode catalyst for DSCs

The transfer of the electrons to the oxidized species in the electrolyte at the cathode surface is also of prime importance. With the conventional iodide/triiodide electrolyte, platinized FTO cathode works the best,[43] however, it has been observed that the platinized FTO surface is a poor electrocatalyst for the cobalt(III) reduction. Thus, a number of different materials have been considered to achieve better electrocatalytic activity and electrochemical stability of the catalyst. These approaches include the use of gold NPs coated cathodes, screen-printed carbon on FTO, graphene nanoplatelets (GNP), coated FTO and conducting polymers like PEDOT and its derivatives coated FTO cathodes (the structures shown in Figure 2.10).[44] GNP coating on FTO forms thin semitransparent film and shows superior electrochemical stability under prolonged potential cycling. As photocathodes, in combination with $[Co(bpy)_3]^{2+/3+}$, it shows higher efficiency especially at full sun intensity and improved fill factor compared to conventional thermally-coated Pt photocathodes[44b]. Utilizing a new redox couple $[Co(bpy\text{-}pz)_2]^{2+/3+}$, where bpy-pz = 6-(1*H*-pyrazol-1-yl)-2,2′-bipyridine, with organic dye Y123, Grätzel *et al.* (2012) reported an efficiency of 10 % under full sun illumination conditions. The benefits of using the conducting polymer PProDOT as cathode material are evident, not only resulting in higher overall efficiency but also producing V_{OC} closer to 1V.[44a]

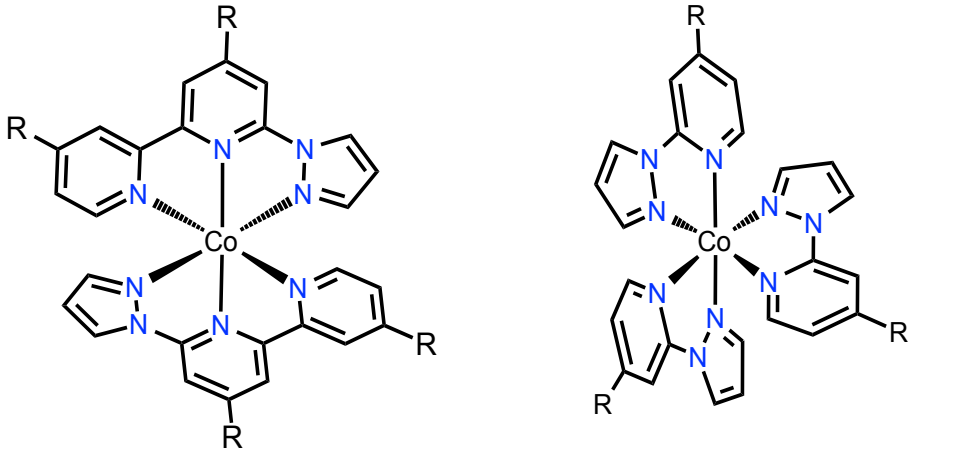

Figure 2.11: Tridentate, bpy-pz and bidentate py-pz-based redox mediators with corresponding redox potential vs. NHE

With all this available knowledge and material, Grätzel *et al.* published a seminal paper exploiting co-sensitization based on zinc-complex porphyrin dye (YD2-*o*-C8) and the Y123 organic dye. Cocktail sensitization in conjunction with the use of $[Co(bpy)_3]^{2+/3+}$ as redox couple lead to the record power conversion efficiency of 12.3 % under 100 mW cm^{-2} simulated AM 1.5 G illumination.[45]

In the earlier part of this section, we learned that Co^{2+} and Co^{3+} have $3d^7$ and $3d^6$ electronic structures, respectively. When the metal center is surrounded by ligands, the degenerated five *d* orbitals split further into a more stable set of three *d* orbitals (t_{2g}) and a less stable set of two *d* orbitals (e_g). The extent of splitting is affected by many factors, including the oxidation state of the metal and the nature of the ligand sphere. For bpy ligand, the cobalt(II) complex, is "high spin" whereas the cobalt(III) complex is "low spin" under ambient conditions of temperature and pressure (see Figure 2.13).

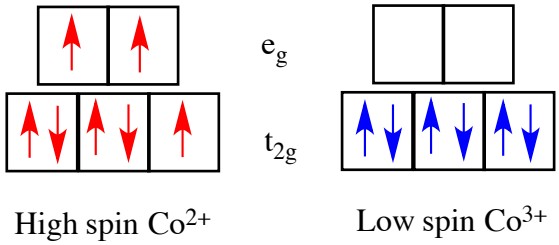

Figure 2.13: Schematic representation of the electronic distribution of *d*-orbitals in high spin state and low spin state for Co^{2+} and Co^{3+} respectively.

Conversely, in case of stronger field ligands, a larger splitting of the 5*d* orbitals is realized which results in following spin states (see Figure 2.14).

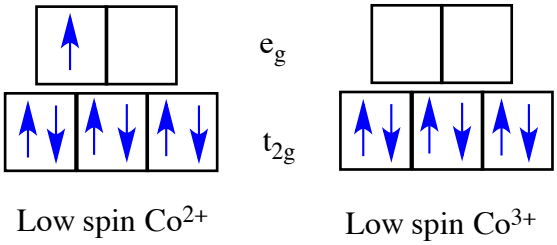

Figure 2.14: Schematic representations of the electronic distribution of d-orbitals in low spin states for Co^{2+} and Co^{3+}

All the cobalt(II)/(III) polypyridyl complexes we have studied thus far have high spin configurations for Co^{2+} complexes but always low spin configuration for Co^{3+} complexes. That is, $[Co(bpy)_3]^{2+}$ is always in the high spin state and $[Co(bpy)_3]^{3+}$ in the low spin state. Thus, an important feature of $[Co(bpy)_3]^{2+/3+}$ is that, in the process of electron self-exchange reactions, a large inner-sphere reorganization energy is involved due to the transition of $[Co(bpy)_3]^{2+}$ from high spin to low spin in $[Co(bpy)_3]^{3+}$. This feature is very beneficial in terms of retarding electron recombination reactions to the oxidized species of the redox couple. However, this large inner-sphere reorganization energy associated to the complex will also limit the dye-regeneration process.

On the basis of these observations, Hamann *et al.* used a redox couple capable of shuttling in a low-spin state in both the Co^{2+} and Co^{3+} oxidation states. They used a strong field ligand, trithiacyclononane (ttcn), to make the $[Co(ttcn)_2]^{2+/3+}$ redox couple. The photovoltaic behavior of DSCs based on $[Co(ttcn)_2]^{2+/3+}$ was compared to the archetypal $[Co(bpy)_3]^{2+/3+}$ redox shuttle using an organic and inorganic dye.

By using $[Co(ttcn)_2]^{2+/3+}$ as redox shuttles they were able to achieve quantitative dye-regeneration with a driving force of only ~ 200 mV.[46] However, using organic dye, MK2, an efficiency of 2 % was achieved.

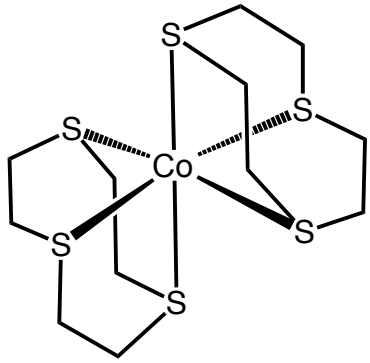

Figure 2.15: Co-trithiacyclononane comples, used to make the redox shuttle $[Co(ttcn)_2]^{2+/3+}$ which is low-spin complex in its both oxidation states, 2+ and 3+

The effect of driving force for recombination or dye-regeneration has been studied comprehensively for cobalt(II)/(III) based redox shuttles. Hagfeldt and co-authors studied this for a variety of polypyridyl-based cobalt(II)/(III) complexes. Using the $[Co(Cl\text{-}phen)_3]^{2+/3+}$ redox shuttle, a driving force of 390 mV was found to be sufficient to regenerate more than 80 % of D35 dye. Also, in the case of $[Co(NO_2\text{-}phen)_3]^{2+/3+}$/D35 system, a driving force of 260 mV was insufficient and it only regenerated 60 % of the dye molecules. In another very recent study, Hagfeldt *et al.* investigated a variety of polypyridyl cobalt complexes with potential in the range of 0.34 to 1.2 V vs. NHE. They found that DSC devices based on polypyridyl complexes with a driving force for dye-regeneration of 0.4 eV, efficiently regenerated 84 % of the D35 dye molecules.[47]

In a very recent paper Grätzel *et al.*, reported the synthesis and application of ruthenium-based dyes (3a and 3b), compatible with cobalt(II)/(III)-based electrolyte systems. Previously, Z907, a ruthenium-based dye has shown a power conversion efficiency of 6.5 % with cobalt(II)/(III)-based redox couples. In this new dye, an insulation effect caused by C_{12} alkoxy chains prevents the intimate contact of the oxidized form of the redox couple (cobalt(III) complex) with the TiO_2 surface. Using a $[Co(phen)_3]^{2+/3+}$ based redox couple, an efficiency of 8.6 % is obtained for the DSC devices sensitized using the new ruthenium-based dye.[48]

In the following, structures of the dyes mentioned in this chapter are shown.

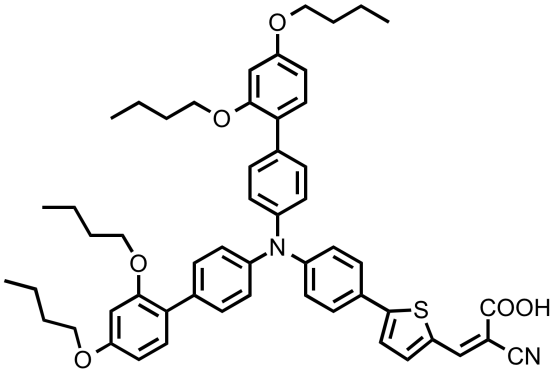

D35

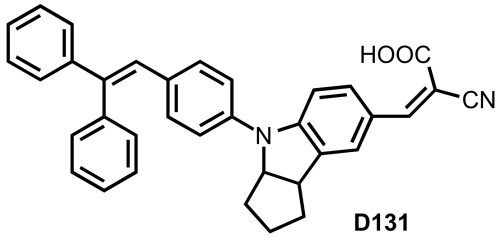

D131

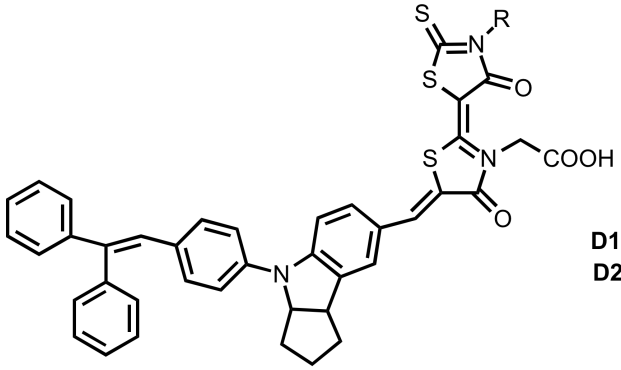

D149 = R = C_2H_5
D205 = R = C_8H_{17}-n

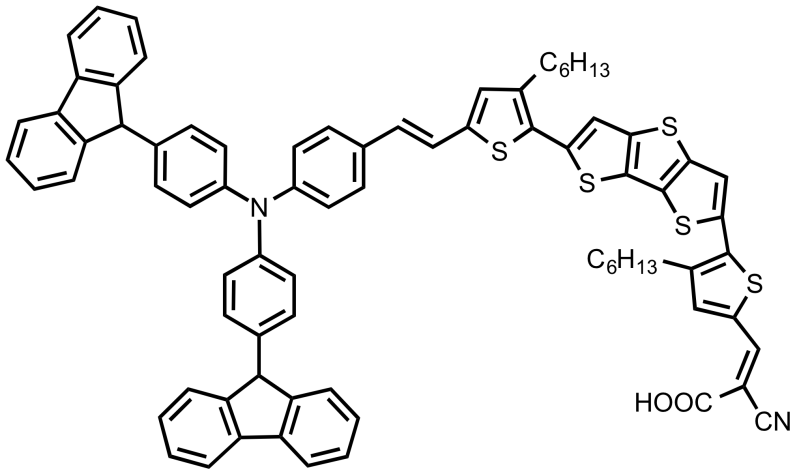

CARB-PAHTDTT

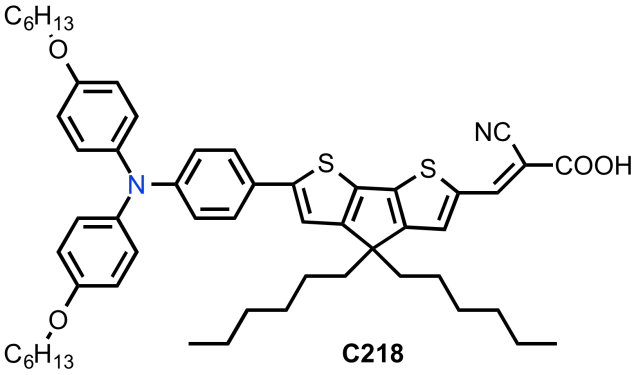

C218

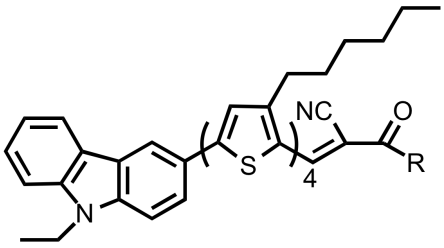

MK-2; R = OH
MKZ-35; R = NH-CH_2COOH
MKZ-36; R = NH-CH_2-CH_2COOH

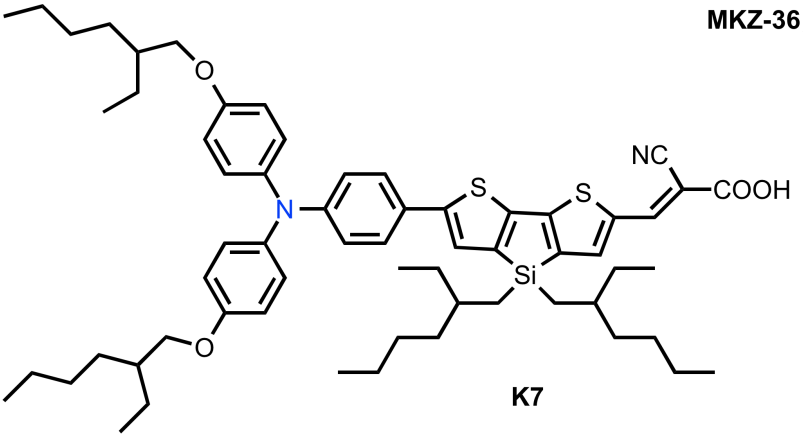

K7

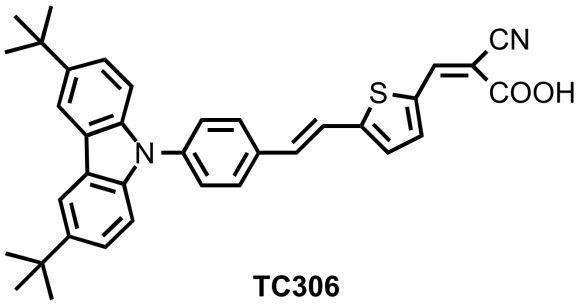

TC306

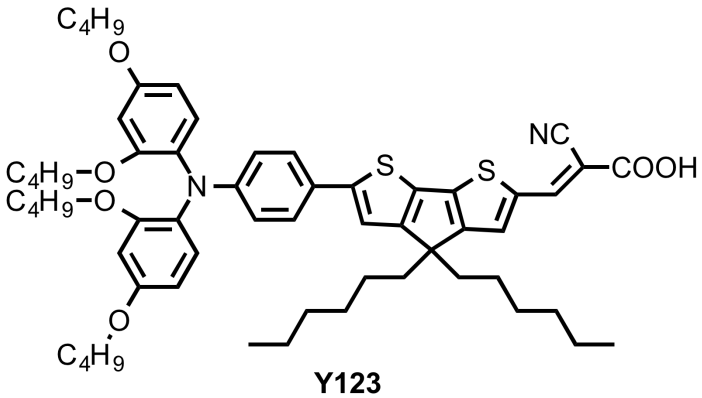

Y123

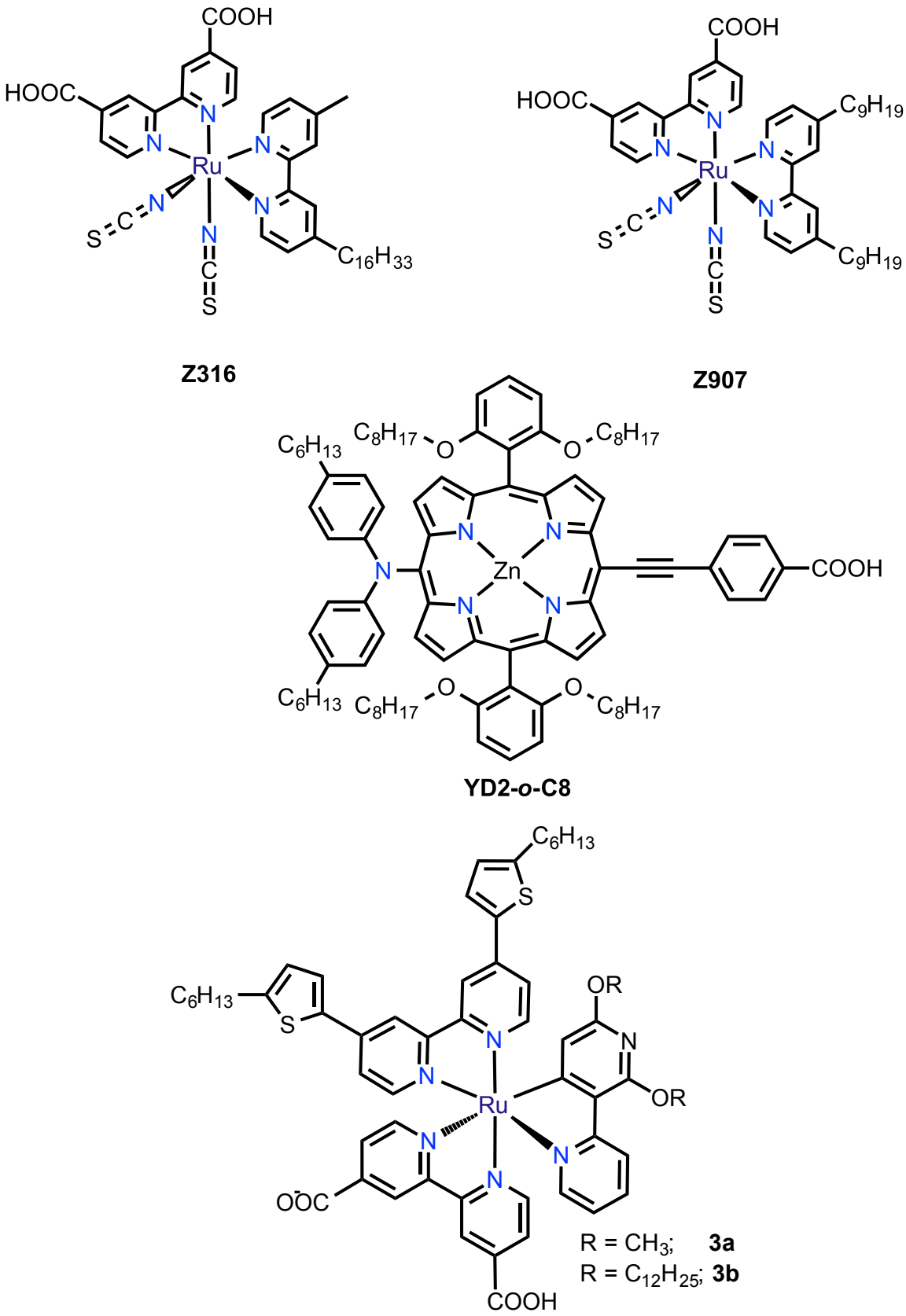

Figure 2.16: Molecular structures of sensitizers used in DSCs shown with their common names

2.4 Research Motivation

From the literature reviewed, it is clear that the dye-sensitized solar cell (DSC) is a promising, inexpensive technology that could help the world meet future energy requirements. DSCs are attractive alternatives to classical photovoltaics because they can potentially be produced at low cost via well-established commercial printing technologies. They also have the advantage of being able to operate in diffuse sunlight.

However, industrial production of large-scale DSCs is still imminent. One aspect crucial for the industrial application of DSCs is a non-corrosive and robust electrolyte system. A major drawback associated with the hitherto ubiquitous I^-/I_3^- based electrolyte is its corrosive nature. In addition, much energy is wasted due to the fixed redox potential of I^-/I_3^- and the mismatch in potential between commonly used dyes and this redox couple. Ideally, the use of a tunable redox couple would provide the opportunity to adjust the redox potential corresponding to the highest occupied molecular orbital (HOMO) level of the dye. This will successively reduce the dye-regeneration driving forces and maximize achievable overall efficiency.

A number of organic and inorganic redox couples have been explored to find the optimal redox couple to enable the industrial production of efficient and stable solar cells. Very recently, the polypyridyl ligand (L) based cobalt(II)/(III) complexes of type $[Co(L)_n]^{2+/3+}$ has received much attention. An attractive feature of these complexes, in particular, is the tunability of their structural, electronic, and redox properties through the ligand environment. The stability of metal complexes is yet another feature that can potentially be achieved by controlling the ligand architecture. Recent studies show that, for related families of polypyridyl ligands, a higher denticity results in a higher overall stability constant (β) of the complex through the chelate effect. Thus, stability is an important feature when contemplating their applications in many fields, including renewable energy research focusing on DSCs and solar light-driven hydrogen generation from water.

Most of the cobalt(II)/(III) complexes applied as redox mediators in literature contained bidentate or tridentate polypyridyl ligands and, at the start of this research, no work had been reported on the application of the cobalt complexes of high

denticity polypyridyl ligands. Thus our research into alternative redox mediators focused on the synthesis of cobalt(II)/(III) complexes with polypyridyl ligands of higher denticity (pentadentate and hexadentate) and their application as redox mediators in DSCs.

The work presented in the thesis can be summarized as follows:

- A general introduction to the energy requirement and mitigation through PV technologies is provided in the first chapter of the thesis. Detailed mechanistic description and working principle for DSC based PV technology is provided. The importance of developing alternative DSC redox mediators is also discussed.

- Chapter 2 summarizes prior work on the exploration of alternative redox mediators to the more traditional iodide/triiodide. This work is divided into two major classes: organic and inorganic redox mediators. Progress in the synthesis of sensitizer dyes along with the introduction of new redox couples is explained.

- In Chapter 3, a new approach for the optimization of the DSC redox couples is presented. This method utilizes an octahedral cobalt(II)/(III) complex, $[Co(L)(MeCN)]^{2+/3+}$, where L = pentapyridyl ligand and MeCN is a weakly binding ligand. Lewis bases, such as *t*BP (4-*tert*-butylpyridine) or NMBI (*N*-methylbenzimidazole), which are important DSC electrolyte components, are shown to displace the monodentate MeCN ligand. Thus, for the first time, the *in-situ* fine-tuning of the redox couple potential has been achieved enabling the optimization of the device energetics. This method offers fine adjustment of the redox couple through the judicious choice of the Lewis base, which then allows the selection of dyes with varying energetics. The binding of the Lewis bases to the cobalt metal center of the redox couple has been investigated using a range of techniques including single crystal X-ray crystallography. Determination of the X-ray crystal structures ($[Co(L)(tBP)]^{2+/3+}$ and $[Co(L)(NMBI)]^{2+/3+}$) in both oxidation states of the

redox couple (Co^{2+} and Co^{3+}) has allowed the estimation of the inner-sphere reorganization energy, which was found to be closely related to the dynamics of electron transfer reactions. The devices constructed using these redox couples in combination with two Lewis bases resulted in high efficiency and cell voltages.

- In Chapter 4, a new cobalt complex was synthesized using a judiciously engineered hexapyridyl ligand. The complex $[Co(L')]^{2+/3+}$, where L' = a hexapyridyl ligand, is characterized using various techniques. The redox mediator based on this complex resulted in higher DSC efficiencies than the $[Co(bpy)_3]^{2+/3+}$ couple. Most importantly, the lab scale devices made with this redox mediator exhibited much improved stability under full sun aging experiments as compared to those based on $[Co(bpy)_3]^{2+/3+}$, highlighting the potentially pivotal role played by the high denticity metal complex in the future development of DSC redox mediators.

- In addition to the synthesis of ($[Co(L)(tBP)]^{2+/3+}$ and $[Co(L)(NMBI)]^{2+/3+}$, the versatility of binding monodentate Lewis bases to the sixth coordination site of the complex $[Co(L)(MeCN)]^{2+}$ is highlighted in Chapter 5 with the characterization of $[Co(L)(F)]^{2+}$ using single crystal X-ray crystallography. This complex has one of the shortest bonds Co^{III}—F bonds reported to date. For comparison, we also report the X-ray crystal structure of the $[Co(L)(DMF)]^{3+}$ formed by oxidation of $[Co(L)(MeCN)]^{2+}$ with AgTFSI and subsequent reaction with DMF. Chapter 5 of the thesis describes the synthesis and characterization of these two complexes; their evaluation as DSC redox couple will be carried out in future.

2.5 References (chapter 2)

1. Boschloo, G.; Gibson, E. A.; Hagfeldt, A., Photomodulated Voltammetry of Iodide/Triiodide Redox Electrolytes and Its Relevance to Dye-Sensitized Solar Cells. *J. Phys. Chem. Lett.* **2011,** *2*, 3016–3020.

2. Pichot, F.; Gregg, B. A., The Photovoltage-Determining Mechanism in Dye-Sensitized Solar Cells. *J. Phys. Chem. B* **1999,** *104*, 6-10.

3. Yella, A.; Lee, H. W.; Tsao, H. N.; Yi, C. Y.; Chandiran, A. K.; Nazeeruddin, M. K.; Diau, E. W. G.; Yeh, C. Y.; Zakeeruddin, S. M.; Grätzel, M., Porphyrin-Sensitized Solar Cells with Cobalt (II/III)-Based Redox Electrolyte Exceed 12% Efficiency. *Science* **2011**, *334*, 629- 634.

4. a) Daeneke, T.; Attila, T.; Mozer, J., Uemura, Y.; Makuta, S.; Fekete, M.; Tachibana, Y.; Koumura, N.; Bach, U.; Spiccia, L., Dye Regeneration Kinetics in Dye-Sensitized Solar Cells. *J. Am. Chem. Soc.* **2012**, *134,* 16925-16928.; b) Daeneke, T.; Mozer, A. J.; Kwon, T-H.; Duffy, N. W.; Holmes, A. B.; Bach, U.; Spiccia, L., Dye Regeneration and Charge Recombination in Dye-Sensitized Solar Cells with Ferrocene Derivatives as Redox Mediators. *Energy Environ. Sci***. 2012**, *5*, 7090-7099. c) Mozer, A. J.; Panda, D. K.; Gambhir, S.; Winther-Jensen, B.; Wallace, G. G., Microsecond Dye Regeneration Kinetics in Efficient Solid State Dye-Sensitized Solar Cells Using a Photoelectrochemically Deposited PEDOT Hole Conductor. *J. Am. Chem. Soc.* **2010**, *132,* 9543-9545.

5. a) Caneschi, D. Gatteschi and P. Rey, The Chemistry and Magnetic Properties of Metal Nitronyl Nitroxide Complexes. *Prog. Inorg. Chem.* **1991**, *39*, 331-429. b) Keana, J. F. W., Newer Aspects of the Synthesis and Chemistry of Nitroxide Spin Labels. *Chem. Rev.* **1978**, *78*, 37-64. c) Veciana, J.; Cirujeda, J.; Novoa, J.; Deumal, M., Magnetic Properties of Organic Materials. Marcel-Dekker, New York (NY), **1999**, p: 573ff.

6. a) Zhang, Z.; Chen, P.; Murakami, T. N.; Zakeeruddin, S. M.; Grätzel, M., The 2,2,6,6-Tetramethyl-1-piperidinyloxy Radical: An Efficient, Iodine-Free Redox Mediator for Dye-Sensitized Solar Cells. *Adv. Funct. Mater.* **2008,** *18*, 341-346. b) Kato, F.; Hayashi, N.; Murakami, T.; Okumura, C.; Oyaizu, K.; Nishide, H., Nitroxide Radicals for Highly Efficient Redox Mediation in Dye-sensitized Solar Cells. *Chem. Lett.* **2010**, *39*, 464–465. c) Kato, F.; Kikuchi, A.; Okuyama, T.; Oyaizu, K.; Nishide, H., Nitroxide Radicals as Highly Reactive Redox Mediators in Dye-Sensitized Solar Cells. *Angew. Chem. Int. Ed.* **2012**, *51*, 10177-10180. d) Gryn'ova, G.; Barakat, J. M.; Blinco, J. P.; Bottle, S. E.; Coote, M. L., Computational Design of Cyclic Nitroxides as Efficient Redox Mediators for Dye-Sensitized Solar Cells. *Chem. Eur. J.* **2012**, *18*, 7582-7593. e) Zhang, S.; Yang, X.; Numata, Y.; Han, L., Highly Efficient Dye-Sensitized Solar Cells: Progress and Future Challenges. *Energy Environ. Sci.* **2013**, *6*, 1443-1464.

7. Hagfeldt, A.; Boschloo, G.; Sun, L.; Kloo, L.; Pettersson, H., Dye-Sensitized Solar Cells. *Chem. Rev.* **2010,** *110*, 6595-6663.

8. Li, D.; Li, H.; Luo,Y.; Li, K.; Meng, Q.; Armand, M.; Chen, L., Non-Corrosive, Non-Absorbing Organic Redox Couple for Dye-Sensitized Solar Cells. *Adv. Funct. Mater.* **2010**, *20*, 3358-3365.

9. Wang, M.; Chamberland, N.; Breau, L.; Moser, J.-E.; Humphry-Baker, R.; Marsan, B.; Zakeeruddin, S. M.; Grätzel, M., An Organic Redox Electrolyte to Rival Triiodide/iodide in Dye-sensitized Solar Cells. *Nat. Chem.* **2010**, *2*, 385-389.

10. Tian, H.; Jiang, X.; Yu, Z.; Kloo, L.; Hagfeldt, A.; Sun, L., Efficient Organic-Dye-Sensitized Solar Cells Based on an Iodine-Free Electrolyte. *Angew. Chem. Int. Ed.*, **2010**, *49*, 7328-7331.

11. Tian, H.; Yu, Z.; Hagfeldt, A; Kloo, L.; Sun, L., Organic Redox Couples and Organic Counter Electrode for Efficient Organic Dye-Sensitized Solar Cells. *J. Am. Chem. Soc.*, **2011**, *133*, 9413-9422.

12. Cheng, M.; Yang, X.; Li, S.; Wang, X.; Sun, L., Efficient Dye-Sensitized Solar Cells based on an Iodine-free Electrolyte using L-Cysteine/L-Cystine as a Redox Couple. *Energy Environ. Sci.* **2012**, *5,* 6290-6293.

13. Zhang, Z., PhD thesis, Enhancing the Open-circuit Voltage of Dye-Sensitized Solar Cells: Coadsorbents and alternative Redox Couples, EPFL, **2008**.

14. Yu, Z.; Tian, H.; Gabrielsson, E.; Boschloo, G.; Gorlov, M.; Sun, L.; Kloo, L., Tetrathiafulvalene as a One-Electron Iodine-free Organic Redox Mediator in Electrolytes for Dye-sensitized Solar Cells. *RSC Adv.* **2012**, *2,* 1083-108.

15. a) Zhu, R.; Jiang, C-Y.; Liu, B.; Ramakrishna, S. Highly Efficient Nanoporous TiO_2-Polythiophene Hybrid Solar Cells Based on Interfacial Modification Using a Metal-Free Organic Dye. *Adv. Mater.* **2009**, *21,* 994-1000. b) Kumar R. S. S.; Grancini, G.; Petrozza A.; Abrusci, A.; Snaith H. J.; Lanzani G., Effect of polymer morphology on P3HT-based solid-state dye sensitized solar cells: an ultrafast spectroscopic investigation. *Optics Express.* **2013**, *21*, 469-474. c) Johansson, E. M. J.; Pradhan, S.; Wang, E.; Unger, E. L.; Hagfeldt, A.; Andersson, M. R., Efficient Infiltration of Low Molecular Weight Polymer in Nanoporous TiO_2. **2011**, *502,* 225-230. d) Karlsson, M.; unpublished work, Dept. Chemistry, Uppsala University, Sweden, 2008-2012 (reference through Sandra Feldt's e-thesis, 2013). e) Panells, M.; Abate, A.; Hollman, D. J.; Stranks, D. S.; Bharti, V.; Gaure, J.; Moanty, D.; Cand, S.; Snaith, H. J.; Robertson, N., Diacetylene Bridged Triphenylamines as Hole Transport Materials for Solid State Dye sensitized Solar Cells. *J. Mater. Chem. A* **2013**, *1,* 6949-6960. f) Snaith, H. J; Zakeeruddin, S. M.; Wang, Q.; Pechy, P.; Grätzel, M., Dye-Sensitized Solar Cells Incorporating a "Liquid" Hole-Transporting Material, *Nano Lett.* **2006**, *6,* 2000-2003. g) Yang, L.; Xu, B.; Bi, D.; Tian, H.; Boschloo, G.; Sun, L.; Hagfeldt, A.; Johansson, E. M. J., Initial Light Soaking Treatment Enables Hole Transport Material to Outperform Spiro-OMeTAD in Solid-State Dye-Sensitized Solar Cells. *J. Am. Chem. Soc.*

2013, *135*, 7378-7385. h) Murakoshi, K.; Kogure, R.; Wada, Y.; Yanagida, S., Solid State Dye-Sensitized TiO_2 Solar Cell with Polypyrrole as Hole Transport Layer. *Chem. Lett.* **1997**, 26, 471-472. i) Saito, Y.; Fukuri, N.; Senadeera, R.; Kitamura, T.; Wada, Y.; Yanagida, S., Solid State Dye Sensitized Solar Cells using in situ Polymerized PEDOTs as Hole Conductor. *Electrochem. Commun.* **2004,** *6,* 71-74. j) Xia, J.; Masaki, N.; Lira-Cantu, M.; Kim, Y.; Jiang, K.; Yanagida, S., Influence of Doped Anions on Poly(3,4-ethylenedioxythiophene) as Hole Conductors for Iodine-Free Solid-State Dye-Sensitized Solar Cells. *J. Am. Chem. Soc.* **2008,** *130,* 1258-1263. k) Fukuri, N.; Masaki, N.; Kitamura, N.; Wada, Y.; Yanagida, S., Electron Transport Analysis for Improvement of Solid-State Dye-Sensitized Solar Cells Using Poly(3,4-ethylenedioxythiophene) as Hole Conductors. *J. Phys. Chem. B* **2006**, *110*, 25251-25258.

16. a) Lee, M. M., Teuscher, J.; Miyasaka, T.; Murakami, T. N.; Snaith, H. J., Efficient Hybrid Solar Cells based on Meso-superstructured Organometal Halide Perovskites. *Science* **2012**, *338*, 643-647. b) Ball, J. M.; Lee, M. M.; Hey, A.; Snaith, H. J., Low-temperature Processed Meso-Superstructured to Thin-film Perovskite Solar Cells. *Energy Environ. Sci.* **2013**, *6,* 1739-1743. c) Heo, J. H.; Im, S. K.; Noh, J. H.; Mandal, T. N.; Lim, C. S.; Chang, J. A. ; Lee, Y. H.; Kim, H. J., Sarkar, A.; Nazeeruddin, M. K.; Grätzel, M.; Seok, S., Efficient Inorganic–organic Hybrid Heterojunction Solar Cells containing Perovskite Compound and Polymeric Hole Conductors. *Nature Photon.* **2013**, *7*, 486-492. d) Burschka, J.; Pellet, N.; Moon, S. J.; Humphry-Baker, R.; Gao, P.; Nazeeruddin, M.; Grätzel, M., Sequential Deposition as a Route to High-performance Perovskite-sensitized Solar Cells. *Nature* **2013**, *499*, 316-319.

17. Hara, K.; Horiguchi, T.; Kinoshita, T.; Sayama, K.; Arakawa, H., Influence of Electrolytes on the Photovoltaic Performance of Organic Dye-Sensitized Nanocrystalline TiO_2 Solar Cells. *Sol. Energy Mat. Sol. Cells* **2001**, *70*, 151-161.

18. Wang, Z -S.; Sayama, K.; Sugihara, H., Efficient Eosin Y Dye-Sensitized Solar Cell Containing Br^-/Br_3^- Electrolyte. *J. Phys. Chem. B* **2005**, *109*, 22449-22455.

19. Teng, C.; Yang, X.; Yuan, C.; Li, C.; Chen, R.; Tian, H.; Li, S.; Hagfeldt, A.; Sun, L., Two Novel Carbazole Dyes for Dye-Sensitized Solar Cells with Open-Circuit Voltages up to 1 V Based on Br^-/Br_3^- Electrolytes. *Org. Lett.* **2009**, *11*, 5542-5545.

20. Teng, C.; Yang, X.; Li, S.; Cheng, M.; Hagfeldt, A.; Wu, L.-Z.; Sun, L., *Chem. Eur. J.*, **2010**, *16*, 13127-13138.

21. Gorlov, M.; Pettersson, H.; Hagfeldt, A.; Kloo, L., Electrolytes for Dye-Sensitized Solar Cells Based on Interhalogen Ionic Salts and Liquids. *Inorg. Chem.* **2007**, *46*, 3566-3575.

22. Bergeron, B. V.; Marton, A.; Oskam, G.; Meyer, G. J., Dye-Sensitized SnO_2 Electrodes with Iodide and Pseudohalide Redox Mediators. *J. Phys. Chem. B* **2004**, *109*, 937-943.

23. Wang, P.; Zakeeruddin, S. M.; Moser, J.-E.; Humphry-Baker, R.; Grätzel, M., A Solvent-Free, $SeCN^-/(SeCN)_3^-$ Based Ionic Liquid Electrolyte for High-Efficiency Dye-Sensitized Nanocrystalline Solar Cells. *J. Am. Chem. Soc.* **2004**, *126*, 7164-7165.

24. a) Gregg, B. A.; Pichot, F.; Ferrere, S.; Fields, C. L., Interfacial Recombination Processes in Dye-Sensitized Solar Cells and Methods To Passivate the Interfaces. *J. Phys. Chem. B*, **2001**, *105,* 1422-1429. b) Feldt, S. M.; Cappel, U. B.; Johansson, E. M. J.; Boschloo, G.; Hagfeldt, A., Characterization of Surface Passivation by Poly(methylsiloxane) for Dye-Sensitized Solar Cells Employing the Ferrocene Redox Couple. *J. Phys. Chem. C*, **2010**, *114*, 10551-10558. c) Hamann, T. W.; Farha, O. K.; Hupp, J. T., Outer-Sphere Redox Couples as Shuttles in Dye-Sensitized Solar Cells. Performance Enhancement Based on Photoelectrode Modification via Atomic Layer Deposition. *J. Phys. Chem. C*, **2008**, *112,* 19756-19764. d) Waita, S. M.; Aduda, B. O.; Mwabora, J. M.; Niklasson, G. A.; Granqvist, C. G.; Boschloo, G., Electrochemical characterization of TiO_2 blocking layers

prepared by reactive DC magnetron sputtering. *J. Electroanal. Chem.* **2009**, *637,* 79-83.

25. Daeneke, T.; Attila, T.; Mozer, J., Uemura, Y.; Makuta, S.; Fekete, M.; Tachibana, Y.; Koumura, N.; Bach, U.; Spiccia, L., Dye Regeneration Kinetics in Dye-Sensitized Solar Cells. *J. Am. Chem. Soc.* **2012**, *134,* 16925-16928.

26. Cazzanti, S.; Caramori, S.; Argazzi, R.; Elliott, C. M.; Bignozzi, C. A., Efficient Non-corrosive Electron-Transfer Mediator Mixtures for Dye-Sensitized Solar Cells. *J. Am. Chem. Soc.* **2006,** *128*, 9996-9997.

27. a) Caramori, S.; Husson, J.; Beley, M.; Bignozzi, C. A.; Argazzi, R.; Gros, P. C., Combination of Cobalt and Iron Polypyridine Complexes for Improving the Charge Separation and Collection in Ru(terpyridine)$_2$-Sensitised Solar Cells. *Chem. Eur. J.* 2010, **16**, 2611-2618. b) Rutkowska, I., Andrearczyk, A.; Zoladek, S.; Goral, M.; Darowicki, K.; Kulesza, P., Electrochemical characterization of Prussian blue type Nickel Hexacyanoferrate Redox Mediator for Potential Application as Charge Relay in Dye-Sensitized Solar Cells, *J. Solid State Electrochem.* **2011**, *15*, 2545-2552. c) Daeneke, Y. Uemura, Y.; Duffy, N. W.; Mozer, A. J.; Koumura, N.; Bach, N.; Spiccia, L., Aqueous Dye-Sensitized Solar Cell Electrolytes Based on the Ferricyanide–Ferrocyanide Redox Couple. *Adv. Mater.* **2012**, *24,* 1222-1225.

28. Li, T. C.; Spokoyny, A. M.; She, C.; Farha, O. K.; Mirkin, C. A.; Marks, T. J.; Hupp, J. T., Ni(III)/(IV) Bis(dicarbollide) as a Fast, Noncorrosive Redox Shuttle for Dye-Sensitized Solar Cells. *J. Am. Chem. Soc.* **2010,** *132*, 4580-4582.

29. Spokoyny, A.; Li, T.; Farha, O.; Machan, C.; She, C.; Stern, C.; Marks, T.; Hupp, J.; Mirkin, C., Electronic Tuning of Nickel-Based Bis(dicarbollide) Redox Shuttles in Dye-Sensitized Solar Cells. *Angew. Chem. Int. Ed.* **2010,** *49,* 5339-5343.

30. Hattori, S.; Wada, Y.; Yanagida, S.; Fukuzumi, S., Blue Copper Model Complexes with Distorted Tetragonal Geometry Acting as Effective Electron-Transfer Mediators in Dye-Sensitized Solar Cells. *J. Am. Chem. Soc.* **2005,** *127*, 9648-9654.

31. Bai, Y.; Yu, Q.; Cai, N.; Wang, Y.; Zhang, M.; Wang, P., High-efficiency Organic Dye-Sensitized Mesoscopic Solar Cells with a Copper Redox Shuttle. *Chem. Commun.*, **2011**, *47,* 4376-4378.

32. Nusbaumer, H.; Moser, J.-E.; Zakeeruddin, S. M.; Nazeeruddin, M. K.; Grätzel, M., Co^{II}(dbbip) Complex Rivals Tri-iodide/Iodide Redox Mediator in Dye-Sensitized Photovoltaic Cells. *J. Phys. Chem. B* **2001,** *105*, 10461-10464.

33. Sapp, S. A.; Elliott, C. M.; Contado, C.; Caramori, S.; Bignozzi, C. A., Substituted Polypyridine Complexes of Cobalt(II/III) as Efficient Electron-Transfer Mediators in Dye-Sensitized Solar Cells. *J. Am. Chem. Soc.* **2002,** *124*, 11215-11222.

34. Nusbaumer, H.; Zakeeruddin, S. M., Moser, J.-E.; Grätzel, M.; *Chem. Eur. J.* An Alternative Efficient Redox Couple for the Dye-Sensitized Solar Cell System. **2003**, *9*, 3756–3763.

35. Nakade, S.; Makimoto, Y.; Kubo, W.; Kitamura, T.; Wada, Y.; Yanagida, S., Roles of Electrolytes on Charge Recombination in Dye-Sensitized TiO_2 Solar Cells (2): The Case of Solar Cells Using Cobalt Complex Redox Couples. *J. Phys. Chem. B*, **2005**, *109*, 3488–3493.

36. Klahr, B. M.; Hamann, T. W., Performance Enhancement and Limitations of Cobalt Bipyridyl Redox Shuttles in Dye-Sensitized Solar Cells. *J. Phys. Chem. C* **2009,** *113*, 14040-14045.

37. a) Hagberg, D. P.; Jiang, X.; Gabrielsson, E.; Linder, M.; Marinado, T.; Brinck, T.; Hagfeldt, A.; Sun, L., Symmetric and Unsymmetric Donor Functionalization. Comparing Structural and Spectral Benefits of

Chromophores for Dye-Sensitized Solar Cells. *J. Mater. Chem.* **2009**, *19,* 7232-7238. b) Feldt, S. M.; E. A. Gibson, E. A.; Gabrielsson, E.; Sun, L.; Boschloo, G.; Hagfeldt, A., Design of Organic Dyes and Cobalt Polypyridine Redox Mediators for High-Efficiency Dye-Sensitized Solar Cells. *J. Am. Chem. Soc.* **2010,** *132,* 16714-16724.

38. Zhou, D.; Yu, Q.; Cai, N.; Bai, Y.; Wang, Y.; Wang, P., Efficient Organic Dye-Sensitized Thin-Film Solar Cells based on the Tris(1,10-phenanthroline)cobalt(II/III) redox shuttle. *Energy Environ. Sci.* **2011**, *4*, 2030-2034.

39. a) Bai, Y.; Zhang, J.; Zhou, D.; Wang, Y.; Zhang, M.; Wang, P., Engineering Organic Sensitizers for Iodine-Free Dye-Sensitized Solar Cells: Red-Shifted Current Response Concomitant with Attenuated Charge Recombination. *J. Am. Chem. Soc.*, **2011**, *133,* 11442-11445. b) Liu, J.; Zhang, J.; Xu, M.; Zhou, D.; Jing, X.; Wang, P., Mesoscopic Titania Solar Cells with the Tris(1,10-phenanthroline)cobalt Redox Shuttle: Uniped versus Biped Organic Dyes. *Energy Environ. Sci.* **2011**, *4,* 3021-3029.

40. Aribia, K. B.; Moehl, T.; Zakeeruddin, S. M.; Grätzel, M., Tridentate Cobalt Complexes as Alternative Redox Couples for High-efficiency Dye-Sensitized Solar Cells. *Chem. Sci***. 2013**, *4*, 454-459.

41. Tsao, H. N.; Yi, C.; Moehl, T.; Yum, J.-H.; Zakeeruddin, S. M.; Nazeeruddin, M. K.; Grätzel, M., Cyclopentadithiophene Bridged Donor–Acceptor Dyes Achieve High Power Conversion Efficiencies in Dye-Sensitized Solar Cells Based on the Tris-Cobalt Bipyridine Redox Couple. *ChemSusChem*. **2011**, *4,* 591-594.

42. Kim, H.-S.; Ko, S.-B.; Jang, I.-H.; Park, N.-G., Improvement of Mass Transport of the $[Co(bpy)_3]^{II/III}$ Redox Couple by Controlling Nanostructure of TiO_2 Films in Dye-Sensitized Solar Cells. *Chem. Commun.* **2011**, *47,* 12637-12639.

43. Chiba, Y.; Islam, A.; Watanabe, Y.; Komiya, R.; Koide, N.; Han, L., Dye-sensitized Solar Cells with Conversion Efficiency of 11.1%. *Jpn. J. Appl. Phys.* **2006**, *45*, 638-640.

44. a) Yum, J. H.; Baranoff, E.; Kessler, F.; Moehl, T.; Ahmad, S.; Bessho, T.; Marchioro, A.; Ghadiri, E.; Moser, J. E.; Nazeeruddin, M. K.; Grätzel, M. Rationally Designed Cobalt Complexes as Redox Shuttle for Dye-Sensitized Solar Cells to Exceed 1000 mV. *Nat. Commun.* **2012**, *3*, 631-639. b) Kavan, L.; Yum, J. H.; Nazeeruddin, M. K.; Grätzel, M. Graphene Nanoplatelet Cathode for Co(III/II) Mediated Dye-Sensitized Solar Cells. *ACS Nano* **2011**, *5*, 9171- 9178. c) Sapp, S. A.; Elliot, M.; Contado, C.; Caramori, S.; Bignozzi, C. A., Substituted Polypyridine Complexes of Cobalt(II/III) as Efficient Electron-Transfer Mediators in Dye-Sensitized Solar Cells. *J. Am. Chem. Soc.* **2002**, *124*, 11215-11222. d) Ghamouss, F.; Pitson, R.; Odobel, F.; Boujtita, M.; Caramori, S.; Bignozzi, C. A., Characterization of Screen Printed Carbon Counterelectrodes for Co(II)/(III) Mediated Photoelectrochemical Cells. *Electrochim. Acta* **2010**, *55*, 6517-6522. e) Ahmad, S.; Bessho, T.; Kessler, F.; Baranoff, E.; Frey, J.; Yi, C.; Grätzel, M.; Nazeeruddin, M. K., A New Generation of Platinum and Iodine Free Efficient Dye-Sensitized Solar Cells. *Phys. Chem. Chem. Phys.* **2012**, *14*, 10631-10639.

45. Yella, A.; Lee, H. W.; Tsao, H. N.; Yi, C. Y.; Chandiran, A. K.; Nazeeruddin, M. K.; Diau, E. W. G.; Yeh, C. Y.; Zakeeruddin, S. M.; Grätzel, M., Porphyrin-Sensitized Solar Cells with Cobalt (II/III)-Based Redox Electrolyte Exceed 12% Efficiency. *Science* **2011**, *334*, 629- 634.

46. Xie, Y.; Hamann, T. W., Fast Low-Spin Cobalt Complex Redox Shuttles for Dye-Sensitized Solar Cells. *J. Phys. Chem. Lett.* **2013**, *4*, 328-332.

47. Feldt, S. M.; Wang, G.; Boschloo, G.; Hagfeldt, A., Effects of Driving Forces for Recombination and Regeneration on the Photovoltaic Performance of Dye-Sensitized Solar Cells using Cobalt Polypyridine Redox Couples. *J. Phys. Chem. C.* **2011**, *115*, 21500-21507. b) Feldt, S. M.; Lohse, P. W.; Kessler, F.; Nazeeruddin, M. K.; Grätzel, M.; Boschloo, G.; Hagfeldt, A., Regeneration and Recombination Kinetics in Cobalt Polypyridine based Dye-Sensitized Solar Cells, Explained Using Marcus Theory. *Phys. Chem. Chem. Phys.* **2013**, *15,* 7087-7097.

48. Polander, L. E.; Yella, A.; Curchod, B. F. E.; Ashari A. N.; Teuscher, J.; Scopelliti, R.; Gao, P.; Mathew, S.; Moser, J.-E.; Tavernelli, I.; Rothlisberger, U.; Grätzel, M.; Nazeeruddin, M. K.; Frey, J., Towards Compatibility between Ruthenium Sensitizers and Cobalt Electrolytes in Dye-Sensitized Solar Cells. *Angew. Chem. Int. Ed.* **2013**, *125*, 8893-8897.

Chapter 3

A New Direction in Dye-Sensitized Solar Cells Redox Mediator Development: In Situ Fine-Tuning of the Cobalt(II)/(III) Redox Potential through Lewis Base Interactions

Monash University

Declaration for Thesis Chapter [3]

Declaration by candidate

In the case of Chapter [3], the nature and extent of my contribution to the work was the following:

Nature of contribution	Extent of contribution (%)
Synthesis of the Co-complexes and characterisation, fabrication of the solar cells, IV-and electrochemical data collection, results interpretation, preparation and editing of the manuscript.	65 %

The following co-authors contributed to the work. If co-authors are students at Monash University, the extent of their contribution in percentage terms must be stated:

Name	Nature of contribution	Extent of contribution (%) for student co-authors only
Jordan C. Axelson	Synthesis of the ligand and Cobalt(II) complex	N/A
Noel W. Duffy	Helping with IMVS-IMPS	N/A
Craig M. Forsyth	Helping with crystallography	N/A
Christoper J. Chang	Experimental design and editting	N/A
Jeffrey R. Long	Experimental design and editting	N/A
Leone Spiccia	Experimental design, planning, drafting and editing	N/A
Udo Bach	Experimental design, planning, drafting and editing	N/A

The undersigned hereby certify that the above declaration correctly reflects the nature and extent of the candidate's and co-authors' contributions to this work*.

Candidate's Signature	[redacted]	**Date** 30/08/2013
Main Supervisor's Signature	[redacted]	**Date** 30/08/2013

JACS
JOURNAL OF THE AMERICAN CHEMICAL SOCIETY
Article
pubs.acs.org/JACS

A New Direction in Dye-Sensitized Solar Cells Redox Mediator Development: In Situ Fine-Tuning of the Cobalt(II)/(III) Redox Potential through Lewis Base Interactions

Muhammad K. Kashif,[†] Jordan C. Axelson,[‡] Noel W. Duffy,[§] Craig M. Forsyth,[⊥] Christopher J. Chang,[¶] Jeffrey R. Long,[‡] Leone Spiccia,*[,⊥] and Udo Bach*[,†,#,&]

[†]Department of Materials Engineering, Monash University, Victoria 3800, Australia

[‡]Department of Chemistry, University of California, Berkeley, California 94720-1460, United States

[§]Commonwealth Scientific and Industrial Research Organization, Energy Technology, Clayton South, Victoria 3169, Australia

[⊥]School of Chemistry, Monash University, Victoria 3800, Australia

[¶]Department of Chemistry and the Howard Hughes Medical Institute, University of California, Berkeley, California 94720-1460, United States, and Chemical Sciences Division, Lawrence Berkeley National Laboratory, Berkeley, California, 94720, United States

[#]Commonwealth Scientific and Industrial Research Organization, Materials Science and Engineering, Clayton South, Victoria 3169, Australia

[&]Melbourne Centre for Nanofabrication, 151 Wellington Road, Clayton, Victoria 3168, Australia

Supporting Information

ABSTRACT: Dye-sensitized solar cells (DSCs) are an attractive renewable energy technology currently under intense investigation. In recent years, one area of major interest has been the exploration of alternatives to the classical iodide/triiodide redox shuttle, with particular attention focused on cobalt complexes with the general formula $[Co(L)_n]^{2+/3+}$. We introduce a new approach to designing redox mediators that involves the application of $[Co(PY5Me_2)(MeCN)]^{2+/3+}$ complexes, where $PY5Me_2$ is the pentadentate ligand, 2,6-bis(1,1-bis(2-pyridyl)ethyl)pyridine. It is shown, by X-ray crystallography, that the axial acetonitrile (MeCN) ligand can be replaced by more strongly coordinating Lewis bases (B) to give complexes with the general formula $[Co(PY5Me_2)(B)]^{2+/3+}$, where B = 4-*tert*-butylpyridine (tBP) or *N*-methylbenzimidazole (NMBI). These commonly applied DSC electrolyte components are used for the first time to fine-tune the potential of the redox couple to the requirements of the dye through coordinative interactions with the $Co^{II/III}$ centers. Application of electrolytes based on the $[Co(PY5Me_2)(NMBI)]^{2+/3+}$ complex in combination with a commercially available organic sensitizer has enabled us to attain DSC efficiencies of 8.4% and 9.2% at a simulated light intensity of 100% sun (1000 W m^{-2} AM1.5 G) and at 10% sun, respectively, higher than analogous devices applying the $[Co(bpy)_3]^{2+/3+}$ redox couple, and an open circuit voltage (V_{oc}) of almost 1.0 V at 100% sun for devices constructed with the tBP complex.

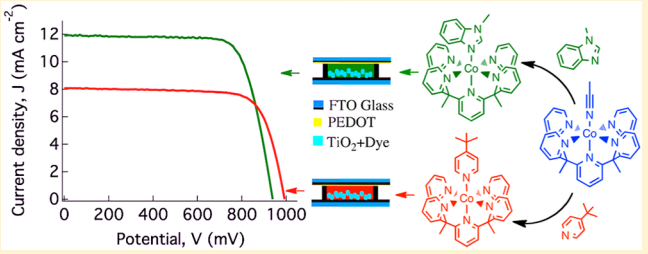

INTRODUCTION

The ever-increasing energy demands and concerns over climate change are motivating scientists to tackle present and future energy challenges. Dye-sensitized solar cells (DSCs) are considered to be a promising green technology capable of meeting our future energy demands. The unique design of DSCs offers a wide range of choices for its components, such as nanocrystalline metal oxides, photosensitizers, counter electrode materials, redox mediators, and electrolytes. In these devices, upon optical excitation of the photosensitizer and subsequent electron injection into the nanocrystalline metal oxide, the redox mediator present in the electrolyte regenerates the photosensitizer. The redox mediator not only ensures efficient dye regeneration but also transports positive charge to the catalyst-coated counter electrode. Lewis bases, such as 4-*tert*-butylpyridine (tBP) and less commonly *N*-methylbenzimidazole (NMBI), have been used as additives in the electrolyte.[1−3] The resultant increase in the efficiency of DSC performance upon addition of these Lewis bases has been attributed to the negative shift of the titania conduction band edge as well as to a reduction in the rates of interfacial charge recombination reactions.[4−9] Periodic density-functional calculations have also shown that adsorbate molecules with nitrogen donor atoms induce a negative shift of the TiO_2 conduction band edge.[10]

Until recently, iodide/triiodide (I^-/I_3^-) was the redox mediator of choice for the construction of highly efficient

Received: June 18, 2012
Published: September 11, 2012

dx.doi.org/10.1021/ja305897k | J. Am. Chem. Soc. 2012, 134, 16646−16653

DSCs. Recognition of the need to address some of the shortcomings of this redox couple, such as incompatibility with metallic conductors and a significant loss in energy arising from the large driving force required for the regeneration of the photooxidized dye, is now stimulating interest in new redox mediators.[11−21] Of all the alternatives examined thus far, $Co^{II/III}$ polypyridyl redox couples have emerged as leading candidates to replace the I^-/I_3^- redox shuttle.[22−29] $Co^{II/III}$ complexes are generally noncorrosive toward most metals, and modification in the ligand architecture can be used to fine-tune the $Co^{II/III}$ redox potential so as to achieve efficient dye regeneration and at the same time maximize the open circuit potential (V_{OC}).[19,24] The advantage of these redox mediators was recently demonstrated by the use of the $[Co(bpy)_3]^{2+/3+}$ couple in DSCs, which achieved a record efficiency of 12.3% and V_{OC} of 965 mV.[30]

A large inner-sphere reorganization energy in the cases of $[Co(bpy)_3]^{2+/3+}$ and $[Co(phen)_3]^{2+/3+}$ has been suggested to result in slow rates of interfacial recombination between photoinjected electrons and the Co^{III} complexes, thus leading to high efficiencies.[31−34] In a further recent development, a cobalt complex of formula $[Co(L^1)_2]^{2+/3+}$, where L^1 is the tridentate ligand [6-(1*H*-pyrazol-1-yl)-2,2′-bipyridine)], achieved a high V_{OC} of 998 mV and an impressive efficiency of 10%.[19]

The denticity and spatial arrangement of the donor atoms are features of a ligand that can be manipulated to design metal complexes with particular properties and coordination geometries. In addition to the electron-donating properties of the ligands, the rigidity and number of donor atoms are important in determining the stability and electrochemical properties of a particular complex. Moreover, the ligand properties can be used to modulate the relative activation energies for electron-transfer processes involving the metal complexes.

Here, we report a new approach to designing redox mediators, which exploits the coordination properties of Lewis bases commonly added to DSC electrolyte solutions. The pair of cobalt complexes chosen for this purpose have the formula $[Co(PY5Me_2)(MeCN)](OTf)_2$ (**1a**) and $[Co(PY5Me_2)(MeCN)](TFSI)_3$ (**1b**) ($PY5Me_2$ = (2,6-(bis(bis-2-pyridyl)methylmethane)pyridine, see Scheme 1). The nitrogen donors in the pentadentate polypyridyl ligand, $PY5Me_2$, occupy the corners of a square-pyramid when bound to the metal center. In complexes **1a**/**1b**, the sixth coordination site of the octahedral ligand field is occupied by a weakly bound acetonitrile (MeCN) molecule, which can be readily replaced by more strongly binding ligands. This feature provides an opportunity to fine-tune the potential of the $Co^{II/III}$ redox couple through the addition of suitable strongly coordinating Lewis bases to form complexes of composition $[Co(PY5Me_2)(B)](OTf)_2$ (see Scheme 1). Furthermore, we examined whether the introduction of the chelating pentadentate ligand offers advantages in terms of the key electron transfer processes occurring in DSCs.

We describe the synthesis and characterization of two pairs of $[Co(PY5Me_2)(B)]^{2+/3+}$ complexes, where B corresponds to tBP (**2a**/**2b**) and NMBI (**3a**/**3b**), two bases commonly used as additives in DSC electrolytes, and the application of these complexes as redox mediators in DSCs using the D-π-A organic dye, MK2 (2-cyano-3-[5‴-(9-ethyl-9H-carbazol-3-yl)-3′,3″,3‴,4-tetra-*n*-hexyl-[2,2′,5′,2″,5″,2‴]-quarter thiophen-5-yl] acrylic acid) (see Figure 1). The exciting finding to emerge from this study is the significantly improved efficiency of DSCs constructed with the NMBI complex in comparison to the efficiencies obtained when using the tBP analogue or $[Co(bpy)_3]^{2+/3+}$ complex.

Scheme 1. Shown are the 1a, 2a and 3a Cations for the Co^{II} Complexes and the 1b, 2b and 3b Cations for the Co^{III} Complexes[a]

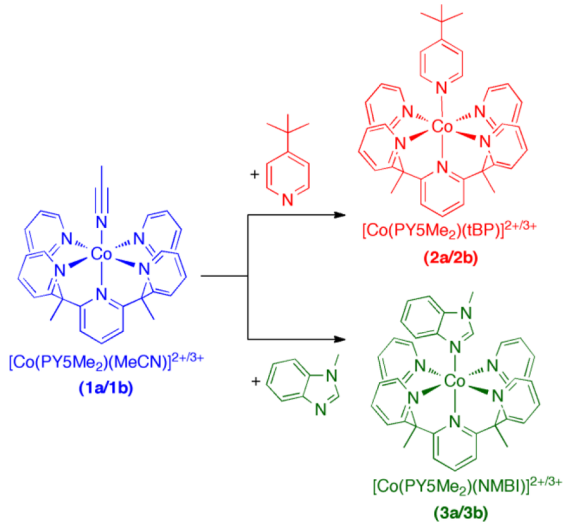

[a]The syntheses are described in the Experimental Section.

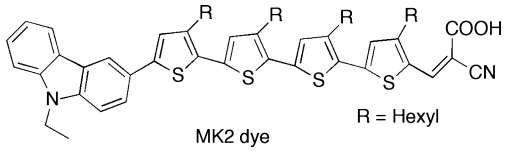

Figure 1. Structure of the MK2 dye.

EXPERIMENTAL SECTION

Materials and Methods. All general reagents and solvents were obtained from commercial sources. Anhydrous solvents were stored in the glovebox. The compounds MK2, bpy (2,2′-bipyridine), tBP (4-*tert*-butylpyridine), NMBI (*N*-methylbenzimidazole), LiTFSI (lithium bis(trifluoromethane)sulfonimide), EDOT (3,4-ethylenedioxythiophene), MeCN and other solvents were purchased from Sigma Aldrich. AgTFSI (silver bis(trifluoromethane)sulfonimide), AgOTf (silver trifluoromethansulfonate) and $NOBF_4$ were purchased from Strem Chemicals Inc. TiO_2 nanoparticles (Ø 30 and 400 nm particles) were obtained from JGC Catalysts and Chemicals Ltd. ^1H and ^{19}F NMR spectra were measured on a Bruker DRX 400 spectrometer, using the signal of the deuterated solvent as an internal standard. The chemical shifts δ are reported in parts per million (ppm) relative to tetramethylsilane (TMS). The values of coupling constants (J) are given in Hertz (Hz). Peak multiplicities are abbreviated as follows: s (singlet), d (doublet), t (triplet), and m (multiplet). Microanalyses were carried out by the Campbell Microanalytical Laboratory, University of Otago, New Zealand. UV−visible spectra were recorded with a Lambda 950 Perkin-Elmer spectrophotometer. All electrochemistry experiments were performed at 22 °C in a three-electrode cell joined to a VSP workstation. The reference electrode was a CH Instruments $Ag/AgNO_3$ nonaqueous electrode. $Fc^{0/+}$ was used as a reference system and a conversion factor of 635 mV was used to convert electrochemical potential vs ferrocene to NHE.

Synthesis of the Cobalt Complexes. Unless otherwise noted, all synthetic procedures as well as electrolyte filling of the DSCs were performed under inert N_2 atmosphere, using standard glovebox techniques. The ligand $PY5Me_2$ was synthesized as previously described.[35] The complex $[Co(PY5Me_2)(MeCN)](OTf)_2$ (**1a**) was

obtained with use of the method of Zadrozny et al.,[36] but substituting AgOTf for $TlPF_6$.

*[Co(PY5Me$_2$)(tBP)](OTf)$_2$·2MeCN (**2a**).* This compound was accessed by the addition of tBP (6.8 mg, 0.050 mmol) into a stirred mixture of **1a** (42 mg, 0.050 mmol) in 10 mL of acetonitrile, at room temperature. Compound **1a** is very poorly soluble in acetonitrile. However, it becomes soluble upon addition of tBP. The solution was stirred for 1 h at room temperature to ensure ligand exchange was complete. Layering with Et_2O induced crystallization. Yield: 45 mg (96%) of **2a** as pink crystals. Crystals of the diacetonitrile solvate suitable for X-ray diffraction analysis were obtained by the diffusion of Et_2O into a concentrated acetonitrile solution of **2a**. Elemental analysis: Found (Calcd) for $C_{42s}H_{41}CoF_6N_7O_6S_2$ (**2**): C, 51.64 (51.34); H, 4.23 (4.09); N, 8.74 (8.98).

*[Co(PY5Me$_2$)(NMBI)](OTf)$_2$·2MeCN. (**3a**).* Compound **3a** was prepared by the addition of NMBI (6.6 mg, 0.050 mmol) into an acetonitrile mixture of **1a** (42 mg, 0.050 mmol) following the procedure described for compound **2a**. Yield: 43 mg (95%) of **3a** as pink crystals. Crystals of the diacetonitrile solvate suitable for X-ray diffraction analysis were obtained by the diffusion of Et_2O into an acetonitrile solution of **3a**. Elemental analysis: Found (Calcd) for $C_{39}H_{33}CoF_6N_7O_6S_2$ (**3**): C, 49.98 (50.22); H, 3.66 (3.57); N, 11.14 (10.51).

*[Co(PY5Me$_2$)(MeCN)](TFSI)$_3$ (**1b**), [Co(PY5Me$_2$)(tBP)](TFSI)$_3$ (**2b**), and [Co(PY5Me$_2$)(NMBI)](TFSI)$_3$·3CH$_2$Cl$_2$ (**3b**).* The synthesis of **2b** and **3b** followed a similar procedure to that described for **2a** and **3a**. However, high-quality crystals could not be grown for complexes **2b** and **3b** when $NOBF_4$ was used as the oxidant. In addition, following oxidation of the Co^{II} complex to the corresponding Co^{III} complex with use of $NOBF_4$ it was found that the BF_4^- slowly decomposes generating fluoride ions, which then coordinate to the Co^{III} center. Hence, AgTFSI was used as the oxidant and the products isolated as TFSI salts. To prepare **1b** solid AgTFSI (35 mg, 0.13 mmol) and **1a** (34 mg, 0.043 mmol) were added to 10 mL of CH_2Cl_2 and the mixture was stirred for 1 h, giving a light orange mixture containing Ag particles, which were removed by filtration through diatomaceous earth. Orange crystals of [Co(PY5Me$_2$)(MeCN)](TFSI)$_3$·3(CH$_2$Cl$_2$) (**1b**) were obtained by layering with Et_2O. Yield: 45 mg (75%) as orange crystals. **1b** was then reacted (as described for **2a** and **3a**) with tBP and NMBI to give **2b** and **3b**, respectively. A high yield (97%) was obtained for complexes **2b** and **3b.** Crystals of [Co(PY5Me$_2$)(NMBI)](TFSI)$_3$·3CH$_2$Cl$_2$ (**3b**) suitable for X-ray diffraction studies were obtained by vapor diffusion of Et_2O into a concentrated solution of **3b** in acetonitrile. Despite numerous attempts, crystals of **2b** suitable for X-ray crystallography could not be obtained.

[Co(PY5Me$_2$)(tBP))](TFSI)$_3$ (**2b**): ^{1}H NMR (400 MHz, CD_3CN, 22 °C) δ 9.63 (d, J_{HH} = 8 Hz, 4H, py-H), 8.35−8.32 (m, 1 H, py-H), 8.30−8.24 (m, 6 H, py-H), 8.18−8.16 (M, 4H, py-H), 8.07−8.04 (m, 1H, tBP-H), 7.97−7.95 (m, 1H, tBP-H), 7.90−7.87 (m, 4H, py-H), 7.72−7.68 (m, 2H, tBP-H), 5.47 (s, 9H, tBP-3CH_3), 2.96−2.81 (m, 6H, Me_2−H).

[Co(PY5Me$_2$)(NMBI))](TFSI)$_3$ (**3b**): ^{1}H NMR (400 MHz, CD_3CN, 22 °C) δ 9.67 (m, 1H, NMBI-H), 8.81 (d,, J_{HH} = 8 Hz, 2 H, NMBI-H), 8.57 (d,, J_{HH} = 8 Hz, 2 H, NMBI-H), 8.37−8.16 (m, 11 H, py-H), 8.01−7.90 (m, 2H, py-H), 7.70−7.60 (m, 2 H, py-H), 7.56−7.52 (m, 1 H, py-H), 7.37−7.34 (m, 2 H, py-H), 6.85 (s, 1 H, py-H), 4.05−3.94 (m, 3 H, CH_3−NMBI), 3.01−2.98 (m, 6 H, Me_2−H).

Data Collection. Representative orange or orange-red prismatic crystals of **2a**, **3a**, and **3b** were mounted on an Oxford Gemini Ultra CCD diffractometer equipped with an Oxford Cryosystems 700 Cryostream and cooled to 123(1) K. Data were collected with Mo Kα radiation (λ = 0.71073 Å) and processed with CrysAlisPro software; Lorentz, polarization, and absorption corrections (multiscan) were applied. The structures were solved and refined with SHELX-97.[37] All non-hydrogen atoms were refined with anisotropic thermal parameters and hydrogen atoms were placed in calculated positions, using a riding model with C−H = 0.95−0.98 Å and U_{iso}(H) = xU_{iso}(C), x = 1.2 or 1.5. For **3a**, one of the CF_3SO_3 counterions was modeled as disordered with the CF_3 and SO_3 groups each occupying two positions rotated by approximately 15° about the S−C bond. The disordered atoms were refined with occupancies fixed at 0.5, with equivalent C−F and S−O distances restrained to be the same and with the anisotropic thermal parameters for some atoms restrained to be similar. A summary of crystallographic data can be found in Table 1.

Table 1. Crystallographic Data for 2a, 3a, and 3b

	2a	3a	3b
formula	$C_{44}H_{44}CoF_6N_8O_6S_2$	$C_{43}H_{39}CoF_6N_9O_6S_2$	$C_{46}H_{39}Cl_6CoF_{18}N_{10}O_{12}S_6$
fw	1017.94	1014.88	1729.86
crystal system	monoclinic	triclinic	triclinic
space group	$P2_1/c$	$P\bar{1}$	$P\bar{1}$
a (Å)	14.4264(9)	12.5214(7)	13.4281(6)
b (Å)	14.7665(11)	13.0143(11)	13.7502(5)
c (Å)	21.3870(14)	15.4881(8)	19.9835(9)
α (deg)	90	108.227(6)	74.802(4)
β (deg)	93.340(6)	90.845(4)	87.534(4)
γ (deg)	90	113.083(7)	66.118(4)
V (Å^3)	4548.3(5)	2177.9(2)	3247.5(2)
Z	4	2	2
μ_{calcd} (mm^{-1})	0.551	0.576	0.821
ρ_{calcd} (g·cm^{-1})	1.487	1.548	1.769
2θ range (deg)	3.96−55.0	3.74−64.70	3.82−60.0
N_t	26161	28652	40980
$N(R_{int})$	10440 (0.057)	14035 (0.051)	18933 (0.033)
N_o	8023	9473	13918
$R1$ ($I > 2\sigma I$)	0.056	0.059	0.058
wR ($I > 2\sigma I$)	0.143	0.137	0.136
R(all data)	0.076	0.094	0.086
wR(all data)	0.159	0.164	0.167
GoF	1.051	1.037	1.027
$\Delta\rho_{max/min}$ (e)	1.05; −0.82	1.20; −1.05	1.74; −1.32

Device Fabrication. Established procedures were followed for DSC fabrication.[12] A 1 μm thick film (4 × 4 mm) of 30 nm-sized TiO_2 particles was screen printed on fluorine-doped SnO_2 (FTO) conducting glass electrodes (4 mm thick and 10 Ω/□). A second layer was printed by using 400 nm-sized particles to produce a titania layer with overall thickness of 3 μm. A 2 μm thick transparent TiO_2 film (4 × 4 mm) with 30 nm-sized TiO_2 particles was deposited for the IMVS-IMPS studies. Following the application of a first sintering process (500 °C) to the screen-printed films, a $TiCl_4$ treatment was carried out by submerging the films in an aqueous solution containing 40 mM $TiCl_4$ at 70−75 °C. After heating the films with a heat gun at 570 ± 25 °C for 40 min, the films were immersed for 6 h in a 0.2 mM solution of MK2 in an acetonitrile:toluene (1:1) mixture. The PEDOT counter electrodes were prepared by electropolymerizing EDOT on the FTO substrate.[38] Working electrode and counter electrode were bonded together with a 25 μm thick hot melt Surlyn gasket. Electrolytes were filled into the space between the two electrodes by using a backfilling technique under vacuum. The electrolyte-injecting hole was sealed with hot melt Surlyn backed by aluminum foil.

IV and IPCE Instrumentation. An Oriel sun simulator equipped with a filtered 1000 W xenon lamp was used as a source of simulated solar irradiation (AM 1.5 G, 1000 W/m^2). A calibrated silicon photodiode provided by Peccell Technologies was used to adjust the output of the light source and a color filter was used to minimize the optical mismatch between the calibration diode and the DSCs. The IV characteristics of the cells under these conditions were recorded with use of a Keithley 2400 source meter. Light intensities below one sun were achieved by using a filter wheel fitted with a series of mesh filters. Incident photon conversion efficiency was measured by an Oriel system fitted with a 150 W xenon lamp, linked to a Cornerstone 260

monochromator. IPCE photocurrents of the DSCs were recorded under short circuit conditions by means of a Keithley 2400 source meter. The monochromatic photon flux was quantified by using a calibrated silicon photodiode (Peccell Technologies).

Intensity Modulated Photovoltage Spectroscopy, Intensity Modulated Photocurrent Spectroscopy (IMVS-IMPS) and Charge Extraction Instrumentation. IMVS-IMPS studies were carried out on complete DSCs by using a combination of red and white light LEDs. The light intensity of the red LED powered by an adjustable DC voltage source was modulated to a depth of 2% by the integral function generator of a Stanford lock-in-amplifier (SR810). The lock-in-amplifier is capable of providing a sine wave modulation between 0.1 Hz and 30 kHz. To achieve one sun equivalent, an additional white light diode array controlled by a commercial DC power source was used. All experiments were carried out in an earthed Faraday dark box to remove electrical noise at low light intensities. The photovoltage was recorded with the help of a high impedance voltage follower (input impedance 10^{12} Ω), powered by a battery. The amplitude and phase of the resulting AC photovoltages were captured by using the lock-in amplifier run under a computer-controlled program Labview. A fitting program written in Labview was used for the data analysis. An unmodulated white light illuminated the DSC for 10 s to attain equilibrium between charge injection and recombination under open circuit conditions. An integrated computer-controlled mercury-wetted relay switch was used to switch the light off and to put the device to short circuit. The resultant extracted charge was measured across a 50 Ω resistor, using an NI-6251 data logger.

RESULTS AND DISCUSSION

A key step in fine-tuning the redox potential of the $Co^{II/III}$ redox shuttle involved ligation of the Lewis bases to the parent complex **1a**. The complexes $[Co(PY5Me_2)(tBP)](OTf)_2$ (**2a**) and $[Co(PY5Me_2)(NMBI)](OTf)_2$ (**3a**) were accessed by the addition of tBP and NMBI, respectively, to an acetonitrile solution of **1a** (see Scheme 1). The axial MeCN ligand in **1a** is readily displaced by these more strongly binding monodentate ligands. The preparation of the Co^{III} complexes was achieved by first preparing $[Co(PY5Me_2)(MeCN)](TFSI)_3$, through oxidation of **1a** with AgTFSI, and then reacting the product with tBP and NMBI to afford $[Co(PY5Me_2)(tBP)](TFSI)_3$ (**2b**) and $[Co(PY5Me_2)(NMBI)](TFSI)_3$ (**3b**), respectively.

Crystallography. Single crystals of $[Co^{II}(PY5Me_2)(tBP)](OTf)_2\cdot 2MeCN$ (**2a**) and $[Co^{II}(PY5Me_2)(NMBI)](OTf)_2\cdot 2MeCN$ (**3a**) suitable for X-ray analysis were obtained on addition of tBP and NMBI to an acetonitrile solution of the Co^{II} complex **1a**, respectively. Similarly, $[Co(PY5Me_2)(NMBI)](TFSI)_3\cdot 3(CH_2Cl_2)$ (**3b**) was obtained by the addition of tBP to the trivalent analogue of complex **1a**. All three complexes display a distorted octahedral $Co^{II/III}$ geometry with either the tBP or NMBI ligands in the axial position (Figures 2 and S4, SI).

The coordination spheres for complexes **2a** and **3a** are very similar, with the $Co-N_{Py}$ distances (see Table 2) in the range of 2.122(2)−2.156(1) Å (**2a**) and 2.108(2)−2.156(2) Å (**3a**). These bond lengths are marginally longer than those for the MeCN complex **1a** (2.095(3)−2.142(3) Å).[39] The $Co-N_6$ (*N*-atom of the base) distances of 2.122(3) (**1a**), 2.129(2) (**2a**), and 2.108(2) Å (**3a**) also show little difference. The longer $Co-N_{Py}$ bond lengths in **2a** and **3a** are accompanied by a displacement of the Co atom out of the equatorial plane by 0.139(1) and 0.149(1) Å (cf., the Co in **3b** is coplanar with the four equatorial pyridyl donors, −0.037(1) Å). The ability of the $PY5Me_2$ ligand to absorb the structural effects arising from changes in the oxidation state of the central metal atoms (e.g., two-electron $Mo^{II}-Mo^{IV}$ changes) has been previously established.[40] However, in the current structures, the shortening of the Co−N bonds from **3a** to **3b** results in an unusually close approach (1.81 Å for **3b** cf. 2.15 Å for **3a**) of two neighboring *o*-H atoms on the terminal pyridyl groups (Figures 2 and S4, SI). A top view of the complex cations of **2a**, **3a**, and **3b** shows a highly symmetrical alignment of the axial ligand (tBP and NMBI) and the $Me_2C-PY_1-CMe_2$ plane (see Figure S3, SI).

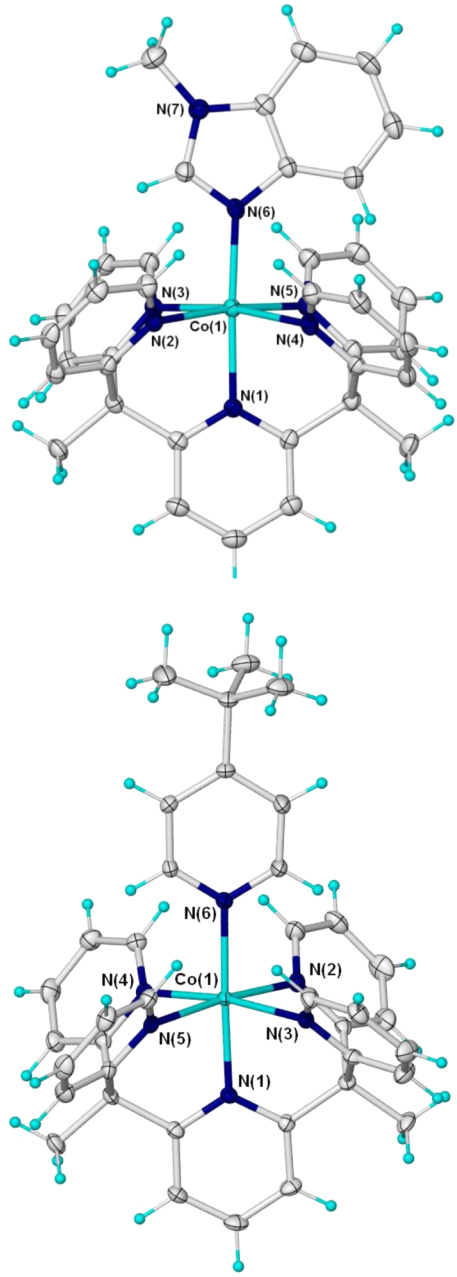

Figure 2. Crystal structures of the octahedral complexes $[Co(PY5Me_2)(tBP)]^{2+}$ (**2a** cation) and $[Co(PY5Me_2)(NMBI)]^{2+}$ (**3a** cation), with the pale blue, gray, and dark blue spheres representing Co, C, and N, respectively. Ellipsoids are depicted at the 50% probability level.

The Co−N bond lengths for $[Co(PY5Me_2)(NMBI)]^{2+}$ (**3a** cation) and $[Co(PY5Me_2)(NMBI)]^{3+}$ (**3b** cation) indicate that oxidation of the Co center results in an average decrease in the Co−N bond distances of 0.150(6) Å (calculated as the average difference in bond lengths for pairs of identical Co−N bonds in each complex). The corresponding change in bond distances

Table 2. Selected Bond Distances (Å) and Angles (deg) for 2a, 3a, and 3b

bond/angle	2a	3a	3b
Co−N(1)[a]	2.122(2)	2.122(2)	1.976(2)
Co−N(2)	2.132(2)	2.145(2)	1.989(2)
Co−N(3)	2.156(2)	2.156(2)	1.999(2)
Co−N(4)	2.145(2)	2.140(2)	1.999(2)
Co−N(5)	2.135(2)	2.140(2)	1.991(2)
Co−N(6)[b]	2.129(2)	2.108(2)	1.960(2)
N(1)−Co−N(6)	177.88(9)	177.26(8)	179.1(1)
N(2)−Co−N(5)	173.59(9)	172.61(8)	176.9(1)
N(3)−Co−N(4)	171.32(9)	170.87(8)	177.4(1)
N(2)−Co−N(4)	97.22(9)	99.11(8)	93.4(1)
N(5)−Co−N(3)	98.29(9)	96.48(8)	96.7(1)
N(3)−Co−N(2)	82.64(9)	80.21(8)	84.4(1)
N(5)−Co−N(4)	80.89(9)	83.10(8)	85.4(1)
N(1)−Co−N(3)	85.42(8)	86.26(8)	89.2(1)
N(1)−Co−N(2)	86.62(9)	87.12(8)	89.0(1)
N(1)−Co−N(4)	85.91(9)	84.61(8)	89.4(1)
N(1)−Co−N(5)	87.14(9)	86.07(7)	88.1(1)

[a]Axial $PY5Me_2$ pyridyl donor. [b]Axial Co−N(NMBI) bond.

for $[Co(bpy)_3]^{2+/3+}$ is 0.198(6) Å.[42,43] Thus, the constrained nature of the $PY5Me_2$ ligand appears to have a significant influence on the Co^{III} geometry. As a consequence, oxidation/reduction reactions involving the $[Co(PY5Me_3)(B)]^{2+/3+}$ complexes are likely to require less inner-sphere reorganization (vide infra).

Electrochemistry. The electrochemical properties of complexes **1a**−**3a** were investigated by using cyclic voltammetry under nitrogen. For compound **1a**, two quasi-reversible redox reactions are observed at half-wave potentials of $E_{1/2}$ = −0.845 V and +0.803 V vs NHE, corresponding to the $[Co(PY5Me_2)(MeCN)]^{1+/2+}$ and $[Co(PY5Me_2)(MeCN)]^{2+/3+}$ redox reactions, respectively (Figure S1a in the SI). This is consistent with previous literature reports.[36,39] Upon introduction of tBP and NMBI to form **2a** and **3a**, the $Co^{II/III}$ redox potential was lowered to a more negative value relative to that of **1a**. The $E_{1/2}$ for $[Co(PY5Me_2)(tBP)]^{2+/3+}$ shifted slightly to +0.780 V vs NHE, whereas $E_{1/2}$ for $[Co(PY5Me_2)(NMBI)]^{2+/3+}$ shifted to +0.714 V vs NHE (see Figure 3a). The corresponding redox potential for $[Co(bpy)_3]^{2+/3+}$ is 0.56 V vs NHE and is virtually unaffected by the addition of the bases. The redox potentials (vs NHE) derived for complexes **2a** and **3a**, $[Co(bpy)_3]^{2+/3+}$, and the HOMO LUMO levels of MK2 are compared in Figure 3b. These redox properties indicate that these complexes are well suited for DSC electrolyte development. The displacement of a monodentate ligand by an alternative Lewis base, which in turn affects the electrochemical properties of the complex, is not unprecedented. A study[44] carried out on a series of complexes with the formula $[Fe(PY5)(Y)]^{n+}$, where PY5 = 2,6-(bis(bis-2-pyridyl)-methoxymethane)pyridine and Y represents a series of neutral and anionic exogenous monodentate ligands, revealed that the MeOH ligand in $[Fe(PY5)(MeOH)]^{n+}$ can be displaced by the addition of a Lewis base and that the anionic ligands enhance the reversibility of the $Fe^{II/III}$ redox reaction on Pt disk electrodes.

Photovoltaic Performance. Two new electrolytes based on redox shuttles, **2a**/**2b** and **3a**/**3b**, were optimized and tested for their performance in DSCs and compared to a standard electrolyte employing $[Co(bpy)_3]^{2+/3+}$ as redox couple. An

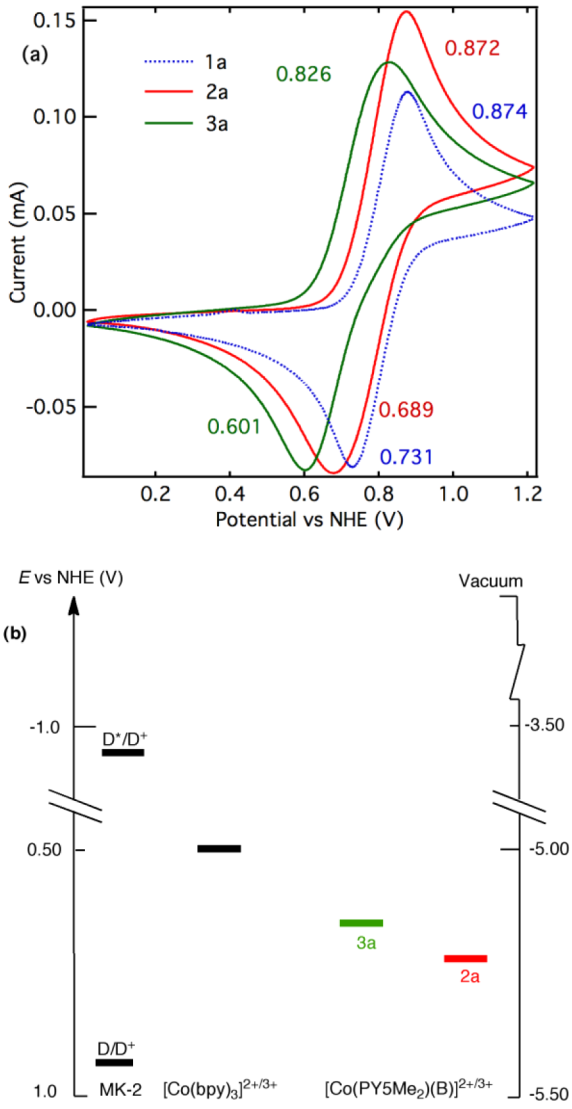

Figure 3. Cyclic voltammetry and energy level diagram. (a) Cyclic voltammogram of 10 mM solutions of $[Co(PY5Me_2)(MeCN)](OTf)_2$ in MeCN (blue wave 1), with 10 mM tBP added (red wave **2a**) and 10 mM NMBI added (green wave **3a**). The measurements were performed with use of a glassy carbon disk electrode and 100 mM $(Bu_4N)PF_6$ as supporting electrolyte at a scan rate of 100 mV/s. (b) Energy level diagram of DSC components, approximate redox potentials of the electrolytes[7] based on $[Co(bpy)_3]^{2+/3+}$ and complexes **2a** and **3a**. Data for MK2 dye and cobalt complexes are relative to the normal hydrogen electrode (NHE).

efficient, commercially available carbazole dye, MK2, was used as the photosensitizer. The redox potential (0.92 V versus NHE) of MK2 was measured on ITO films in acetonitrile containing 0.10 M $TBAPF_6$ as supporting electrolyte. The dye has a high molar extinction coefficient (38 400 M^{-1} cm^{-1})[49] and ensures excellent light harvesting, even when adsorbed onto relatively thin (2−5 μm) TiO_2 films. It is therefore a convenient sensitizer for DSCs based on one-electron-transfer redox couples, where the use of thinner than usual TiO_2 film thicknesses is preferred due to increased charge recombination as compared to I^-/I_3^-.

The highest energy conversion efficiency of 8.4% under simulated sunlight (AM 1.5 G, 1000 W/m^2) was achieved by using an electrolyte based on redox couple **3a**/**3b** (see Table

dx.doi.org/10.1021/ja305897k | J. Am. Chem. Soc. 2012, 134, 16646−16653

Table 3. Tabulated Photovoltaic Performance Data of DSCs Made with Different Redox Mediators and MK2 Dye under Simulated Sunlight (AM 1.5 G, 1000 W/m^2)[a]

redox couple	2a/b	3a/b	$[Co(bpy)_3]^{2+/3+}$	$[Co(bpy)_3]^{2+/3+}$
base[b]	tBP	NMBI	tBP	NMBI
RP (mV)[c]	684	633	496	498
V_{OC} (mV)	993 ± 2	940 ± 1	802 ± 1	795 ± 1
J_{SC} (mA cm^{-2})	8.1 ± 0.01	11.8 ± 0.4	14.1 ± 0.2	13.0 ± 0.3
FF	0.76 ± 0.01	0.77 ± 0.01	0.66 ± 0.01	0.67 ± 0.01
η (%)	6.1 ± 0.1	8.4 ± 0.3	7.4 ± 0.1	7.0 ± 0.2

[a]Double-layer TiO_2 films (1 μm mesoporous TiO_2 (30 nm) and 2 μm scattering TiO_2 (400 nm)) were used for the construction of all DSCs. A 0.5 μm thick PEDOT was used as counter electrode, which was grown electrochemically on FTO, using a 20 mM solution of EDOT monomer in acetonitrile and 100 mM LiTFSI as supporting electrolyte. The average performance values and standard deviation over a sample of three cells is given. [b]The electrolyte consists of 0.20 M Co^{II} complex, 0.075 M Co^{III} complex, 0.10 M LiTFSI, and 0.50 M of either tBP or NMBI as indicated. [c]The redox potential of the electrolytes were determined from the potential difference between a Pt wire and a reference electrode (Ag/Ag^+), immersed in the electrolyte.[7]

3). These DSCs clearly outperform devices based on the more conventional $[Co(bpy)_3]^{2+/3+}$ redox couple. The efficiency gain is primarily due to a significant increase in V_{OC} and fill factor (FF), which compensate for a drop in short-circuit current density (J_{SC}). The interpretation of changes in V_{OC} and J_{SC} for these cells is not straightforward, as the added bases influence the electronic properties of the mesoporous TiO_2 electrode (e.g., flat band position, surface states), while also creating different redox mediators through in situ reactions with **1a**/**1b**. The more positive redox potential of electrolytes based on **2a**/**2b** relative to $[Co(bpy)_3]^{2+/3+}$ is reflected in a higher V_{OC} of 993 mV for devices made with electrolytes containing **2a**/**2b**.

The performance of DSCs based on $Co^{II/III}$ polypyridyl electrolytes is highly dependent on the mesostructure of the TiO_2 film used to construct the cells. In this study, the TiO_2 films have been optimized for the use of MK2 in conjunction with $[Co(bpy)_3]^{2+/3+}$ based electrolytes (see the Experimental Section), yielding efficiencies (η) of up to 7.4%. This represents a substantial improvement over the 5.5% efficiency reported recently for DSCs based on MK2 and $[Co(bpy)_3]^{2+/3+}$ electrolyte.[45] Again, the key point to make here is that sensitizers with very high molar extinction coefficients are ideal for one-electron redox mediators, as a very thin film of 1 μm transparent TiO_2 nanoparticles is sufficient to ensure efficient light harvesting.

The IV curves for the best performing DSCs for each redox couple are shown in Figure 4, measured at AM1.5 G; 1000 W/m^2. The devices made with the NMBI complex, **3**, show a 140 mV higher V_{OC} and a significant increase in FF compared to devices employing a $[Co(bpy)_3]^{2+/3+}$ electrolyte. The 140 mV gain in V_{OC} is primarily attributed to the differences in the redox potentials[7] of the two electrolytes.

The measured redox potential for the $[Co(bpy)_3]^{2+/3+}$ electrolyte was in very close agreement with the standard Nernst potential calculated by Grätzel et al. for $[Co(bpy)_3]^{2+/3+}$ at very similar concentrations.[46] The lower J_{SC} values for devices based on **2a**/**2b** could be a consequence of less efficient dye-regeneration, and may arise from the lower driving force for this reaction (0.24 V). Photocurrent dynamics measurements, using simple on/off experiments (see Figure S5 in the SI), revealed that the photocurrents at 1 sun were somewhat limited by mass-transport limitations. This effect was slightly more pronounced for devices based on **3a**/**3b** compared to $[Co(bpy)_3]^{2+/3+}$. Inefficient dye regeneration could result in a significantly higher equilibrium concentration of photooxidized dye and therefore a faster rate of recombination between

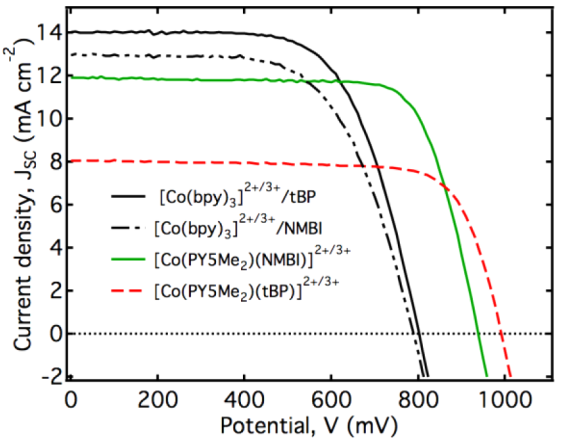

Figure 4. Comparison of DSC performance for optimized devices sensitized with MK2 based on **3a**/**3b** (green line), **2a**/**2b** (red dashed), $[Co(bpy)_3]^{2+/3+}$/tBP (black solid), and $[Co(bpy)_3]^{2+/3+}$/NMBI (black dotted) electrolytes in acetonitrile. IV characteristics are summarized in Table 3.

conduction band electrons and photooxidized dye molecules. In the future, we intend to investigate the electron transfer processes limiting the performance of these devices.

The incident photon-to-electron conversion efficiency (IPCE) spectra of DSCs sensitized with MK2 are shown in Figure 5. Comparable IPCEs are observed for the devices fabricated by using $[Co(bpy)_3]^{2+/3+}$ with either tBP or NMBI added as Lewis base. The devices fabricated with electrolytes based on complexes **2a**/**2b** and **3a**/**3b** show lower IPCEs compared to DSCs constructed from $[Co(bpy)_3]^{2+/3+}$ electrolytes. This is anticipated from the lower J_{SC} values measured under simulated sunlight (see Table 3).

IMVS-IMPS Spectroscopy. Further insights into the electron lifetime and mean transient time of photoinjected charge carriers were gained by using the intensity-modulated photovoltage and photocurrent spectroscopy (IMVS and IMPS), as complemented by charge extraction experiments. Figure 6a shows the IMPS results, which compare mean electron transient times (τ_c) as a function of J_{SC}. The observed τ_c for the devices based on redox systems **2a**/**2b**, **3a**/**3b**, and $[Co(bpy)_3]^{2+/3+}$ with tBP and NMBI are similar, as expected. It can be seen in Figure 6b that for each of the electrolyte systems, linear plots for electron lifetime measurements (τ_n) vs electron density were observed.

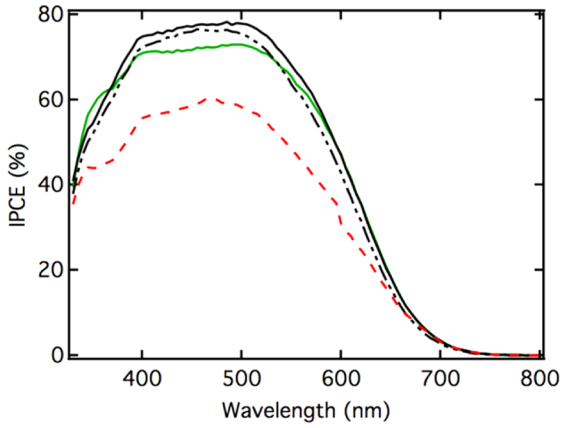

Figure 5. IPCE spectra for the DSCs sensitized with MK2 based on **3a**/**3b** (green line), **2a**/**2b** (red dashed), $[Co(bpy)_3]^{2+/3+}$/tBP (black solid), and $[Co(bpy)_3]^{2+/3+}$/NMBI (black dotted) electrolytes in acetonitrile.

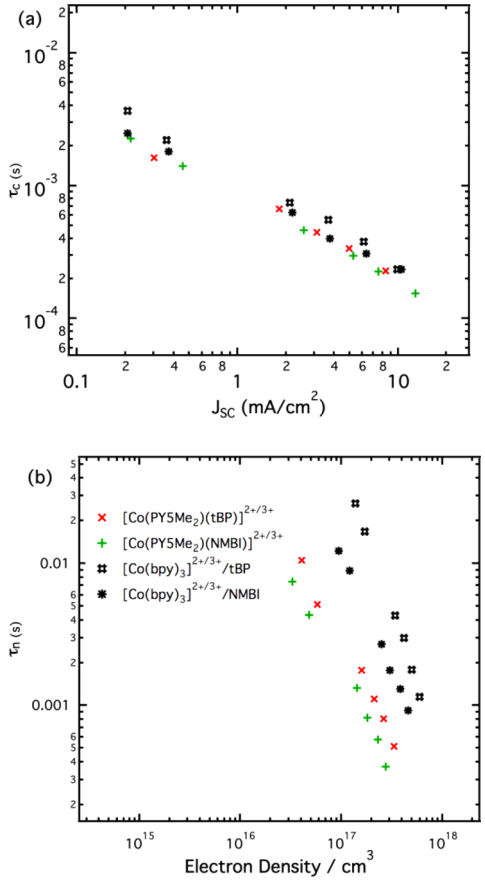

Figure 6. IMVS and IMPS spectroscopy. (a) Mean electron transient time versus short circuit current. (b) Electron lifetimes are plotted vs extracted charge for MK2-sensitized DSCs. The devices were constructed with use of 2 μm thick TiO_2 (30 nm) mesoporous films and contained the corresponding redox shuttle in their electrolyte. The electrolyte composition is given in Table 3.

The results are consistent with recombination occurring via electron transfer from the conduction band[47] to the oxidized form of the redox couple, despite large differences in the redox potentials of electrolytes as well as different reorganizational energies of the cobalt complexes. In general, faster electron transfer rates associated with redox systems based on complexes **2a**/**2b** and **3a**/**3b** can result in comparatively short electron lifetimes for photoinjected charge carriers. In contrast, the high-energy activation barrier relative to the $[Co(bpy)_3]^{2+/3+}$ redox couple brings about a 10-fold improvement in the lifetime of photoinjected charge carriers, at a similar charge density.

The classical inner-sphere reorganization energy associated with electron-exchange reactions of metal complexes can be estimated by the following equation:[41]

$$\Delta G_{inner} = \frac{n}{2}\frac{f_{III}f_{II}}{f_{III}+f_{II}}\Delta X^2$$

where f_i = force constants for the Co^{II} and Co^{III}-ligand bonds and ΔX = change in bond distances of n bonds. Assuming f_i and n to be similar for the $[Co(PY5Me_2)(NMBI)]^{2+/3+}$ (**3a**/**3b**) and $[Co(bpy)_3]^{2+/3+}$ redox couples, the estimated inner-sphere reorganizational energy varies with the square of the displacement. Compared with $[Co(bpy)_3]^{2+/3+}$ (where ΔX = 0.20 Å), a decrease in inner-sphere reorganizational energy of almost 50% is predicted for **3a**/**3b** (for which ΔX = 0.15 Å).[42,43] This is expected to result in faster dye regeneration but also in faster recombination between injected electrons and the oxidized redox mediator. Faster recombination for electrolytes with higher redox potentials is also expected as the driving force for dye regeneration is decreased for electron transfer processes operating in the Marcus normal region.[26] According to Hupp et al.[48] the open-circuit quasi-Fermi level drops (becomes less negative) with a positive increase in the redox potential of the redox couple and, hence, it reduces the attainable V_{OC}.

CONCLUSIONS

We have explored the application of a new class of redox mediators based on the complex $[Co(PY5Me_2)(MeCN)]^{2+/3+}$, where $PY5Me_2$ is a pentapyridyl ligand. Using a number of techniques, including X-ray crystallography, we have demonstrated that the MeCN ligand can be replaced by a more strongly binding monodentate ligand. Thus, the use of a pentadentate ligand allows the potential of the $Co^{II/III}$ redox couple to be tuned through the single-site coordination of tBP or NMBI, two Lewis bases commonly added to DSC electrolytes. Metal complexes based on the pentadentate ligand are also predicted to result in a lower reorganizational energy for electron transfer when compared to the $[Co(bpy)_3]^{2+/3+}$ redox couple. Application of electrolytes based on the cobalt-NMBI complexes in DSCs, in combination with a strongly absorbing organic sensitizer, MK2, have yielded devices with efficiencies of 9.2% and 8.4% at 0.1 and 1 sun irradiation, respectively, outperforming analogous devices constructed with the $[Co(bpy)_3]^{2+/3+}$ redox couple. In addition, an open circuit voltage approaching 1.0 V was measured for devices based on the tBP complexes **2a**/**2b**, as a consequence of the higher redox potential of this redox couple.

The ability of complexes, such as **1a**, to react with monodentate ligands opens a new avenue in DSC electrolyte research. That is, fine-tuning of the redox potential of the electrolyte through the judicious choice of the Lewis base. Moreover, complexes like **1a** are ideal model compounds for fundamental studies of recombination kinetics,[47] since different reaction driving forces can be achieved through the addition of appropriate ligands with little change in reorganization energy.

■ ASSOCIATED CONTENT

Supporting Information

Cyclic voltammogram for complexes **1a, 2a** and **3a**; electronic spectra for complexes **2a/b** and **3a/b**; crystal structure of complex **3b**, and cif files for complexes **2a**, **3a** and **3b**; pulsed light current transients for **3a/3b** and $[Co(bpy)_3]^{2+/3+}$; photovoltaic performance data at different light intensities for the devices made with **3a/3b**; and IMVS-IMPS spectroscopy of the cells made with complexes **2a/2b**, **3a/3b**, and $[Co(bpy)_3]^{2+/3+}$. This material is available free of charge via the Internet at http://pubs.acs.org.

■ AUTHOR INFORMATION

Corresponding Author

[redacted]

Notes

The authors declare no competing financial interest.

■ ACKNOWLEDGMENTS

Financial support from the Australian Research Council through the Discovery, Australian Research Fellowship and LIEF programs, the Commonwealth Scientific and Industrial Research Organization (Australia), the Australian Solar Institute, the Victorian State Government Department of Primary Industry (SERD Program, Victorian Organic Solar Cells Consortium), and Monash University is gratefully acknowledged. Valuable discussions with Torben Daeneke are gratefully acknowledged. This work was performed in part at the Melbourne Centre for Nanofabrication, an initiative partly funded by the Commonwealth of Australia and the Victorian Government. Work at Berkeley was supported by NSF Grant CHE-1111900 (J.R.L.), DOE/LBNL Grant 403801 (C.J.C.), and an NSF Graduate Research Fellowship (J.C.A.).

■ REFERENCES

(1) Zhang, C.; Dai, J.; Huo, Z.; Pan, X.; Hu, L.; Kong, F.; Huang, Y.; Sui, Y.; Fang, X.; Wang, K.; Dai, S. *Electrochim. Acta* **2008**, *53*, 5503.
(2) Nakade, S.; Makimoto, Y.; Kubo, W.; Kitamura, T.; Wada, Y. *J. Phys. Chem B* **2005**, *109*, 3488.
(3) Fabregat, F. S.; Bisquert, J. *Sol. Energy Mater. Sol. Cells* **2005**, *87*, 117.
(4) Krüger, J.; Plass, R.; Cevey, L.; Piccirelli, M.; Grätzel, M. *Appl. Phys. Lett.* **2001**, *2085*, 10.
(5) Nakade, S.; Kanzaki, T.; Kubo, W.; Kitamura, T.; Wada, Y.; Yanagida, S. *J. Phys. Chem B* **2005**, *109*, 3480.
(6) Bach, U.; Tachibana, Y.; Moser, J.-E.; Haque, S. A.; Durrant, J. R.; Grätzel, M.; Klug, D. R. *J. Am. Chem. Soc.* **1999**, *121*, 7445.
(7) Boschloo, G.; Haeggman, L.; Hagfeldt, A. *J. Phys. Chem B* **2006**, *110*, 13144.
(8) Huang, S. Y.; Schlichtho, G.; Nozik, A. J.; Grätzel, M.; Frank, A. J. *J. Phys. Chem B* **1997**, *101*, 2576.
(9) Nazeeruddin, M. K.; Kay, A.; Mueller, E.; Liska, P.; Vlachopoulos, N.; Grätzel, M. *J. Am. Chem. Soc.* **1993**, *115*, 6382.
(10) Kusama, H.; Orita, H.; Sugihara, H. *Langmuir* **2008**, *24*, 4411.
(11) Daeneke, T.; Uemura, Y.; Duffy, N. W.; Mozer, A. J.; Koumura, N.; Bach, U.; Spiccia, L. *Adv. Mater.* **2012**, *24*, 1222.
(12) Daeneke, T.; Kwon, T.-H.; Holmes, A. B.; Duffy, N. W.; Bach, U.; Spiccia, L. *Nature Chem.* **2011**, *3*, 211.
(13) Daeneke, T, A.; Mozer, A. J.; Kwon, T.-H.; Holmes, A. B.; Duffy, N. W.; Bach, U.; Spiccia, L. *Energy Environ. Sci.* **2012**, *5*, 7090.
(14) Bai, Y.; Yu, Q.; Cai, N.; Wang, Y.; Zhang, M.; Wang, P. *Chem. Commun.* **2011**, *47*, 4376.
(15) Teng, C.; Yang, X.; Yuan, C.; Li, C.; Chen, R.; Tian, H.; Li, S.; Hagfeldt, A.; Sun, L. *Org. Lett.* **2009**, *11*, 5542.
(16) Liu, J.; Zhang, J.; Xu, M.; Zhou, D.; Jing, X.; Wang, P. *Energy Environ. Sci.* **2011**, *4*, 3021.
(17) Tian, H.; Yu, Z.; Hagfeldt, A.; Kloo, L.; Sun, L. *J. Am. Chem. Soc.* **2011**, *133*, 9413.
(18) Rowley, J. G.; Farnum., H. B.; Ardo, S.; Meyer, J.G. . *J. Phsy. Chem. Lett.* **2010**, *1*, 3132.
(19) Yum, J.-H.; Baranoff, E.; Kessler, F.; Moehl, T.; Ahmad, S.; Bessho, T.; Marchioro, A.; Ghadiri, E.; Moser, J.-e.; Yi, C.; Nazeeruddin, K.; Grätzel, M. *Nature Commun.* **2012**, *3*, 631.
(20) Wang, M.; Chamberland, N.; Breau, L.; Humphry-baker, R.; Zakeeruddin, S. M.; Grätzel, M. *Nature Chem.* **2010**, *2*, 385.
(21) Cheng, M.; Yang, X.; Li, S.; Sun, L. *Energy Environ. Sci.* **2012**, *5*, 6290.
(22) Liu, J.; Zhang, J.; Xu, M.; Zhou, D.; Wang, P. *Energy Environ. Sci.* **2011**, *4*, 3021.
(23) Bai, Y.; Zhang, J.; Zhou, D.; Wang, Y.; Zhang, M.; Wang, P. *J. Am. Chem. Soc.* **2011**, *133*, 11442.
(24) Feldt, S. M.; Wang, G.; Boschloo, G.; Hagfeldt, A. *J. Phys. Chem. C* **2011**, *115*, 21500.
(25) Kavan, L.; Yum, J.-H.; Grätzel, M. *Nano Lett.* **2011**, *11*, 5501.
(26) Feldt, S. M.; Gibson, E. A.; Gabrielsson, E.; Sun, L.; Boschloo, G.; Hagfeldt, A. *J. Am. Chem. Soc.* **2010**, *132*, 16714.
(27) Cazzanti, S.; Caramori, S.; Argazzi, R.; Elliott, C. M.; Bignozzi, C. A.; Chimica, D.; Borsari, V. L. *J. Am. Chem. Soc.* **2006**, *128*, 9996.
(28) Moser, J. E.; Zakeeruddin, S. M.; Nazeeruddin, M. K.; Grätzel, M. *J. Phys. Chem. B* **2001**, *105*, 10461.
(29) Sapp, S. A.; Elliott, C. M.; Contado, C.; Caramori, S.; Bignozzi, C. A. *J. Am. Chem. Soc.* **2002**, *124*, 11215.
(30) Yella, a.; Lee, H.-W.; Tsao, H. N.; Yi, C.; Chandiran, a. K.; Nazeeruddin, M. K.; Diau, E. W.-G.; Yeh, C.-Y.; Zakeeruddin, S. M.; Grätzel, M. *Science* **2011**, *334*, 629.
(31) Hamann, T. W. *Dalton Trans.* **2012**, *41*, 3111.
(32) Weaver, M. J.; Yee, E. L. *Inorg. Chem.* **1980**, *19*, 1936.
(33) Sutin, N. *Acc. Chem. Res.* **1982**, *15*, 275.
(34) Marcus, R. A. *Annu. Rev. Phys. Chem.* **1964**, *15*, 155.
(35) Bechlars, B.; Alessandro, D. M. D.; Jenkins, D. M.; Iavarone, A. T.; Glover, S. D.; Kubiak, C. P.; Long, J. R. *Nature Chem.* **2010**, *2*, 362.
(36) Zadrozny, J. M.; Freedman, D. E.; Jenkins, D. M.; Harris, T. D.; Iavarone, A. T.; Mathoniere, C.; Clerac, R.; Long, J. R. *Inorg. Chem.* **2010**, *49*, 8886.
(37) Sheldrick, G. M. *Acta Crystallogr., Sect. A* **2008**, *64*, 112.
(38) Tsao, H. N.; Burschka, J.; Yi, C.; Kessler, F.; Nazeeruddin, M. K.; Grätzel, M. *Energy Environ. Sci.* **2011**, *4*, 4921.
(39) Sun, Y.; Bigi, J. P.; Piro, N. A.; Tang, M. L.; Long, J. R.; Chang, C. J. *J. Am. Chem. Soc.* **2011**, *133*, 9212.
(40) Karunadasa, H. I.; Chang, C. J.; Long, J. R. *Nature* **2010**, *464*, 1329.
(41) Endicott, J. F.; Brubaker, G. R.; Ramasami, T.; Kumar, K.; Dwarakanath, K.; Cassel, J.; Johnson, D. *Inorg. Chem.* **1983**, *22*, 3754.
(42) Yao, J.-C.; Ma, L.-F.; Yao, F-J. *Z. Kristallogr.—New Cryst. Struct.* **2005**, *220*, 483.
(43) Du, M.; Zhao, X.-J.; Cai, H. *Z. Kristallogr.—New Cryst. Struct.* **2004**, *219*, 463.
(44) Goldsmith, C. R.; Jonas, R. T.; Cole, A. P.; Stack, T. D. P. *Inorg. Chem.* **2002**, *41*, 4642.
(45) Kim, H.-S.; Ko, S.-B.; Jang, I.-H.; Park, N.-G. *Chem. Commun.* **2011**, *47*, 12637.
(46) Tsao, H. N.; Yi, C.; Moehl, T.; Yum, J.-H.; Zakeeruddin, S. M.; Nazeeruddin, M. K.; Grätzel, M. *ChemSusChem* **2011**, *4*, 591.
(47) Ondersma, J. W.; Hamann, T. W. *J. Am. Chem. Soc.* **2011**, *133*, 8264.
(48) Devries, M. J.; Pellin, M. J.; Hupp, J. T. *Langmuir* **2010**, *26*, 9082.
(49) Wang., Z.-S.; Koumura., N.; Cui., Y.; Takahashi, M.; Sekiguchi., H.; Mori., A.; Kubo., T.; Furube., A.; Hara., K. *Chem. Mater.* **2008**, *20*, 3993.

Supporting Information for:
A New Direction in Dye-Sensitized Solar Cells Redox Mediator Development: *In-Situ* Fine-Tuning of the Cobalt(II)/(III) Redox Potential through Lewis Base Interactions

Muhammad K. Kashif[a], Jordan C. Axelson[b], Noel Duffy[c], Craig M. Forsyth[d], Christopher J. Chang[e], Jeffrey R. Long[b], Leone Spiccia[*d] and Udo Bach[*a,f,g]

KEYWORDS. Dye-sensitized solar cell, redox mediators, cobalt(II)/(III) pentapyridyl complexes, Lewis base interactions, tuning redox potentials

Corresponding Authors:
leone.spiccia@monash.edu
udo.bach@monash.edu

[a]Department of Materials Engineering, Monash University, Victoria 3800, Australia
[b]Department of Chemistry, University of California, Berkeley, California 94720-1460, United States
[c] Commonwealth Scientific and Industrial Research Organization, Energy Technology, Clayton South, Victoria 3169, Australia
[d]School of Chemistry, Monash University, Victoria 3800, Australia
[e]Department of Chemistry and the Howard Hughes Medical Institute, University of California, Berkeley, and Chemical Sciences Division, Lawrence Berkeley National Laboratory, Berkeley, California, 94720, United States
[f]Commonwealth Scientific and Industrial Research Organization, Materials Science and Engineering, Clayton South, Victoria 3169, Australia
[g]Melbourne Centre for Nanofabrication, 151 Wellington Road, Clayton, Victoria 3168, Australia

Cyclic voltammogram of $[Co(PY5Me_2)(X)](OTf)_2$

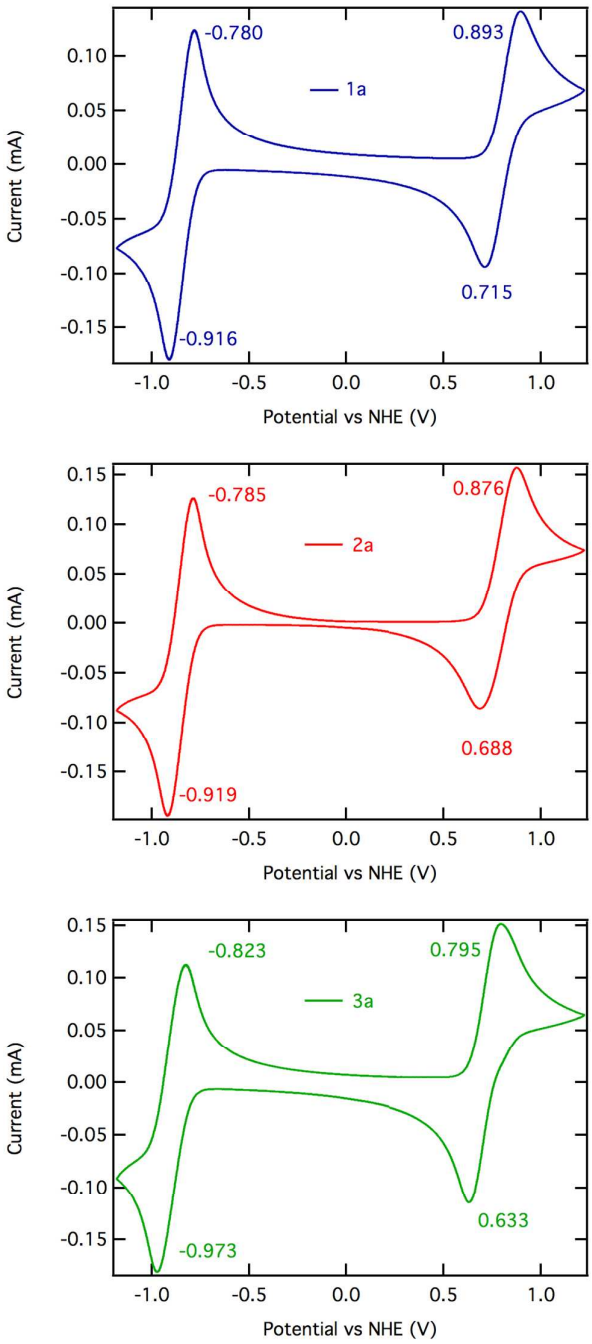

Figure S1: Cyclic voltammogram of $[Co(PY5Me_2)(MeCN)](OTf)_2$ **(1a)**, $[Co(PY5Me_2)(tBP)](OTf)_2$ **(2a)**, $[Co(PY5Me_2)(NMBI)](OTf)_2$ **(3a)** measured using a 10 mM solution in MeCN on a glassy carbon disk electrode and 100 mM $(Bu_4N)PF_6$ as supporting electrolyte at a scan rate of 100 mV/sec.

Electronic Spectra of Complexes 1a-3a

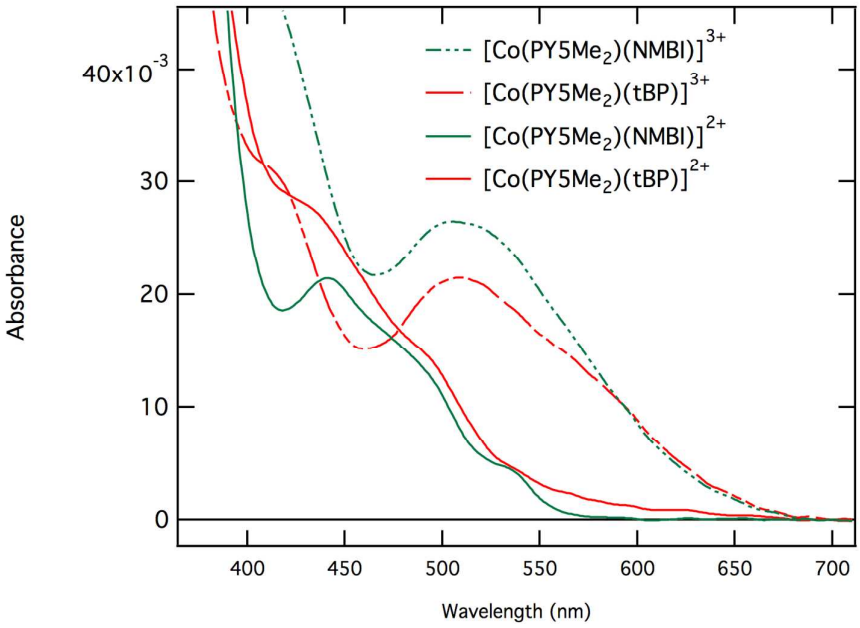

Figure S2: UV-Vis spectra of **2a**, **2b**, **3a** and **3b** measured for a 5 mM MeCN solutions of each complex (1 cm path length cuvette).

Crystal Structures of 2a and 3a

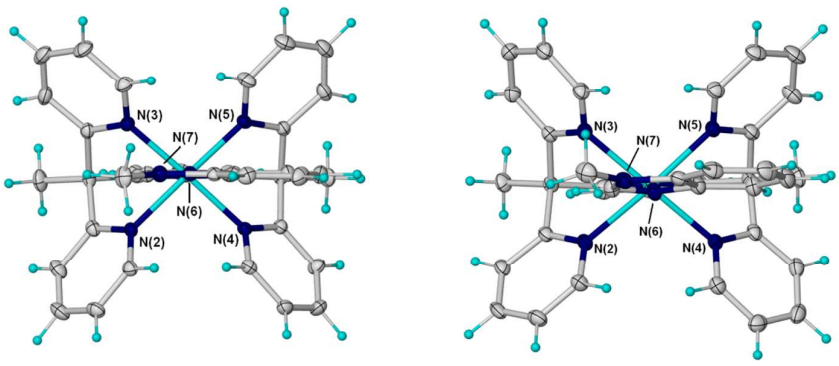

Figure S3. Top view of $[Co(PY5Me_2)(tBP)]^{2+}$ (**2a** cation) and $[Co(PY5Me_2)(NMBI)]^{2+}$ cations (**3a** cation) with pale blue, grey and dark blue spheres representing Co, C, and N respectively. The O_3SCF_3 anions and solvent MeCN molecules have been omitted for clarity. The complexes are highly symmetrical along the PY1-Me_2 and axial ligand (tBP and NMBI) axis.

Crystal Structure of $[Co(PY5Me_2)(NMBI)](TFSI)_3 \cdot 3(CH_2Cl_2)$ (3b)

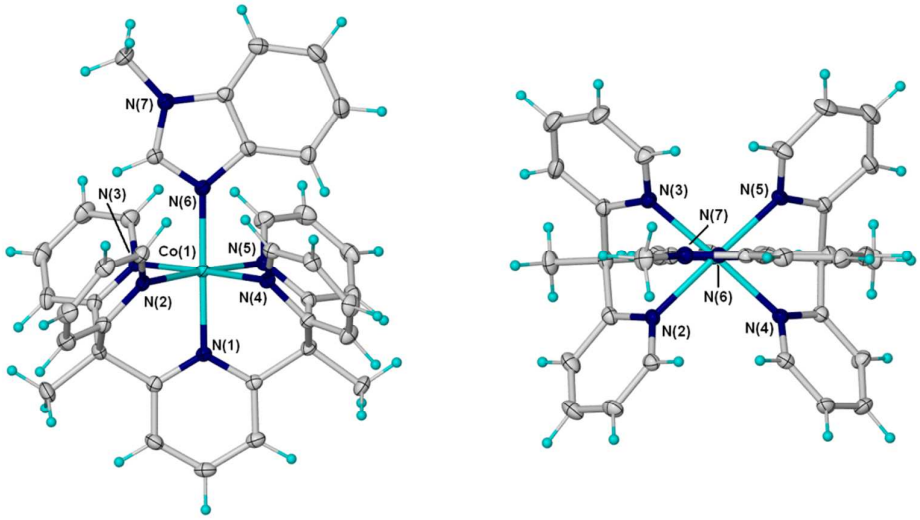

Figure S4. View of the $[Co(PY5Me_2)(NMBI)]^{2+}$ cation of $[Co(PY5Me_2)(NMBI)](TFSI)_3 \cdot 3(CH_2Cl_2)$ (**3b**) with non-hydrogen atoms represented by 50% thermal ellipsoids and hydrogen atoms as spheres of arbitrary size; the counter anions and lattice solvent molecules have been omitted for clarity.

Table S1. Tabulated photovoltaic performance data of devices made with the redox couple **3a/b** and the MK2 dye. All the devices are measured at given simulated sunlight intensities.

Electrolyte[b]	Intensity	V_{OC} (mV)	J_{SC} ($mAcm^{-2}$)	*FF*	η (%)
3a/3b	100	940±1	11.8±0.4	0.77±0.01	8.4±0.3
	40	909±1	4.6±0.5	0.78±0.02	8.9±0.2
	10	862±2	1.4±0.4	0.80±0.02	9.2±0.2

[a]Double-layer TiO_2 films (1 µm mesoporous TiO_2 (30 nm) and 2 µm scattering TiO_2 (400 nm)) were used for the construction of all DSCs. 0.5 µm thick PEDOT was used as counter electrode, which was grown electrochemically on FTO using a 20 mM solution of EDOT monomer in acetonitrile and 100 mM LiTFSI as supporting electrolyte. IV characteristic data is averaged for three DSCs. [b]The electrolyte consists of Co^{II}, 0.2 M, Co^{III} 0.75 M, lithium trifluoromethanesulfonimide (LiTFSI) 0.1 M.

Pulsed Light Current Transients

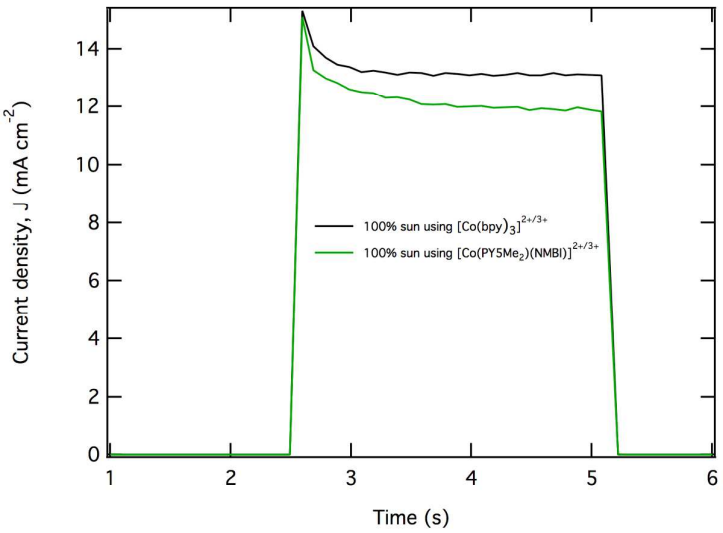

Figure S5: Photocurrent dynamics during a 2.5 sec 'on'-stage under simulated sunlight (AM 1.5G, 1,000 W/cm^2).

IMVS-IMPS Spectroscopy of the Devices

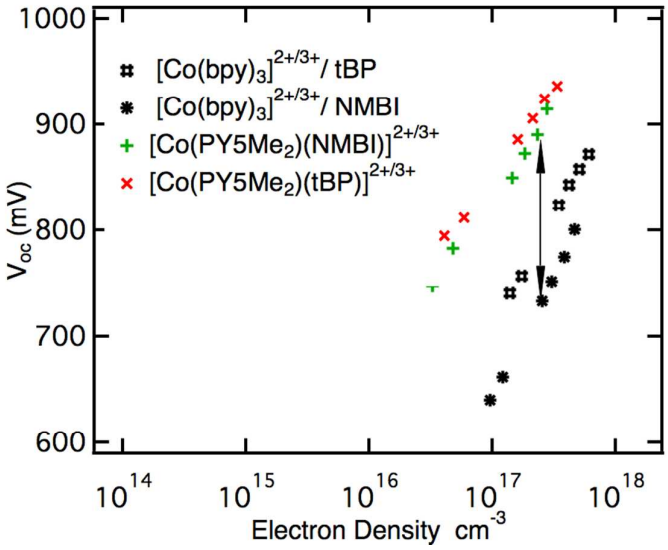

Figure S6. Extracted charge per film area vs open circuit voltage. Measured by IMVS and charge extraction method for MK2-sensitized DSCs. The devices were constructed using 2 μm thick mesoporous TiO_2 (30 nm) films and filled with corresponding redox shuttle (explained in graph). The electrolyte concentration was consistent as explained in the Table 2. The average diffusion length (L_n) was estimated to be 3.4 μm from $[T_n \times D_n]^{1/2}$, so it is expected that the charge collection at short circuit is efficient.

Chapter 4

Stable Dye-Sensitized Solar Cell Electrolytes Based on Cobalt(II)/(III) Complexes of a Hexadentate Pyridyl Ligand

Monash University

Declaration for Thesis Chapter [4]

Declaration by candidate

In the case of Chapter [4], the nature and extent of my contribution to the work was the following:

Nature of contribution	Extent of contribution (%)
Synthesis of the Co-complexes and characterisation, fabrication of the solar cells, IV-and electrochemical data collection, results interpretation, preparation and editing of the manuscript.	65 %

The following co-authors contributed to the work. If co-authors are students at Monash University, the extent of their contribution in percentage terms must be stated:

Name	Nature of contribution	Extent of contribution (%) for student co-authors only
Michael Nippe	Synthesis of the ligand and Cobalt(II) complex	N/A
Noel W. Duffy	Helping with IMVS-IMPS	N/A
Craig M. Forsyth	Helping with crystallography	N/A
Christoper J. Chang	Experimental design and editting	N/A
Jeffrey R. Long	Experimental design and editting	N/A
Leone Spiccia	Experimental design, planning, drafting and editing	N/A
Udo Bach	Experimental design, planning, drafting and editing	N/A

The undersigned hereby certify that the above declaration correctly reflects the nature and extent of the candidate's and co-authors' contributions to this work*.

Candidate's Signature	[redacted]	**Date** 30/08/2013
Main Supervisor's Signature	[redacted]	**Date** 30/08/2013

Dye-Sensitized Solar Cells

DOI: 10.1002/anie.201300070

Stable Dye-Sensitized Solar Cell Electrolytes Based on Cobalt(II)/(III) Complexes of a Hexadentate Pyridyl Ligand**

Muhammad K. Kashif, Michael Nippe, Noel. W. Duffy, Craig M. Forsyth, Christopher J. Chang, Jeffrey R. Long,* Leone Spiccia,* and Udo Bach**

Dye-sensitized solar cells (DSCs) can be fabricated from low-cost components with simple high-throughput printing techniques thereby providing a viable alternative to conventional photovoltaics.[1] A recent step-change in DSC research has been the successful application of transition-metal complexes (e.g., $[Co(bpy)_3]^{2+/3+}$, bpy = 2,2′-bipyridine), organometallics (e.g., ferrocene), and organic compounds as redox mediators,[2,3] replacing formerly used corrosive iodine/iodide electrolytes while maintaining impressive energy conversion efficiencies.[4]

An attractive feature of cobalt complexes, in particular, is that the structure, electronic properties, and redox chemistry can be tuned by varying the ligand environment. In this respect, the type and number of donor atoms (denticity) that the ligands used to form the cobalt coordination sphere is of paramount importance. First, for related families of ligands, such as polypyridyls, a higher denticity results in a higher overall stability constant (β) of the complex through the chelate effect.[5] The stability of complexes is important when contemplating their application in many fields, including renewable energy research focusing on DSCs and solar-driven hydrogen generation from water. Dissociation of the bpy ligands from $[Co(bpy)_3]^{2+}$ was recently identified as a significant issue for its applicability as a catalyst in photo-electrochemical water splitting devices, which was overcome by replacing the bpy ligands with a pentadentate ligand.[6] Secondly, the denticity of the ligands will affect the reorganization energies associated with electron transfer processes involving the $Co^{2+/3+}$ redox states,[7] and will influence the rates of important charge-transfer steps, such as charge recombination and dye regeneration. The latter will affect the driving force required for efficient dye regeneration and therefore ultimately the maximum obtainable DSC efficiency.[8,9]

To date only a small number of cobalt complexes have been tested in DSCs, with the majority based on bidentate ligands such as bpy and phen (1,10-phenanthroline) and their derivatives. In a recent article about applying $Co^{II/III}$-tpy complexes (tpy = 2,2′;6′,2″-terpyridine) as DSC redox mediators, Grätzel and co-workers highlight the importance of ligand substitution to achieve higher open-circuit photovoltage (V_{OC}).[3g] We recently reported a study of DSCs employing cobalt complexes based on a combination of a pentadentate ligand (2,6-bis(1,1-bis(2-pyridyl)ethyl)pyridine, $PY5Me_2$) and a weakly bound monodentate ligand. We were able to fine-tune the redox potential of the complex by choosing monodentate ligands with varying Lewis basicity, thereby creating the opportunity to adjust the driving force for dye regeneration.[10] Here we report for the first time the application of the Co complex of a hexapyridyl ligand (6,6′-bis(1,1-di(pyridin-2-yl)ethyl)-2,2′-bipyridine, bpyPY4) as a redox mediator in DSCs, and compare its photovoltaic performance and stability to the reference mediator $[Co(bpy)_3]^{2+/3+}$ (Co-bpy). A major motivation for using a hexadentate ligand was to develop a redox shuttle based on complexes with very high thermodynamic stability.

[*] M. K. Kashif, Prof. Dr. U. Bach
Department of Materials Engineering, Monash University
Clayton, Victoria 3800 (Australia)
[redacted]
Dr. M. Nippe, Prof. Dr. J. R. Long
Department of Chemistry, University of California
Berkeley, CA 94720-1460 (USA)
[redacted]
Prof. Dr. C. J. Chang
Departments of Chemistry and Molecular and Cell Biology
and the Howard Hughes Medical Institute
University of California, Berkeley, CA 94720-1460 (USA)
[redacted]
Dr. M. Nippe, Prof. Dr. C. J. Chang, Prof. Dr. J. R. Long
Materials or Chemical Sciences Division
Lawrence Berkeley National Laboratory
Berkeley, CA 94720-1460 (USA)
Dr. C. M. Forsyth, Prof. Dr. L. Spiccia
Department of Chemistry, Monash University
Clayton, Victoria 3800 (Australia)
[redacted]
Prof. Dr. U. Bach
Melbourne Centre for Nanofabrication
151 Wellington Road, Clayton, Victoria 3168 (Australia)
and
CSIRO, Materials Science and Engineering
Clayton South, Victoria 3169 (Australia)
N. W. Duffy
CSIRO, Energy Technology
Clayton South, Victoria 3169 (Australia)

[**] The authors acknowledge the Australian Research Council for providing equipment and fellowship support and the Australian Solar Institute, the Victorian State Government (DBI-VSA and DPI-ETIS) for financial support. The CSIRO is acknowledged for providing support through an OCE Science Leader position (UB). Part of the synthetic work was carried out at the Joint Center for Artificial Photosynthesis supported by the Office of Science of the U.S. Department of Energy under award number DE-SC0004993.

Supporting information for this article, including details of the synthesis, device characterization, and crystal structure determination, is available on the WWW under http://dx.doi.org/10.1002/anie.201300070.

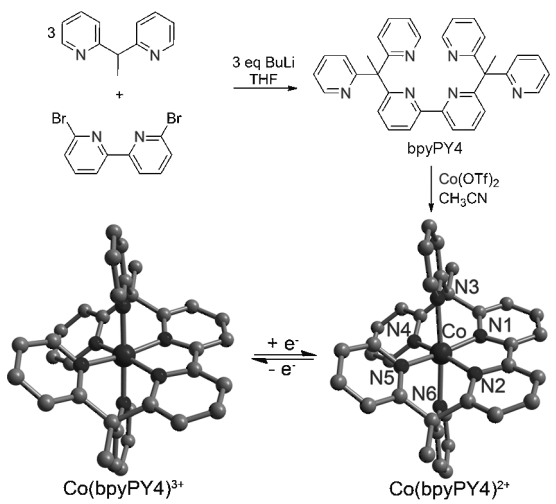

Figure 1. Synthetic route to bpyPY4 and molecular structures of $[Co(bpyPY4)]^{2+/3+}$ in crystals of **1a**/**1b**.

Full details of the synthesis and characterization of bpyPY4, $[Co(bpyPY4)](CF_3SO_3)_2$ (**1a**) and $[Co(bpyPY4)](CF_3SO_3)_3$ (**1b**) (CF_3SO_3 = trifluoromethanesulfonate) are in the Supporting Information. In brief, the new bpyPY4 ligand was synthesized through the reaction of deprotonated 1,1-bis(2-pyridyl)ethane and 6,6′-dibromo-2,2′-dipyridyl (Figure 1). Complexation of bpyPY4 with $Co(CF_3SO_3)_2$ in acetonitrile (MeCN) and subsequent crystallization from MeCN/Et_2O yielded dark red crystals of **1a**. Oxidation of **1a** with stoichiometric amounts of $Ag(CF_3SO_3)$ afforded **1b**, which could be crystallized by Et_2O diffusion into a MeCN solution. The results of the crystal structure analyses are depicted in Figures 1, S1, S2, and Table 1. Comparison of the

Table 1: Metal ligand bond lengths in **1a** and **1b**.

Compound	**1a** [Å]	**1b** [Å]
Co–N1	1.926(2)	1.929(3)
Co–N2	1.941(4)	1.917(3)
Co–N3	2.216(3)	1.952(3)
Co–N4	1.965(4)	1.944(3)
Co–N5	1.955(4)	1.940(3)
Co–N6	2.235(3)	1.943(3)

Co–N bond lengths for cobaltous **1a** and cobaltic **1b** reveals that the major change upon oxidation of the Co^{II} to the Co^{III} complex is a contraction along the N3–Co–N6 axis, with relatively minor changes to the equatorial bond lengths (Table 1). In contrast, all Co–N bond lengths in $[Co(bpy)_3]^{2+/3+}$ and $[Co(PY5Me_2)NMBI]^{2+/3+}$ changed significantly.[10,11] The rigidity of the preorganized cavity of the hexadentate ligand appears to restrict structural changes upon reduction/oxidation to axial elongation/compression of the cobalt(II)/(III) coordination sphere (NMBI = *N*-methylbenzimidazole).

The cyclic voltammogram of **1a** in MeCN (0.1 M NBu_4PF_6; Figure S3) shows reversible processes centered at −170 and −90 mV vs. Fc/Fc^+ corresponding to the $[Co(bpyPY4)]^{2+/3+}$ and $[Co(bpyPY4)]^{1+/2+}$ redox reactions, respectively (Fc = ferrocene). Features observed at more negative potentials are ascribed to ligand-based reduction processes. Thus, the redox potential related to $Co^{2+/3+}$ in **1a** is calculated to be 465 mV versus the normal hydrogen electrode (NHE), whereas the corresponding redox potential for $[Co(bpy)_3]^{2+/3+}$ is 560 mV. The cathodic and anodic current responses associated with the Co-based redox processes are linearly proportional to the square root of the scan rate (ν), indicating diffusion-controlled behavior as is expected for a homogeneous system. A comparison of the redox potentials (vs. NHE) for **1a**/**1b**, $[Co(bpy)_3]^{2+/3+}$, and the $E(D/D^+)$ levels of MK2 (Figure 2) reveals that **1a**/**1b** will provide a substantial

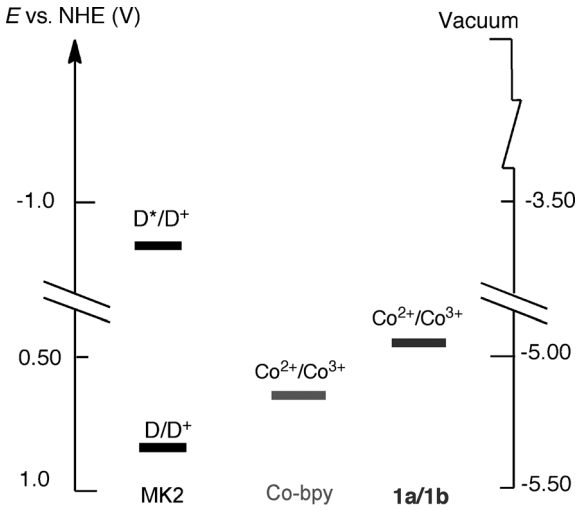

Figure 2. Energy level diagram showing the approximate redox potentials of DSC components relative to the normal hydrogen electrode (NHE) in acetonitrile.

electrochemical driving force for dye regeneration (> 400 mV). The redox properties of **1a** indicate that it is well suited for DSC electrolyte development using dyes with $E(D/D^+)$ energies ≥ 800 mV vs. NHE. In this study, MK2, a dye with a high molar extinction coefficient of 38 400 $M^{-1}cm^{-1}$ and excellent light-harvesting properties was considered a good photosensitizer for use with one-electron-transfer redox couples.[12]

The **1a**/**1b**-based electrolytes were optimized by varying the concentrations of **1a**, **1b** and the additives, NMBI and lithium bis(trifluoromethanesulfonyl)imide (LiTFSI). The data for the optimized devices are shown in Table 2. Previously, we have shown that very thin (1 μm) transparent titania films can be successfully used to harvest most of the incident light.[10] However, in this study, we have successfully applied thicker titania films, consisting of 6 μm transparent layers of 30 nm particles coated with 4 μm thick scattering layers (400 nm particles). With these 10 μm mesostructured films, an efficiency of 7.8% for the MK2/Co-bpy electrolyte combination was achieved, which is higher than reported recently (7.3%).[12a] An impressive efficiency of 8.3% was achieved for the DSCs based on the new redox couple **1a**/**1b**. A reduction in V_{OC} of 100 mV is observed for **1a**/**1b**-based

Table 2: Photovoltaic performance of DSCs assembled with the two redox couples and MK2 dye with simulated sunlight (AM 1.5 G, 1000 $W m^{-2}$).[a]

Redox couple[b]	**1a**/**1b**	Co-bpy
$E_{1/2}(Co^{2+/3+})$ [mV][c]	465	560
V_{OC} [mV]	757 ± 2	826 ± 3
J_{SC} [mA cm^{-2}]	14.7 ± 0.2	13.7 ± 0.3
FF	0.75 ± 0.02	0.69 ± 0.01
η [%]	8.3 ± 0.1	7.8 ± 0.2

[a] Double-layer TiO_2 films [6 μm mesoporous TiO_2 (30 nm) and 4 μm scattering TiO_2 (400 nm)] and a Pt counter electrode were used for the fabrication of all DSCs. The devices were measured immediately after fabrication and the average performance of at least three devices with standard deviation is provided. [b] The electrolyte consists of 0.20 M Co^{II} complex, 0.10 M of Co^{III} complex, 0.05 M of LiTFSI and 0.50 M of NMBI in pure acetonitrile (MeCN). [c] Redox potentials of the **1a** and Co-bpy are reported vs NHE.

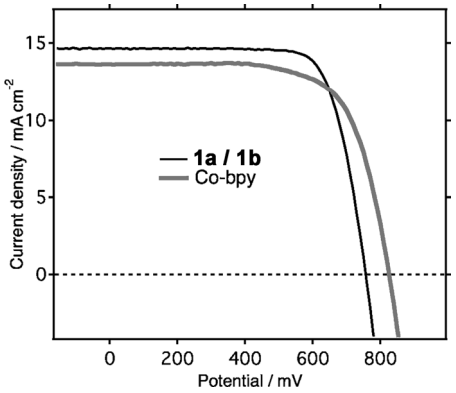

Figure 3. Current density (*J*)–potential (*V*) characteristics of the best-performing DSCs fabricated using electrolytes **1a**/**1b** and Co-bpy. For photovoltaic performance data and details on the electrolyte composition see Table 2.

devices, as compared to Co-bpy-based devices, which is in agreement with the about 100 mV difference in the $Co^{II/III}$ redox potentials of **1a** and Co-bpy.

Figure 3 shows the current density (*J*)–potential (*V*) characteristics of the best performing DSCs based on redox couples **1a**/**1b** and Co-bpy, measured under simulated air mass (AM) and 1.5 G, 1000 $W m^{-2}$. The electrolyte included NMBI as an additive. The devices employing **1a**/**1b** in the electrolyte show a higher current density (J_{SC}) and a significant increase in the fill factor (*FF*) compared to the devices based on Co-bpy, indicating that **1a**/**1b** clearly outperforms Co-bpy as a redox mediator. This is likely due to the lower electrochemical driving force for dye regeneration in case of Co-bpy ($\Delta E = 340$ mV), compared to **1a**/**1b** ($\Delta E = 435$ mV). This is in agreement with previous studies on DSCs employing cobalt mediators, where the minimum electrochemical driving force for quantitative dye regeneration was found to be around 500 mV.[3b,h] Furthermore, light soaking the devices made with **1a**/**1b** for 20 min under AM 1.5 G and 1000 $W m^{-2}$ irradiation resulted in an increase in J_{SC} and a slight decrease in V_{OC}, giving rise to an overall efficiency of 9.4% (see Table S2). Similar light-soaking effects have been previously linked to a shift in conduction band edge.[13] The incident photon-to-electron conversion efficiency (IPCE) spectra of DSCs, made using either electrolytes are comparable (see Figure S5) with a few percent higher IPCE for **1a**/**1b** resulting in a slight increase in J_{SC}.

Intensity-modulated photovoltage spectroscopy (IMVS), complemented by charge extraction measurements, was used to compare the electron lifetimes for DSCs assembled with **1a**/**1b** and Co-bpy-based electrolytes as a function of the extracted charge (Figure 4). Interestingly, the two DSCs

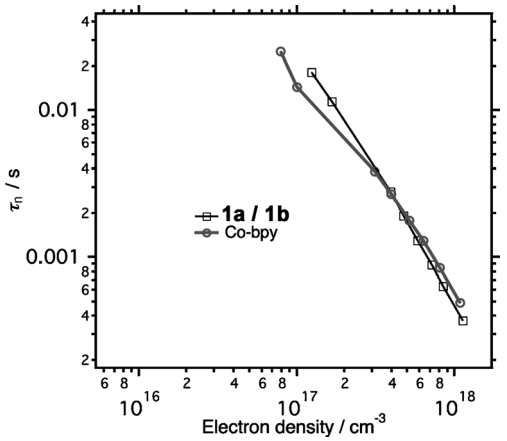

Figure 4. Electron lifetime (τ_n) determined via IMVS spectroscopy versus extracted charge for DSCs based on electrolyte **1a**/**1b** and Co-bpy. The electron density per volume of mesoporous TiO_2 film was determined by charge extraction experiments.

exhibit similar lifetimes for the electrons injected into the TiO_2 conduction band, indicating comparable charge-recombination rates for both electrolyte systems.

The evolution of DSC performance for devices based on **1a**/**1b** and Co-bpy redox mediators was also tested under continuous simulated full sun irradiation. In this comparison, we also studied the effect of additives on device stability by using two different Lewis base additives. Keeping in mind that the Lewis bases added to the electrolytes may interact with the polypyridyl complexes, a comparatively milder Lewis base, *p*-trifluoromethylpyridine (TFMP), was examined as an electrolyte additive in parallel to NMBI, which is commonly applied in iodide/triiodide-based DSCs to improve the long-term stability.[14] In choosing TFMP, the excellent thermal, hydrolytic, and oxidative stability of fluorinated aromatic hydrocarbons and the relatively small size of the $-CF_3$ group were considered beneficial features.[15] The *J*–*V* results for cells fabricated using **1a**/**1b** and Co-bpy using TFMP as an additive are shown in Table S1 and Figure S5. The addition of TFMP to Co-bpy leads to a green precipitate and, as a consequence, the devices made with this electrolyte show poor performance reproducibility and very poor stability. In contrast, no precipitation was observed in the **1a**/**1b**/TFMP electrolytes and the DSCs gave comparable efficiencies to the **1a**/**1b**/NMBI electrolyte system.

Preliminary stability tests were then carried out to compare devices with NMBI and TFMP added to **1a**/**1b**

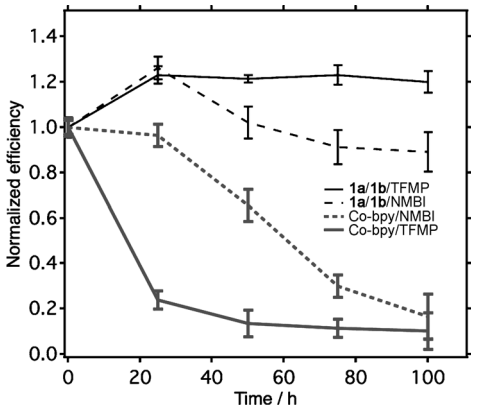

Figure 5. Normalized efficiencies of the devices under full sun irradiation aging experiment is shown with a 400 nm UV-cut off filter. Two Lewis bases, NMBI and TFMP, were alternatively used with **1a**/**1b** and Co-bpy (4:1, MeCN:VN).

and Co-bpy-based electrolytes abbreviated **1a**/**1b**/NMBI, **1a**/**1b**/TFMP, Co-bpy/NMBI, and Co-bpy/TFMP (Figure 5).

A mixture of acetonitrile and valeronitrile (4:1) was used to reduce the volatility of the electrolyte. An environmental chamber equipped with a Hg lamp was automated to maintain the DSCs under continuous full sun irradiation at 45% humidity and a device temperature of 25–30°C to test the devices. Figure 5 shows the normalized efficiencies of the DSCs over a period of 100 h. DSCs based on electrolyte **1a**/**1b** clearly outperformed those assembled with the reference mediator Co-bpy, showing a >20% performance increase over the first 24 h of continuous illumination. When TFMP was used, the DSCs based on **1a**/**1b** initially showed a 20% increase in performance, which maintained across the full 100 h testing period. In the case of NMBI, the DSCs showed the same initial improvement in performance but there was a gradual decrease and stabilization at about 90% of the original value after 100 h testing. Over the 100 h period, a decrease in performance of over 80% was observed for DSCs based on the Co-bpy electrolyte and NMBI. In the presence of TFMP, this performance decrease was even more pronounced, with a drop of 76% observed after the first 24 h illumination period. In general, the Co-bpy electrolyte was found to be incompatible with TFMP, leading to a green precipitate and poor device performance.

In conclusion, we have prepared and structurally characterized the Co^{II} and Co^{III} complexes of a new hexadentate polypyridyl ligand and, for the first time, applied such types of complexes as redox mediators in DSC electrolytes. The devices constructed with these complexes were found to outperform the prototypical Co-bpy redox mediator both in terms of overall efficiency and stability under full sun irradiation conditions. The design of multidentate ligands leading to very stable cobalt complexes under DSC test conditions is likely to become a major area of endeavor in the quest for high-performance cobalt-based DSC electrolytes that meet the stringent stability requirements of commercial applications. For further optimization of the cobalt-based redox mediators, studies are underway to evaluate the minimum electrochemical energy required for quantitative dye regeneration in line with our previous work on ferrocene derivatives.[16]

Received: January 4, 2013
Revised: March 19, 2013
Published online: April 18, 2013

Keywords: cobalt electrolytes · dye-sensitized solar cells · energy conversion · ligand engineering

[1] a) M. Graetzel, R. A. J. Jenssen, D. B. Mitzi, E. H. Sargent, *Nature* **2012**, *488*, 304–312; b) F. Kato, A. Kikuchi, T. Okuyama, K. Oyaizu, H. Nishide, *Angew. Chem.* **2012**, *124*, 10324–10327; *Angew. Chem. Int. Ed.* **2012**, *51*, 10177–10180.

[2] a) S. Powar, T. Daeneke, M. T. Ma, D. Fu, N. W. Duffy, G. Gotz, M. Weidelener, A. Mishra, P. Baeuerle, L. Spiccia, U. Bach, *Angew. Chem.* **2013**, *125*, 630–633; *Angew. Chem. Int. Ed.* **2013**, *52*, 602–605; b) T. Daeneke, Y. Uemura, N. W. Duffy, A. J. Mozer, N. Koumura, U. Bach, L. Spiccia, *Adv. Mater.* **2012**, *24*, 1222–1225; c) T. Daeneke, T. H. Kwon, A. B. Holmes, N. W. Duffy, U. Bach, L. Spiccia, *Nat. Chem.* **2011**, *3*, 211–215; d) J. Liu, J. Zhang, M. Xu, D. Zhou, X. Jing, P. Wang, *Energy Environ. Sci.* **2011**, *4*, 3021–3029; e) H. Tian, Z. Yu, A. Hagfeldt, L. Kloo, L. Sun, *J. Am. Chem. Soc.* **2011**, *133*, 9413–9422; f) J.-H. Yum, E. Baranoff, F. Kessler, T. Moehl, S. Ahmad, T. Bessho, A. Marchioro, E. Ghadiri, J.-E. Moser, C. Yi, M. K. Nazeeruddin, M. Grätzel, *Nat. Commun.* **2012**, *3*, 631–638; g) M. Wang, N. Chamberland, L. Breau, J.-E. Moser, R. Humphry-Baker, S. M. Zakeeruddin, M. Grätzel, *Nature Chem.* **2010**, *2*, 385–389; h) M. Cheng, X. Yang, S. Li, L. Sun, *Energy Environ. Sci.* **2012**, *5*, 6290–6293.

[3] a) Y. Bai, J. Zhang, D. Zhou, Y. Wang, M. Zhang, P. Wang, *J. Am. Chem. Soc.* **2011**, *133*, 11442–11445; b) S. M. Feldt, G. Wang, G. Boschloo, A. Hagfeldt, *J. Phys. Chem. C* **2011**, *115*, 21500–21507; c) S. M. Feldt, E. A. Gibson, E. Gabrielsson, L. Sun, G. Boschloo, A. Hagfeldt, *J. Am. Chem. Soc.* **2010**, *132*, 16714–16724; d) S. Cazzanti, S. Caramori, R. Argazzi, C. M. Elliott, C. A. Bignozzi, *J. Am. Chem. Soc.* **2006**, *128*, 9996–9997; e) H. Nusbaumer, J. E. Moser, S. M. Zakeeruddin, M. K. Nazeeruddin, M. Grätzel, *J. Phys. Chem. B* **2001**, *105*, 10461–10464; f) S. A. Sapp, C. M. Elliott, C. Contado, S. Caramori, C. A. Bignozzi, *J. Am. Chem. Soc.* **2002**, *124*, 11215–11222; g) K. B. Aribia, T. Moehl, S. M. Zakeeruddin, M. Graetzel, *Chem. Sci.* **2013**, *4*, 454–459; h) K. C. D. Robson, K. Hu, G. J. Meyer, C. P. Berlinguette, *J. Am. Chem. Soc.* **2013**, *135*, 1961–1971.

[4] A. Yella, H.-W. Lee, H. N. Tsao, C. Yi, A. K. Chandiran, M. K. Nazeeruddin, E. W.-G. Diau, C.-Y. Yeh, S. M. Zakeeruddin, M. Grätzel, *Science* **2011**, *334*, 629–634.

[5] a) R. M. Izatt, K. Pawlak, J. S. Bradshaw, R. L. Bruening, *Chem. Rev.* **1991**, *91*, 1721–2085; b) R. D. Hancock, A. E. Martell, *Chem. Rev.* **1989**, *89*, 1875–1914.

[6] a) H. I. Karunadasa, C. J. Chang, J. R. Long, *Nature* **2010**, *464*, 1329–1333; b) Y. Sun, J. P. Bigi, N. A. Piro, M. L. Tang, J. R. Long, C. J. Chang, *J. Am. Chem. Soc.* **2011**, *133*, 9212–9215; c) H. I. Karunadasa, E. Montalvo, Y. Sun, M. Majda, J. R. Long, C. J. Chang, *Science* **2012**, *335*, 698–702; d) M. Guttentag, A. Rodenberg, C. Bachmann, A. Senn, P. Hamm, R. Alberto, *Dalton Trans.* **2013**, *42*, 334–337.

[7] J. F. Endicott, G. Brubaker, T. Ramasami, K. Kumar, K. Dwarakanath, J. Cassel, D. Johnson, *Inorg. Chem.* **1983**, *22*, 3754–3762.

[8] R. A. Marcus, *Annu. Rev. Phys. Chem.* **1964**, *15*, 155–196.

[9] B. E. Hardin, H. J. Snaith, M. D. McGehee, *Nat. Photonics* **2012**, *6*, 162–169.

[10] M. K. Kashif, J. C. Axelson, N. W. Duffy, C. M. Forsyth, C. J. Chang, J. R. Long, L. Spiccia, U. Bach, *J. Am. Chem. Soc.* **2012**, *134*, 16646 – 16653.
[11] J. C. Yao, L.-F. Ma, F.-J. Yao, *Z. Kristallogr. New Cryst. Struct.* **2005**, *220*, 483 – 485.
[12] a) T. N. Mukarami, N, Koumura, T. Uchiyama, Y. Uemeura, K. Obuchi, N. Masaki, M. Kimura, S. Mori, *J. Mater. Chem. A* **2013**, *1*, 792 – 798; b) Z.-S. Wang, N. Koumura, Y. Cui, M. Takahashi, H. Sekiguchi, A. Mori, T. Kubo, A. Furube, K. Hara, *Chem. Mater.* **2008**, *20*, 3993 – 4003.
[13] a) A. Listorti, C. Creager, P. Sommeling, J. Kroon, E. Palomares, A. Fornelli, B. Breen, P. R. F. Barnes, J. R. Durrant, C. Law, B. O'Regan, *Energy Environ. Sci.* **2011**, *4*, 3494 – 3501; b) S. Guarnera, A. Bonucci, S. Perissinotto, R. Giannantonio, G. Lanzani, A. Petrozza, *RSC Adv.* **2013**, *3*, 2163 – 2166.
[14] a) C. Zhang, J. Dai, Z. Huo, X. Pan, L. Hu, F. Kong, Y. Huang, Y. Sui, X. Fang, K. Wang, S. Dai, *Electrochim. Acta* **2008**, *53*, 5503 – 5508; b) S. Nakade, Y. Makimoto, W. Kubo, T. Kitamura, Y. Wada, S. Yanagida, *J. Phys. Chem. B* **2005**, *109*, 3488 – 3493; c) F. Fabregat-Santiago, G. Garcia-Belmont, J. Bisquert, G. Boschloo, A. Hagfeldt, *Sol. Energy Mater. Sol. Cells* **2005**, *87*, 117 – 131; d) J. Krüger, R. Plass, L. Cevey, M. Piccirelli, M. Grätzel, U. Bach, *Appl. Phys. Lett.* **2001**, *79*, 2085 – 2087; e) S. Nakade, T. Kanzaki, W. Kubo, T. Kitamura, Y. Wada, S. Yanagida, *J. Phys. Chem. B* **2005**, *109*, 3480 – 3487; f) U. Bach, Y. Tachibana, J.-E. Moser, S. A. Haque, J. R. Durrant, M. Grätzel, D. R. Klug, *J. Am. Chem. Soc.* **1999**, *121*, 7445 – 7446; g) G. Boschloo, L. Haeggman, A. Hagfeldt, *J. Phys. Chem. B* **2006**, *110*, 13144 – 13150; h) S. Y. Huang, G. Schlichthorl, A. J. Nozik, M. Grätzel, A. J. Frank, *J. Phys. Chem. B* **1997**, *101*, 2576 – 2582; i) M. K. Nazeeruddin, A. Kay, E. Mueller, P. Liska, N. Vlachopoulos, M. Grätzel, *J. Am. Chem. Soc.* **1993**, *115*, 6382 – 6390.
[15] a) M. A. García-Monforte, S. Martínez-Salvador, B. Menjón, *Eur. J. Inorg. Chem.* **2012**, 4945 – 4966; b) M. Schlosser, M. Marull, *Eur. J. Inorg. Chem.* **2003**, 1569 – 1575; c) M. J. Katz, M. J. D. Vermeer, O. K. Farha, M. J. Pellin, J. T. Hupp, *Langmuir* **2013**, *29*, 806 – 814.
[16] T. Daeneke, A. J. Mozer, Y. Uemura, S. Makuta, M. Fekete, Y. Tachibana, N. Koumura, U. Bach, L. Spiccia, *J. Am. Chem. Soc.* **2012**, *134*, 16925 – 16928.

Angewandte Chemie
Eine Zeitschrift der Gesellschaft Deutscher Chemiker

Supporting Information

69451 Weinheim, Germany

Stable Dye-Sensitized Solar Cell Electrolytes Based on Cobalt(II)/(III) Complexes of a Hexadentate Pyridyl Ligand**

Muhammad K. Kashif, Michael Nippe, Noel. W. Duffy, Craig M. Forsyth, Christopher J. Chang, Jeffrey R. Long,* Leone Spiccia,* and Udo Bach**

anie_201300070_sm_miscellaneous_information.pdf

Materials and Methods

Anhydrous solvents CH_3CN, THF, and Et_2O were purified using a commercial solvent purification system from JC-Meyer-Solvent systems (jcmeyer-solventsystems.com). 6,6'-Dibromo-2,2'-dipyridyl (3B Scientific), ethyl acetate (Fisher), CH_2Cl_2 (Fisher) and NBu_4PF_6 (Strem) were purchased and used as received. 1,1-*bis*(2-pyridyl)ethane and $Co(CF_3SO_3)_2 \cdot 2CH_3CN$ were prepared according to published procedures {B. Bechlars, D. M. D'Alessandro, David. M. Jenkins, A. T. Lavarone, S. D. Glover, C. P. kubiak, J. R. Long, *Nature Chemistry,* **2012**, *2,*362-368; M. Seitz, A. Kaiser, D. R. Powell, A. S. Borovik, O. Reiser, *Adv. Synth. Catal.* **2004**, *346*, 737-741}.

Infrared spectra were obtained on a Nicolet Avatar 360 FTIR with an attenuated total reflectance (ATR) accessory. Carbon, hydrogen, and nitrogen analyses were obtained from the Microanalytical Laboratory of the University of California, Berkeley. ^{1}H-NMR spectra were obtained using a Bruker AVQ-400 or AVB-300 instrument and peaks were referenced to residual solvent peaks. Electrospray ionization mass spectrometry (ESI-MS) measurements were performed using a quadrupole time-of-flight mass spectrometer (Q-tof Premier, Waters, Milford, MA). High-resolution mass spectrometry (HRMS) measurements were performed using an Autospec mass spectrometer (Waters). Both instruments are located in the QB3/Chemistry Mass Spectrometry Facility at UC Berkeley. Cyclic voltammograms were recorded using a BASi CV-50W potentiostat and a three-electrode setup, with glassy carbon disk (working), Pt-wire (auxiliary), and Ag/AgCl (aq) or $Ag/AgPF_6$ (non-aq) electrode (reference). The ferrocene/ferrocenium couple (640 mV vs. NHE) was used as internal standard and potentials were converted to NHE accordingly.

X-ray crystallography. Data collection was performed on single crystals coated with Paratone-N oil and mounted on Kaptan loops. The crystals were frozen under a stream of N_2 (100 K; Oxford Cryostream 700) during measurements. Data were collected using a Bruker APEX II QUAZAR diffractometer equipped with a Microfocus Sealed Source (Incoatec IμS; Mo-Ka λ = 0.71073 Å) and APEX-II detector. Raw data were integrated and corrected for Lorentz and polarization effects using Bruker APEX2 v. 2009.1.{APEX2, v. 2009 ; Bruker Analytical X-Ray Systems, Inc: Madison, WI, 2009} Absorption corrections were applied using SADABS.{Sheldrick, G. M. SADABS, Version 2.03; Bruker Analytical X-ray

Systems, Inc: Madison, WI, 2000} Space group assignments were determined by examination of systematic absences, E-statistics, and successive refinement of the structures. Structures were solved using direct methods and refined by least-squares refinement on F^2 followed by difference Fourier synthesis.{OLEX2} All hydrogen atoms were included in the final structure factor calculation at idealized positions and were allowed to ride on the neighboring atoms with relative isotropic displacement coefficients. Thermal parameters were refined anisotropically for all non-hydrogen atoms.

In the structure of Co(bpyPY4)$(CF_3SO_3)_2$, the hexadentate ligand is disordered over two positions with a occupancy ratio of 90/10 (Figure S1). This disorder could be conveniently modeled and anisotropic refinement was stable utilizing solely EADP constraints of those ligand based atoms that are involved in the disorder. Similarly, one of the triflate counter-ions shows partial disorder with 25/75 relative occupations over two positions.

Scheme S1. Synthetic route to **bpyPY4**

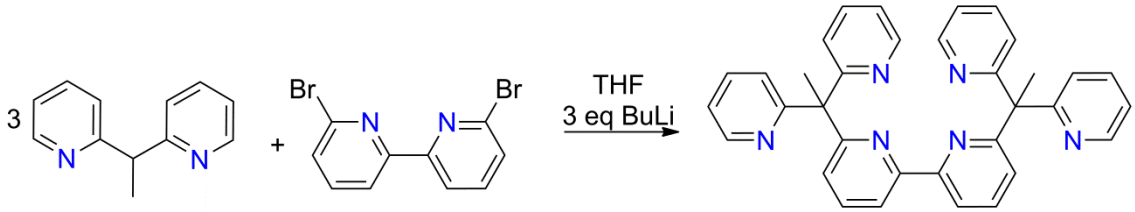

Synthesis of bpyPY4. Under a dry N_2 atmosphere, nBuLi (2.5 M in hexanes, 4.30 mL, 10.8 mmol) was added to a solution of 1,1-bis(2-pyridyl)ethane (2.00 g, 10.9 mmol) in THF (80 mL) at 0°C. After stirring for 30 min at 0°C the red mixture was allowed to warm to room temperature and stirred for an additional 60 min after which a THF (40 mL) solution of 6,6'-dibromo-2,2'-dipyridyl (1.14 g, 3.62 mmol) was added via cannula transfer. After stirring for 30 min the mixture was heated to reflux for 36 h. The reaction mixture was then allowed to cool to room temperature and quenched with H_2O (50 mL). The organic layer was separated and the aqueous layer was extracted three times with CH_2Cl_2 (60 mL). The combined organic phases were dried over $MgSO_4$, filtered, and the solvent removed under reduced pressure. The sticky white mixture was suspended in ethyl acetate (30 mL) and sonicated. The liquid was

decanted and the white solid product was then repeatedly washed with more ethyl acetate and isolated by filtration. Yield 1.39 g (74 %).
^{1}H-NMR (CD3Cl, 300 MHz, ppm): d 8.60 (4H, d, J = 3 Hz), 8.03 (2H, d, 6 Hz), 7.62-7.53 (6H, m), 7.14-7.08 (10H, m), 2.40 (6H, s). IR (neat, cm^{-1}): 1583 (m), 1563 (s), 1466 (s), 1428 (vs), 1380 (w), 1362 (w), 1293 (vw), 1276 (vw), 1155 (m), 1119 (w), 1103 (m), 1091 (m), 1064 (m), 1046 (m), 991 (m), 886 (vw), 862 (w), 799 (m), 784 (s), 776 (s), 765 (w), 745 (vs), 704 (vw), 655 (s), 629 (m), 619 (m), 604 (vw), 573 (s), 514 (w), 500 (w).

Synthesis of [Co(bpyPY4)]$(CF_3SO_3)_2$ (1a). Using a N_2 filled glove box, CH_3CN (14 mL) was added to a solid mixture of bpyPY4 (200 mg, 0.384 mmol) and $Co(CF_3SO_3)_2 \cdot 2CH_3CN$ (167 mg, 0.384 mmol). The mixture was stirred for 4 h at 60°C after which it had turned dark-red. After cooling to ambient temperature the solution was filtered through celite and layered with Et_2O. Solvent diffusion over 2 days yielded large dark-red crystals of **1a** that were washed with Et_2O and dried. Yield: 184 mg (55 %). Anal. Calcd. for $C_{36}H_{28}N_6F_6O_6S_2Co$ [Co(bpyPY4)]$(CF_3SO_3)_2$: C, 49.26 %; H, 3.22 %; N, 9.58 %. Found: C, 49.0 %; H, 3.33 %; N, 9.49 %. IR (neat, cm^{-1}): 1591 (m), 1467 (m), 1436 (m), 1391 (w), 1258 (vs), 1222 (s), 1143 (s), 1056 (w), 1028 (vs), 909 (w), 847 (m), 817 (w), 793 (w), 770 (m), 752 (s), 652 (m), 634 (vs), 571 (s), 541 (w), 514 (s), 486 (w). ESI-MS (m/z, amu): 728.13 $[M^{2+}+ CF_3SO_3]^+$, 289.59 $[M^{2+}]^{2+}$.

Synthesis of [Co(bpyPY4)]$(CF_3SO_3)_3$ (1b). Using a N_2 filled glovebox, CH_3CN (10 mL) was added to a mixture of [Co(bpyPY4)]$(CF_3SO_3)_2$ (150 mg, 0.171 mmol) and $Ag(CF_3SO_3)$ (43.9 mg, 0.171 mmol). The mixture was stirred for 0.5 h at RT after which it had turned light red. The solution was filtered through celite and layered with Et_2O. Large dark-red crystals of **1b** were obtained after two days that were washed with Et_2O and dried. Yield: 123 mg (70 %). Anal. Calcd. for $C_{37}H_{28}N_6F_9O_9S_3Co$ [Co(bpyPY4)]$(CF_3SO_3)_3$: C, 43.28 %; H, 2.75 %; N, 8.18 %. Found: C, 43.66 %; H, 2.54 %; N, 7.9 %; ^{1}H-NMR (CD_3Cl, 300 MHz, ppm): 8.72-8.54 (8H, m), 8.44 (2H, t, 9 Hz), 8.23-8.08 (6H, m), 7.56 (2H, d, 7.5 Hz), 7.43 (2H, d, 7.5 Hz), 7.22 (2H, t, 7.5 Hz), 3.10 (6h, s).

Crystal data for **1a:** triclinic, space group $P\bar{1}$, a=10.3779(6) Å, b=11.8365(7) Å, c=16.5638(10) Å, α=97.280(2) °, β=98.397(2) °, γ=115.098(2)°, total reflections=20293, r_{calcd}(g cm^{-3})=1.636, independent reflections=6347, GOF=1.051 R=0.1335, wR_2=0.1436.
Crystal data for **1b:** monoclinic, space group $P2_1/c$, a=13.5709(4) Å, b=15.0108(5) Å, c=23.09125(6) Å, α=90 °, β=97.949(2) °, γ=90 °, total reflections=28628, independent reflections=11091, r_{calcd}(g cm^{-3})=1.583 GOF=1.035 R=0.0644, wR_2=0.1798.

Device Fabrication: A process established in our lab was followed for DSCs fabrication. A 6 μm thick film (4×4 mm) of 30 nm-sized TiO_2 particles was screen-printed on fluorine doped SnO_2 (FTO) conducting glass electrode (4 mm thick and 10 Ω per square). More layers were printed using 400 nm-sized particles to develop an overall thickness of 10 μm, TiO_2 nanoparticles. A 2 μm thick transparent TiO_2 film (4×4 mm) using 30 nm-sized TiO_2 particles was screen-printed on FTO conducting glass for the IMVS-IMPS studies. After a first sintering process at 500°C applied to the screen-printed films, a $TiCl_4$ treatment was done by dipping the films into a 20 mM $TiCl_4$ solution at 70°C in water. After heating the films in a heat gun at 570±25°C for 40 minutes, the films were immersed for 24 hours in 1 μM solution of MK2 in acetonitrile:toluene (1:1) mixture. The Pt counter electrodes were prepared by thermal decomposition of 10 mM solution of $PtCl_6$ in isopropanol on the FTO substrate. Working electrode and counter electrode were joined together using a 25 μM thick Surlyn gasket. Electrolytes were filled into the space between the two electrodes using a back-filling technique with the help of vacuum. The electrolyte-injecting hole was sealed with hot melt Surlyn backed by glass slide.

IV and IPCE Instrumentation. An Oriel sun simulator using a filtered 1000 W xenon lamp was used to provide simulated solar irradiation (AM 1.5, 1000W/m^2). A calibrated silicon photodiode by Peccell Technologies was used to adjust the output of the light source and a color filter was employed to reduce the optical mismatch between the calibration diode and the DSCs. A Keithley 2400 source meter was used to record the IV-characteristics of the cells under provided condition. Light intensities lower than one sun were obtained by using a filter wheel fitted with a series of

different sized mesh filters. Incident photon conversion efficiency was measured by an Oriel system fitted with a 150W xenon lamp and linked to a Cornerstone 260 as a monochromator light source. A Keithley 2400 source meter was used to record IPCE photocurrents of the devices under tests. The monochromatic photon flux was quantified by using a calibrated silicon photodiode provided by Peccell Technologies. Stability studies were done using an environmental chamber provided by the ATLAS, with model number SC^3 340 Solar Simulator.

Intensity Modulated Photovoltage Spectroscopy (IMVS) and Charge Extraction Instrumentation: IMVS studies were carried out on fully functional DSC devices employing a combination of red and white light LEDs. A DC voltage source was used to control the light intensity of red LED, modulated to a depth of 2% using the integral function generator of a Stanford lock-in-amplifier (SR810). SR810 then provided a sine wave modulation between 0.1 Hz and 30 kHz. The additional white diode array was controlled by a commercial DC power source. A battery powered, high impedence voltage follower with an input impedence of 10^{12} Ω, was used to record the photovoltage. A computer controlled programme Labview was used to control a lock-in amplifier to capture the amplitude and phase of the resulting AC photovoltages. A Labview fitting programme was used for the data analysis. The DSC was illuminated using an unmodulated white light for 10 s to attain equilibrium between charge injection and recombination under open circuit conditions. A computer controlled mercury-wetted relay switch was used to switch the light off and to put the device to short circuit and the resultant extracted charge was measured across a 50 Ω resistor, using an NI-6251 data logger. Devices were constructed using a 1.3 μm thick TiO_2 (30 nm) mesoporous film sensitized with MK2 dye.

Crystal Structures of Complex 1a and 1b:

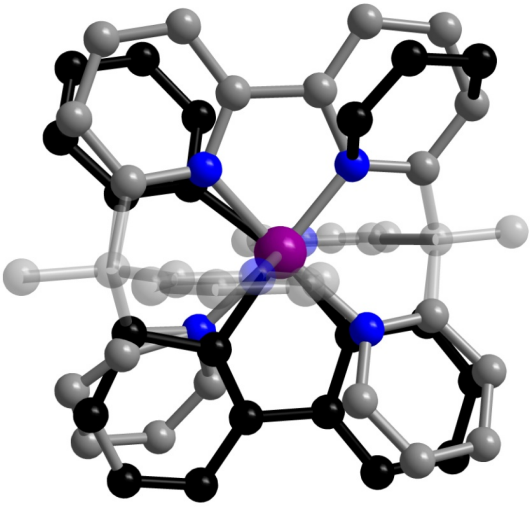

Figure S1. Molecular structure of the dication $[Co(bpyPY4)]^{2+}$ of **1a** emphasizing the disorder of the ligand.

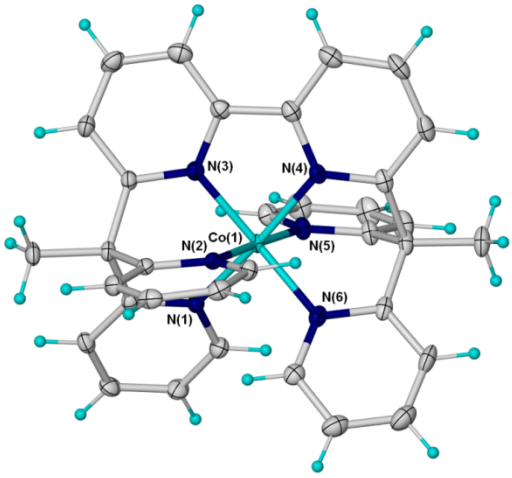

Figure S2. View of the $[Co(bpyPY4)]^{3+}$ trication of $[Co(bpyPY4)](CF_3SO_3)_3 \cdot MeCN$ (**1b**) with non-hydrogen atoms represented by 50% thermal ellipsoids and hydrogen atoms as spheres of arbitrary size; the counter anions and lattice solvent molecules have been omitted for clarity.

Cyclic Voltammetry of Complex 1a:

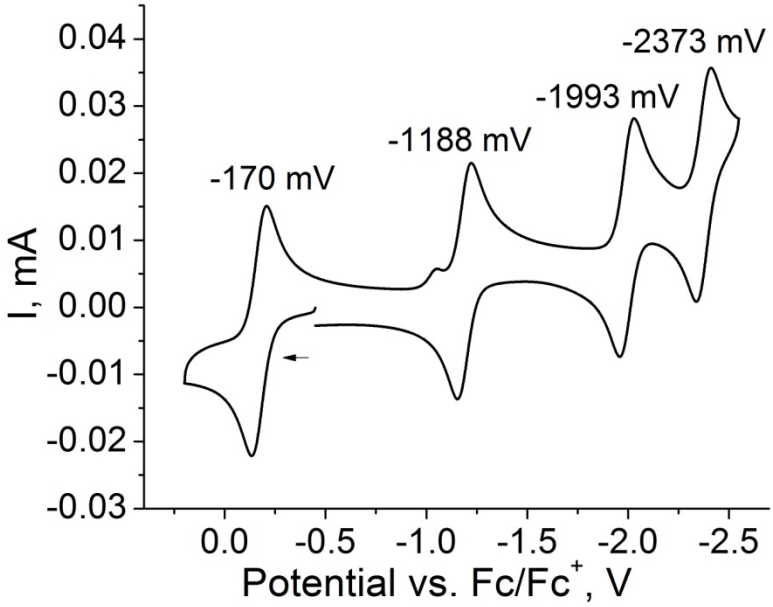

Figure S3. Cyclic voltammogram of $[Co(bpyPY4)](CF_3SO_3)_2$ (1 mM) in MeCN (0.1 M NBu_4PF_6).

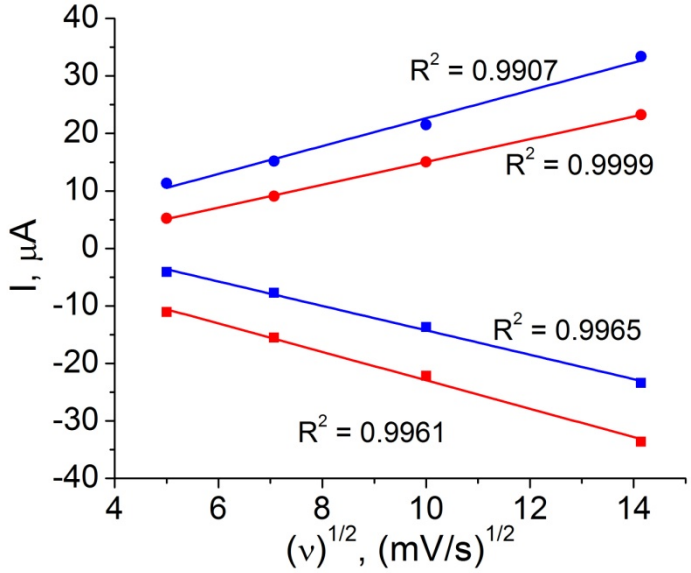

Figure S4. Linear relationship of anodic (squares) and cathodic (circles) currents of the $Co^{3+/2+}$ (red) and $Co^{2+/1+}$ (blue) redox couples versus the square root of the scan-rate (n) (n = 25, 50, 100, 200 mV/s^{-1})

IPCE and IV Characterization:

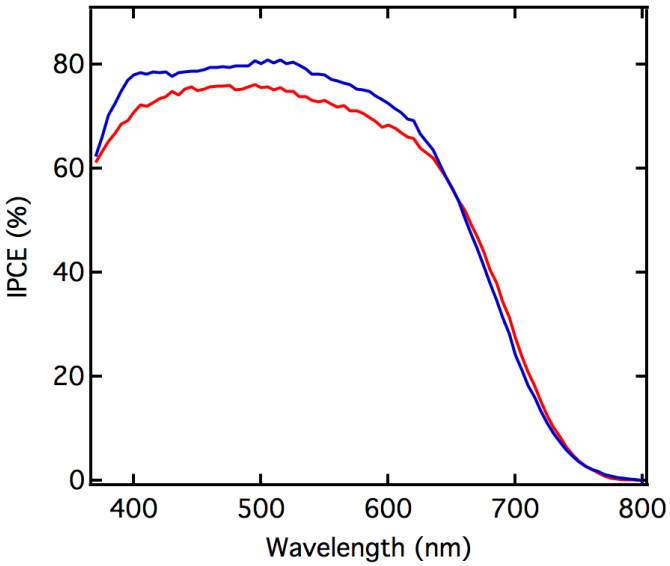

Figure S5. IPCE spectra of the best-performing DSCs fabricated using electrolytes **1a/1b** and Co-bpy in combination with NMBI Lewis base. For average photovoltaic performance data and details on the electrolyte composition see Table 2.

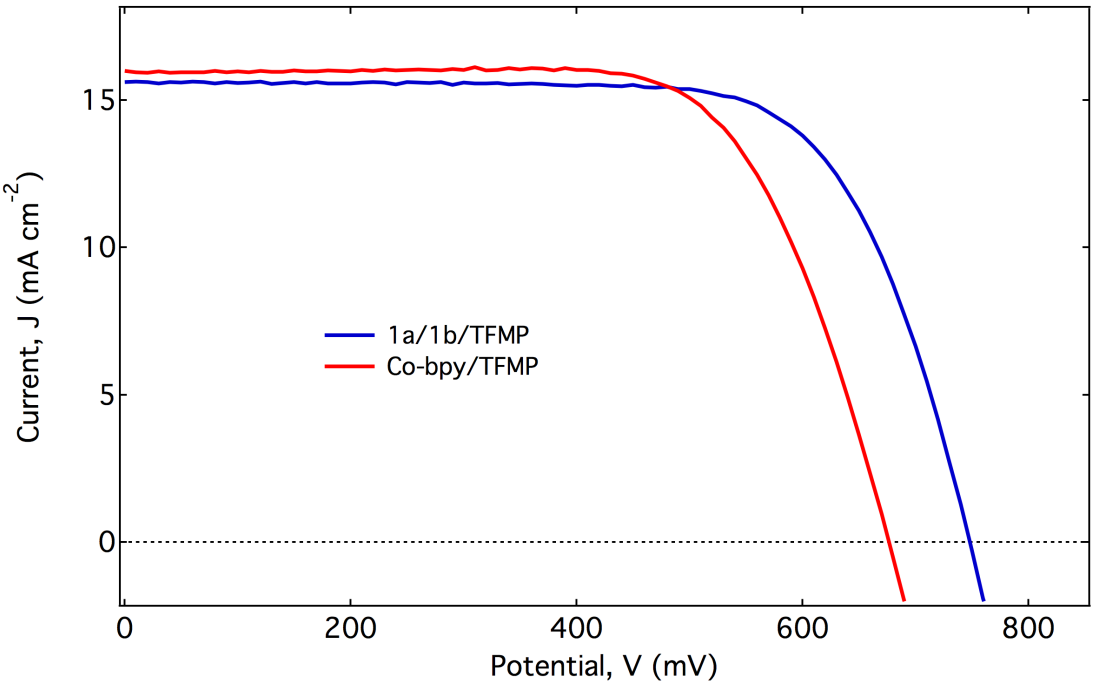

Figure S6. IV curves showing a comparison of the DSCs performance for the best devices made using electrolyte **1a/1b** and Co-bpy in combination with the TFMP Lewis base. Other photovoltaic characteristics and electrolyte components are explained in Table 2.

IV characteristics of DSCs based on electrolyte systems using 1a/1b/TFMP and Co-bpy/TFMP, redox couple/Lewis base in acetonitrile as solvent

***Table S1*:** Tabulated photovoltaic data of the DSC devices made **1a/1b/TFMP** and **Co-bpy/TFMP** as electrolytes and MK2 dye, under simulated sunlight (AM 1.5 G, 1000 W/m^2) [a]

Redox couple[b]	**1a/1b/TFMP**	**Co-bpy/TFMP**
$E_{1/2}$ (mV) [c]	465	560
V_{OC} (mV)	748±3	689±19
J_{SC} (mA.cm^{-2})	15.6±0.2	14.9±0.6
FF	0.71±0.04	0.70±0.03
η (%)	8.3±0.2	7.2±0.3

[a] Double-layer TiO_2 films (6 µm mesoporous TiO_2 (30 nm) and 4 µm scattering TiO_2 (400 nm)) and a platinum counter electrode were used for the fabrication of all DSCs. The average performance at least three devices with standard deviation is provided. [b] The electrolyte consists of 0.20 M Co^{II} complex, 0.100 M of Co^{III} complex, 0.05 M of LiTFSI and 0.50 M of NMBI in pure MeCN. [c] Redox potentials of the **1a** and Co-bpy are reported vs NHE.

Comparison of the efficiencies of DSCs measured before and after light soaking, based on electrolyte 1a/1b/NMBI using acetonitrile as solvent

Table S2. Photovoltaic performance of DSCs assembled with the **1a/1b/NMBI**[a] redox couple and MK2 dye, under simulated sunlight (AM 1.5 G, 1000 W/m^2) [b]

Testing conditions	**No light soaking**	**20 min light soaking**
V_{OC} (mV)	748±5	732±3
J_{SC} (mA.cm^{-2})	15.6±0.3	16.9±0.3
FF	0.72±0.02	0.74±0.01
η (%)	8.3±0.2	9.4±0.1

[a] Double-layer TiO_2 films (6 µm mesoporous TiO_2 (30 nm) and 4 µm scattering TiO_2 (400 nm)) and a Pt counter electrode were used for the fabrication of all DSCs. The average performance of at least three devices with standard deviation is provided. [b] The electrolyte consists of 0.20 M Co^{II} complex, 0.10 M Co^{III} complex, 0.05 M LiTFSI and 0.50 M NMBI in acetonitrile.

Monash University

Declaration for Thesis Chapter [5]

Declaration by candidate

In the case of Chapter [5], the nature and extent of my contribution to the work was the following:

Nature of contribution	Extent of contribution (%)
Synthesis of the Co-complexes and characterisation, fabrication of the solar cells, IV-and electrochemical data collection, results interpretation, preparation and editing of the manuscript.	70 %

The following co-authors contributed to the work. If co-authors are students at Monash University, the extent of their contribution in percentage terms must be stated:

Name	Nature of contribution	Extent of contribution (%) for student co-authors only
Jordan C. Axelson	Synthesis of the ligand and Cobalt(II) complex	N/A
Craig M. Forsyth	Helping with crystallography	N/A
Christoper J. Chang	Experimental design and editing	N/A
Jeffrey R. Long	Experimental design and editing	N/A
Leone Spiccia	Experimental design, planning, drafting and editing	N/A
Udo Bach	Experimental design, planning, drafting and editing	N/A

The undersigned hereby certify that the above declaration correctly reflects the nature and extent of the candidate's and co-authors' contributions to this work*.

Candidate's Signature	[redacted]	**Date** 30/08/2013
Main Supervisor's Signature	[redacted]	**Date** 30/08/2013

Chapter 5

Stabilization of a Very Short Co-F Bond with a Cobalt Pentapyridyl Ligand Cavity

Muhammad K. Kashif[a], Jordan C. Axelson[b], Craig M. Forsyth[c], Christopher J. Chang[d], Jeffrey R. Long[b], Udo Bach[a,e,f], Leone Spiccia[c]

Corresponding Authors:
[redacted]

[a]Department of Materials Engineering, Monash University, Victoria 3800, Australia
[b]Department of Chemistry, University of California, Berkeley, California 94720-1460, United States
[c]School of Chemistry, Monash University, Victoria 3800, Australia
[d]Department of Chemistry and the Howard Hughes Medical Institute, University of California, Berkeley, and Chemical Sciences Division, Lawrence Berkeley National Laboratory, Berkeley, California, 94720, United States
[e]Commonwealth Scientific and Industrial Research Organization, Materials Science and Engineering, Clayton South, Victoria 3169, Australia
[f]Melbourne Centre for Nanofabrication, 151 Wellington Road, Clayton, Victoria 3168, Australia

Stabilization of a Very Short Co-F Bond within a Pentapyridyl Ligand

Abstract: The reaction of $[Co(PY5Me_2)(CH_3CN)]^{2+}$ with tetrabutylammonium fluoride and $NOBF_4$ has resulted in the formation of $[Co(PY5Me_2)(F)]^{2+}(OTf)_2$, where $PY5Me_2$ = (2,6-(bis(bis-2-pyridyl)methylmethane)pyridine) and OTf = trifluoromethanesulfonate anion, a complex which has been characterized using single crystal X-ray crystallography, NMR and elemental analysis. In the complex cation, five coordination sites are occupied by nitrogen donors from the pentapyridyl ligand and the sixth site by a fluoride anion. The pentapyridyl ligand around cobalt(III) metal centre forms a cavity that stabilizes the shortest Co-F bond distance reported to date (1.819(2) Å). The complex was initially isolated from a solution containing $[Co(PY5Me_2)(CH_3CN)]^{2+}$ and $NOBF_4$. On standing, the BF_4^- anion had dissociated to form fluoride coordinated to the cobalt(III) centre. For comparison, we also report the X-ray crystal structure of the $[Co(PY5Me_2)(DMF)]^{3+}(OTf)_2(TFSI)$, where TFSI = bis(trifluoromethane)sulfonimide anion formed by oxidation of **1** with AgTFSI and subsequent reaction with DMF.

Key words: cobalt fluoride complex, pentadentate ligands, ploypyridylx, fluorinating agent, X-ray crystal structure

Introduction:

In coordination chemistry, the design of the ligands is of prime importance in manipulating the structure and properties of the resulting metal complex. A number of structural designs have been applied in the quest to develop novel metal complexes with interesting properties and for a variety applications.[1] Pentadentate ligands have been an area of interest as the ligand cavity can be appropriately designed to bind strongly to the metal ion in question while at the same time leaving one site available for further fine-tuning of the complexes properties. These efforts include, for example, cyclam derivatives, (cyclam= 1,4,8,11,-tetraazacyclotetradecane), tacn derivatives (tacn = 1,4,7-triazacyclononane) a noncyclic pentadentate ligands containing a combination of

a wide variety of donor atoms located on functional groups such as amines, pyridyls, imidazole, carboxylates, etc...[2]

A recent interesting example of such a ligand is the ligand $PY5H_2$ and its derivatives $PY5R_2$ (R = Me, OH, OMe). The molybdenum and cobalt complexes of this family of ligands have proven very useful in the exploration of alternative energy resources, including hydrogen generation catalysis, redox mediators for dye-sensitized solar cells (DSCs), modelling of metalloenzyme active sites and the construction of single-molecule magnets.[3] The synthesis of $PY5Me_2$ and its analogues was initially motivated by lipoxygenase, a mononuclear iron enzyme, possessing a single labile coordination site.[4] The coordination behaviour of the pentadentate polypyridyl ligand $PY5Me_2$ have been extensively studied using a variety of transition metals. The ligand binds to the metal centre in a square pyramidal fashion and enforces an octahedral geometry on a variety of metal centres. The sixth coordination site in the *para* position of the central pyridine ring that is left occupied by a monodentate ligand offers the possibility of substituting other ligands. Although the $PY5Me_2$ framework is quite rigid and has limited flexibility, the cavity of $PY5Me_2$ ligand and its analogues adapts cleverly to accommodate a variety of metal centres in different oxidation states. Concomitant angular and torsional changes induced according to the size of the metal centre are absorbed by the ligand cavity.

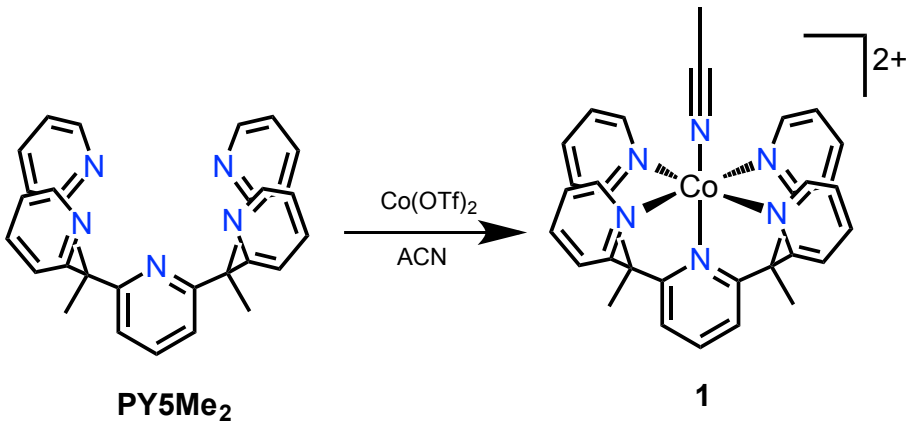

Figure 1: Structure of the ligand $PY5Me_2$ and its cobalt(II) metal complex **1**

For example, this feature has been successfully used in the application of these complexes in the reduction of hydrogen ions to hydrogen gas.[5] In a recent publication, we have shown that the weakly bound acetonitrile in **1** can be replaced by a stronger binding ligand such as 4-*tert*-butylpyridine (tBP) or *N*-methylbenzimidazole (NMBI). As a consequence tuning of the $Co^{2+/3+}$ redox potential was achieved which led to the development of efficient dye-sensitized solar cells (DSCs).[6] In this paper, we describe the synthesis and structural characterisation of two Co(III) derivatives of the compound **1**, in which the axial ligand has been replaced by either fluoride or *N, N*-dimethylformamide (DMF). In the fluoro complex, $[Co(PY5Me_2)(F)]^{2+}$, a ligand centre was found to stabilize the shortest known Co-F bond was stabilised within the "$[Co(PY5Me_2)]$" cavity. To the best of our knowledge, and as suggested by a recent review, there is only one known example of a complex with general formula $[Co^{III}(L)_n(F)_m]$, where L = pyridine and n, m = 2-3. To further study the effects of coordination of a larger ligand in the sixth coordination site, we have also synthesized the $[Co(P5Me_2)(DMF)]^{3+}$ complex (**3**). For the DMF ligand, linkage isomers are possible as it can either bind through an oxygen (*O*-isomer) or nitrogen (*N*-isomer) donor atom. Sargeson *et al.* for example, have studied the rate of base hydrolysis of coordinated DMF in $[Co(NH_3)_5(DMF)]^{3+}$.[7]

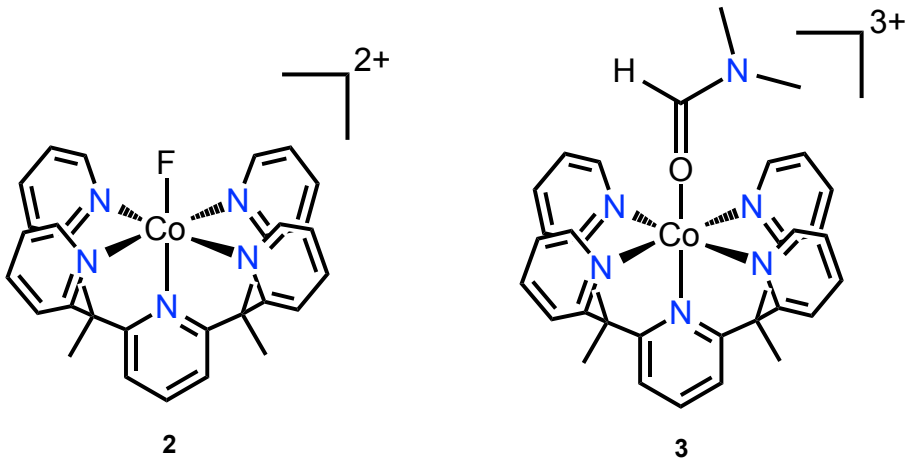

2 **3**

Figure 2: Structures of two cobalt(III) complexes, compound **2** (left) and **3** (right) synthesised using compound **1** shown in figure 1

Experimental

Materials and Methods: General reagents and solvents were obtained from commercial sources and used as supplied. Anhydrous solvents were used and stored in glove box under nitrogen. ^{1}H NMR spectra were measured on a Bruker DRX 400 spectrometer, using the signal of the deuterated solvent as an internal standard. The ^{1}H NMR chemical shifts δ are reported in parts per million (ppm) relative to tetramethylsilane (TMS). The values of coupling constants (*J*) are given in Hertz (Hz) and peak multiplicities are abbreviated as follows: s (singlet), d (doublet), t (triplet), and m (multiplet). The ^{19}F-NMR spectra were also measured on a Briker DRX 400 spectrometer but with $CFCl_3$ as an internal standard. Microanalyses were carried out by the Campbell Microanalytical Laboratory, University of Otago, New Zealand. Solution UV−visible spectra were recorded with a Lambda 950 Perkin-Elmer spectrophotometer. ATR FTIR spectra were recorded using a Bruker Equinox 55 Infrared Spectrometer fitted with a Specac Diamond ATR source.

Synthesis of cobalt complexes

Unless otherwise noted the synthesis and crystallization of the complexes was carried out in glove box under nitrogen. The ligand $PY5Me_2$ and complex $[Co(PY5Me_2)(CH_3CN)](OTf)_2$ (**1)** where, OTf = trifluoromethanesulfonate, were synthesized as described previously.[5]

$[Co(PY5Me_2)(F)](OTf)_2 \cdot CH_3CN$ (2)

Method A: Compound **2** was initially isolated from the reaction of compound **1** and $NOBF_4$. $NOBF_4$ (5.84 mg, 0.05 mmol) was added to acetonitrile solution of **1** (42.1 mg, 0.05 mmol) and left for stirring for half an hour in order to oxidize the metal centre from Co^{2+} to Co^{3+}. The solution was then reduced in volume and left standing whereupon single crystals suitable for X-ray study were obtained. The structural analysis, however, revealed that compound **2** had formed and not the expected $[Co(PY5Me_2)(CH_3CN)]^{3+}$ complex. A low percentage yield of 11.6 mg (25%) was obtained for this reaction.

Method B: An improved higher yielding synthesis for **2** was then developed. An acetonitrile solution of **1** {[Co(PY5Me$_2$)(CH$_3$CN)](OTf)$_2$} (25.2 mg, 0.03 mmol) was reacted with NOBF$_4$ (3.5 mg, 0.03 mmol) and a tetrabutylammonium fluoride (8.6 µl of 1M solution in THF, 0.03 mmol). Upon stirring at room temperature a light red coloured solution of [Co(PY5Me$_2$)(F)]$^{3+}$ was obtained together with a precipitate of tetrabutylammonium tetrafluoroborate (TBABF$_4$). The mixture was stirred for 30 minutes and the precipitated TBABF$_4$ removed by the filtration through diatomaceous earth. The resultant solution was reduced in volume under vacuum to obtain the product as a red solid. The red solid was then dissolved in acetonitrile and layered with a diethyl ether/CH$_2$Cl$_2$ mixture to crystallise the product. Yield: (14.7 mg, 60%). [Co^{III}(PY5Me$_2$)(F)](OTf)$_2$·CH$_3$CN (**2**): ^{1}H NMR (400MHz, CD$_3$CN, 22 °C) δ 9.56 (d, J_{HH} = 6.4Hz, 4H, py-H); 8.25-8.23 (m, 1 H, py-H), 8.21-8.19 (m, 6 H, py-H); 8.07-8.04 (M, 4H, py-H); 7.81-7.77 (m, 4H, py-H); 2.76 (s, 6H, Me$_2$-H); ^{19}F NMR (400MHz, CD$_3$CN, CFCl$_3$ as internal standard, 22 °C) -150.56 and -150.51 (two peaks, BF$_4$); -143.16 (s, F, Co-F); -78.07 (s, F, CF$_3$). Elemental analysis: Found (Calcd.) for C$_{33}$H$_{29}$Cl$_4$CoF$_7$N$_5$O$_6$S$_2$: C, 39.72 (40.06); H, 3.47 (2.95); N, 7.44 (7.08); S, 7.05 (6.48)

[Co(PY5Me$_2$)(DMF)](OTf)$_2$(TFSI)·3(CH$_2$Cl$_2$) (3)

Compound **1** was oxidized to obtain **1$_b$** {[Co^{III}(PY5Me$_2$)(CH$_3$CN)](OTf)$_2$(TFSI)}, where TFSI = bis(trifluoromethane)sulfonimide anion, using AgTFSI according to a previously reported method.[6] Then, the acetonitrile solution of **1** (25.2 mg, 0.03 mmol) was reacted with DMF (2.30 µl, 0.03 mmol) to obtain a pink solution. The solution was stirred for 1 h and then layered with mixture of dichloromethane and dry diethyl ether to produce high quality crystals. The crystals were collected by filtration and dried under vacuum (20 mg, 75%). [Co^{III}(PY5Me$_2$)(DMF)](OTf)$_2$(TFSI) (**2**): ^{1}H NMR (400MHz, CD$_3$CN, 22 °C) δ 9.62 (d, J_{HH} = 6.4 Hz, 4H, py-H); 9.08 and 8.57 (d, J_{HH} = 6.8 Hz, amide H); 8.29-7.94 (m, 11 H, py-H); 7.34-7.58 (m, 4H, py-H); 2.90-2.60 (m, 6H, Me$_2$-H); 2.90-2.60 (m, 6H, Me$_2$-DMF); Elemental analysis: Found (Calcd) for C$_{38}$H$_{35}$CoF$_{12}$N$_8$O$_{11}$S$_4$: C, 39.02 (38.20); H, 2.38 (2.95); N, 8.75 (9.38); S, 6.94

(6.54); ATR-FTIR (thin film): 3509, 3082, 2950, 1660, 1598, 1459, 1386, 1348, 1264, 1225, 1182, 1135, 1055, 1025, 910, 865, 786, 762, 634 cm^{-1}.

Data Collection: Crystal data were recorded using an Oxford Gemini Ultra CCD diffractometer equipped with an Oxford Cryosystems 700 Cryostream and cooled to 123(1) K. Representative orange or orange-yellow prismatic crystals of **2** and **3** were mounted on the diffractometer for analysis. The data were collected with Mo Kα radiation (λ = 0.71073 Å) and processed using CrysAlisPro software. Lorentz, polarization and multi scan absorption were applied. The refinement of structures was carried out using SHELX-97.[8] Anisotropic thermal parameters were used to refine all non-hydrogen atoms. Hydrogen atoms were placed using a riding model with C-H = 0.95-0.98 Å and U_{iso}(H) = xU_{iso}(C), x = 1.2 or 1.5. Crystallographic data, being reported in this manuscript will be deposited with the Cambridge Crystallographic Data Centre (full details of the crystal structure determination is provided in the appendix of the thesis). Crystallographic data (Table S1) as well as Tables of key bond length and angles for complex **2** (Table S2) and complex **3** (Table S3) are provided in the supporting information.

Results and discussion

Polypyridyl cobalt(III) coordination complexes in which the fluoride ion is directly bound to the cobalt(III) centre are rare. Recent studies have shown that fluorides coordinated to a metal centre can become involves in extensive intermolecular and/or intramolecular hydrogen bonding.[9] Potential application of such complexes in biochemistry,[10] crystal engineering,[11] supramolecular, coordination and organometallic chemistry have been proposed. Such metal complexes are also finding applications in radio imaging.[12] Following an initial observation that a novel cobalt(III)-fluoride complex $[Co(PY5Me_2)(F)](OTf)_2$ was formed in solution containing complex **1** and $NOBF_4$, an improved synthesis was developed which involved the conversion of $[Co(PY5Me_2)(CH_3CN)]^{2+}$ into the corresponding cobalt(III) complex followed by reaction with TBAF. The second complex, $[Co(PY5Me_2)(DMF)](OTf)_2(TFSI)$ was obtained by reacting the corresponding cobalt complex with DMF. The two complexes were characterized by elemental analysis, NMR, IR and UV-Vis spectroscopy

Crystallography

The single crystal X-ray structures of $[Co(PY5Me_2)(F)](OTf)_2$ (**2**) and $[Co^{III}(PY5Me_2)(DMF)](OTf)_2(TFSI)$ (**3**) are reported here. The binding of two monodentate ligands with different sizes and steric requirements to the cobalt(III) centre highlights the accommodating behaviour of the $PY5Me_2$ cavity. The structures of the $[Co(PY5Me_2)(NMBI)]^{3+}$ and $[Co(PY5Me_2)(MeCN)]^{3+}$ complexes have already been reported elsewhere and key structural parameters will be used in the discussion to follow.[6] The cobalt(III) metal centre in each metal complex is coordinated in square-pyramidal fashion by the $PY5Me_2$ ligand with four pyridyls forming the equatorial plane and the central pyridyl in the ligand occupying an axial position. Binding of the monodentate ligand to the sixth coordination site results in a final distorted octahedral geometry. The Co-F bond distance (1.819(2) Å) is, to our knowledge, the shortest measured so far for the cobalt(III) complex. The cavity generated by the $PY5Me_2$ ligand. The ligation of F^- to cobalt(III) is further stabilized by $F^{\cdots}H$ interactions. The Co-X_{axi} (where, X_{axi} represents F^-, an N or an O donor atom from the axially ligated fluoride acetonitrile, DMF, NMBI) distances highlight the close approach of the F^- anion to the cobalt(III) centre. One striking observation for these different exogenous ligands is the perfect alignment of the axial ligand with the plane made by the central pyridine ring and the C_2Me_2 moiety of the $PY5Me_2$ cavity. This feature is absent in the complexes of $PY5(OMe)_2$, due to the distortion of the central pyridine ring induced by the methoxy substituents.[13] The coordination sphere for the four complexes compared herein is very similar, however, the cavity expands or contracts in response to the size of the exogenous ligand. As can be seen from table1, for the small fluoro complex the $PY5Me_2$ ligand forms a very small cavity around the cobalt(III) centre and as the size of the axial monodentate ligand increases there is a clear expansion of the coordination sphere to accommodate the corresponding ligands. The size of the cavity follows a general trend for ligand size; $F^- < DMF \approx CH_3CN < NMBI$.

Table 1: Axial and average equatorial bond distances for cobalt(III) complexes with different monodentate exogenous ligands

Exogenous ligand X =	**Average bond distances (Å) for**		
	Co-axial ligand bond distance	*Co-axial N_{Py} bond distances*	*Co-equatorial N_{Py} bond distances*
F	1.819(2)	1.944(2)	1.962(1)
DMF {$(CH_3)_2NCHO$}	1.908(3)	1.950(4)	1.979(6)
ACN (CH_3CN)	1.923(5)	1.940(5)	1.977(6)
NMBI (*N*-methylbenzimidazole)	1.960(2)	1.976(2)	1.994(5)

One of very important feature of complex **2** is the involvement of the cobalt(III) bound fluoride ion in moderate strength F···H interactions. The interactions of the fluoride ion bound to cobalt(III) metal centre with the solvent molecules of acetonitrile are shown in the table 2. These interactions, which can be attributed to the high electron density of fluoride ion, restrict further bridging to other cobalt metal centres. The observed bond distances in this case are approximately 2.50 Å. Hulliger et al have suggested that distances up to 2.9 Å can be considered F···H, hydrogen-bonding interactions based on sum of the van der Waals radii of fluorine and hydrogen 2.67 Å.[14] However, F···F interactions which have been observed for other metal halides is absent in this case of cobalt fluoride.[9a] The importance of intermolecular hydrogen bonding is a well-understood phenomenon in crystal engineering and supramolecular chemistry. Theoretical and experimental results have demonstrated that F^- is the best H-bond acceptors.[15] The negative inductive effect ($\sigma_I = 0.51$) and the positive mesomeric effect ($\sigma_R = -0.34$) are operative factors responsible for this reactivity.

In case of DMF ligand, the ligand is also observed to be strongly involved with the oxygen atoms of the counterion molecule, OTf. The strongest hydrogen bond (2.27 Å) involves the interaction of the formyl hydrogen of the DMF and oxygen of the OTf molecule.

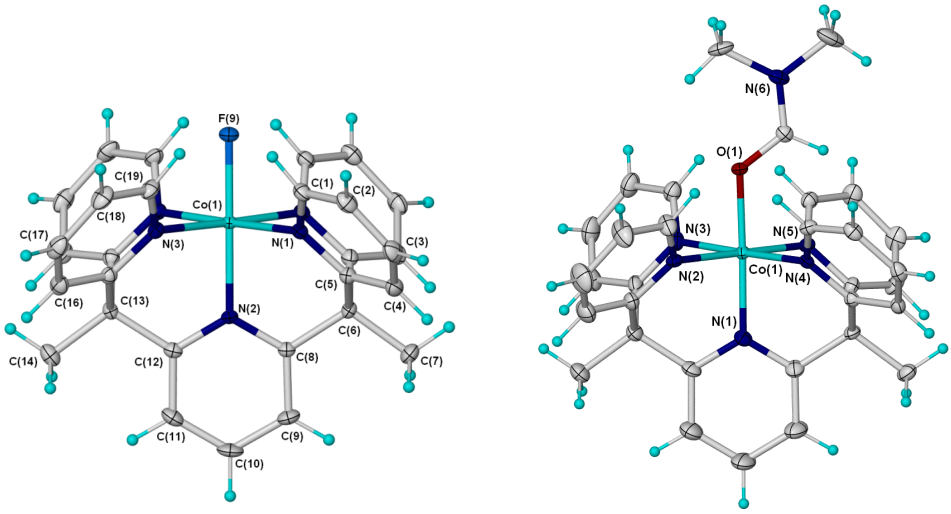

cation **2** cation **3**

Figure 3. Crystal structures of the complex $[Co(Py5Me_2)(F)]^{2+}$ (cation **2**) and $[Co(Py5Me_2)(DMF)]^{3+}$ (cation **3**) with non-hydrogen atoms represented by 50% thermal ellipsoids and hydrogen atoms as spheres of arbitrary size; the counter ions and lattice solvent have been omitted for clarity.

Table 2: Hydrogen bond or weak interaction bond distances within crystal structures

Hydrogen bonds or weak interactions for $[Co^{III}(PY5Me_2)(X)]$	Distances (Å)
X = F	
Co(1)-F(9)·····H(36C) (acetonitrile)	2.51
Co(2)-F(10)·····H(38A) (acetonitrile)	2.49
Co(1)-F(9)·····C(36) (acetonitrile)	3.08
Co(2)-F(10)·····C (C38) (acetonitrile)	2.99
X = DMF	
(formyl) C(30)-H(30)·····O(7) (OTf)	2.27
(dimethyl) C(31)-H(31B)·····O(9) (OTF)	2.62
(amide) N(6)·····O(11) (OTf)	2.93

Conclusion: We have synthesised and characterized two cobalt(III) complexes of a pentadentate $PY5Me_2$ ligand which have fluoride and DMF ligands occupying the sixth coordination site. Two particularly striking structural features are the very short Co···F distance for the fluoro complex and the ability of the cavity generated by the $PY5Me_2$ ligand on coordination of the cobalt(III) to be tuned in response to the size and steric constraints introduced by the axially coordinated monodentate ligand. These features highlight the possibility to further explore these structural features, for example, the development of new redox mediators for DSCs and catalysts for hydrogen generation.[5]

References:

(1) a) D. Desbouis, I. P. Troitsky, M. J. Belousoff, L. Spiccia, *Coord. Chem. Rev.* **2012**, *256*, 897. b) A. Singh, L. Spiccia, *Coord. Chem. Rev.* **2013**, *257*, 2607. c) J. M. Zadrozny, D. E. Freedman, D. M. Jenkins, T. D. Harris, A. T. Iavarone, C. Mathoniere, R. Clerac, J. R. Long, *Inorg. Chem.* **2010**, *49*, 8886. (d) H. I. Karunadasa, C. J. Chang, J. R. Long, *Nature*, **2010**, *464,* 1329.

(2) a) A. Grohmann, F. Knoch, *Inorg. Chem.* **1996**, *35*, 7932. b) S. Tamagaki, Y. Kanamaru, M. Ueno, W. Tagaki, *Bull. Chem. Soc. Jpn.* **1991**, *64*, 165. c) M. Lubben, A. Meetsma, E. C. Wilkinson, B. L. Feringa, L. Jr. Que, *Angew. Chem., Int. Ed. Engl.* **1995**, *34*, 1512. d) L. Jr. Que, G. Roelfes, M. Lubben, K. Chen, R. Y. N. Ho, A. Meetsma, S. Genseberger, R. M. Hermant, R. Hage, S. K. Mandal, V. G. Young, Y. Zang, H. Kooijman, A. L. Spek, B. L. Feringa, *Inorg. Chem.* **1999**, *38*, 1929.

(3) a) R. T. Jonas, T. D. P. Stack, *J. Am. Chem. Soc.* **1997**, *119*, 8566. b) C. R. Goldsmith, R. T. Jonas, T. D. P. Stack, *J. Am. Chem. Soc.* **2002**, *124*, 83. c) C. R. Goldsmith, A. P. Cole, T. D. P. Stack, *J. Am. Chem. Soc.* **2005**, *127*, 9904. d) C. R. Goldsmith, T. D. P. Stack, *Inorg. Chem.* **2006**, *45*, 6048. (e) D.E. Freedman, D. M. Jenkins, A. T. Iavarone, J. R. Long, *J. Am. Chem. Soc.* **2008**, *130*, 2884. f) D. E. Freedman, D. M. Jenkins, J. R. Long, *Chem. Comm.* **2009**, 4829. g) B. Bechlars, D. M. D'Alessandro, D. M. Jenkins, A. T. Iavarone, S. D. Glover, C. P. Kubiak, J. R. Long, *Nat. Chem.* **2010**, *2*, 362.

(4) C. R. Goldsmith, R. T. Jonas, A. P. Cole, T. D. P. Stack, *Inorg. Chem.* **2002**, *41*, 4633.

(5) Y. Sun, J. P. Bigi, N. A. Piro, M. L. Tang, J. R. Long, C. J. Chang, *J. Am. Chem. Soc.* **2011**, *133*, 9212.

(6) M. K. Kashif, C. J. Axelson, N. W. Duffy, C. M. Forsyth, C. J. Chang, J. R. Long, L. Spiccia, U. Bach, *J. Am. Chem. Soc.,* **2012,** *134,* 16646. b) A. E. King, Y,

Surendranath, N. A. Piro, J. P. Bigi, J. R. Long, C. J. Chang, *Chem. Sci.* **2013**, *4*, 1578.

(7) a) D.A. Buckingham, J. M. Harrowfield, A. M. Sargeson, *J. Am. Chem. Soc.* **1974**, *96*, 1726. b). C. J. Boreham, D. A. Buckingham, D. J. Francis, A. M. Sargeson, L. G. Warner, *J. Am. Chem. Soc.* **1981**, *103*, 1975. c) D. A. Buckingham, F. R. Keene, A. M. Sargeson, *J. Am. Chem. Soc.* **1974**, *96*, 4981.

(8) G. M. Sheldrick, *Acta Crystallogr. Sect. A,* **2008**, *64*, 112.

(9) a) L. Brammer, E. A. Bruton, P. Sherwood, *Cryst. Growth Des.* **2001**, *1*, 277. b) P. Politzer , J. W. Timberlake, *J. Org. Chem.* **1972**, *37*, 3557.

(10) J. Emsley, N. M. Reza, H. M. Dawes, M. B. Hursthouse, *J. Chem. Soc., Dalton Trans.* **1986**, 313.

(11) L. Brammer, J. K. Swearingen, E. A. Bruton, P. Sherwood, *Proc. Nat. Acad. Sci. U.S.A.* **2002**, *99*, 4956.

(12) J. B. Aitken, S. Antony, C. M. Weekley, B. Lai, L. Spiccia, H. H. Harris, *Metallomics*, **2012**, *4*, 1051.

(13) J. M. Robertus, G. Klein, T. J. Robert, R. G. Christian, T. D. P. Stack, *Inorg. Chem.,* **2002**, *41*, 4633.

(14) K. Reichenbächer, H. I. Süss, J. Hulliger, *Chem. Soc. Rev.* **2005**, *34*, 22.

(15) E. Espinosa, I. Alkorta, J. Elguero, E. Molius, *J. Chem. Phys.* **2002**, *117*, 5529.

Supporting Information for:

Stabilization of a Very Short Co-F Bond with a Cobalt Pentapyridyl Ligand Cavity

Muhammad K. Kashif[a], Jordan C. Axelson[b], Craig M. Forsyth[c], Christopher J. Chang[d], Jeffrey R. Long[b], Udo Bach[a,e,f], Leone Spiccia[c]

Corresponding Authors:
[redacted]

[a]Department of Materials Engineering, Monash University, Victoria 3800, Australia
[b]Department of Chemistry, University of California, Berkeley, California 94720-1460, United States
[c]School of Chemistry, Monash University, Victoria 3800, Australia
[d]Department of Chemistry and the Howard Hughes Medical Institute, University of California, Berkeley, and Chemical Sciences Division, Lawrence Berkeley National Laboratory, Berkeley, California, 94720, United States
[e]Commonwealth Scientific and Industrial Research Organization, Materials Science and Engineering, Clayton South, Victoria 3169, Australia
[f]Melbourne Centre for Nanofabrication, 151 Wellington Road, Clayton, Victoria 3168, Australia

Table S1: Crystallographic Data for complex **2** and **3**

	2	**3**
Formula	$C_{68}H_{59}Co_2F_{14}N_{13}O_{12}S_4$	$C_{37}H_{34}Cl_2CoF_{12}N_7O_{11}S_4$
fw	1762.38	1238.78
Crystal system	orthorohombic	monoclinic
space group	C*mc*2$_1$	*P*2$_1$/*c*
a(Å)	14.7310(4)	19.0821(9)
b(Å)	21.9915(8)	13.1795(7)
c(Å)	21.9340(8)	19.0210(9)
α(º)	90	90
β(º)	90	97.481(5)
γ(º)	90	90
V(Å^3)	7105.7(4)	4742.9(4)
Z	4	4
m_{calcd}(mm^{-1})	0.694	0.764
r_{calcd}(g.cm^{-1})	1.647	1.735
2*q* range(º)	2.07-32.37	1.88-27.50
N_t	42139	26122
$N(R_{int})$	11729 (0.038)	10884 (0.062)
N_o	10126	6657
*R*1(*I*>2σ*I*)	0.031	0.074
w*R*(*I*>2σ*I*)	0.074	0.180
R(all data)	0.037	0.131
w*R*(all data)	0.077	0.215
GoF	1.036	1.030
Dρ$_{max/min}$(e)	0.533;-0.455	0.95;-1.35

Table S2: Selected Bond Distances (Å) and angles (deg) for complex **2**

Bond/angle	**2**
Co1-F1	1.820(2)
Co1-N1	1.959(3)
Co1-N2	1.961(2)
Co1-N3	1.963(2)
Co1-N2	1.961(2)
Co1-N3	1.963(2)
Co(2)-F(2)	1.819(2)
Co(2)-N(11)	1.943(2)
Co(2)-N(12)	1.961(2)
Co(2)-N(13)	1.972(2)
Co(2)-N(12)	1.961(2)
Co(2)-N(13)	1.972(2)
F(1)-Co(1)-N(1)	179.9(1)
F(1)-Co(1)-N(2)	89.71(8)
F(1)-Co(1)-N(3)	89.08(8)
F(1)-Co(1)-N(2)	89.71(8)
F(1)-Co(1)-N(3)	89.08(8)
N(1)-Co(1)-N(2)	90.37(9)
N(1)-Co(1)-N(3)	90.83(9)
N(1)-Co(1)-N(2)	90.37(9)
N(1)-Co(1)-N(3)	90.83(9)
N(2)-Co(1)-N(3)	97.40(7)
N(2)-Co(1)-N(2)	83.19(7)
N(2)-Co(1)-N(3)	178.66(8)
N(3)-Co(1)-N(2)	178.66(8)
N(3)-Co(1)-N(3)	81.98(7)
N(2)-Co(1)-N(3)	97.40(7)
F(2)-Co(2)-N(11)	179.13(9)
F(2)-Co(2)-N(12)	89.78(8)
F(2)-Co(2)-N(13)	88.97(8)
F(2)-Co(2)-N(12)	89.78(8)
F(2)-Co(2)-N(13)	88.97(8)
N(11)-Co(2)-N(12)	90.80(9)
N(11)-Co(2)-N(13)	90.45(9)
N(11)-Co(2)-N(12)	90.80(9)
N(11)-Co(2)-N(13)	90.45(9)
N(12)-Co(2)-N(13)	82.76(7)
N(12)-Co(2)-N(12)	96.83(7)
N(12)-Co(2)-N(13)	178.69(8)
N(13)-Co(2)-N(12)	178.69(8)
N(13)-Co(2)-N(13)	97.61(7)
N(12)-Co(2)-N(13)	82.76(7)

Table S3: Selected Bond Distances (Å) and angles (deg) for complex **3**

Bond distances/angle	**3**
Co-O(1)	1.908(3)
Co-N(1)^{b}	1.950(4)
Co-N(2)	1.987(4)
Co-N(3)	1.975(4)
Co-N(4)	1.981(4)
Co-N(5)	1.974(4)
N(1)-Co- O(1)	178.3(2)
N(2)-Co-O(1)	87.6(2)
N(3)-Co-O(1)	87.7(2)
N(4)-Co-O(1)	90.6(1)
N(5)-Co-O(1)	93.1(2)
N(2)- Co-N(5)	177.1(2)
N(3)- Co-N(4)	178.1(2)
N(2)- Co-N(4)	97.1(2)
N(5)- Co-N(3)	95.3(2)
N(3)- Co-N(2)	81.9(2)
N(5)- Co-N(4)	85.7(2)
N(1)- Co-N(3)	91.7(2)
N(1)- Co-N(2)	90.7(2)
N(1)- Co-N(4)	89.9(2)
N(1)- Co-N(5)	88.5(2)

Chapter 6

Conclusion

6.1 Conclusion

At the commencement of this PhD thesis research, a large research effort was underway aimed at finding alternative redox couples. Many new organic and inorganic redox mediators were being discovered and implemented. Several groups revisited previously researched redox couples with new strategies to improve the efficiency. Our group also reconsidered the use of the Fc/Fc^{+} redox couple. Using an organic dye and improved fabrication techniques, high efficiency solar cells were successfully produced. In 2010, a first breakthrough was reported by the group of Hagfeldt who achieved a DSC high efficiency by combining an organic sensitizer with, the $[Co(bpy)_3]^{2+/3+}$ redox mediator. In 2012, the Grätzel group was successful in pushing the DSC efficiency to 12.3 % by using a cocktail of two dyes and again the $[Co(bpy)_3]^{2+/3+}$ redox mediator. After these important advances in the development of alternative redox mediator research, many groups have focused on the improvement of cobalt(II)/(III) based redox mediators. This included the use of different ligand systems based on bidentate and tridentate nitrogen-donor ligands.

The research presented in this thesis contributes another advance in the field of alternative redox mediators based on cobalt(II)/(III) redox mediators. The application of cobalt(II)/(III) complexes of higher denticity polypyridyl ligands not only provided redox mediators with tunable geometric features (using a pentadentate ligand) but also furnished stability (utilizing hexadentate ligand) to the cobalt(II)/(III)-based redox mediators.

The molecular structures of the new cobalt complexes applied as redox mediators have been determined in both oxidation states, using single crystal X-ray crystallography, to explore the structural changes accompanying the redox process and to elucidate their effect on the performance of the DSCs. Using a number of analytical techniques, it was shown that the sixth coordination site, left unoccupied by the pentadentate ligand and occupied by a solvent molecule, could be substituted by stronger binding monodentate Lewis bases. This strategy led us to put forward the concept of *in-situe* fine-tuning the redox potential of the electrolyte using the $[Co(PY5Me_2)(CH_3CN)]^{2+/3+}$ complex. Single crystal X-ray

characterization of the complexes, $[Co(PY5Me_2)(tBP)]^{2+/3+}$ and $[Co(PY5Me_2)(NMBI)]^{2+/3+}$ revealed structural changes which could be related to the recombination kinetics in the corresponding DSC devices.

For the pentadentate ligand based complexes, $[Co(PY5Me_2)(B)]^{2+/3+}$, the changes in internal reorganization of the complexes resulting from the redox process were estimated and compared to those observed for the typical $[Co(bpy)_3]^{2+/3+}$ redox mediator. The smaller reorganization energy associated with the new redox couple $[Co(PY5Me_2)(NMBI)]^{2+/3+}$ as compared to the $[Co(bpy)_3]^{2+/3+}$ resulted in shorter electron lifetimes.

The pair of cobalt(II)/(III) complexes based on a hexadentate ligand (L') $\{[Co(L')]^{2+/3+}\}$ was also applied as redox mediator. The structural characterization of the complex showed unsymmetrical changes in the bond distances upon oxidation of the cobalt(II) complex; viz, oxidation was accompanied by significant contraction of the two axial Co-N bonds with little changes in the equatorial Co-N distances. The thermodynamic stability associated with the $[Co(L')]^{2+}$ complex was assessed by comparing the results of full sun illumination experiments on the DSC devices filled with $[Co(L')]^{2+/3+}$ redox couple and the devices made using $[Co(bpy)_3]^{2+/3+}$ based redox mediator. Two Lewis bases of varying basicity were used as electrolyte additives. An outstanding stability was found for devices made using $[Co(L')]^{2+/3+}$ based redox mediator in conjunction with comparatively weak Lewis base (4-trifluoromethyl-pyridine).

The importance of using AgTFSI as an oxidant was realized when the oxidation of $[Co(PY5Me_2)(CH_3CN)]^{2+}$ using $NOBF_4$ resulted in the formation of an unwanted but rather novel cobalt(III)-fluoride complex: $[Co(PY5Me_2)(F)]^{2+}$. Thus, in Chapter 3, an alternative oxidation method of cobalt(II) complexes using AgTFSI is suggested. Chapter 5 describes a more direct method for the synthesis of the novel $[Co(PY5Me_2)(F)]^{2+}$ complex together with the X-ray crystal structure determination and a comparison of this structure to that of related complexes.

6.2 Outlook

This thesis emphasizes the value of using high denticity polypyridyl ligands for the synthesis of cobalt(II)/(III) based complexes and defines new directions to obtain thermodynamically stable cobalt(II)/(III) based redox couples. Future work will focus on the fundamental studies of regeneration and recombination kinetics for redox couples derived from the $[Co(PY5Me_2)(CH_3CN)]^{2+}$ complex. Variation in the redox potential through the replacement of the acetonitrile ligand with a range of Lewis bases will allow the further elucidation of fundamental electron transfer processes and the optimization of the structure and properties of the complex. The hexadentate ligand based redox couple, $[Co(L')]^{2+/3+}$, can potentially be applied in high boiling solvents; therefore, the thermodynamic stability of the complex will be investigated under extended full sun illumination at elevated temperatures (60-84 °C). These studies will be important if commercial development of such devices is to be contemplated.

From a broader perspective, the successful implementation of cobalt complexes incorporating high denticity ligands as DSC redox mediators points to the desirability of custom designing new ligands not only for use in developing cobalt complexes but also redox couples based on a variety of other metals.

Chapter 7

Appendix

Experimental for Complex $[Co(PY5Me_2)(F)](OTf)_2 \cdot CH_3CN$ (2)

Crystal data

$2(C_{29}H_{25}CoFN_5) \cdot 4(CF_3O_3S) \cdot 3(C_2H_3N)$	V = 7105.7 (4) Å^3
M_r = 1762.38	Z = 4
Orthorhombic, $Cmc2_1$	Mo Ka radiation, l = 0.71073 Å
a = 14.7310 (4) Å	m = 0.69 mm^{-1}
b = 21.9915 (8) Å	T = 123 K
c = 21.9340 (8) Å	0.25 × 0.25 × 0.25 mm

Data collection

Xcalibur, Ruby, Gemini ultra diffractometer	11729 independent reflections
Absorption correction: multi-scan *CrysAlis PRO*, Agilent Technologies, Version 1.171.35.15 (release 03-08-2011 CrysAlis171 .NET) (compiled Aug 3 2011,13:03:54) Empirical absorption correction using spherical harmonics, implemented in SCALE3 ABSPACK scaling algorithm.	10126 reflections with $I > 2s(I)$
T_{min} = 0.467, T_{max} = 1.000	R_{int} = 0.038
42139 measured reflections	

Refinement

$R[F^2 > 2s(F^2)]$ = 0.031	H-atom parameters constrained
$wR(F^2)$ = 0.077	Dñ$_{max}$ = 0.53 e Å^{-3}
S = 1.04	Dñ$_{min}$ = -0.45 e Å^{-3}
8374 reflections	Absolute structure: Flack H D (1983), Acta Cryst. A39, 876-881
576 parameters	Flack parameter: -0.023 (9)
7 restraints	

Data collection: *CrysAlis PRO*, Agilent Technologies, Version 1.171.35.15 (release 03-08-2011 CrysAlis171 .NET) (compiled Aug 3 2011,13:03:54); cell refinement: *CrysAlis PRO*, Agilent Technologies, Version 1.171.35.15 (release 03-08-2011 CrysAlis171 .NET) (compiled Aug 3 2011,13:03:54); data reduction: *CrysAlis PRO*, Agilent Technologies, Version 1.171.35.15 (release 03-08-2011 CrysAlis171 .NET) (compiled Aug 3 2011,13:03:54); program(s) used to solve structure: *SHELXS97* (Sheldrick, 1990); program(s) used to refine structure: *SHELXL97* (Sheldrick, 1997); molecular graphics: *X-SEED*; software used to prepare material for publication: CIFTAB.

Supplementary Materials:

$[Co(PY5Me_2)(F)](OTf)_2 \cdot CH_3CN$ (2)

Complex $[Co(PY5Me_2)(F)](OTf)_2 \cdot CH_3CN$ (2)

Crystal data

$2(C_{29}H_{25}CoFN_5) \cdot 4(CF_3O_3S) \cdot 3(C_2H_3N)$	$F(000) = 3592$
$M_r = 1762.38$	$D_x = 1.647$ Mg m^{-3}
Orthorhombic, $Cmc2_1$	Mo $K\alpha$ radiation, $\lambda = 0.71073$ Å
Hall symbol: C 2c -2	Cell parameters from 3868 reflections
$a = 14.7310$ (4) Å	$\theta = 2.2–32.4°$
$b = 21.9915$ (8) Å	$\mu = 0.69$ mm^{-1}
$c = 21.9340$ (8) Å	$T = 123$ K
$V = 7105.7$ (4) Å^3	Prism, orange
$Z = 4$	0.25 × 0.25 × 0.25 mm

Data collection

Xcalibur, Ruby, Gemini ultra diffractometer	11729 independent reflections
Radiation source: Enhance (Mo) X-ray Source	10126 reflections with $I > 2\sigma(I)$
graphite	$R_{int} = 0.038$
Detector resolution: 10.3389 pixels mm^{-1}	$\theta_{max} = 32.4°$, $\theta_{min} = 2.1°$
ω scans	$h = -22 \rightarrow 19$
Absorption correction: multi-scan *CrysAlis PRO*, Agilent Technologies, Version 1.171.35.15 (release 03-08-2011 CrysAlis171 .NET) (compiled Aug 3 2011,13:03:54) Empirical absorption correction using spherical harmonics, implemented in SCALE3 ABSPACK scaling algorithm.	$k = -32 \rightarrow 32$
$T_{min} = 0.467$, $T_{max} = 1.000$	$l = -27 \rightarrow 32$
42139 measured reflections	

Refinement

Refinement on F^2	Secondary atom site location: difference Fourier map
Least-squares matrix: full	Hydrogen site location: inferred from neighbouring sites
$R[F^2 > 2s(F^2)] = 0.031$	H-atom parameters constrained
$wR(F^2) = 0.077$	$w = 1/[s^2(F_o^2) + (0.0422P)^2 + 4.130P]$ where $P = (F_o^2 + 2F_c^2)/3$
$S = 1.04$	$(D/s)_{max} = 0.001$
8374 reflections	$Dñ_{max} = 0.53$ e Å^{-3}
576 parameters	$Dñ_{min} = -0.45$ e Å^{-3}
7 restraints	Absolute structure: Flack H D (1983), Acta Cryst. A39, 876-881
Primary atom site location: structure-invariant direct methods	Flack parameter: -0.023 (9)

Special details

Geometry. All esds (except the esd in the dihedral angle between two l.s. planes) are estimated using the full covariance matrix. The cell esds are taken into account individually in the estimation of esds in distances, angles and torsion angles; correlations between esds in cell parameters are only used when they are defined by crystal symmetry. An approximate (isotropic) treatment of cell esds is used for estimating esds involving l.s. planes.

Refinement. Refinement of F^2 against ALL reflections. The weighted R-factor wR and goodness of fit S are based on F^2, conventional R-factors R are based on F, with F set to zero for negative F^2. The threshold expression of $F^2 > 2\text{sigma}(F^2)$ is used only for calculating R-factors(gt) etc. and is not relevant to the choice of reflections for refinement. R-factors based on F^2 are statistically about twice as large as those based on F, and R- factors based on ALL data will be even larger.

Fractional atomic coordinates and isotropic or equivalent isotropic displacement parameters (Å^2)

	x	*y*	*z*	U_{iso}*/U_{eq}	Occ. (<1)
Co1	0.5000	0.359286 (18)	0.448768 (18)	0.01210 (9)	
Co2	0.5000	0.279771 (18)	0.085253 (17)	0.01142 (9)	
S1	0.26458 (4)	0.53300 (3)	0.29428 (3)	0.02034 (12)	
S2	0.5000	0.00776 (4)	0.54750 (4)	0.02066 (17)	
S3	0.0000	0.24136 (4)	0.29829 (4)	0.02306 (17)	
F1	0.5000	0.41734 (8)	0.38966 (8)	0.0185 (4)	
F2	0.5000	0.21770 (8)	0.03047 (8)	0.0187 (4)	
F3	0.1166 (2)	0.46905 (14)	0.28463 (13)	0.1024 (11)	
F4	0.12820 (17)	0.51831 (14)	0.36808 (10)	0.0848 (8)	
F5	0.09554 (13)	0.56500 (14)	0.28356 (11)	0.0794 (8)	
F6	0.57256 (17)	-0.01137 (12)	0.65408 (10)	0.0739 (7)	
F7	0.5000	0.07134 (12)	0.64792 (14)	0.0808 (12)	
F8	0.0622 (4)	0.3420 (3)	0.3337 (2)	0.0560 (16)	0.50
F9	-0.0735 (3)	0.3535 (3)	0.3091 (4)	0.094 (3)	0.50
F10	0.0395 (3)	0.3404 (2)	0.24128 (16)	0.0719 (16)	0.50
O3	0.27201 (13)	0.53130 (8)	0.22898 (8)	0.0272 (4)	
O4	0.30947 (17)	0.48365 (11)	0.32498 (10)	0.0529 (7)	
O5	0.27734 (18)	0.59148 (10)	0.32109 (10)	0.0499 (6)	
O6	0.41820 (12)	0.03875 (10)	0.52959 (9)	0.0365 (5)	
O7	0.5000	-0.05698 (13)	0.53935 (15)	0.0490 (8)	
O8	-0.0772 (6)	0.2318 (6)	0.2592 (4)	0.0313 (17)	0.50
O9	0.0841 (6)	0.2187 (6)	0.2742 (4)	0.047 (3)	0.50
O10	-0.0232 (3)	0.23124 (19)	0.36141 (13)	0.0431 (16)	0.50
N1	0.5000	0.29667 (12)	0.51228 (11)	0.0122 (5)	
N2	0.41161 (12)	0.40712 (8)	0.49537 (8)	0.0145 (4)	
N3	0.41259 (12)	0.31229 (8)	0.40036 (8)	0.0141 (4)	
N11	0.5000	0.34520 (11)	0.14480 (11)	0.0118 (5)	
N12	0.40044 (12)	0.31861 (8)	0.04049 (8)	0.0149 (4)	
N13	0.39926 (12)	0.23955 (8)	0.12862 (8)	0.0146 (4)	
N9	0.5000	0.54749 (15)	0.51802 (18)	0.0341 (7)	
N10	0.23043 (19)	0.20926 (12)	0.01862 (13)	0.0419 (6)	
C1	0.5000	0.31293 (14)	0.57153 (13)	0.0151 (6)	
C2	0.5000	0.26913 (16)	0.61810 (15)	0.0252 (7)	
H2	0.5000	0.2809	0.6598	0.030*	
C3	0.5000	0.20872 (17)	0.60177 (17)	0.0302 (8)	
H3	0.5000	0.1782	0.6324	0.036*	

C4	0.5000	0.19240 (16)	0.54187 (17)	0.0248 (7)	
H4	0.5000	0.1506	0.5307	0.030*	
C5	0.5000	0.23690 (14)	0.49733 (14)	0.0168 (6)	
C6	0.5000	0.38041 (14)	0.58588 (15)	0.0177 (6)	
C7	0.5000	0.39161 (16)	0.65538 (14)	0.0233 (7)	
H7A	0.5000	0.4355	0.6634	0.035*	
H7B	0.5543	0.3732	0.6734	0.035*	0.50
H7C	0.4457	0.3732	0.6734	0.035*	0.50
C8	0.41579 (15)	0.40912 (10)	0.55682 (10)	0.0171 (4)	
C9	0.34858 (16)	0.43754 (10)	0.59056 (11)	0.0218 (5)	
H9	0.3516	0.4377	0.6338	0.026*	
C10	0.27690 (17)	0.46577 (11)	0.56106 (12)	0.0247 (5)	
H10	0.2287	0.4835	0.5837	0.030*	
C11	0.27676 (17)	0.46772 (11)	0.49825 (12)	0.0230 (5)	
H11	0.2296	0.4881	0.4769	0.028*	
C12	0.34644 (15)	0.43959 (10)	0.46670 (11)	0.0180 (4)	
H12	0.3485	0.4432	0.4236	0.022*	
C13	0.5000	0.22190 (14)	0.42951 (14)	0.0160 (6)	
C14	0.5000	0.15238 (15)	0.41979 (17)	0.0239 (7)	
H14A	0.5000	0.1435	0.3760	0.036*	
H14B	0.4457	0.1348	0.4386	0.036*	0.50
H14C	0.5543	0.1348	0.4386	0.036*	0.50
C15	0.41691 (15)	0.25100 (10)	0.39980 (10)	0.0159 (4)	
C16	0.35041 (16)	0.21714 (11)	0.36937 (11)	0.0209 (5)	
H16	0.3529	0.1740	0.3698	0.025*	
C17	0.28115 (16)	0.24652 (12)	0.33875 (11)	0.0248 (5)	
H17	0.2332	0.2241	0.3206	0.030*	
C18	0.28314 (16)	0.30868 (13)	0.33515 (11)	0.0252 (5)	
H18	0.2385	0.3298	0.3121	0.030*	
C19	0.35043 (16)	0.34040 (11)	0.36520 (10)	0.0195 (5)	
H19	0.3530	0.3834	0.3610	0.023*	
C20	0.42093 (15)	0.36799 (9)	0.16639 (10)	0.0158 (4)	
C21	0.41901 (17)	0.41249 (11)	0.21141 (11)	0.0237 (5)	
H21	0.3627	0.4276	0.2262	0.028*	
C22	0.5000	0.43448 (16)	0.23442 (16)	0.0259 (8)	
H22	0.5000	0.4644	0.2657	0.031*	
C23	0.33358 (15)	0.34155 (10)	0.14019 (10)	0.0175 (4)	
C24	0.24993 (17)	0.37334 (12)	0.16694 (12)	0.0273 (6)	
H24A	0.1948	0.3555	0.1494	0.041*	
H24B	0.2523	0.4168	0.1572	0.041*	

H24C	0.2492	0.3680	0.2113	0.041*	
C25	0.33355 (15)	0.34806 (10)	0.07041 (10)	0.0175 (5)	
C26	0.26563 (17)	0.37855 (11)	0.03906 (13)	0.0271 (5)	
H26	0.2195	0.3995	0.0608	0.032*	
C27	0.26546 (19)	0.37825 (12)	-0.02384 (13)	0.0297 (6)	
H27	0.2212	0.4008	-0.0458	0.036*	
C28	0.33021 (17)	0.34492 (11)	-0.05459 (12)	0.0267 (5)	
H28	0.3300	0.3426	-0.0978	0.032*	
C29	0.39527 (16)	0.31504 (10)	-0.02083 (10)	0.0195 (5)	
H29	0.4386	0.2908	-0.0417	0.023*	
C30	0.33133 (15)	0.27287 (10)	0.15294 (10)	0.0161 (4)	
C31	0.26116 (17)	0.24542 (11)	0.18494 (11)	0.0221 (5)	
H31	0.2143	0.2695	0.2023	0.027*	
C32	0.25957 (17)	0.18286 (11)	0.19149 (11)	0.0222 (5)	
H32	0.2138	0.1638	0.2153	0.027*	
C33	0.32524 (17)	0.14874 (11)	0.16302 (11)	0.0224 (5)	
H33	0.3242	0.1056	0.1653	0.027*	
C34	0.39280 (15)	0.17838 (10)	0.13100 (10)	0.0177 (4)	
H34	0.4365	0.1547	0.1098	0.021*	
C35	0.5000	0.55129 (16)	0.4666 (2)	0.0291 (9)	
C36	0.5000	0.55688 (18)	0.3999 (2)	0.0352 (9)	
H36A	0.5612	0.5491	0.3843	0.053*	0.50
H36B	0.4811	0.5980	0.3884	0.053*	0.50
H36C	0.4577	0.5272	0.3825	0.053*	0.50
C37	0.2865 (2)	0.18320 (14)	-0.00647 (15)	0.0384 (7)	
C38	0.3578 (2)	0.15038 (15)	-0.03933 (17)	0.0482 (8)	
H38A	0.4025	0.1794	-0.0551	0.072*	
H38B	0.3308	0.1278	-0.0733	0.072*	
H38C	0.3879	0.1219	-0.0115	0.072*	
C39	0.1445 (2)	0.51979 (17)	0.30765 (14)	0.0475 (8)	
C40	0.5000	0.01452 (16)	0.63013 (18)	0.0286 (8)	
C41	0.0000	0.32384 (19)	0.29361 (14)	0.0379 (9)	

Atomic displacement parameters (Å^2)

	U^{11}	U^{22}	U^{33}	U^{12}	U^{13}	U^{23}
Co1	0.01409 (19)	0.01098 (19)	0.01122 (18)	0.000	0.000	0.00185 (15)
Co2	0.01383 (18)	0.01030 (19)	0.01012 (18)	0.000	0.000	0.00033 (15)
S1	0.0234 (3)	0.0210 (3)	0.0166 (3)	0.0060 (2)	-0.0024 (2)	-0.0002 (2)
S2	0.0171 (4)	0.0164 (4)	0.0284 (4)	0.000	0.000	-0.0001 (3)
S3	0.0220 (4)	0.0335 (5)	0.0138 (4)	0.000	0.000	0.0010 (3)
F1	0.0229 (9)	0.0159 (9)	0.0168 (9)	0.000	0.000	0.0041 (7)
F2	0.0235 (9)	0.0170 (9)	0.0157 (9)	0.000	0.000	-0.0038 (7)
F3	0.114 (2)	0.119 (2)	0.0741 (18)	-0.0918 (19)	0.0038 (16)	-0.0039 (16)
F4	0.0662 (15)	0.154 (3)	0.0342 (11)	-0.0179 (17)	0.0223 (10)	0.0026 (14)
F5	0.0306 (10)	0.146 (2)	0.0619 (14)	0.0298 (13)	-0.0044 (9)	-0.0036 (15)
F6	0.0770 (15)	0.1027 (19)	0.0420 (11)	0.0384 (14)	-0.0221 (11)	0.0090 (12)
F7	0.174 (4)	0.0285 (15)	0.0403 (16)	0.000	0.000	-0.0118 (13)
F8	0.056 (3)	0.054 (4)	0.058 (3)	-0.042 (2)	0.003 (2)	-0.014 (2)
F9	0.032 (2)	0.025 (2)	0.224 (10)	0.0141 (18)	-0.032 (4)	0.019 (4)
F10	0.120 (4)	0.065 (3)	0.0306 (18)	-0.050 (2)	0.003 (2)	0.0168 (17)
O3	0.0318 (10)	0.0322 (10)	0.0178 (9)	0.0088 (8)	0.0019 (7)	0.0040 (7)
O4	0.0718 (16)	0.0586 (15)	0.0282 (11)	0.0429 (13)	0.0016 (11)	0.0130 (10)
O5	0.0736 (16)	0.0332 (11)	0.0429 (12)	-0.0095 (11)	-0.0152 (11)	-0.0147 (10)
O6	0.0207 (9)	0.0490 (12)	0.0398 (12)	0.0058 (9)	-0.0040 (8)	0.0092 (10)
O7	0.081 (2)	0.0205 (15)	0.0454 (19)	0.000	0.000	-0.0072 (13)
O8	0.019 (3)	0.043 (5)	0.032 (3)	-0.016 (2)	0.000 (3)	0.005 (3)
O9	0.018 (2)	0.048 (6)	0.076 (7)	0.018 (3)	-0.017 (3)	-0.016 (4)
O10	0.062 (5)	0.051 (2)	0.0159 (16)	-0.008 (2)	-0.0001 (16)	0.0099 (15)
N1	0.0106 (11)	0.0136 (12)	0.0124 (12)	0.000	0.000	0.0019 (10)
N2	0.0165 (9)	0.0117 (9)	0.0151 (9)	-0.0002 (7)	0.0001 (7)	0.0008 (7)
N3	0.0142 (9)	0.0169 (9)	0.0112 (8)	0.0009 (7)	0.0015 (7)	-0.0008 (7)
N11	0.0173 (12)	0.0087 (12)	0.0094 (11)	0.000	0.000	0.0002 (9)
N12	0.0167 (9)	0.0119 (9)	0.0162 (9)	-0.0049 (7)	-0.0023 (7)	0.0034 (7)
N13	0.0141 (8)	0.0154 (9)	0.0143 (9)	-0.0015 (7)	-0.0021 (7)	0.0022 (7)
N9	0.0355 (18)	0.0185 (17)	0.048 (2)	0.000	0.000	0.0048 (14)
N10	0.0452 (16)	0.0355 (14)	0.0451 (15)	-0.0127 (13)	-0.0174 (13)	0.0092 (12)
C1	0.0156 (14)	0.0150 (15)	0.0146 (15)	0.000	0.000	0.0029 (11)
C2	0.037 (2)	0.0260 (19)	0.0128 (16)	0.000	0.000	0.0071 (13)
C3	0.043 (2)	0.0206 (18)	0.0271 (19)	0.000	0.000	0.0151 (14)
C4	0.0324 (19)	0.0119 (16)	0.0301 (19)	0.000	0.000	0.0028 (14)
C5	0.0176 (15)	0.0149 (15)	0.0180 (15)	0.000	0.000	0.0038 (12)

C6	0.0229 (15)	0.0168 (15)	0.0134 (14)	0.000	0.000	0.0001 (13)
C7	0.0318 (18)	0.0229 (18)	0.0151 (16)	0.000	0.000	-0.0002 (13)
C8	0.0208 (11)	0.0141 (11)	0.0165 (10)	-0.0004 (9)	0.0012 (8)	0.0005 (8)
C9	0.0294 (12)	0.0167 (11)	0.0193 (11)	-0.0025 (9)	0.0065 (10)	-0.0016 (9)
C10	0.0249 (12)	0.0189 (12)	0.0302 (13)	0.0038 (10)	0.0085 (10)	-0.0029 (10)
C11	0.0209 (11)	0.0179 (12)	0.0300 (13)	0.0022 (9)	0.0005 (10)	0.0001 (10)
C12	0.0204 (11)	0.0129 (10)	0.0206 (11)	0.0006 (8)	-0.0015 (8)	0.0011 (8)
C13	0.0170 (14)	0.0129 (15)	0.0182 (16)	0.000	0.000	-0.0025 (12)
C14	0.0254 (17)	0.0161 (16)	0.0302 (18)	0.000	0.000	-0.0019 (13)
C15	0.0159 (10)	0.0176 (11)	0.0141 (10)	0.0003 (8)	0.0020 (8)	0.0000 (8)
C16	0.0217 (12)	0.0206 (12)	0.0206 (11)	-0.0071 (9)	0.0013 (9)	-0.0024 (9)
C17	0.0207 (11)	0.0374 (15)	0.0163 (11)	-0.0084 (10)	-0.0016 (9)	-0.0027 (10)
C18	0.0215 (12)	0.0366 (15)	0.0174 (11)	0.0056 (10)	-0.0057 (9)	-0.0001 (10)
C19	0.0204 (11)	0.0242 (12)	0.0139 (10)	0.0055 (9)	-0.0012 (8)	-0.0006 (9)
C20	0.0201 (11)	0.0117 (10)	0.0155 (10)	-0.0002 (8)	0.0019 (8)	0.0011 (8)
C21	0.0294 (12)	0.0212 (12)	0.0205 (12)	0.0024 (10)	0.0070 (10)	-0.0049 (9)
C22	0.040 (2)	0.0168 (17)	0.0210 (17)	0.000	0.000	-0.0076 (13)
C23	0.0166 (10)	0.0129 (10)	0.0229 (11)	0.0020 (8)	0.0022 (8)	0.0009 (8)
C24	0.0208 (12)	0.0207 (12)	0.0405 (16)	0.0047 (9)	0.0093 (11)	0.0000 (11)
C25	0.0162 (10)	0.0120 (10)	0.0243 (12)	-0.0020 (8)	-0.0020 (8)	0.0008 (8)
C26	0.0240 (12)	0.0157 (12)	0.0416 (15)	0.0000 (9)	-0.0107 (11)	0.0020 (11)
C27	0.0289 (13)	0.0182 (12)	0.0419 (15)	-0.0035 (10)	-0.0229 (12)	0.0100 (11)
C28	0.0314 (13)	0.0260 (13)	0.0226 (11)	-0.0141 (10)	-0.0125 (11)	0.0083 (11)
C29	0.0211 (12)	0.0212 (12)	0.0161 (11)	-0.0087 (9)	-0.0034 (8)	0.0036 (9)
C30	0.0165 (10)	0.0144 (11)	0.0175 (10)	-0.0002 (8)	-0.0012 (8)	-0.0010 (8)
C31	0.0231 (12)	0.0211 (12)	0.0221 (12)	-0.0038 (9)	0.0041 (9)	-0.0024 (10)
C32	0.0239 (12)	0.0206 (12)	0.0220 (11)	-0.0090 (9)	0.0045 (9)	0.0010 (9)
C33	0.0253 (12)	0.0186 (11)	0.0234 (12)	-0.0060 (9)	-0.0022 (10)	0.0051 (9)
C34	0.0178 (11)	0.0158 (11)	0.0196 (11)	-0.0005 (8)	-0.0024 (8)	0.0007 (9)
C35	0.0201 (17)	0.0150 (17)	0.052 (3)	0.000	0.000	0.0002 (16)
C36	0.037 (2)	0.0201 (19)	0.048 (2)	0.000	0.000	-0.0053 (17)
C37	0.0415 (17)	0.0296 (15)	0.0441 (17)	-0.0180 (14)	-0.0195 (15)	0.0141 (13)
C38	0.0390 (16)	0.0467 (18)	0.059 (2)	-0.0093 (14)	-0.0172 (15)	0.0058 (16)
C39	0.0450 (18)	0.066 (2)	0.0314 (16)	-0.0158 (17)	0.0051 (13)	-0.0039 (15)
C40	0.040 (2)	0.0131 (17)	0.033 (2)	0.000	0.000	0.0028 (14)
C41	0.050 (2)	0.038 (2)	0.0251 (18)	0.000	0.000	0.0030 (17)

Geometric parameters (Å, º)

Co1—F1	1.8196 (18)	N11—C20	1.353 (2)
Co1—N1	1.959 (3)	N11—C20^{i}	1.353 (2)
Co1—N2^{i}	1.9613 (18)	N12—C29	1.349 (3)
Co1—N2	1.9613 (18)	N12—C25	1.349 (3)
Co1—N3	1.9630 (18)	N13—C34	1.350 (3)
Co1—N3^{i}	1.9630 (18)	N13—C30	1.350 (3)
Co2—F2	1.8186 (18)	N9—C35	1.131 (5)
Co2—N11	1.943 (2)	N10—C37	1.146 (4)
Co2—N12	1.9608 (18)	C1—C2	1.404 (4)
Co2—N12^{i}	1.9608 (18)	C1—C6	1.517 (4)
Co2—N13^{i}	1.9723 (18)	C2—C3	1.376 (5)
Co2—N13	1.9723 (18)	C3—C4	1.362 (5)
S1—O5	1.427 (2)	C4—C5	1.383 (5)
S1—O3	1.4368 (17)	C5—C13	1.524 (4)
S1—O4	1.438 (2)	C6—C8	1.531 (3)
S1—C39	1.816 (3)	C6—C8^{i}	1.531 (3)
S2—O7	1.435 (3)	C6—C7	1.544 (4)
S2—O6	1.4391 (19)	C8—C9	1.385 (3)
S2—O6^{i}	1.4391 (19)	C9—C10	1.385 (4)
S2—C40	1.819 (4)	C10—C11	1.378 (4)
S3—O9^{ii}	1.436 (4)	C11—C12	1.384 (3)
S3—O9	1.436 (4)	C13—C15	1.527 (3)
S3—O8	1.439 (3)	C13—C15^{i}	1.527 (3)
S3—O8^{ii}	1.439 (3)	C13—C14	1.544 (4)
S3—O10^{ii}	1.443 (3)	C15—C16	1.400 (3)
S3—O10	1.443 (3)	C16—C17	1.382 (4)
S3—C41	1.817 (4)	C17—C18	1.370 (4)
F3—C39	1.292 (4)	C18—C19	1.380 (3)
F4—C39	1.347 (4)	C20—C21	1.391 (3)
F5—C39	1.337 (4)	C20—C23	1.524 (3)
F6—C40	1.320 (3)	C21—C22	1.383 (3)
F7—C40	1.309 (4)	C22—C21^{i}	1.383 (3)
F8—F9^{ii}	0.619 (8)	C23—C24	1.533 (3)
F8—C41	1.332 (4)	C23—C30	1.536 (3)
F9—F8^{ii}	0.619 (8)	C23—C25	1.537 (3)
F9—C41	1.309 (4)	C25—C26	1.387 (3)
F9—F10^{ii}	1.597 (8)	C26—C27	1.380 (4)
F10—F10^{ii}	1.165 (10)	C27—C28	1.379 (4)

F10—C41	1.338 (3)	C28—C29	1.378 (3)
F10—F9^{ii}	1.597 (8)	C30—C31	1.388 (3)
O8—O9^{ii}	0.448 (13)	C31—C32	1.384 (4)
O9—O8^{ii}	0.448 (13)	C32—C33	1.374 (4)
O10—O10^{ii}	0.685 (9)	C33—C34	1.382 (3)
N1—C1	1.348 (4)	C35—C36	1.468 (6)
N1—C5	1.355 (4)	C37—C38	1.464 (5)
N2—C8	1.350 (3)	C40—F6^{i}	1.320 (3)
N2—C12	1.352 (3)	C41—F9^{ii}	1.309 (4)
N3—C19	1.347 (3)	C41—F8^{ii}	1.332 (4)
N3—C15	1.349 (3)	C41—F10^{ii}	1.338 (3)
F1—Co1—N1	179.89 (10)	C2—C1—C6	121.3 (3)
F1—Co1—N2^{i}	89.72 (7)	C3—C2—C1	118.2 (3)
N1—Co1—N2^{i}	90.36 (8)	C4—C3—C2	120.4 (3)
F1—Co1—N2	89.72 (7)	C3—C4—C5	119.7 (3)
N1—Co1—N2	90.36 (8)	N1—C5—C4	121.0 (3)
N2^{i}—Co1—N2	83.19 (10)	N1—C5—C13	116.5 (3)
F1—Co1—N3	89.09 (7)	C4—C5—C13	122.4 (3)
N1—Co1—N3	90.83 (8)	C1—C6—C8	108.48 (18)
N2^{i}—Co1—N3	178.66 (8)	C1—C6—C8^{i}	108.48 (18)
N2—Co1—N3	97.40 (7)	C8—C6—C8^{i}	108.2 (3)
F1—Co1—N3^{i}	89.09 (7)	C1—C6—C7	111.2 (3)
N1—Co1—N3^{i}	90.83 (8)	C8—C6—C7	110.20 (18)
N2^{i}—Co1—N3^{i}	97.40 (7)	C8^{i}—C6—C7	110.20 (18)
N2—Co1—N3^{i}	178.66 (8)	N2—C8—C9	121.0 (2)
N3—Co1—N3^{i}	81.99 (10)	N2—C8—C6	116.1 (2)
F2—Co2—N11	179.12 (10)	C9—C8—C6	122.9 (2)
F2—Co2—N12	89.78 (7)	C8—C9—C10	119.8 (2)
N11—Co2—N12	90.80 (7)	C11—C10—C9	118.8 (2)
F2—Co2—N12^{i}	89.78 (7)	C10—C11—C12	119.0 (2)
N11—Co2—N12^{i}	90.80 (7)	N2—C12—C11	122.0 (2)
N12—Co2—N12^{i}	96.84 (10)	C5—C13—C15	109.01 (16)
F2—Co2—N13^{i}	88.97 (7)	C5—C13—C15^{i}	109.01 (16)
N11—Co2—N13^{i}	90.45 (7)	C15—C13—C15^{i}	106.5 (3)
N12—Co2—N13^{i}	178.69 (8)	C5—C13—C14	110.4 (3)
N12^{i}—Co2—N13^{i}	82.77 (7)	C15—C13—C14	110.86 (17)
F2—Co2—N13	88.97 (7)	C15^{i}—C13—C14	110.86 (17)
N11—Co2—N13	90.45 (7)	N3—C15—C16	120.2 (2)
N12—Co2—N13	82.77 (7)	N3—C15—C13	116.9 (2)
N12^{i}—Co2—N13	178.69 (8)	C16—C15—C13	122.8 (2)

N13^{i}—Co2—N13	97.61 (10)	C17—C16—C15	120.0 (2)
O5—S1—O3	115.11 (13)	C18—C17—C16	118.6 (2)
O5—S1—O4	115.26 (15)	C17—C18—C19	119.5 (2)
O3—S1—O4	114.33 (12)	N3—C19—C18	122.0 (2)
O5—S1—C39	101.88 (16)	N11—C20—C21	121.8 (2)
O3—S1—C39	103.36 (13)	N11—C20—C23	116.96 (19)
O4—S1—C39	104.55 (16)	C21—C20—C23	121.3 (2)
O7—S2—O6	115.85 (11)	C22—C21—C20	119.2 (2)
O7—S2—O6^{i}	115.85 (11)	C21—C22—C21^{i}	119.3 (3)
O6—S2—O6^{i}	113.72 (17)	C20—C23—C24	111.12 (19)
O7—S2—C40	101.84 (18)	C20—C23—C30	108.94 (18)
O6—S2—C40	103.49 (11)	C24—C23—C30	111.17 (19)
O6^{i}—S2—C40	103.49 (11)	C20—C23—C25	109.87 (18)
O9^{ii}—S3—O9	119.3 (12)	C24—C23—C25	109.77 (19)
O9^{ii}—S3—O8	17.9 (5)	C30—C23—C25	105.83 (18)
O9—S3—O8	114.3 (3)	N12—C25—C26	121.2 (2)
O9^{ii}—S3—O8^{ii}	114.3 (3)	N12—C25—C23	116.06 (19)
O9—S3—O8^{ii}	17.9 (5)	C26—C25—C23	122.6 (2)
O8—S3—O8^{ii}	104.4 (10)	C27—C26—C25	119.7 (3)
O9^{ii}—S3—O10^{ii}	120.3 (4)	C28—C27—C26	119.4 (2)
O9—S3—O10^{ii}	95.4 (4)	C29—C28—C27	118.1 (2)
O8—S3—O10^{ii}	137.4 (4)	N12—C29—C28	123.2 (2)
O8^{ii}—S3—O10^{ii}	111.1 (4)	N13—C30—C31	121.0 (2)
O9^{ii}—S3—O10	95.4 (4)	N13—C30—C23	116.47 (19)
O9—S3—O10	120.3 (4)	C31—C30—C23	122.4 (2)
O8—S3—O10	111.1 (4)	C32—C31—C30	119.8 (2)
O8^{ii}—S3—O10	137.4 (4)	C33—C32—C31	118.9 (2)
O10^{ii}—S3—O10	27.4 (3)	C32—C33—C34	118.7 (2)
O9^{ii}—S3—C41	109.0 (5)	N13—C34—C33	122.7 (2)
O9—S3—C41	109.0 (5)	N9—C35—C36	179.4 (4)
O8—S3—C41	96.5 (5)	N10—C37—C38	179.2 (3)
O8^{ii}—S3—C41	96.5 (5)	F3—C39—F5	108.4 (3)
O10^{ii}—S3—C41	102.0 (2)	F3—C39—F4	107.8 (3)
O10—S3—C41	102.0 (2)	F5—C39—F4	108.1 (3)
F9^{ii}—F8—C41	74.4 (5)	F3—C39—S1	112.7 (3)
F8^{ii}—F9—C41	78.5 (4)	F5—C39—S1	110.0 (2)
F8^{ii}—F9—F10^{ii}	130.9 (6)	F4—C39—S1	109.7 (2)
C41—F9—F10^{ii}	53.7 (3)	F7—C40—F6	107.0 (2)
F10^{ii}—F10—C41	64.2 (2)	F7—C40—F6^{i}	107.0 (2)
F10^{ii}—F10—F9^{ii}	108.3 (3)	F6—C40—F6^{i}	108.1 (4)

C41—F10—F9^{ii}	52.1 (2)	F7—C40—S2	112.0 (3)
O9^{ii}—O8—S3	80.6 (7)	F6—C40—S2	111.2 (2)
O8^{ii}—O9—S3	81.5 (7)	F6^{i}—C40—S2	111.2 (2)
O10^{ii}—O10—S3	76.28 (17)	F9—C41—F9^{ii}	111.6 (7)
C1—N1—C5	119.4 (3)	F9—C41—F8	104.3 (4)
C1—N1—Co1	119.9 (2)	F9^{ii}—C41—F8	27.1 (4)
C5—N1—Co1	120.7 (2)	F9—C41—F8^{ii}	27.1 (4)
C8—N2—C12	118.66 (19)	F9^{ii}—C41—F8^{ii}	104.3 (4)
C8—N2—Co1	120.51 (15)	F8—C41—F8^{ii}	86.9 (6)
C12—N2—Co1	120.82 (15)	F9—C41—F10^{ii}	74.2 (4)
C19—N3—C15	119.02 (19)	F9^{ii}—C41—F10^{ii}	116.6 (5)
C19—N3—Co1	120.91 (16)	F8—C41—F10^{ii}	141.7 (5)
C15—N3—Co1	119.99 (15)	F8^{ii}—C41—F10^{ii}	100.7 (3)
C20—N11—C20^{i}	118.8 (3)	F9—C41—F10	116.6 (5)
C20—N11—Co2	120.61 (13)	F9^{ii}—C41—F10	74.2 (4)
C20^{i}—N11—Co2	120.61 (13)	F8—C41—F10	100.7 (3)
C29—N12—C25	118.13 (19)	F8^{ii}—C41—F10	141.7 (5)
C29—N12—Co2	121.06 (16)	F10^{ii}—C41—F10	51.6 (4)
C25—N12—Co2	120.78 (15)	F9—C41—S3	118.9 (3)
C34—N13—C30	118.27 (19)	F9^{ii}—C41—S3	118.9 (3)
C34—N13—Co2	121.24 (15)	F8—C41—S3	105.2 (4)
C30—N13—Co2	120.31 (15)	F8^{ii}—C41—S3	105.2 (4)
N1—C1—C2	121.3 (3)	F10^{ii}—C41—S3	108.7 (3)
N1—C1—C6	117.4 (3)	F10—C41—S3	108.7 (3)

Symmetry codes: (i) -*x*+1, *y*, *z*; (ii) -*x*, *y*, *z*.

Experimental for Complex 3

Crystal data

$C_{32}H_{32}CoN_6O \cdot C_2F_6NO_4S_2 \cdot 2(CF_3O_3S) \cdot CH_2Cl_2$	V = 4742.9 (4) Å^3
M_r = 1238.78	Z = 4
Monoclinic, $P2_1/c$	Mo Ka radiation, l = 0.71073 Å
a = 19.0821 (9) Å	m = 0.76 mm^{-1}
b = 13.1795 (7) Å	T = 123 K
c = 19.0210 (9) Å	0.20 × 0.10 × 0.02 mm
b = 97.481 (5)°	

Data collection

Xcalibur, Ruby, Gemini ultra diffractometer	10884 independent reflections
Absorption correction: multi-scan *CrysAlis PRO*, Agilent Technologies, Version 1.171.35.15 (release 03-08-2011 CrysAlis171 .NET) (compiled Aug 3 2011,13:03:54) Empirical absorption correction using spherical harmonics, implemented in SCALE3 ABSPACK scaling algorithm.	6657 reflections with $I > 2s(I)$
T_{min} = 0.940, T_{max} = 1.000	R_{int} = 0.062
26122 measured reflections	

Refinement

$R[F^2 > 2s(F^2)] = 0.074$	0 restraints
$wR(F^2) = 0.215$	H-atom parameters constrained
$S = 1.03$	$D\rho_{max} = 0.95$ e Å^{-3}
10884 reflections	$D\rho_{min} = -1.35$ e Å^{-3}
669 parameters	

Data collection: *CrysAlis PRO*, Agilent Technologies, Version 1.171.35.15 (release 03-08-2011 CrysAlis171 .NET) (compiled Aug 3 2011,13:03:54); cell refinement: *CrysAlis PRO*, Agilent Technologies, Version 1.171.35.15 (release 03-08-2011 CrysAlis171 .NET) (compiled Aug 3 2011,13:03:54); data reduction: *CrysAlis PRO*, Agilent Technologies, Version 1.171.35.15 (release 03-08-2011 CrysAlis171 .NET) (compiled Aug 3 2011,13:03:54); program(s) used to solve structure: *SHELXS97* (Sheldrick, 1990); program(s) used to refine structure: *SHELXL97* (Sheldrick, 1997); molecular graphics: *X-SEED*; software used to prepare material for publication: CIFTAB.

Supplementary Materials for Complex 3:

$[Co(PY5Me_2)(DMF)](OTf)_2(TFSI)\cdot(CH_2Cl_2)$

Complex 3; $[Co(PY5Me_2)(DMF)](OTf)_2(TFSI)\cdot(CH_2Cl_2)$

Crystal data

$C_{32}H_{32}CoN_6O\cdot C_2F_6NO_4S_2\cdot 2(CF_3O_3S)\cdot CH_2Cl_2$	$F(000) = 2504$
$M_r = 1238.78$	$D_x = 1.735$ Mg m^{-3}
Monoclinic, $P2_1/c$	Mo $K\alpha$ radiation, $\lambda = 0.71073$ Å
Hall symbol: -P 2ybc	Cell parameters from 3819 reflections
$a = 19.0821$ (9) Å	$\theta = 1.9–30.2°$
$b = 13.1795$ (7) Å	$\mu = 0.76$ mm^{-1}
$c = 19.0210$ (9) Å	$T = 123$ K
$\beta = 97.481$ (5)°	Plate, red-orange
$V = 4742.9$ (4) Å^3	0.20 × 0.10 × 0.02 mm
$Z = 4$	

Data collection

Xcalibur, Ruby, Gemini ultra diffractometer	10884 independent reflections
Radiation source: Enhance (Mo) X-ray Source	6657 reflections with $I > 2\sigma(I)$
graphite	$R_{int} = 0.062$
Detector resolution: 10.3389 pixels mm^{-1}	$\theta_{max} = 27.5°$, $\theta_{min} = 1.9°$
ω scans	$h = -24$Æ24
Absorption correction: multi-scan *CrysAlis PRO*, Agilent Technologies, Version 1.171.35.15 (release 03-08-2011 CrysAlis171 .NET) (compiled Aug 3 2011,13:03:54) Empirical absorption correction using spherical harmonics, implemented in SCALE3 ABSPACK scaling algorithm.	$k = -17$Æ12
$T_{min} = 0.940$, $T_{max} = 1.000$	$l = -24$Æ17
26122 measured reflections	

Refinement

Refinement on F^2	Primary atom site location: structure-invariant direct methods
Least-squares matrix: full	Secondary atom site location: difference Fourier map
$R[F^2 > 2s(F^2)] = 0.074$	Hydrogen site location: inferred from neighbouring sites
$wR(F^2) = 0.215$	H-atom parameters constrained
$S = 1.03$	$w = 1/[s^2(F_o^2) + (0.0995P)^2 + 8.3637P]$ where $P = (F_o^2 + 2F_c^2)/3$
10884 reflections	$(D/s)_{max} = 0.001$
669 parameters	$D\rho_{max} = 0.95$ e Å^{-3}
0 restraints	$D\rho_{min} = -1.35$ e Å^{-3}

Special details

Geometry. All esds (except the esd in the dihedral angle between two l.s. planes) are estimated using the full covariance matrix. The cell esds are taken into account individually in the estimation of esds in distances, angles and torsion angles; correlations between esds in cell parameters are only used when they are defined by crystal symmetry. An approximate (isotropic) treatment of cell esds is used for estimating esds involving l.s. planes.

Refinement. Refinement of F^2 against ALL reflections. The weighted R-factor wR and goodness of fit S are based on F^2, conventional R-factors R are based on F, with F set to zero for negative F^2. The threshold expression of $F^2 > 2\text{sigma}(F^2)$ is used only for calculating R-factors(gt) etc. and is not relevant to the choice of reflections for refinement. R-factors based on F^2 are statistically about twice as large as those based on F, and R- factors based on ALL data will be even larger.

Fractional atomic coordinates and isotropic or equivalent isotropic displacement parameters (Å^2)

	x	*y*	*z*	U_{iso}*/U_{eq}
Co1	0.26947 (3)	0.91770 (5)	0.18068 (3)	0.01368 (17)
Cl1	0.23183 (12)	0.74105 (18)	0.49707 (11)	0.0689 (6)
Cl2	0.15631 (16)	0.7377 (3)	0.35356 (14)	0.1044 (10)
S1	0.08520 (8)	0.33266 (12)	0.22552 (8)	0.0334 (4)
S2	0.04588 (10)	0.28222 (17)	0.08148 (10)	0.0525 (5)
S3	0.45595 (7)	0.56234 (10)	0.31461 (6)	0.0207 (3)
S4	0.33791 (7)	0.11245 (10)	0.46421 (6)	0.0206 (3)
F1	0.21969 (18)	0.3491 (3)	0.2122 (2)	0.0493 (10)
F2	0.1803 (2)	0.1965 (3)	0.2046 (2)	0.0533 (10)
F3	0.1980 (2)	0.2683 (4)	0.3045 (2)	0.0644 (12)
F4	0.1789 (3)	0.2621 (5)	0.0611 (2)	0.0818 (17)
F5	0.1036 (2)	0.2559 (4)	-0.0346 (2)	0.0709 (14)
F6	0.1267 (3)	0.3979 (4)	0.0147 (3)	0.0901 (18)
F7	0.35058 (19)	0.4756 (3)	0.23499 (17)	0.0439 (9)
F8	0.32203 (17)	0.5427 (3)	0.33055 (18)	0.0417 (9)
F9	0.3795 (2)	0.4014 (3)	0.33594 (18)	0.0446 (9)
F10	0.3106 (2)	0.1002 (3)	0.59553 (18)	0.0565 (11)
F11	0.2613 (2)	-0.0147 (3)	0.5276 (2)	0.0600 (12)
F12	0.3725 (2)	-0.0236 (3)	0.5632 (2)	0.0515 (10)
O1	0.31533 (16)	0.8656 (3)	0.26836 (16)	0.0170 (7)
O2	0.0925 (3)	0.4269 (4)	0.2630 (3)	0.0524 (13)
O3	0.0432 (2)	0.2568 (4)	0.2508 (3)	0.0538 (13)
O4	0.0465 (3)	0.1779 (4)	0.0963 (3)	0.0604 (14)
O5	-0.0138 (3)	0.3214 (5)	0.0382 (3)	0.0772 (18)
O6	0.4375 (2)	0.6537 (3)	0.2752 (2)	0.0339 (9)
O7	0.5033 (2)	0.4957 (3)	0.2846 (2)	0.0359 (10)
O8	0.47057 (18)	0.5754 (3)	0.39056 (17)	0.0249 (8)
O9	0.40244 (19)	0.1643 (3)	0.4890 (2)	0.0340 (9)
O10	0.2775 (2)	0.1770 (3)	0.4490 (2)	0.0369 (10)
O11	0.3439 (2)	0.0333 (3)	0.41299 (19)	0.0389 (10)
N1	0.2205 (2)	0.9678 (3)	0.0910 (2)	0.0173 (8)
N2	0.2128 (2)	0.7908 (3)	0.1712 (2)	0.0170 (8)
N3	0.1917 (2)	0.9622 (3)	0.2325 (2)	0.0179 (9)
N4	0.34821 (19)	0.8694 (3)	0.13102 (19)	0.0149 (8)
N5	0.3215 (2)	1.0474 (3)	0.19143 (19)	0.0149 (8)
N6	0.4055 (2)	0.8523 (3)	0.3562 (2)	0.0203 (9)

N7	0.0700 (3)	0.3613 (4)	0.1455 (3)	0.0469 (14)
C1	0.1499 (3)	0.9527 (4)	0.0736 (3)	0.0226 (11)
C2	0.1157 (3)	0.9797 (5)	0.0072 (3)	0.0355 (14)
H2	0.0664	0.9678	-0.0042	0.043*
C3	0.1525 (3)	1.0232 (5)	-0.0416 (3)	0.0390 (16)
H3	0.1299	1.0400	-0.0875	0.047*
C4	0.2237 (3)	1.0424 (5)	-0.0227 (3)	0.0333 (14)
H4	0.2500	1.0760	-0.0548	0.040*
C5	0.2565 (3)	1.0127 (4)	0.0430 (3)	0.0213 (11)
C6	0.1121 (3)	0.9011 (4)	0.1293 (3)	0.0222 (11)
C7	0.0321 (3)	0.8940 (5)	0.1041 (3)	0.0308 (13)
H7A	0.0243	0.8567	0.0592	0.046*
H7B	0.0123	0.9624	0.0973	0.046*
H7C	0.0088	0.8582	0.1399	0.046*
C8	0.1439 (3)	0.7948 (4)	0.1431 (3)	0.0207 (11)
C9	0.1044 (3)	0.7073 (5)	0.1307 (3)	0.0324 (13)
H9	0.0568	0.7114	0.1088	0.039*
C10	0.1335 (3)	0.6144 (5)	0.1498 (4)	0.0424 (16)
H10	0.1073	0.5537	0.1395	0.051*
C11	0.2016 (3)	0.6114 (5)	0.1841 (4)	0.0378 (15)
H11	0.2224	0.5487	0.2000	0.045*
C12	0.2391 (3)	0.7007 (4)	0.1950 (3)	0.0253 (12)
H12	0.2854	0.6984	0.2204	0.030*
C13	0.1242 (3)	0.9592 (4)	0.1991 (3)	0.0207 (11)
C14	0.0696 (3)	0.9978 (5)	0.2326 (3)	0.0291 (13)
H14	0.0227	0.9972	0.2087	0.035*
C15	0.0826 (3)	1.0370 (5)	0.2999 (3)	0.0367 (15)
H15	0.0456	1.0671	0.3215	0.044*
C16	0.1497 (3)	1.0321 (5)	0.3355 (3)	0.0318 (13)
H16	0.1594	1.0548	0.3832	0.038*
C17	0.2030 (3)	0.9933 (4)	0.3005 (3)	0.0237 (11)
H17	0.2494	0.9885	0.3254	0.028*
C18	0.3357 (2)	1.0305 (4)	0.0650 (2)	0.0171 (10)
C19	0.3685 (3)	1.0859 (4)	0.0066 (3)	0.0240 (11)
H19A	0.3618	1.0453	-0.0369	0.036*
H19B	0.4191	1.0959	0.0216	0.036*
H19C	0.3455	1.1519	-0.0023	0.036*
C20	0.3711 (2)	0.9264 (4)	0.0800 (2)	0.0152 (9)
C21	0.4270 (2)	0.8943 (4)	0.0453 (2)	0.0179 (10)
H21	0.4419	0.9348	0.0086	0.021*

C22	0.4613 (3)	0.8035 (4)	0.0639 (3)	0.0211 (11)
H22	0.4991	0.7805	0.0399	0.025*
C23	0.4391 (3)	0.7473 (4)	0.1182 (3)	0.0205 (11)
H23	0.4621	0.6857	0.1333	0.025*
C24	0.3831 (3)	0.7821 (4)	0.1502 (2)	0.0172 (10)
H24	0.3681	0.7431	0.1875	0.021*
C25	0.3447 (2)	1.0903 (4)	0.1336 (2)	0.0176 (10)
C26	0.3767 (3)	1.1849 (4)	0.1384 (3)	0.0241 (11)
H26	0.3900	1.2162	0.0971	0.029*
C27	0.3895 (3)	1.2341 (4)	0.2034 (3)	0.0272 (12)
H27	0.4114	1.2990	0.2072	0.033*
C28	0.3697 (3)	1.1862 (4)	0.2629 (3)	0.0251 (12)
H28	0.3793	1.2162	0.3086	0.030*
C29	0.3360 (3)	1.0946 (4)	0.2540 (3)	0.0187 (10)
H29	0.3220	1.0625	0.2947	0.022*
C30	0.3795 (2)	0.8839 (4)	0.2944 (2)	0.0176 (10)
H30	0.4087	0.9219	0.2672	0.021*
C31	0.4776 (3)	0.8796 (6)	0.3868 (3)	0.0394 (16)
H31A	0.4992	0.9220	0.3532	0.059*
H31B	0.5057	0.8177	0.3967	0.059*
H31C	0.4760	0.9172	0.4310	0.059*
C32	0.3640 (3)	0.7934 (4)	0.4015 (3)	0.0287 (12)
H32A	0.3167	0.7809	0.3761	0.043*
H32B	0.3600	0.8316	0.4450	0.043*
H32C	0.3876	0.7285	0.4136	0.043*
C33	0.1769 (3)	0.2853 (5)	0.2383 (4)	0.0427 (16)
C34	0.1191 (5)	0.3002 (7)	0.0290 (4)	0.061 (2)
C35	0.3732 (3)	0.4914 (5)	0.3037 (3)	0.0292 (13)
C36	0.3200 (3)	0.0400 (5)	0.5413 (3)	0.0328 (13)
C37	0.1764 (5)	0.8003 (10)	0.4369 (5)	0.093 (3)
H37A	0.1964	0.8678	0.4284	0.112*
H37B	0.1316	0.8115	0.4568	0.112*

Atomic displacement parameters (Å^2)

	U^{11}	U^{22}	U^{33}	U^{12}	U^{13}	U^{23}
Co1	0.0130 (3)	0.0148 (3)	0.0131 (3)	0.0005 (3)	0.0010 (2)	0.0027 (3)
Cl1	0.0763 (14)	0.0714 (15)	0.0619 (12)	-0.0012 (12)	0.0202 (11)	0.0191 (11)
Cl2	0.107 (2)	0.132 (3)	0.0725 (16)	-0.0341 (19)	0.0074 (14)	0.0094 (17)
S1	0.0291 (8)	0.0341 (8)	0.0384 (8)	0.0061 (6)	0.0098 (6)	0.0023 (7)
S2	0.0473 (11)	0.0675 (14)	0.0428 (10)	-0.0162 (10)	0.0055 (8)	-0.0050 (9)
S3	0.0237 (6)	0.0226 (7)	0.0162 (6)	0.0070 (5)	0.0037 (5)	0.0021 (5)
S4	0.0236 (6)	0.0201 (7)	0.0173 (6)	0.0004 (5)	0.0001 (5)	-0.0015 (5)
F1	0.034 (2)	0.039 (2)	0.077 (3)	-0.0017 (17)	0.0167 (19)	0.007 (2)
F2	0.048 (2)	0.039 (2)	0.075 (3)	0.0110 (19)	0.017 (2)	0.007 (2)
F3	0.053 (3)	0.074 (3)	0.062 (3)	0.006 (2)	-0.008 (2)	0.020 (2)
F4	0.052 (3)	0.137 (5)	0.059 (3)	-0.020 (3)	0.017 (2)	-0.012 (3)
F5	0.080 (3)	0.086 (4)	0.051 (3)	-0.035 (3)	0.023 (2)	-0.027 (2)
F6	0.123 (5)	0.076 (4)	0.079 (3)	-0.042 (3)	0.043 (3)	-0.010 (3)
F7	0.045 (2)	0.056 (3)	0.0286 (18)	-0.0032 (18)	-0.0050 (15)	-0.0164 (17)
F8	0.0265 (18)	0.058 (2)	0.042 (2)	-0.0008 (17)	0.0081 (15)	-0.0137 (18)
F9	0.075 (3)	0.0223 (19)	0.039 (2)	-0.0117 (18)	0.0148 (18)	-0.0063 (16)
F10	0.097 (3)	0.050 (3)	0.0258 (19)	0.005 (2)	0.023 (2)	-0.0014 (18)
F11	0.060 (3)	0.056 (3)	0.066 (3)	-0.028 (2)	0.016 (2)	0.011 (2)
F12	0.066 (3)	0.040 (2)	0.045 (2)	0.014 (2)	-0.0052 (19)	0.0175 (18)
O1	0.0169 (16)	0.0213 (19)	0.0123 (15)	-0.0003 (14)	-0.0008 (13)	0.0042 (14)
O2	0.048 (3)	0.043 (3)	0.071 (3)	0.004 (2)	0.022 (2)	-0.005 (3)
O3	0.037 (3)	0.053 (3)	0.075 (3)	0.003 (2)	0.019 (2)	0.018 (3)
O4	0.063 (3)	0.059 (4)	0.062 (3)	-0.007 (3)	0.018 (3)	0.001 (3)
O5	0.051 (3)	0.106 (5)	0.071 (4)	-0.002 (3)	-0.006 (3)	0.006 (4)
O6	0.045 (2)	0.025 (2)	0.030 (2)	0.0072 (19)	0.0022 (18)	0.0128 (18)
O7	0.033 (2)	0.046 (3)	0.031 (2)	0.015 (2)	0.0089 (17)	-0.0032 (19)
O8	0.0269 (19)	0.033 (2)	0.0143 (17)	0.0050 (17)	-0.0001 (14)	0.0007 (16)
O9	0.026 (2)	0.034 (2)	0.041 (2)	-0.0079 (18)	-0.0029 (17)	0.0028 (19)
O10	0.032 (2)	0.033 (2)	0.044 (2)	0.0117 (19)	-0.0008 (18)	0.006 (2)
O11	0.067 (3)	0.032 (2)	0.0168 (19)	0.004 (2)	0.0046 (18)	-0.0103 (17)
N1	0.015 (2)	0.016 (2)	0.020 (2)	0.0048 (17)	-0.0005 (16)	0.0014 (17)
N2	0.018 (2)	0.019 (2)	0.0141 (19)	0.0022 (17)	-0.0001 (15)	0.0062 (17)
N3	0.014 (2)	0.019 (2)	0.022 (2)	-0.0018 (17)	0.0059 (16)	0.0026 (18)
N4	0.0116 (18)	0.019 (2)	0.0141 (19)	0.0001 (16)	-0.0002 (15)	0.0005 (16)
N5	0.0160 (19)	0.015 (2)	0.0142 (19)	0.0028 (16)	0.0022 (15)	0.0026 (16)
N6	0.019 (2)	0.024 (2)	0.016 (2)	0.0061 (18)	-0.0026 (16)	-0.0031 (18)
N7	0.050 (3)	0.039 (3)	0.050 (3)	0.001 (3)	0.001 (3)	0.011 (3)

C1	0.017 (2)	0.027 (3)	0.022 (3)	0.005 (2)	-0.0038 (19)	0.004 (2)
C2	0.023 (3)	0.051 (4)	0.030 (3)	0.006 (3)	-0.004 (2)	0.008 (3)
C3	0.028 (3)	0.058 (4)	0.029 (3)	0.010 (3)	-0.003 (2)	0.018 (3)
C4	0.030 (3)	0.043 (4)	0.026 (3)	0.008 (3)	0.002 (2)	0.015 (3)
C5	0.022 (3)	0.019 (3)	0.023 (3)	0.003 (2)	0.001 (2)	0.006 (2)
C6	0.015 (2)	0.029 (3)	0.021 (3)	0.001 (2)	0.0012 (19)	0.003 (2)
C7	0.018 (3)	0.042 (4)	0.030 (3)	-0.001 (2)	-0.003 (2)	0.005 (3)
C8	0.017 (2)	0.023 (3)	0.021 (2)	-0.005 (2)	0.0009 (19)	0.001 (2)
C9	0.024 (3)	0.034 (3)	0.037 (3)	-0.009 (3)	-0.003 (2)	0.001 (3)
C10	0.037 (4)	0.028 (3)	0.060 (4)	-0.014 (3)	0.002 (3)	-0.005 (3)
C11	0.031 (3)	0.021 (3)	0.060 (4)	-0.005 (3)	-0.001 (3)	0.006 (3)
C12	0.022 (3)	0.018 (3)	0.036 (3)	0.001 (2)	0.001 (2)	0.006 (2)
C13	0.015 (2)	0.024 (3)	0.024 (3)	0.000 (2)	0.0037 (19)	0.005 (2)
C14	0.017 (3)	0.035 (3)	0.036 (3)	0.000 (2)	0.005 (2)	-0.001 (3)
C15	0.031 (3)	0.041 (4)	0.041 (3)	-0.003 (3)	0.020 (3)	-0.002 (3)
C16	0.033 (3)	0.036 (3)	0.029 (3)	-0.006 (3)	0.015 (2)	-0.003 (3)
C17	0.025 (3)	0.025 (3)	0.023 (3)	-0.002 (2)	0.007 (2)	-0.001 (2)
C18	0.018 (2)	0.019 (3)	0.015 (2)	0.002 (2)	0.0023 (18)	0.005 (2)
C19	0.030 (3)	0.024 (3)	0.019 (2)	-0.005 (2)	0.003 (2)	0.004 (2)
C20	0.016 (2)	0.015 (2)	0.015 (2)	-0.0019 (19)	0.0001 (18)	-0.0014 (19)
C21	0.015 (2)	0.022 (3)	0.017 (2)	-0.004 (2)	0.0023 (18)	-0.002 (2)
C22	0.016 (2)	0.023 (3)	0.024 (3)	-0.001 (2)	0.003 (2)	-0.006 (2)
C23	0.018 (2)	0.018 (3)	0.024 (3)	0.002 (2)	0.000 (2)	-0.003 (2)
C24	0.022 (2)	0.015 (2)	0.014 (2)	0.000 (2)	0.0016 (19)	0.0002 (19)
C25	0.019 (2)	0.014 (2)	0.020 (2)	0.001 (2)	0.0065 (19)	0.003 (2)
C26	0.034 (3)	0.018 (3)	0.023 (3)	-0.002 (2)	0.010 (2)	0.005 (2)
C27	0.036 (3)	0.014 (3)	0.033 (3)	-0.005 (2)	0.009 (2)	-0.007 (2)
C28	0.031 (3)	0.020 (3)	0.025 (3)	-0.005 (2)	0.006 (2)	-0.007 (2)
C29	0.019 (2)	0.019 (3)	0.018 (2)	0.001 (2)	0.0041 (19)	0.001 (2)
C30	0.018 (2)	0.017 (2)	0.018 (2)	0.001 (2)	0.0024 (19)	-0.003 (2)
C31	0.023 (3)	0.064 (5)	0.028 (3)	0.010 (3)	-0.009 (2)	-0.009 (3)
C32	0.045 (3)	0.027 (3)	0.013 (2)	0.001 (3)	0.000 (2)	0.005 (2)
C33	0.041 (4)	0.042 (4)	0.046 (4)	0.004 (3)	0.008 (3)	0.012 (3)
C34	0.072 (6)	0.053 (5)	0.061 (5)	-0.027 (5)	0.020 (4)	-0.015 (4)
C35	0.033 (3)	0.030 (3)	0.025 (3)	0.002 (3)	0.006 (2)	-0.010 (2)
C36	0.044 (4)	0.024 (3)	0.031 (3)	0.002 (3)	0.010 (3)	-0.002 (3)
C37	0.067 (6)	0.129 (10)	0.083 (7)	0.015 (6)	0.011 (5)	-0.021 (7)

Geometric parameters (Å, º)

Co1—O1	1.907 (3)	N2—C12	1.345 (6)
Co1—N1	1.951 (4)	N2—C8	1.355 (6)
Co1—N3	1.974 (4)	N3—C17	1.348 (6)
Co1—N5	1.974 (4)	N3—C13	1.361 (6)
Co1—N4	1.981 (4)	N4—C20	1.345 (6)
Co1—N2	1.987 (4)	N4—C24	1.354 (6)
Cl1—C37	1.651 (11)	N5—C29	1.339 (6)
Cl2—C37	1.784 (10)	N5—C25	1.361 (6)
S1—O3	1.404 (5)	N6—C30	1.284 (6)
S1—O2	1.430 (5)	N6—C32	1.465 (7)
S1—N7	1.558 (6)	N6—C31	1.467 (7)
S1—C33	1.845 (7)	C1—C2	1.392 (7)
S2—O4	1.403 (6)	C1—C6	1.518 (7)
S2—O5	1.413 (6)	C2—C3	1.361 (8)
S2—N7	1.623 (6)	C3—C4	1.383 (8)
S2—C34	1.835 (8)	C4—C5	1.378 (7)
S3—O7	1.431 (4)	C5—C18	1.533 (7)
S3—O6	1.438 (4)	C6—C13	1.525 (7)
S3—O8	1.445 (3)	C6—C8	1.536 (7)
S3—C35	1.824 (6)	C6—C7	1.543 (7)
S4—O10	1.431 (4)	C8—C9	1.381 (7)
S4—O9	1.433 (4)	C9—C10	1.374 (9)
S4—O11	1.442 (4)	C10—C11	1.376 (9)
S4—C36	1.820 (6)	C11—C12	1.379 (8)
F1—C33	1.314 (7)	C13—C14	1.385 (7)
F2—C33	1.340 (8)	C14—C15	1.373 (8)
F3—C33	1.289 (8)	C15—C16	1.370 (8)
F4—C34	1.321 (10)	C16—C17	1.383 (7)
F5—C34	1.341 (9)	C18—C25	1.514 (7)
F6—C34	1.328 (9)	C18—C19	1.530 (6)
F7—C35	1.338 (6)	C18—C20	1.539 (7)
F8—C35	1.341 (6)	C20—C21	1.393 (6)
F9—C35	1.335 (7)	C21—C22	1.388 (7)
F10—C36	1.331 (6)	C22—C23	1.383 (7)
F11—C36	1.329 (7)	C23—C24	1.375 (7)
F12—C36	1.331 (7)	C25—C26	1.386 (7)
O1—C30	1.283 (6)	C26—C27	1.390 (7)
N1—C5	1.348 (6)	C27—C28	1.391 (7)

N1—C1	1.359 (6)	C28—C29	1.367 (7)
O1—Co1—N1	178.32 (16)	C4—C5—C18	121.3 (4)
O1—Co1—N3	87.70 (15)	C1—C6—C13	110.6 (4)
N1—Co1—N3	91.75 (16)	C1—C6—C8	108.4 (4)
O1—Co1—N5	93.07 (15)	C13—C6—C8	107.3 (4)
N1—Co1—N5	88.56 (17)	C1—C6—C7	110.7 (4)
N3—Co1—N5	95.25 (16)	C13—C6—C7	109.4 (4)
O1—Co1—N4	90.63 (15)	C8—C6—C7	110.5 (4)
N1—Co1—N4	89.89 (16)	N2—C8—C9	121.0 (5)
N3—Co1—N4	178.12 (17)	N2—C8—C6	116.4 (4)
N5—Co1—N4	85.72 (16)	C9—C8—C6	122.5 (5)
O1—Co1—N2	87.64 (15)	C10—C9—C8	120.4 (5)
N1—Co1—N2	90.72 (16)	C9—C10—C11	118.3 (6)
N3—Co1—N2	81.96 (17)	C10—C11—C12	119.2 (6)
N5—Co1—N2	177.09 (16)	N2—C12—C11	122.6 (5)
N4—Co1—N2	97.10 (16)	N3—C13—C14	119.8 (5)
O3—S1—O2	118.1 (3)	N3—C13—C6	116.6 (4)
O3—S1—N7	117.7 (3)	C14—C13—C6	123.2 (5)
O2—S1—N7	105.7 (3)	C15—C14—C13	120.7 (5)
O3—S1—C33	106.7 (3)	C16—C15—C14	119.2 (5)
O2—S1—C33	101.4 (3)	C15—C16—C17	118.5 (5)
N7—S1—C33	105.3 (3)	N3—C17—C16	122.6 (5)
O4—S2—O5	117.4 (4)	C25—C18—C19	111.5 (4)
O4—S2—N7	119.0 (3)	C25—C18—C5	108.2 (4)
O5—S2—N7	109.3 (4)	C19—C18—C5	110.8 (4)
O4—S2—C34	104.4 (4)	C25—C18—C20	107.9 (4)
O5—S2—C34	104.4 (4)	C19—C18—C20	110.4 (4)
N7—S2—C34	99.4 (3)	C5—C18—C20	107.9 (4)
O7—S3—O6	115.5 (2)	N4—C20—C21	120.9 (4)
O7—S3—O8	115.0 (2)	N4—C20—C18	117.1 (4)
O6—S3—O8	115.1 (2)	C21—C20—C18	121.9 (4)
O7—S3—C35	102.8 (3)	C22—C21—C20	120.4 (4)
O6—S3—C35	102.7 (3)	C23—C22—C21	118.1 (4)
O8—S3—C35	103.1 (2)	C24—C23—C22	119.0 (5)
O10—S4—O9	114.7 (3)	N4—C24—C23	123.2 (4)
O10—S4—O11	115.2 (3)	N5—C25—C26	120.4 (4)
O9—S4—O11	115.2 (3)	N5—C25—C18	117.9 (4)
O10—S4—C36	104.1 (3)	C26—C25—C18	121.6 (4)
O9—S4—C36	103.2 (3)	C25—C26—C27	120.2 (5)
O11—S4—C36	101.8 (3)	C26—C27—C28	118.5 (5)

C30—O1—Co1	125.2 (3)	C29—C28—C27	118.3 (5)
C5—N1—C1	118.4 (4)	N5—C29—C28	124.0 (5)
C5—N1—Co1	120.8 (3)	O1—C30—N6	121.9 (4)
C1—N1—Co1	120.6 (3)	F3—C33—F1	110.5 (6)
C12—N2—C8	117.9 (4)	F3—C33—F2	106.7 (6)
C12—N2—Co1	122.6 (3)	F1—C33—F2	107.9 (5)
C8—N2—Co1	119.5 (3)	F3—C33—S1	110.9 (5)
C17—N3—C13	118.7 (4)	F1—C33—S1	111.0 (5)
C17—N3—Co1	122.2 (3)	F2—C33—S1	109.7 (5)
C13—N3—Co1	119.1 (3)	F4—C34—F6	110.7 (7)
C20—N4—C24	118.3 (4)	F4—C34—F5	109.1 (7)
C20—N4—Co1	120.1 (3)	F6—C34—F5	104.7 (7)
C24—N4—Co1	121.4 (3)	F4—C34—S2	111.9 (6)
C29—N5—C25	118.3 (4)	F6—C34—S2	110.3 (6)
C29—N5—Co1	122.5 (3)	F5—C34—S2	109.9 (5)
C25—N5—Co1	119.2 (3)	F9—C35—F7	108.0 (5)
C30—N6—C32	122.4 (4)	F9—C35—F8	107.4 (4)
C30—N6—C31	121.0 (5)	F7—C35—F8	107.0 (5)
C32—N6—C31	116.5 (4)	F9—C35—S3	112.2 (4)
S1—N7—S2	125.2 (4)	F7—C35—S3	110.8 (4)
N1—C1—C2	121.1 (5)	F8—C35—S3	111.2 (4)
N1—C1—C6	116.3 (4)	F11—C36—F10	106.2 (5)
C2—C1—C6	122.6 (5)	F11—C36—F12	107.4 (5)
C3—C2—C1	120.2 (5)	F10—C36—F12	107.8 (5)
C2—C3—C4	118.5 (5)	F11—C36—S4	111.6 (4)
C5—C4—C3	119.8 (5)	F10—C36—S4	111.8 (4)
N1—C5—C4	121.8 (5)	F12—C36—S4	111.7 (4)
N1—C5—C18	116.9 (4)	Cl1—C37—Cl2	116.2 (7)

ChemPubSoc Europe

DOI: 10.1002/cssc.201200636

Cyanomethylbenzoic Acid: An Acceptor for Donor–π–Acceptor Chromophores Used in Dye-Sensitized Solar Cells

Wanchun Xiang,[a] Akhil Gupta,[b, c] Muhammad Kalim Kashif,[a] Noel Duffy,[c] Ante Bilic,[d] Richard A. Evans,*[c] Leone Spiccia,*[a] and Udo Bach*[b, e, f]

During the past two decades, dye-sensitized solar cells (DSCs) have received great attention due to their low fabrication cost compared to conventional silicon solar cells.[1] Energy conversion efficiencies of up to 11% have been reported for DSCs based on iodide/iodine liquid electrolytes and ruthenium(II) dyes.[2] However, in terms of practical applications, these high-performance iodine-based electrolytes are afflicted with a number of potential disadvantages, such as their high volatility, significant coloration, and corrosive nature. The latter gives rise to major incompatibility issues with a number of metals and sealing materials, limiting the use of metal substrates or charge-collecting grids in the construction of DSC modules.

Iodine-free, one-electron outer-sphere redox couples, such as cobalt(II)/(III) polypyridyl complexes, are promising alternative redox mediators due to their weak coloration and their compatibility with a wide range of metal substrates.[3] DSCs based on these mediators can reach high conversion efficiencies, especially when used in conjunction with organic sensitizers, featuring high molar extinction coefficients and TiO_2 electrodes of only a few microns in thickness.[4] Yella et al. recently reported a DSC with a new benchmark efficiency of 12.3%, which used $[Co(bpy)_3]^{2+/3+}$ (bpy = 2,2′-bipyridine) as redox mediator, causing a paradigm shift in dye-sensitized solar cells.[5] Thus, the best-performing DSC features neither a ruthenium(II) polypyridyl complex as sensitizer, nor an iodide-based electrolyte. Previous studies suggested that the performance of cobalt redox mediators in DSCs is hindered by rapid recombination of electrons in the TiO_2 conduction band with the cobalt(III) species and, furthermore, by slow dye regeneration.[6] These issues can be overcome by: (1) matching sensitizers with cobalt polypyridyl complexes, such that a sufficient driving force is available to ensure efficient dye regeneration;[6] and (2) applying sensitizers with high molar extinction coefficients to ensure excellent light harvesting even when using thin TiO_2 films.[7]

A number of organic sensitizers have been tested in conjunction with cobalt electrolytes. Most of these dyes are donor–π-bridge–acceptor (D–π–A) dyes. Among donor groups, triphenylamine and its derivatives have shown promise in the development of DSCs due to their nonplanar structure suppressing the aggregation of dye molecules.[8] Oligothiophenes, and their derivatives, have been widely used as conjugated π-bridges, due to their high polarizability as well as their tunable spectroscopic and electrochemical properties.[7,9] The focus of electron-acceptor groups has been largely on carboxyl acid, cyanoacrylic acid, and the rhodanine-3-acetic-acid moiety as they bind strongly to the TiO_2 semiconductor surface.[5,10] In particular, much attention has been paid to cyanoacrylic acid because of its strong electron-withdrawing ability, which may result in an efficient electron–hole separation within the dye molecule. In contrast, few studies have ever been reported that examine whether the structural alternatives of this particular acceptor improve the performance of DSCs. In this work, cyanomethylbenzoic acid is introduced as a new acceptor moiety for DSC sensitizers and is compared to the more established cyanoacetic acid moiety. It was thought that the cyanomethylbenzoic acid may provide better performance as it will cause a redshift of the absorption spectrum. For this purpose, two new dyes were synthesized. K6 (see Figure 1) is a structural analogue of dye C240,[11] differing slightly in the degree and type of alkoxy-substitution on the phenyl rings of the triarylamine unit. K7 is a structural analogue of K6, in which cyanoacrylic acid was replaced with the new cyanomethylbenzoic-acid acceptor. Molecular orbital calculations show similar highest occupied and lowest unoccupied molecular orbital (HOMO/LUMO) electron distributions for the two dyes (Figure 1).

The K6 and K7 dyes were synthesized by reacting the aldehyde precursor, 6-[4-(bis{4-[(2-ethylhexyl)oxy]phenyl}amino)-

[a] Dr. W. Xiang,[+] M. K. Kashif, Prof. Dr. L. Spiccia
School of Chemistry
Monash University
Victoria 3800 (Australia)
[redacted]

[b] A. Gupta,[+] Prof. Dr. U. Bach
Department of Materials Engineering
Monash University
Victoria 3800 (Australia)
[redacted]

[c] A. Gupta,[+] Dr. N. Duffy, Prof. Dr. R. A. Evans
CSIRO Materials Science and Engineering
Flexible Electronics Theme
Bayview Avenue, Clayton South, 3169, Victoria (Australia)
[redacted]

[d] Dr. A. Bilic
CSIRO Mathematics Informatics and Statistics
Bayview Avenue, Clayton 3169, Victoria (Australia)

[e] Prof. Dr. U. Bach
Commonwealth Scientific and Industrial Research Organization
Materials Science and Engineering
Flexible Electronics Theme
Clayton South, Victoria 3169 (Australia)

[f] Prof. Dr. U. Bach
Melbourne Centre for Nanofabrication
151 Wellington Road, Clayton, VIC 3168 (Australia)

[+] These authors contributed equally to this work.

Supporting Information for this article is available on the WWW under http://dx.doi.org/10.1002/cssc.201200636.

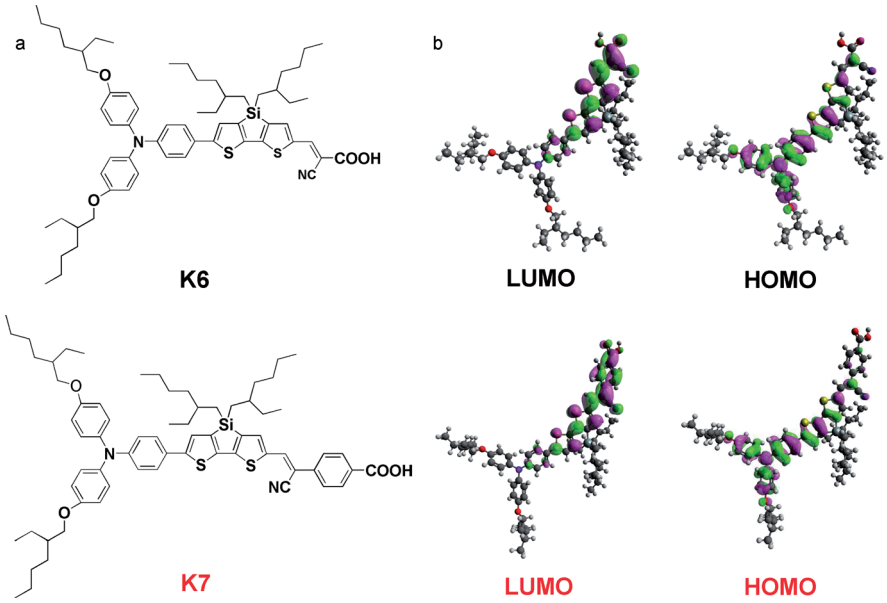

Figure 1. a) Chemical structures of sensitizers K6 and K7. b) Electron-density distribution for the LUMOs and HOMOs of K6 and K7. Density functional theory (DFT) calculations were performed on all the materials using the Gaussian 03 suite of programs and B3LYP/6-311+G(d,p)//B3LYP/6-31G(d) level of theory.

phenyl]-4,4-bis(2-ethylhexyl)-4*H*-silolo[3,2-b:4,5-b′]dithiophene-2-carbaldehyde, at reflux with cyanoacetic acid in a 1:1 (*v*/*v*) acetonitrile/chloroform mixture and 4-(cyanomethyl)benzoic acid in a 9:1 (*v*/*v*) acetonitrile/chloroform solvent mixture, respectively, in the presence of piperidine as base. Synthetic and characterization details are provided in the Supporting Information.

The UV/Vis spectra of K6 and K7 measured in chlorobenzene solution, and when absorbed on a TiO_2 film, are shown in Figure 2. In solution, the absorption maximum of K7 is slightly red-shifted by 25 nm relative to the cyanoacrylic acid dye, K6, whereas the molar extinction coefficient at λ_{max} of K7 (43 700 L mol^{-1} cm^{-1}@521 nm) is slightly higher than that of K6 (40 800 L mol^{-1} cm^{-1}@506 nm). When adsorbed onto TiO_2 films, the absorption maxima for both K6 and K7 shift by about 30 nm to shorter wavelengths when compared to the solution spectrum, which may be due to the deprotonation of the carboxylic acid group on the surface of TiO_2. K7 shows superior light absorption at wavelengths longer than 460 nm.

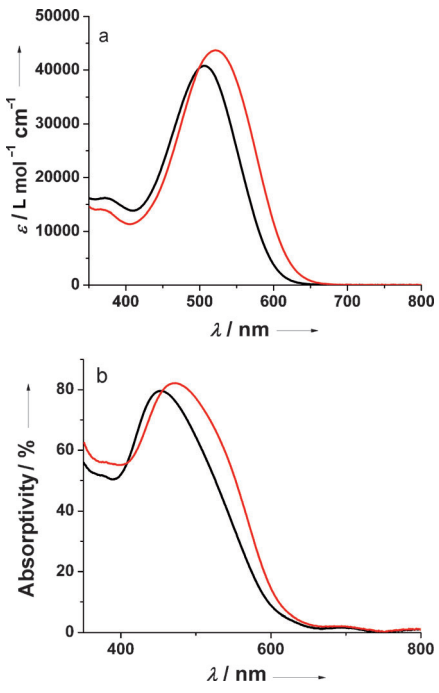

Figure 2. a) Molar extinction coefficients (ε) of K6 (black) and K7 (red) in chlorobenzene. b) Absorptivity spectra of 1.2 μm thick TiO_2 films sensitized with K6 (black) and K7 (red) recorded in air. Sensitization of the films was performed using a 1.5 μM dye solutions in a chlorobenzene and ethanol mixture (*v*/*v* = 1:1) for 8 h.

The dye anchoring in DSCs is critical in achieving high cell efficiencies. K6 contains a cyanoacrylic acid group as anchoring moiety, which is typically introduced into most organic dyes to chemically attach to the TiO_2 surface.[12] To compare the binding ability of K7, which has a cyanomethylbenzoic acid acceptor, with that of K6, the absorption of the two dyes on TiO_2 was investigated. In Figure 3, the absorption of the dye adsorbed on the mesoporous TiO_2 film is plotted as a function of the dye's equilibrium concentration (c_{equ}) in the dye bath. The two dyes show a very similar concentration-dependent absorption behavior with the dye absorption reaching a plateau at $c_{equ} \approx 0.1$ mM. According to classical Langmuir absorption theory[13] the dye-binding constant can be extracted from a plot of the inverse of the surface coverage Γ^{-1} as a function of c_{equ}^{-1} [Eq. (1)].[13] The inset of Figure 3 shows the corresponding plot, confirming Langmuir-type adsorption behavior. The calculated binding constants, *K*, for the two dyes are identical [$(4.42 \pm 0.07) \times 10^5$ and $(4.46 \pm 0.03) \times 10^5$ L mol^{-1} for K6 and K7, respectively], suggesting that the new acceptor moiety attaches to the TiO_2 surface just as strongly as the traditional cyanoacrylic acid group. In keeping with this finding, the dye loading for K7 [6.87 (± 0.03) $\times 10^{-8}$ mol cm^{-2}] and K6 [6.91 (± 0.02) $\times 10^{-8}$ mol cm^{-2}], under the conditions used to dye films for DSC construction, is identical.

$$\left(\frac{1}{\Gamma}\right) = \left(\frac{1}{c_{equ}}\right)\frac{1}{K} + 1 \qquad (1)$$

Cyclic voltammetry was carried out to determine the redox properties of these two dyes (see Figure S1). The oxidation of K7 occurs at a half-wave potential of $E_{1/2}(K7/K7^+) = 1.02$ V

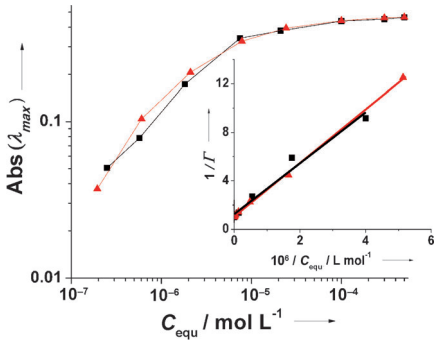

Figure 3. Langmuir isotherms. Dye absorption on 1.2 μm thick mesoporous TiO_2 films at the wavelength of maximum absorption (K6 black and K7 red) as a function of the equilibrium concentration of the dye (c_{equ}) in the solution (chlorobenzene/ethanol = 1:1 *v*/*v*). The films were kept in the dye bath for 20 h. Inset: The inverse of TiO_2 surface coverage Γ^{-1} plotted against the inverse of the dye equilibrium concentration $(c_{equ})^{-1}$ with $\Gamma = Abs(\lambda_{max})/Abs^0(\lambda_{max})$ where $Abs^0(\lambda_{max})$ corresponds to $Abs(\lambda_{max})$ measured at $c_{equ} = 0.5$ mM.

Table 1. Photovoltaic performance of DSCs under simulated AM1.5G solar irradiation (100 mW cm^{-2}).[a]

Dye	Electrolyte	V_{oc}[b] [mV]	J_{sc}[c] [mA cm^{-2}]	*ff*[d]	η[e] [%]
K6	$Co(bpy)_3^{2+/3+}$	846 ± 3	10.0 ± 0.1	0.76 ± 0.01	6.4 ± 0.2
K7		832 ± 1	12.5 ± 0.2	0.73 ± 0.01	7.6 ± 0.1
K6	I^-/I_3^-	745 ± 8	10.7 ± 0.3	0.73 ± 0.01	5.8 ± 0.2
K7		738 ± 7	11.5 ± 0.3	0.71 ± 0.01	6.1 ± 0.2

[a] DSCs were constructed with the K6 and K7 dyes and tested with two electrolyte systems the compositions of which were as follows: (1) cobalt electrolyte: 0.20 M tris(2,2′-bipyridyl)cobalt(II) bis(trifluoromethanesulfonyl)imide ($[Co(bpy)_3](TFSI)_2$), 0.060 M $[Co(bpy)_3](TFSI)_3$, 0.050 M LiTFSI, 1.00 M *tert*-butylpyridine (*t*BP) in acetonitrile; (2) iodide electrolyte: 0.20 M LiI, 0.060 M I_2, 0.050 M LiTFSI, 1.00 M *t*BP in acetonitrile; both K6 and K7 were adsorbed from a 0.3 mM dye solution in a mixture of chlorobenzene and ethanol (*v*/*v* = 1:1) for 12 h. [b] V_{oc} is the open circuit voltage. [c] J_{sc} is the short circuit current density. [d] *ff* is the fill factor. [e] η is the energy conversion efficiency.

versus normal hydrogen electrode (NHE). The corresponding value for K6 is 170 mV higher [$E_{1/2}(K6/K6^+) = 1.19$ V versus NHE]. The spectral properties of the dyes, shown in Figure 2, were combined with the electrochemical data of the dyes in solution to calculate the $E_{1/2}(D^*/D^+)$ energy levels shown in Figure 4.[14] Based on the electrochemical properties, the dye-

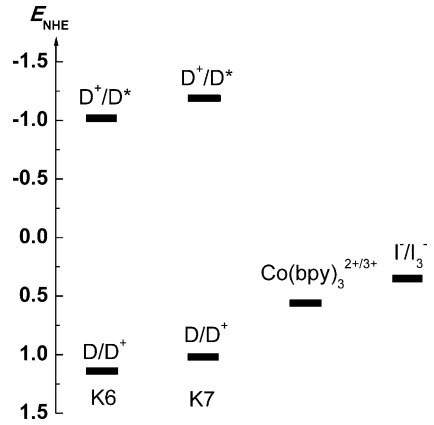

Figure 4. Energy diagram of the sensitizers K6, K7, $[Co(bpy)_3]^{2+/3+}$ and a iodide/triiodide electrolyte based on the results of cyclic voltammetry measurements (see the Supporting Information).

regeneration driving forces for K6 and K7 can be estimated to be 620 and 460 mV, respectively, when these dyes are used in conjunction with a $[Co(bpy)_3]^{2+/3+}$ (bpy = 2,2′-bipyridine) electrolyte. Both driving forces are in excess of 390 mV, which was previously found to be sufficient for efficient dye regeneration by the same redox mediator.[6]

The photovoltaic performance of K6 and K7 was evaluated in DSCs constructed with $[Co(bpy)_3]^{2+/3+}$ as well as a conventional triiodide/iodide-based electrolyte (see Table 1). The TiO_2 electrode structures were optimized to maximize the performance of $[Co(bpy)_3]^{2+/3+}$-based DSCs and consisted of a 4 μm thick transparent layer (30 nm particle size) and a 6 μm thick scattering layer (400 nm particle size). To facilitate the comparison of DSC performance, the concentrations of the oxidized and reduced redox mediators were chosen to be identical for both electrolyte systems. Other additives, such as *t*BP and LiTFSI, were also maintained at the same concentration and acetonitrile was used as solvent.

DSCs sensitized with K7 clearly outperform devices based on the K6 sensitizer in both electrolyte systems. The improvement is mostly due to an increase in the short-circuit current density (J_{SC}). The analysis of the incident-photon-to-current conversion efficiency (IPCE) measurements of these DSCs (see Figure 5a) reveals that the IPCE for K7-sensitized DSCs levels out at values of 82–86% at around 500 nm for the $[Co(bpy)_3]^{2+/3+}$- and iodide-based electrolytes, whereas the values for K6-sensitized cells are somewhat lower reaching maxima of approximately 67% for both electrolyte systems. Only the DSC based on K6 and iodide/triiodide show a weak redshift in the IPCE spectrum. The two dyes show up to 80% light absorption when adsorbed onto a 1.2 μm thick TiO_2 film (see Figure 2b). Light harvesting by the sensitized TiO_2 layers used for the construction of these DSCs (4 μm thick + scattering layer) will, therefore, be close to quantitative over a significant range of the spectral region around the absorption maxima of the sensitizers. To further rationalize the observed IPCE spectra of K6 and K7 in $[Co(bpy)_3]^{2+/3+}$-based DSCs, absorbed-photon-to-electron (APCE) spectra were calculated based on the absorption properties of the sensitized films (see Figure 5b). The average APCE values across the spectral range of 450–550 nm for K6 and K7 are 63 and 70%, respectively, indicating a significantly increased charge conversion efficiency per adsorbed photon for K7-sensitized $[Co(bpy)_3]^{2+/3+}$-based DSCs. This increase can be caused by: (1) improved charge injection; (2) improved dye-regeneration; and/or (3) reduced recombination. To check whether the observed photocurrents during the IPCE and APCE measurements were limited by charge collection, preliminary front/back-IPCE measurements were performed (Figure S3 in the Supporting Information). The results show negligible charge recombination during electron diffusion through TiO_2

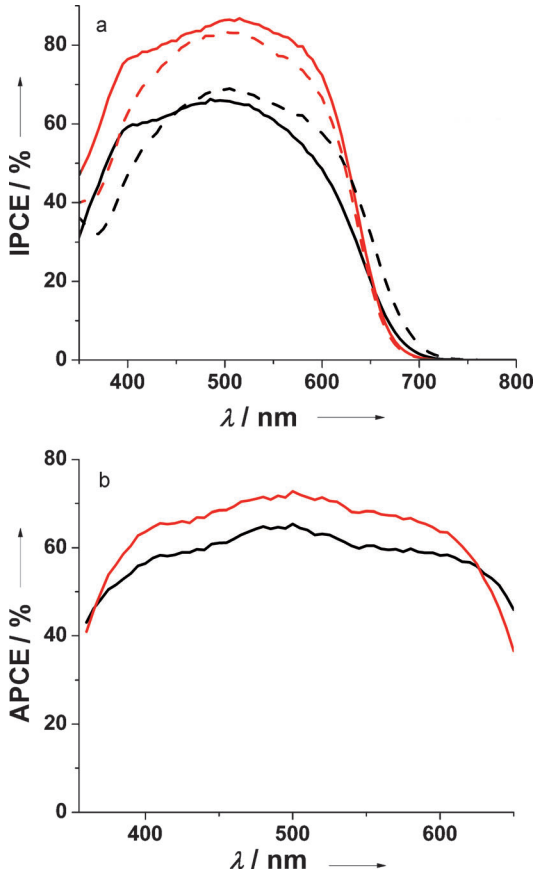

Figure 5. a) Incident-photon-to-electron conversion efficiencies (IPCEs) of DSCs sensitized with K6 (black) and K7 (red) based on $[Co(bpy)_3]^{2+/3+}$ (solid line) and I^-/I_3^- (dashed line) electrolytes (same devices as reported in Table 1). b) Absorbed-photon-to-current generation efficiencies (APCEs) as a function of wavelength for K6 (black) and K7 (red) in conjunction with the $[Co(bpy)_3]^{2+/3+}$ electrolyte described in Table 1. DSCs based on 4 μm thick transparent TiO_2 films were used for this analysis.

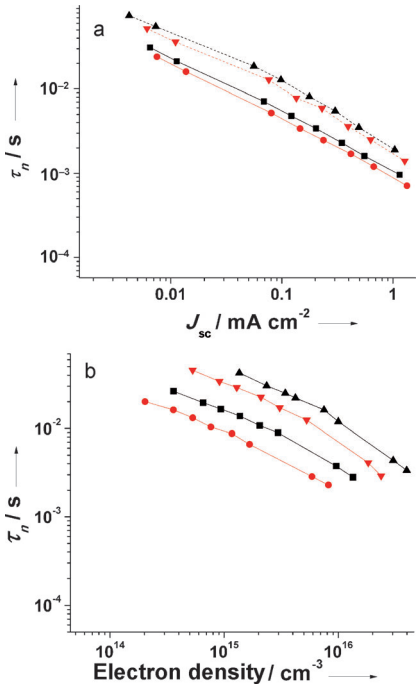

Figure 6. IMVS and IMPS measurements performed on K6- (black) and K7- (red) sensitized DSCs based on $[Co(bpy)_3]^{2+/3+}$ (solid line) and I^-/I_3^- (dashed line) electrolytes (same devices as reported in Table 1). a) Mean charge transient time versus short circuit current. b) Electron lifetime versus electron density.

film, suggesting that the electron diffusion length is well below the thickness of the TiO_2 film.

To further elucidate the origin of the observed differences in photovoltaic performance, the electron lifetime and mean transit time of photo-injected charge carriers were studied by means of intensity modulated photovoltage and photocurrent spectroscopy (IMVS and IMPS)[15] in combination with charge extraction experiments. The IMPS results, shown in Figure 6a, indicate that similar mean electron transit times were observed for both dyes and both electrolytes and suggest comparable electron transport within the TiO_2 layer in all cases. Charge extraction measurements according to Duffy et al[16] were used to determine the amount of charge stored in DSCs as a function of V_{OC} (see Figure S3). The results obtained through IMVS and charge extraction experiments were then combined to yield the electron lifetime as a function of charge stored in the DSC, as shown in Figure 6b. The results for the $[Co(bpy)_3]^{2+/3+}$ electrolytes clearly show an increase in electron lifetime by about a factor of 1.6 for K6-sensitized DSCs over devices sensitized with K7. When I^-/I_3^- is used as redox mediator, there is no apparent difference in electron lifetime for K6- and K7-sensitized DSCs. The somewhat longer electron lifetime observed for K6-sensitized devices is also consistent with the 14 mV increase in V_{OC} and slightly higher *ff* for K6, relative to K7-sensitized $[Co(bpy)_3]^{2+/3+}$ DSCs (see Table 1). This rules out both increased charge recombination as well as inefficient dye-regeneration as a cause for the inferior performance of K6-sensitized DSCs as both effects should result in a reduction, rather than an increase, in electron lifetime. Consequently, superior charge injection properties for K7, relative to K6, are the most likely origin of the observed performance difference. This is also consistent with a 170 mV more negative $E_{1/2}(K7^+/K7^*)$ level compared to $E_{1/2}(K6^+/K6^*)$ (see Figure 4).

In summary, we have evaluated a new cyanomethylbenzoic acid as acceptor for D–π–A DSC sensitizers by comparing its performance to the more widely used cyanoacrylic acid acceptor unit in a pair of analogous dyes. These dyes were modeled on previously reported sensitizers that yielded high DSC performances when combined with $[Co(bpy)_3]^{2+/3+}$ electrolytes (C240).[11] The dye featuring the cyanomethylbenzoic acid acceptor (K7) outperformed the model sensitizer comprising the cyanoacrylic acid group (K6) in terms of its photovoltaic performance. Superior charge injection properties of K7 compared to K6 were identified as the most likely reasons for the observed increases in J_{sc}, efficiency; and IPCE. The performance increase could be realized in spite of a slight electron lifetime decrease for $[Co(bpy)_3]^{2+/3+}$-based DSCs when the cyanoacrylic acid group is replaced with cyanomethylbenzoic acid.

Progress in the development of alternative redox mediators and metal-free sensitizers has accelerated significantly in recent years. The recent work by Yella et al.[5] has highlighted the potential for efficiency improvements beyond those of classical DSCs based on iodide and ruthenium(II) polypyridyl complexes. Until now, however, a limited number of organic dyes have been reported to act as efficient sensitizers when used in conjunction with cobalt(II)/(III) polypyridyl redox mediators. This is anticipated to change radically, given the remarkable progress accomplished recently.[3,4,17] New sensitizers will be required with properties tailored towards their use in conjunction with alternative non-corrosive electrolytes. We believe that the cyanomethylbenzoic-acid acceptor reported herein represents a valuable addition to the library of acceptors that will form the basis for the next generation of custom-designed high-efficiency sensitizers.

Acknowledgements

The authors would like to acknowledge the ARC for providing equipment (LE0883019) and fellowship (U.B., DP110105312) support. This work was further supported by the Australian Solar Institute, the Victorian State Government (DBI-VSA and DPI-ETIS), and was performed in part at the Melbourne Centre for Nanofabrication, an initiative partly funded by the Commonwealth of Australia and the Victorian Government and Monash University. The Commonwealth Scientific and Industrial Research Organization is acknowledged for providing support through an OCE PhD fellowship (A.G.) and an OCE Science Leader position (U.B.).

Keywords: benzoic acid · cobalt complexes · iodine free · solar cells · sensitizers

[1] a) B. O'Regan, M. Grätzel, *Nature* **1991**, *353*, 737 – 740; b) A. Hagfeldt, G. Boschloo, L. C. Sun, L. Kloo, H. Pettersson, *Chem. Rev.* **2010**, *110*, 6595 – 6663; c) P. V. Kamat, K. Tvrdy, D. R. Baker, J. G. Radich, *Chem. Rev.* **2010**, *110*, 6664 – 6688.

[2] M. K. Nazeeruddin, P. Pechy, T. Renouard, S. M. Zakeeruddin, M. Grätzel, *J. Am. Chem. Soc.* **2001**, *123*, 1613 – 1624.

[3] a) Y. Bai, Q. J. Yu, N. Cai, Y. H. Wang, M. Zhang, P. Wang, *Chem. Commun.* **2011**, *47*, 4376 – 4378; b) T. Daeneke, T. H. Kwon, A. B. Holmes, N. W. Duffy, U. Bach, L. Spiccia, *Nat. Chem.* **2011**, *3*, 213 – 215; c) H. N. Tian, E. Gabrielsson, Z. Yu, A. Hagfeldt, L. Kloo, L. C. Sun, *Chem. Commun.* **2011**, *47*, 10124 – 10126; d) M. Cheng, X. C. Yang, S. F. Li, X. N. Wang, L. C. Sun, *Energy Environ. Sci.* **2012**, *5*, 6290 – 6293; e) T. C. Li, F. F. Santiago, O. K. Farha, A. M. Spokoyny, S. R. Raga, J. Bisquert, C. A. Mirkin, T. J. Marks, J. T. Hupp, *J. Phys. Chem. C* **2011**, *115*, 11257 – 11264.

[4] a) D. F. Zhou, Q. J. Yu, N. Cai, Y. Bai, Y. H. Wang, P. Wang, *Energy Environ. Sci.* **2011**, *4*, 2030 – 2034; b) H. N. Tsao, J. L. Burschka, C. Y. Yi, F. Kessler, M. K. Nazeeruddin, M. Grätzel, *Energy Environ. Sci.* **2011**, *4*, 4921 – 4924; c) S. A. Sapp, C. M. Elliott, C. Contado, S. Caramori, C. A. Bignozzi, *J. Am. Chem. Soc.* **2002**, *124*, 11215 – 11222; d) H. N. Tsao, C. Y. Yi, T. Moehl, J. H. Yum, S. M. Zakeeruddin, M. K. Nazeeruddin, M. Grätzel, *ChemSusChem* **2011**, *4*, 591 – 594.

[5] A. Yella, H. W. Lee, H. N. Tsao, C. Yi, A. K. Chandiran, M. K. Nazeeruddin, E. W. G. Diau, C. Y. Yeh, S. M. Zakeeruddin, M. Grätzel, *Science* **2011**, *334*, 629 – 634.

[6] S. M. Feldt, E. A. Gibson, E. Gabrielsson, L. C. Sun, G. Boschloo, A. Hagfeldt, *J. Am. Chem. Soc.* **2010**, *132*, 16714 – 16724.

[7] Y. Bai, J. Zhang, D. F. Zhou, Y. H. Wang, M. Zhang, P. Wang, *J. Am. Chem. Soc.* **2011**, *133*, 11442 – 11445.

[8] a) Y. Liang, B. Peng, J. Chen, *J. Phys. Chem. C* **2010**, *114*, 10992 – 10998; b) T. Marinado, K. Nonomura, J. Nissfolk, M. K. Karlsson, D. P. Hagberg, L. C. Sun, S. Mori, A. Hagfeldt, *Langmuir* **2010**, *26*, 2592 – 2598.

[9] a) T. Maeda, Y. Hamamura, K. Miyanaga, N. Shima, S. Yagi, H. Nakazumi, *Org. Lett.* **2011**, *13*, 5994 – 5997; b) C. J. Qin, W. Q. Peng, K. Zhang, A. Islam, L. Y. Han, *Org. Lett.* **2012**, *14*, 2532 – 2535.

[10] a) J. A. Mikroyannidis, A. Kabanakis, P. Balraju, G. D. Sharma, *J. Phys. Chem. C* **2010**, *114*, 12355 – 12363; b) W. H. Howie, F. Clacysscns, H. Miura, L. M. Peter, *J. Am. Chem. Soc.* **2008**, *130*, 1367 – 1375; c) Y. Hao, X. C. Yang, J. Y. Cong, H. N. Tian, A. Hagfeldt, L. C. Sun, *Chem. Commun.* **2009**, 4031 – 4036; d) A. Abbotto, N. Manfredi, C. Marinzi, F. D. Angelis, E. Mosconi, J. H. Yum, X. X. Zhang, M. K. Nazeeruddin, M. Grätzel, *Energy Environ. Sci.* **2009**, *2*, 1094 – 1101; e) J. Wiberg, T. Marinado, D. P. Hagberg, L. C. Sun, A. Hagfeldt, B. Albinsson, *J. Phys. Chem. C* **2009**, *113*, 3881 – 3886.

[11] M. F. Xu, M. Zhang, M. Pastore, R. Z. Li, F. D. Angelis, P. Wang, *Chem. Sci.* **2012**, *3*, 976 – 983.

[12] a) H. Park, E. Bae, J. J. Lee, J. Park, W. Y. Choi, *J. Phys. Chem. B* **2006**, *110*, 8740 – 8749; b) I. Gillaizeau-Gauthier, F. Odobel, M. Alebbi, R. Argazzi, E. Costa, C. A. Bignozzi, P. Qu, G. J. Meyer, *Inorg. Chem.* **2001**, *40*, 6073 – 6079.

[13] M. Katono, T. Bessho, S. Meng, R. Humphry-Baker, G. Rothenberger, S. M. Zakkeruddin, E. Kaxiras, M. Grätzel, *Langmuir* **2011**, *27*, 14248 – 14252.

[14] H. N. Tian, X. Jiang, Z. Yu, L. Kloo, A. Hagfeldt, L. C. Sun, *Angew. Chem.* **2010**, *122*, 7486 – 7489; *Angew. Chem. Int. Ed.* **2010**, *49*, 7328 – 7331.

[15] A. C. Fisher, L. M. Peter, E. A. Ponomarev, A. B. Walker, K. G. U. Wijayantha, *J. Phys. Chem. B* **2000**, *104*, 949 – 958.

[16] N. W. Duffy, L. M. Peter, R. M. G. Rajapakse, K. G. U. Wijayantha, *Electrochem. Commun.* **2000**, *2*, 658 – 662.

[17] H. N. Tian, L. C. Sun, *J. Mater. Chem.* **2011**, *21*, 10592 – 10601.

Received: August 28, 2012
Published online on January 23, 2013